

# **Design and synthesis of cyclic analogs of the kappa opioid receptor antagonist arodyn**

By

© 2018

Solomon Aguta Gisemba

Submitted to the graduate degree program in Medicinal Chemistry and the Graduate Faculty of the University of Kansas in partial fulfillment of the requirements for the degree of Doctor of Philosophy.

---

Chair: Dr. Blake Peterson

---

Co-Chair: Dr. Jane Aldrich

---

Dr. Michael Rafferty

---

Dr. Teruna Siahaan

---

Dr. Thomas Tolbert

Date Defended: 18 April 2018

The dissertation committee for Solomon Aguta Gisemba certifies that this  
is the approved version of the following dissertation:

**Design and synthesis of cyclic analogs of the kappa opioid  
receptor antagonist arodyn**

---

Chair: Dr. Blake Peterson

---

Co-Chair: Dr. Jane Aldrich

Date Approved: 10 June 2018

## Abstract

Opioid receptors are important therapeutic targets for mood disorders and pain. Kappa opioid receptor (KOR) antagonists have recently shown potential for treating drug addiction and depression. Arodyn (Ac[Phe<sup>1,2,3</sup>,Arg<sup>4</sup>,D-Ala<sup>8</sup>]Dyn A(1-11)-NH<sub>2</sub>), an acetylated dynorphin A (Dyn A) analog, has demonstrated potent and selective KOR antagonism, but can be rapidly metabolized by proteases. Cyclization of arodyn could enhance metabolic stability and potentially stabilize the bioactive conformation to give potent and selective analogs.

Accordingly, novel cyclization strategies utilizing ring closing metathesis (RCM) were pursued. However, side reactions involving olefin isomerization of *O*-allyl groups limited the scope of the RCM reactions, and their use to explore structure-activity relationships of aromatic residues. Here we developed synthetic methodology in a model dipeptide study to facilitate RCM involving Tyr(All) residues. Optimized conditions that included microwave heating and the use of isomerization suppressants were applied to the synthesis of cyclic arodyn analogs. Initial pharmacological data indicates the constraints involving aromatic residues were generally well tolerated at KOR with most of the analogs exhibiting affinities within 3- to 4-fold that of arodyn.

RCM was also used in the synthesis of head to side chain cyclized arodyn analogs. Attempted cyclizations involving Tyr(All) residues proceeded in low yields, in contrast to cyclizations involving AllGly residues. However, ring contraction products as a result of olefin isomerization were also observed during the latter cyclizations. The resulting head to side chain cyclized arodyn analogs exhibited a 5-fold decrease in KOR affinity compared to arodyn.

We further explored synthesis of arodyn analogs cyclized in both the N-terminal and C-terminal segments resulting in bicyclic arodyn analogs. Here, we present the synthesis of two initial bicyclic peptide KOR ligands with different topologies. The RCM-based bicyclic arodyn

analog exhibited KOR affinity within 3-fold that of arodyn, whereas the lactam-based bicyclic analog displayed a substantial loss in affinity for KOR. There are currently no reports of bicyclic opioid peptide ligands and such bicyclic arodyn analogs could be useful as pharmacological tools.

## Acknowledgements

This dissertation is the product of years of work and generous support from more individuals than I could possibly list here. Even so, I wish to express my gratitude to a number of individuals for their kind support. First, I would like to thank my advisor Dr. Jane Aldrich for her mentorship, patience, and support during the course of my PhD. I was very fortunate to have Dr. Aldrich as a mentor; I have gained a wide variety of skill sets and learned a great deal in research and scientific thinking. In addition, I would like to mention my helpful and knowledgeable committee members whose valuable comments improved the quality of my dissertation. My sincere gratitude to Dr. Michael Rafferty, Dr. Blake Peterson, Dr. Teruna Siahaan, and Dr. Thomas Tolbert.

I would also like to thank current and former members of the Aldrich lab for their continuing support and cooperation over the years. I thank Dr. Dmitry Yakovlev and Dr. Tatyana Yakovleva for their helpful discussions and always being there to ensure the lab is running; I was privileged to have their kind support. I cannot forget to thank Dr. Archana Mukhopadhyay for helpful discussions and training in cell culture and biology experiments. I also thank Dr. Michael Ferracane for helpful discussions and performing molecular modeling and docking studies. I would also like to thank Dr. Sanjeewa Senadheera and Dr. Anand Joshi for their help and training at the beginning of my graduate studies. I also thank other members of the Aldrich lab including Christianna Reedy, Dr. Tanvir Khaliq, Dr. Laura Hanold, Grant Simpson, Robyn Pescatore, Jeremy Coleman, and Jan-Louis Cosme. It has been a pleasure to work with all of you.

I would also like to thank Dr. Thomas Murray and his lab members at the University of Creighton for performing pharmacological evaluation of my peptides. I was also fortunate to work with knowledgeable staff members; I thank Dr. Justin Douglas at the University of Kansas NMR

lab and Jim Rocca in the McKnight Brain Institute at the National High Magnetic Field Laboratory's AMRIS facility at the University of Florida for helpful discussions and training in NMR experiments.

Finally, I wish to thank my family: my parents John and Grace, my siblings Chris, Claudia, and Jeremy as well as my fiancée Tiffany for their unwavering commitment and overwhelming support. Words cannot express how thankful I am. Your words of encouragement have been a pillar of strength. This dissertation is dedicated to my family.

## Table of contents

Abstract.....	iii
Acknowledgements.....	v
Abbreviations.....	xii
List of figures.....	xv
List of schemes.....	xx
List of tables.....	xxi
Chapter 1 - Research overview.....	1
1.1 Background and significance .....	2
1.2 Research projects and hypotheses .....	3
1.3 References .....	3
Chapter 2 - Literature review: opioid receptors .....	8
2.1 History and background of opioids .....	9
2.2 Opioid receptors .....	10
2.2.1 Clinically used opioids .....	12
2.2.2 Opioid receptor signaling .....	14
2.2.3 Ligands used for in vitro studies of opioid receptors .....	15
2.2.4 Opioid receptor structures.....	16
2.2.5 Ligand-directed signaling .....	22
2.3 Significance of the KOR .....	24
2.3.1 KOR selective agonists .....	26

2.3.2 KOR selective antagonists .....	29
2.3.2.1 Non-peptidic KOR selective antagonists .....	29
2.3.2.2 Peptidic KOR selective antagonists .....	32
2.4 Conclusions.....	36
2.5 References.....	36
Chapter 3 - Literature review: challenges and opportunities for ring closing metathesis in peptide cyclization.....	56
3.1 Introduction .....	57
3.1.1 Solution phase and solid phase cyclization of peptides .....	60
3.2 Ring closing metathesis (RCM) of peptides .....	62
3.2.1 Polycyclic ligands and RCM .....	67
3.2.2 RCM and opioid peptides .....	72
3.2.2.1 RCM of KOR antagonists.....	75
3.3 Conclusion .....	78
3.4 References .....	78
Chapter 4 -Suppression of desallyl side products in peptide ring closing metathesis involving Tyr(All): a model dipeptide study .....	87
4.1 Introduction .....	88
4.2 Results and discussion.....	92
4.3 Conclusions .....	98



4.4 Experimental .....	99
4.5 References .....	104
Chapter 5 - Conformational constraint of aromatic residues in the “message” sequence of the kappa opioid receptor antagonist arodyn using RCM .....	
5.1 Introduction .....	110
5.2 Results and discussion .....	113
5.2.1 Pharmacophore generation and docking study .....	113
5.2.2 Chemistry .....	118
5.2.2.1 RCM by conventional heating .....	120
5.2.2.2 Microwave Assisted RCM .....	122
5.2.2.3 NMR analysis.....	126
5.2.3 Affinity.....	129
5.3 Conclusions .....	131
5.4 Experimental .....	132
5.5 References .....	140
Chapter 6 - Head to side chain cyclization of arodyn using RCM .....	
6.1 Introduction .....	145
6.2 Results and discussion .....	147
6.2.1 Head to side chain analogs using RCM involving Tyr(All) .....	147
6.2.2 Head to sidechain cyclization involving AllGly .....	148

6.3 Conclusions .....	155
6.4 Experimental .....	155
6.5 References .....	160
Chapter 7 - Synthesis of bicyclic arodyn analogs .....	162
7.1 Introduction .....	163
7.2 Synthesis of a bicyclic arodyn analog using RCM .....	166
7.2.1 Results and discussion .....	167
7.3 Synthesis of a bicyclic arodyn analog using lactam chemistry .....	172
7.3.1 Results and discussion .....	174
7.4 Conclusions .....	177
7.5 Experimental .....	178
7.6 References .....	182
Chapter 8 - Conclusions and future studies .....	184
8.1 Introduction .....	185
8.2 Conclusions and future studies.....	185
8.3 References .....	190
Appendix 1 - Chromatograms of RCM product mixtures from the model dipeptide study .....	191
Appendix 2 - Modeling of arodyn analogs cyclized by RCM between Tyr(All) residues .....	208
A2.1 Methods .....	209
A2.1.1 Conformational searches.....	209

A2.1.2 Receptor preparation .....	209
A2.1.3 Pharmacophore generation.....	210
A2.1.4 Docking.....	211
A2.2 Results and discussion.....	212
A2.2.1 Conformational Searches .....	212
A2.2.2 Receptor Preparation .....	212
A2.2.3 Pharmacophore generation and docking.....	213
A2.4 Conclusions .....	215
A2.5 References .....	217
Appendix 3 - <sup>1</sup> H NMR spectra of arodyn analogs cyclized between adjacent residues using RCM .....	219
Appendix 4 - <sup>1</sup> H NMR spectra of <i>cyclo</i> [5hex,AllGly <sup>5</sup> ]arodyn .....	228

## Abbreviations

Abbreviations used for amino acids follow the rules of the IUPAC-IUB Joint Commission of Biochemical Nomenclature in *Eur. J. Biochem.* **1984**, *138*, 9-37. Amino Acids are in the L-configuration except where indicated otherwise. Additional abbreviations used in this dissertation are as follows:

ATP : adenosine triphosphate

BBB : blood-brain barrier

Boc : *tert*-butyloxycarbonyl

c-AMP : cyclic adenosine monophosphate

CHO : Chinese hamster ovary

COSY : Correlation Spectroscopy

DAMGO : ([D-Ala<sup>2</sup>, N-MePhe<sup>4</sup>, Gly-ol]-enkephalin)

Dap : 2,3-diaminopropionic acid

DCM : dichloromethane

DIEA : *N,N*-diisopropylethylamine

DMF : *N,N*-dimethylformamide

Dmt : 2',6'-dimethyl-Tyr

DMSO : *N,N*-dimethylsulfoxide

DOR : delta ( $\delta$ ) opioid receptor

DPDPE : *cyclo*[D-Pen<sup>2</sup>,D-Pen<sup>5</sup>]enkephalin

Dyn : dynorphin

EL : extracellular loop

ERK : extracellular signal related kinases

ESI-MS : electrospray ionization mass spectroscopy

Fmoc : 9-fluorenylmethoxycarbonyl  
G II : Grubbs 2<sup>nd</sup> generation catalyst  
GDP : guanosine 5'-diphosphate  
GNTI : 5'-guanidinonaltrindole  
GPCR : G protein-coupled receptors  
GRK : G-protein coupled receptor kinase  
GTP : guanosine 5'-triphosphate  
HG II : Hoveyda-Grubbs 2<sup>nd</sup> generation catalyst  
HOAt : 1-hydroxy-7-azabenzotriazole  
HOBt : 1-hydroxy-7-benzotriazole  
i.c.v : intracerebroventricular  
JNK : c-Jun-N-terminal kinase  
KOR : kappa ( $\kappa$ ) opioid receptor  
LC-MS : liquid chromatography mass spectroscopy  
MAPK : mitogen activated protein kinase  
MOR : mu ( $\mu$ ) opioid receptor  
Mtt : 4-methyltrityl  
MVD : mouse vas deferens  
NMP : *N*-methylpyrrolidone  
NMR : nuclear magnetic resonance  
NOPR : nociceptin receptor  
NorBNI : norbinaltorphimine  
ORL : opioid like receptor  
PAL : peptide amide linker  
Pbf : 2,2,4,6,7-pentamethyldihydrobenzofuran-5-sulfonyl

PEG-PS : polyethylene glycol-polystyrene

PyBOP : 7-benzotriazol-1-yl-oxytripyrrolidinophosphonium hexafluorophosphate

RCM : ring closing metathesis

RP-HPLC : reversed phase high performance liquid chromatography

SAR : structure-activity relationships

SEM : standard error of mean

*tBu* : *tert*-butyl

TENA : triethyleneglycolnaltrexamime

TFA : trifluoroacetic acid

Tic : 1,2,3,4-tetrahydroisoquinoline 3-carboxylic acid

TIPS : triisopropylsilane

TM : transmembrane

TMA : Trimesic acid

TOF : time of flight

UPLC : ultra-performance liquid chromatography

## List of figures

	Pg. No.
Figure 1.1 Dyn A(1-11) and arodyn.....	3
Figure 1.2 “Message” and “address” domains of dynorphin A (1-11) and arodyn....	4
Figure 2.1 Structures of opioid ligands; also shown is the prototypical ligand for the sigma receptors.....	10
Figure 2.2. Opioid agonists and antagonists in clinical use discussed in text.....	14
Figure 2.3 Structure of opioid ligands discussed in text.....	16
Figure 2.4 Schematic of the protein structure of the MOR, DOR and KOR showing the percentage of identical residues within the respective segments. Transmembrane helices are indicated by rectangles .....	18
Figure 2.5 Interactions of JDTC in the human KOR ligand binding pocket.....	19
Figure 2.6 Non-nitrogenous KOR agonist salvinorin A and the metabolite salvinorin B.....	20
Figure 2.7 Schematic showing ligand-biased signaling at GPCRs.....	23
Figure 2.8 Structure of G-protein biased a) TRV-130 and b) the triazole chemotype of KOR agonist.....	24
Figure 2.9 Structures of non-peptidic KOR agonists discussed in text a) arylacetamides b) diphenylethylamines, and c) octahydroquinoline carboxamides...	27
Figure 2.10 Structures of peripherally restricted a) non-peptidic and b) peptidic KOR agonists.....	28
Figure 2.11 Structures of Dyn A-based KOR agonists with increased metabolic stability studied <i>in vivo</i> .....	29
Figure 2.12 Non-peptidic KOR antagonists.....	30
Figure 2.13 Peptidic KOR antagonists.....	33
Figure 3.1 Therapeutically relevant cyclic peptides a) ziconotide b) vancomycin, and c) cyclosporine.....	58
Figure 3.2 Cyclization motifs for peptide cyclization a) head to tail b) end (head/tail) to side chain, and c) side chain to side chain.....	58
Figure 3.3 Representative peptide cyclization chemistries showing a) lactam, b) lactone, c) disulfide, d) alkene, e) triazole, and f) ureido cyclizations.....	59
Figure 3.4 Solid phase peptide synthesis using the Fmoc strategy showing a) solution phase and b) on-resin cyclization.....	61
Figure 3.5 a) Structures of ruthenium-based Grubbs catalyst developed by altering the ligands around the metal center to tune catalyst activity and the stability of 1 <sup>st</sup> and 2 <sup>nd</sup> generation catalysts and b) a representative mechanism of RCM.....	62
Figure 3.6 a) General scheme for ring closing metathesis of a resin-bound peptide following incorporation of allylglycine residues b) a representative example of alkene precursors on a peptidic substrate, and c) structure of a hydrogen bond surrogate.....	63
Figure 3.7 Proposed mechanism of formation of ring contraction products following olefin isomerization during RCM.....	65

Figure 3.8 Representative polycyclic peptides: a) schematic structure showing a stitched peptide with contiguous alkene bridging, b) bicyclic HDAC inhibitor, c) romidepsin, d) a Pin 1 inhibitor fused with a cell penetrating peptide, and e) a bicyclic oxytocin analog. Pip = pipercolic acid, Nal = naphthylalanine.....	69
Figure 3.9 Structure of polycyclic peptides synthesized through RCM a) lantacin 3147 A2 synthesized by sequential RCM and b) the carbon-bridged nicin DE ring mimic synthesized in one-step. Dhb= didehydroaminobutyric acid.....	70
Figure 3.10 A representative schematic of the regioselective synthesis of the $\alpha$ -conotoxin Rg1A analog where prenyl glycine residues were used to prevent unwanted cyclization during RCM.....	71
Figure 3.11 One-pot bicyclization of the GTPase Rab8 inhibitor using GI and the molybdenum based RCAM catalyst.....	72
Figure 3.12 Representative examples of opioid peptides cyclized by RCM A) cyclic enkephalin analogs, and b) cyclic dynorphin A analogs.....	73
Figure 3.13 “Message” and “address” regions of opioid peptides illustrated in dynorphin A (1-11). ....	73
Figure 3.14 Schematic representation showing RCM of dynorphin A analogs.....	74
Figure 3.15 Structures of cyclic kappa opioid receptor antagonists.....	76
Figure.3.16 Structure of arodyn.....	76
Figure 3.17 Structure of the cyclic N-methylated arodyn analog. N-Methylation facilitated head to side chain cyclization. ....	76
Figure 3.18 Representative structures of a cyclic arodyn analog, <i>cyclo</i> <sup>2,3</sup> [Tyr <sup>2</sup> (CH <sub>2</sub> -CH=CH-CH <sub>2</sub> )Tyr <sup>3</sup> ,Ile <sup>8</sup> ]arodyn, and the des-allyl products from a side reaction during RCM.....	77
Figure 4.1 Structure of arodyn and Dyn A(1-11), a fragment of the endogenous KOR ligand, Dyn A.....	90
Figure 4.2 Reaction mixture resulting from RCM of [Tyr(All) <sup>2,3</sup> ,Ile <sup>8</sup> ]arodyn .....	90
Figure 4.3 a) Model dipeptide RCM reaction and b) potential desallyl side products	92
Figure 4.4 Chromatograms of the RCM product mixture following RCM at a) 60 °C and b) 40 °C.....	94
Figure 4.5 Chromatograms of the RCM product mixture following RCM (G II 15 mol% in DCM at 40 °C for 2 d) in the presence or absence of the additives 1,4-benzoquinone and phenol (1 equiv each). SM:starting material. Structures of <b>1-4</b> are shown in Figure 4.3.....	96
Figure 4.6 Structures of Grubbs 2 <sup>nd</sup> generation (G II) and Hoveyda-Grubbs 2 <sup>nd</sup> generation (HG II) catalysts .....	96
Figure 4.7 Structure of model tripeptide Fmoc-Tyr(All)-Phe-Tyr(All).....	98
Figure 5.1 Structures of arodyn analogs and possible constraint of aromatic residues.....	112
Figure 5.2 Arodyn analogs cyclized at adjacent tyrosine residues.....	112
Figure 5.3 Docked structure of arodyn (thick green sticks) docked in the KOR model. In this pose, Phe <sup>1</sup> and Phe <sup>3</sup> of arodyn occupy the two aromatic pharmacophoric sites (orange spheres); the guanidinium of Arg <sup>4</sup> lies in one of the basic sites of the pharmacophore (cyan sphere), forming an ionic contact (yellow lines) with Glu297. JDTic (thick gray sticks) and the important nonconserved acidic residues Glu209 and	115



Glu297 – as well as the conserved residues within 5.0 Å of Phe <sup>1</sup> , Phe <sup>2</sup> , and Phe <sup>3</sup> of arodyn – of the minimized receptor are also shown (thin green sticks).....	
Figure 5.4 Structure of the a) p <sup>1</sup> p <sup>2</sup> (magenta sticks) b) m <sup>1</sup> m <sup>2</sup> (purple sticks) c) p <sup>2</sup> p <sup>3</sup> (orange sticks) and d) m <sup>2</sup> m <sup>3</sup> (brown sticks) cyclic arodyn analogs when docked inside the KOR model (not shown). In these poses, Phe <sup>1</sup> and Phe <sup>3</sup> of the analogs occupy the two pharmacophoric aromatic sites (orange spheres) while the guanidinium of Arg <sup>4</sup> lies in one of the basic sites of pharmacophore (cyan sphere); Glu209 and Glu297 of the minimized receptor are also shown. The guanidinium of Arg <sup>4</sup> forms an ionic contact (yellow lines) with the nearby Glu297 in all analogs except a) the p <sup>1</sup> p <sup>2</sup> analog. In b) and d) the guanidinium of Arg <sup>4</sup> also forms an intramolecular ion-dipole interaction with the carbonyl of <i>m</i> -Tyr <sup>2</sup> (yellow lines).....	116
Figure 5.5 Overlay of arodyn and its analogs following docking in the KOR model (not shown). Arodyn (green) and its p <sup>1</sup> p <sup>2</sup> (magenta), m <sup>1</sup> m <sup>2</sup> (purple), p <sup>2</sup> p <sup>3</sup> (orange), and m <sup>2</sup> m <sup>3</sup> (brown) analogs have similar conformations. The acetyl group and backbone of residues 1-3 generally have a similar backbone across the analogs. The side chains of residues 1 and 3 ( $\chi_1$ , $\chi_2$ ) are generally similar, while the conformation of the side chain of residue 2 varies substantially. The conformation of Arg <sup>4</sup> also varies among the different species; only the p <sup>1</sup> p <sup>2</sup> analog does not appear to form an ionic contact with the side chain of Glu297.....	117
Figure 5.6 Arodyn analogs cyclized via conventional heating showing the corresponding yields.....	121
Figure 5.7 a) <sup>1</sup> H NMR of <b>2</b> showing olefin protons and the spectrum following homonuclear decoupling; b) COSY of <b>2</b> .....	127
Figure 6.1 Representative chromatograms showing the RCM of <b>15</b> at various temperatures under microwave heating.....	150
Figure 6.2 Structures of major products following microwave assisted RCM of <b>15</b> at 150 °C. 3 but= 3 butenoic acid.....	150
Figure 6.3 Representative chromatograms showing the RCM <b>16</b> at various temperatures under microwave heating. ....	152
Figure 6.4 Structures of major products following microwave assisted RCM of <b>16</b> at 150 °C. ....	152
Figure 7.1 Structure of bicyclic arodyn analog <i>cyclo</i> [Tyr(All) <sup>2,3</sup> ,AllGly <sup>5,8</sup> ]arodyn ( <b>13</b> ).....	167
Figure 7.2 Synthesis of <i>cyclo</i> [Fmoc-AllGly <sup>5,8</sup> ]arodyn <sup>4-11</sup> ( <b>15</b> ). ....	168
Figure 7.3 Representative chromatograms showing RCM of <b>14</b> at various temperatures under microwave heating.....	168
Figure 7.4 Chromatograms of the synthesis of the <b>13</b> showing major components of the reaction mixtures a) before and b) after RCM involving Tyr(All) residues.....	171
Figure 7.5 Chromatograms and structures of the lactam-based bicyclic arodyn analog and the corresponding linear precursors.....	176
Figure 8.1 Conformational constraint of aromatic residues in arodyn.....	186
Figure 8.2 Products resulting from RCM of [Tyr(All) <sup>2,3</sup> ]arodyn including desallyl products.....	186

Figure 8.3 Olefin isomerization resulting in deallylation during acid catalyzed cleavage from the solid-phase resin.....	186
Figure 8.4 Overlay of arodyn and several analogs following docking in the KOR (not shown). Arodyn (green) and its p <sup>1</sup> p <sup>2</sup> (magenta), m <sup>1</sup> m <sup>2</sup> (purple), p <sup>2</sup> p <sup>3</sup> (orange), and m <sup>2</sup> m <sup>3</sup> (brown) analogs have the same general structure (in referring to arodyn analogs e.g. p <sup>1</sup> p <sup>2</sup> , letters indicate substitution patterns while the superscript indicates residue position in arodyn).....	187
Figure 8.5 Head to side chain arodyn analogs involving AllGly residues showing a ring contraction product. 4pent=4pentenoic acid and 5hex=5hexenoic acid.....	188
Figure A1.1 Reaction mixture resulting from RCM of <b>1</b> showing the RCM product <b>2</b> and desallyl products <b>3</b> , <b>4</b> , and <b>5</b> .....	193
Figure A1.2 Structures of the linear tripeptide <b>6</b> and the cyclic tripeptide <b>7</b> .....	193
Figure A1.3 Reaction mixture resulting from RCM of <b>8</b> showing the RCM product <b>9</b> and desallyl products <b>10</b> , <b>11</b> , and <b>12</b> .....	194
Figure A2.1 Structure of KOR model and pharmacophore for docking. <i>Left</i> : KOR model (gray loops) highlighting the acidic residues Glu209 and Glu297 (gray sticks), the crystallized ligand JD <sub>T</sub> ic (gray sticks), and defined pharmacophore elements (colored spheres). <i>Right</i> : The KOR model was overlaid with crystal structures of the μ and δ opioid receptor (not shown). The pharmacophore consists of one aromatic element (orange sphere) in the same site and plane as the phenol of JD <sub>T</sub> ic (gray sticks), a second aromatic site (orange sphere) between the phenyl rings of BU72 (yellow sticks) and DIPP-NH <sub>2</sub> (magenta sticks), and two basic sites (cyan spheres) adjacent to Glu209 and Glu297.....	211
Figure A2.2 Overlay of arodyn (green) docked in the κ opioid receptor model (green) and the crystal structure of naltrindole (purple) in the δ opioid receptor (not shown). The guanidium of Arg <sup>4</sup> is positioned within 2.5 Å of the 5' position of naltrindole, where the guanidinium group of the κ-selective antagonist 5'-guanidinonaltrindole (5'-GNTI) would lie. This moiety was previously found to bind Glu297 of the κ opioid receptor, a finding that – by extension – supports the results from the docking study.....	216
Figure A2.3 Overlay of arodyn (green) docked in the κ opioid receptor model (green) and the crystal structure of DIPP-NH <sub>2</sub> (magenta) in the δ opioid receptor (not shown). The two peptidic ligands have different sequences, yet they can arrange the aromatic rings of residues 1 and 3 similarly in the pharmacophore (orange spheres). Interestingly, the backbones of the two peptides are strikingly similar from Ca2 to N4, suggesting that peptidic ligands may bind in similar conformations. Phe4 and Arg4 of both peptides do not overlay well, although Phe <sup>4</sup> of DIPP-NH <sub>2</sub> was found to occupy different conformations even in the crystal structure.....	217
Figure A3.1 <sup>1</sup> H-spectra of <b>2</b> . The spectrum of olefinic protons following decoupling of adjacent methylene protons at 4.64 is shown at the bottom as well a COSY showing olefinic and O-methylene protons .....	220
Figure A3.2 <sup>1</sup> H-spectra of <b>3</b> .....	221
Figure A3.3 <sup>1</sup> H-spectra of <b>4</b> .....	222
Figure A3.4 <sup>1</sup> H-spectra of <b>5</b> .....	223
Figure A3.5 <sup>1</sup> H-spectra of <b>6</b> . The spectrum of olefinic protons following decoupling of adjacent methylene protons at 4.68 is shown at the bottom.....	224

Figure A3.6 $^1\text{H}$ -spectra of <b>7</b> .....	225
Figure A3.7 $^1\text{H}$ -spectra of <b>8</b> .....	226
Figure A3.8 $^1\text{H}$ -spectra of <b>9</b> .....	227
Figure A4.1 $^1\text{H}$ -spectra of <b>14 cis</b> .....	229
Figure A4.2 $^1\text{H}$ -spectra of <b>14 trans</b> .....	230

## List of schemes

	Pg. No.
Scheme 4.1 Synthesis of Fmoc-Tyr(All)-Tyr(All)-OH.....	102
Scheme 5.1 Synthesis of the p <sup>2</sup> p <sup>3</sup> analog <b>2</b> with RCM conventional heating using optimized conditions from the model dipeptide study.....	120
Scheme 6.1 Synthesis of [5hex,AllGly <sup>5</sup> ]arodyn ( <b>16</b> ) and <i>cyclo</i> <sup>N,5</sup> [5hex,AllGly <sup>5</sup> ]arodyn ( <b>14</b> ).....	158
Scheme 7.1 Synthesis of <i>cyclo</i> [Tyr(All) <sup>2,3</sup> ,AllGly <sup>5,8</sup> ]arodyn ( <b>13</b> ) using sequential RCM. PyBOP = benzotriazol-1-yl-oxy-tris-pyrrolidino-phosphonium hexafluorophosphate, HOBt = 1-hydroxybenzotriazole, Boc = <i>tert</i> -butoxycarbonyl and Pbf = 2,2,4,6,7-pentamethyldihydrobenzofuran-5-sulfonyl.....	167
Scheme 7.2 Synthesis of <b>13</b> using sequential RCM showing structures of major products in the reaction mixture.....	170
Scheme 7.3 Synthesis of <i>cyclo</i> <sup>N,5,8</sup> [TMA,Dap <sup>5,8</sup> ]arodyn ( <b>29</b> ).....	175

## List of tables

	Pg. No
Table 2.1 Endogenous opioid receptor and related peptides.....	11
Table 3.1 Selected RCM conditions for synthesis of cyclic peptides and corresponding reaction conditions illustrating various reaction optimization and synthetic challenges.....	66
Table 3.2 Binding affinities of Dyn A analogs cyclized by RCM.....	75
Table 4.1 Product profiles for RCM using Grubbs catalyst (G II) .....	93
Table 4.2 Effect of temperature and catalyst concentration on model dipeptide RCM product yields.....	93
Table 4.3 Effect of phenol, temperature, and catalyst concentration on model dipeptide RCM product yields. ....	95
Table 4.4 Model dipeptide RCM product yields under HG II at 40 and 60 °C.....	97
Table 4.5 Tripeptide RCM product yields using optimized conditions with G II and HG II.....	98
Table 4.6 Analytical data of synthesized linear and cyclic peptides.....	101
Table 5.1 Structures of arodyn analogs containing Tyr(All) cyclized by RCM under conventional heating and their linear precursors. In some cases a mixture of <i>cis/trans</i> analogs were obtained (indicated by a wavy bond).....	119
Table 5.2 Results for RCM of <b>10</b> using various reaction conditions.....	120
Table 5.3. Analytical data of purified cyclic peptides <b>2-6</b> and their linear analogs...	122
Table 5.4 Comparison of RCM product yields following cyclization of dipeptide, tripeptide, and arodyn analogs under conventional heating using G II and microwave irradiation using HG II.....	123
Table 5.5 Structures of arodyn analogs containing <i>m</i> -Tyr(All) in positions 1 and 2 cyclized by RCM under .....	125
Table 5.6 HPLC and MS data of purified arodyn analogs <b>7-9</b> and their linear analogs <b>18-20</b> .....	126
Table 5.7 <sup>1</sup> H NMR data of cyclic arodyn analogs <b>2-9</b> . ....	128
Table 5.8 Opioid receptor binding affinities of arodyn analogs cyclized by RCM and their linear counterparts.....	130
Table 5.9 Opioid receptor binding affinities of <i>cyclo</i> [Tyr(All) <sup>x,y</sup> ,Ile <sup>8</sup> ] analogs cyclized by RCM.....	131
Table 5.10 Analytical data of linear peptides synthesized on 2-Chlorotrityl resin and their cyclic analogs.....	136
Table 6.1 Head to side chain arodyn analogs explored using RCM. Only <b>4</b> was obtained.....	146
Table 6.2 Attempted cyclization of head to side chain analogs of arodyn involving Tyr(All).....	148
Table 6.3 Attempted cyclizations of head to side analogs of arodyn involving AllGly and their linear precursors. ....	149
Table 6.4 Cyclization yields following RCM of <b>15</b> under various microwave heating conditions.....	151

Table 6.5 Analytical data of the major products following microwave assisted RCM of <b>15</b> at 150 °C. LC-MS analysis facilitated identification of the ring contraction product <b>17</b> .....	151
Table 6.6 Analytical data of major products following microwave assisted RCM of <b>16</b> at 150 °C.....	153
Table 6.7 <sup>1</sup> H NMR data of cyclic arodyn analogs <b>14 cis</b> and <b>14 trans</b> .....	154
Table 6.8 Analytical data of purified <b>14</b> and its linear precursor <b>16</b> .....	154
Table 6.9 Preliminary KOR binding affinities of <i>cyclo</i> <sup>N,5</sup> [5hex,AllGly <sup>5</sup> ]arodyn and the linear precursor.....	155
Table 7.1. Binding affinities of monocyclic RCM arodyn analogs.....	165
Table 7.2. Preliminary results for activity of cyclic arodyn analogs in the GTPγS assay.....	166
Table 7.3 Analytical data for <b>14</b> and <b>15</b> .....	169
Table 7.4 Synthesis of <b>15</b> under various microwave heating conditions.....	169
Table 7.5 Binding affinities of monocyclic lactam arodyn analogs.....	171
Table 7.6 Initial evaluation of receptor affinity of bicyclic arodyn analog <b>13</b> and related arodyn analogs.....	172
Table 7.7 Binding affinities of monocyclic lactam arodyn analogs.....	174
Table 7.8 Analytical data of <b>27</b> , <b>28</b> , and <b>29</b> .....	175
Table 7.9 Analytical data of bicyclic arodyn analogs.....	181
Table A1.1 Analytical data of synthesized linear and cyclic peptides.....	193
Table A1.2 Product profiles for RCM using initial conditions, 2 <sup>nd</sup> generation Grubbs catalyst (G II).....	194
Table A1.3 Effect of temperature and catalyst concentration on model dipeptide RCM product yields.....	196
Table A1.4 Effect of additives, temperature, and catalyst concentration on model dipeptide RCM product yields.....	199
Table A1.5 Model dipeptide RCM product yields with Hoveyda-Grubbs 2 <sup>nd</sup> generation catalyst (HG II) .....	201
Table A1.6 Tripeptide RCM product yields with optimized conditions with G II and HG II.....	203
Table A1.7 Summary showing yields <sup>a</sup> of model dipeptide ( <b>1</b> ) RCM under various conditions using Grubbs 2 <sup>nd</sup> generation catalyst (G II).....	206
Table A2.1a Energy scores of arodyn analogs cyclized between adjacent residues and conformational data of the first residue from modeling studies.....	214
Table A2.1b Conformational data of the second residue in arodyn analogs cyclized between adjacent residues.....	214
Table A2.1c Conformational data of the third residue in arodyn analogs cyclized between adjacent residues.....	214
Table A2.1d Conformational data of the fourth residue in arodyn analogs cyclized between adjacent residues.....	215

## **Chapter 1 - Research overview**

## 1.1 Background and significance

Over the last century, there has been increasing interest in opioid receptors to understand their physiological and pharmacological effects. The three classical opioid receptors mu (MOR), kappa (KOR), and delta (DOR), were cloned in the 1990's in addition to a fourth structurally related but pharmacologically distinct receptor, the nociceptin (NOPR) receptor.<sup>1</sup> Opioid receptors regulate multiple physiological processes and are important in analgesia, addiction, depression, inflammation, immunity, and the cardiovascular system.<sup>2</sup> MOR selective agonists such as morphine are clinically used analgesics, but have deleterious side effects such as addiction, tolerance, respiratory depression, and constipation.<sup>3</sup> KOR selective agonists are analgesics devoid of MOR associated side effects, but also induce dysphoria and sedation. Recently, KOR selective antagonists have received increasing attention for their potential therapeutic utility in drug addiction, stress-related conditions, and mood disorders.<sup>4,5</sup> Prototypical small molecule selective KOR antagonists such as norBNI and JDTic, however, show prolonged duration of action *in vivo* which has slowed their development and limits their use as pharmacological tools.<sup>6-9</sup>

The majority of peptidic ligands at KOR are derivatives of the endogenous KOR ligand dynorphin A (Dyn A, Figure 1.1). In contrast to small molecule antagonists, peptide antagonists offer a promising profile for potential further development due to their finite duration of action *in vivo*.<sup>10</sup> Arodyn (Ac[Phe<sup>1,2,3</sup>,Arg<sup>4</sup>,D-Ala<sup>8</sup>]Dyn A(1-11)-NH<sub>2</sub>, Figure 1.1), an acetylated Dyn A analog, displays potent and selective KOR antagonism.<sup>11</sup> Further, arodyn prevented stress-induced reinstatement of cocaine seeking behavior in a conditioned place preference assay in mice.<sup>12</sup>



Tyr-Gly-Gly-Phe-Leu-Arg-Arg-Ile-Arg-Pro-Lys

Dyn A(1-11)

Ac-Phe-Phe-Phe-Arg-Leu-Arg-Arg-D-Ala-Arg-Pro-Lys-NH<sub>2</sub>

Arodyn

Figure 1.1 Dyn A(1-11) and arodyn.

In recent years there has been increasing interest in the development of peptides for therapeutic applications;<sup>13</sup> cyclic peptides are particularly promising as they can have enhanced receptor affinity, target selectivity, and metabolic stability.<sup>14-16</sup> Our research has significance in two areas, the exploration of new approaches to peptide cyclization and the potential to identify new and novel potent KOR antagonists as leads for the potential development of treatments for drug addiction. Drug addiction predisposes individuals to various medical complications, violence, and risky behaviors.<sup>17</sup> Effective treatments are needed to alleviate the impact of drug addiction on individuals and society.<sup>18</sup>

This thesis focuses on novel cyclization strategies via ring closing metathesis (RCM) involving aromatic residues to synthesize cyclic derivatives of arodyn. Notably, there are limited reports of cyclizations involving aromatic residues in opioid peptides.<sup>19,20</sup> In contrast to cyclization approaches such as lactam or disulfide bridges that generally involve non-critical residues, RCM allows the cyclization via aromatic residues that contribute to KOR affinity in arodyn. Cyclization can potentially stabilize the bioactive conformation and enhance the proteolytic stability of arodyn. Cyclic arodyn analogs offer complementary tools to small molecule ligands to study KOR pharmacology.

## **1.2 Research projects and hypotheses**

The primary goal of this dissertation is the synthesis of conformationally constrained analogs of the KOR antagonist arodyn to evaluate the effects on KOR affinity, selectivity, efficacy,

and potency. To this effect, the synthesis of arodyn analogs cyclized in the “message” and “address” domains was explored. According to the “message” and “address” concept proposed by Chavkin and Goldstein, the “message” sequence contained in all mammalian opioid peptides is responsible for activating the receptor, while the “address” sequence that is unique to Dyn A (Figure 1.2) imparts affinity for KOR.<sup>21</sup> As in Dyn A, aromatic residues in the “message” sequence of arodyn (Figure 1.2) contribute to its affinity for KOR.<sup>22</sup>

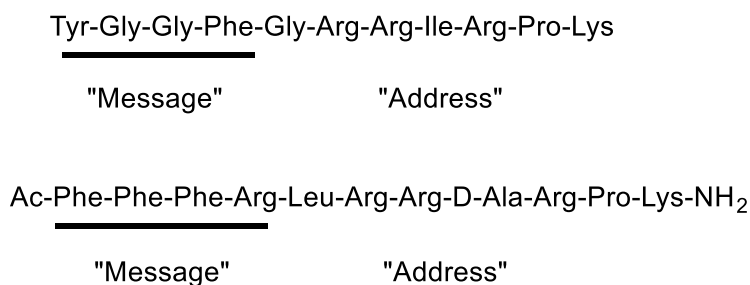


Figure 1.2 “Message” and “address” domains of dynorphin A (1-11) and arodyn.

In chapter 4 we developed synthetic methodology using RCM to optimize the yield of arodyn analogs containing conformationally constrained aromatic residues for pharmacological evaluation. RCM is compatible with peptide synthesis and standard amino acid protecting groups, but side reactions such as olefin isomerization can compromise the product yield.<sup>23</sup> While RCM involving allylglycine (AllGly) residues showed moderate to high yields,<sup>24</sup> reactions involving O-allyl groups in Tyr(All) resulted in desallyl products that compromised reaction yields.<sup>20, 25</sup> A model dipeptide, Fmoc-Tyr(All)-Tyr(All), was used to probe strategies to minimize side reactions and enhance reaction yields. Different reaction parameters, including the examination of reagents reported to suppress side reactions,<sup>23, 26</sup> were examined.

In chapter 5 optimized reaction conditions from the model dipeptide study were applied to the synthesis of conformationally constrained arodyn analogs. Optimized model dipeptide conditions using conventional heating facilitated RCM of arodyn analogs containing Tyr(All) for

pharmacological evaluation, but sequence dependent effects decreased the yields of some analogs. Further optimization using microwave heating was explored to enhance RCM of arodyn analogs containing Tyr(All).

In chapters 6 and 7, additional arodyn analogs cyclized from head to side chain and from side chain to side chain were explored. In chapter 6 microwave assisted RCM using AllGly or Tyr(All) with N-terminal alkenyl amides was explored to synthesize monocyclic arodyn analogs for pharmacological evaluation. In chapter 7, RCM and lactam chemistries were explored to synthesize two different bicyclic arodyn analogs. Notably, there are currently no reported polycyclic opioid peptide ligands.<sup>27</sup> The RCM synthetic methodology developed for cyclization of arodyn was explored to synthesize an initial bicyclic KOR ligand cyclized in both the “message” and “address” domains. A rigid aromatic linker, benzene-1,3,5-tricarboxylic acid (trimesic acid), was used to synthesize a lactam-based bicyclic KOR ligand.

### 1.3 References

1. Snyder, S. H.; Pasternak, G. W. Historical review: Opioid receptors. *Trends Pharmacol. Sci.* **2003**, 24, 198-205.
2. Liang, X.; Liu, R.; Chen, C.; Ji, F.; Li, T. Opioid System Modulates the Immune Function: A Review. *Transl Perioper Pain Med* **2016**, 1, 5-13.
3. Aldrich, J. V.; Vigil-Cruz, S. C.; Abraham, D. J. Narcotic Analgesics. In *Burger's Medicinal Chemistry and Drug Discovery*, John Wiley & Sons, Inc.: 2003.
4. Carroll, F. I.; Carlezon, W. A., Jr. Development of kappa opioid receptor antagonists. *J Med Chem* **2013**, 56, 2178-2195.
5. Li, W.; Sun, H.; Chen, H.; Yang, X.; Xiao, L.; Liu, R.; Shao, L.; Qiu, Z. Major Depressive Disorder and Kappa Opioid Receptor Antagonists. *Transl Perioper Pain Med* **2016**, 1, 4-16.
6. Munro, T. A.; Berry, L. M.; Van't Veer, A.; Béguin, C.; Carroll, F. I.; Zhao, Z.; Carlezon, W. A.; Cohen, B. M. Long-acting  $\kappa$  opioid antagonists nor-BNI, GNTI and JDTC: pharmacokinetics in mice and lipophilicity. *BMC Pharmacol* **2012**, 12, 5.

7. Bruchas, M. R.; Yang, T.; Schreiber, S.; DeFino, M.; Kwan, S. C.; Li, S.; Chavkin, C. Long-acting  $\kappa$  Opioid Antagonists Disrupt Receptor Signaling and Produce Noncompetitive Effects by Activating c-Jun N-terminal Kinase. *J Biol Chem* **2007**, 282, 29803-29811.
8. Melief, E. J.; Miyatake, M.; Carroll, F. I.; Beguin, C.; Carlezon, W. A., Jr.; Cohen, B. M.; Grimwood, S.; Mitch, C. H.; Rorick-Kehn, L.; Chavkin, C. Duration of action of a broad range of selective kappa-opioid receptor antagonists is positively correlated with c-Jun N-terminal kinase-1 activation. *Mol Pharmacol* **2011**, 80, 920-929.
9. Horan, P.; Taylor, J.; Yamamura, H. I.; Porreca, F. Extremely long-lasting antagonistic actions of nor-binaltorphimine (nor-BNI) in the mouse tail-flick test. *J Pharmacol Exp Ther* **1992**, 260, 1237-1243.
10. Aldrich, J. V.; Patkar, K. A.; McLaughlin, J. P. Zyklophin, a systemically active selective kappa opioid receptor peptide antagonist with short duration of action. *Proc Natl Acad Sci* **2009**, 106, 18396-18401.
11. Bennett, M. A.; Murray, T. F.; Aldrich, J. V. Identification of Arodyn, a Novel Acetylated Dynorphin A-(1-11) Analogue, as a  $\kappa$  Opioid Receptor Antagonist. *J Med Chem* **2002**, 45, 5617-5619.
12. Carey, A. N.; Borozny, K.; Aldrich, J. V.; McLaughlin, J. P. Reinstatement of Cocaine Place-Conditioning Prevented by the Peptide kappa-Opioid Receptor Antagonist Arodyn. *Eur J Pharmacol* **2007**, 569, 84-89.
13. Henninot, A.; Collins, J. C.; Nuss, J. M. The Current State of Peptide Drug Discovery: Back to the Future? *J Med Chem* **2017**, 1382-1414.
14. Ong, Y. S.; Gao, L.; Kalesh, K. A.; Yu, Z.; Wang, J.; Liu, C.; Li, Y.; Sun, H.; Lee, S. S. Recent Advances in synthesis and identification of cyclic peptides for bioapplications. *Curr Top Med Chem* **2017**, 17, 2302-2318.
15. Nielsen, D. S.; Shepherd, N. E.; Xu, W.; Lucke, A. J.; Stoermer, M. J.; Fairlie, D. P. Orally Absorbed Cyclic Peptides. *Chem Rev* **2017**, 117, 8094-8128.
16. Zorzi, A.; Deyle, K.; Heinis, C. Cyclic peptide therapeutics: past, present and future. *Curr Opin Chem Biol* **2017**, 38, 24-29.
17. Shorter, D.; Kosten, T. R. Novel pharmacotherapeutic treatments for cocaine addiction. *BMC Medicine* **2011**, 9, 119.

18. Czoty, P. W.; Stoops, W. W.; Rush, C. R. Evaluation of the “Pipeline” for Development of Medications for Cocaine Use Disorder: A Review of Translational Preclinical, Human Laboratory, and Clinical Trial Research. *Pharmacol Rev* **2016**, *68*, 533-562.
19. Siemion, I. Z.; Szewczuk, Z.; Herman, Z. S.; Stachura, Z. To the problem of biologically active conformation of enkephalin. *Molecular and Cellular Biochemistry* **1981**, *34*, 23-29.
20. Fang, W.-J.; Murray, T. F.; Aldrich, J. V. Design, synthesis, and opioid activity of arodyn analogs cyclized by ring-closing metathesis involving Tyr(allyl). *Bioorg Med Chem* **2018**, *26*, 1157-1161.
21. Chavkin, C.; Goldstein, A. Specific receptor for the opioid peptide dynorphin: structure--activity relationships. *Proc Natl Acad Sci U.S.A.* **1981**, *78*, 6543-6547.
22. Bennett, M. A.; Murray, T. F.; Aldrich, J. V. Structure–activity relationships of arodyn, a novel acetylated kappa opioid receptor antagonist. *J Pept Sci* **2005**, *65*, 322-332.
23. Hong, S. H.; Sanders, D. P.; Lee, C. W.; Grubbs, R. H. Prevention of Undesirable Isomerization during Olefin Metathesis. *J Am Chem Soc* **2005**, *127*, 17160-17161.
24. Fang, W.-J.; Cui, Y.; Murray, T. F.; Aldrich, J. V. Design, Synthesis, and Pharmacological Activities of Dynorphin A Analogues Cyclized by Ring-Closing Metathesis. *J Med Chem* **2009**, *52*, 5619-5625.
25. Fang, W. Design and Synthesis of Novel Linear and Cyclic Peptide Ligands for Kappa Opioid Receptors. University of Kansas, 2008.
26. Schmidt, B.; Hauke, S. Cross metathesis of allyl alcohols: how to suppress and how to promote double bond isomerization. *Org Biomol Chem* **2013**, *11*, 4194-4206.
27. Remesic, M.; Lee, Y. S.; Victor, H. J. Cyclic Opioid Peptides. *Curr Med Chem* **2016**, *23*, 1288-1303.

## **Chapter 2 - Literature review: opioid receptors**

## 2.1 History and background of opioids

Opioid analgesics such as morphine (Figure 2.1a) act at opioid receptors and are particularly useful in the treatment of severe pain, despite their deleterious side effect profile including abuse liability and respiratory depression.<sup>1, 2</sup> The therapeutic use of morphine is of particular historical importance. Not long before the isolation of morphine from opium by Sertuner in the 1800's,<sup>3</sup> opium had been the subject of great unrest in the opium war between the British and the Chinese.<sup>4, 5</sup> Despite prevailing opium use, it was not until the 1800's that the use of morphine entered the clinic, spurred by the invention of the hypodermic needle.<sup>5</sup> The use of morphine for pain relief was, however, accompanied by considerable safety and addiction concerns. Ironically, towards the end of the 19<sup>th</sup> century, heroin (diacetyl morphine) was synthesized in the quest to find a safe and non-addicting opioid, but to no avail.<sup>4, 5</sup>

The advent of opiates and opioids with different pharmacological effects came to the forefront in the late 1930's and 1940's. Methadone (Figure 2.1b), a synthetic opioid structurally distinct from morphine, was developed as a replacement for morphine.<sup>6</sup> Similarly, nalorphine (*N*-allylnormorphine, Figure 2.1b) was developed to counter respiratory depression and abuse, both deleterious side effects of morphine.<sup>5</sup> Despite the analgesic activity of nalorphine, accompanying side effects such as dysphoria were a considerable concern leading to the development of compounds such as naloxone (Figure 2.1b), a related compound which was identified but exhibited opioid antagonist activity.<sup>5</sup>

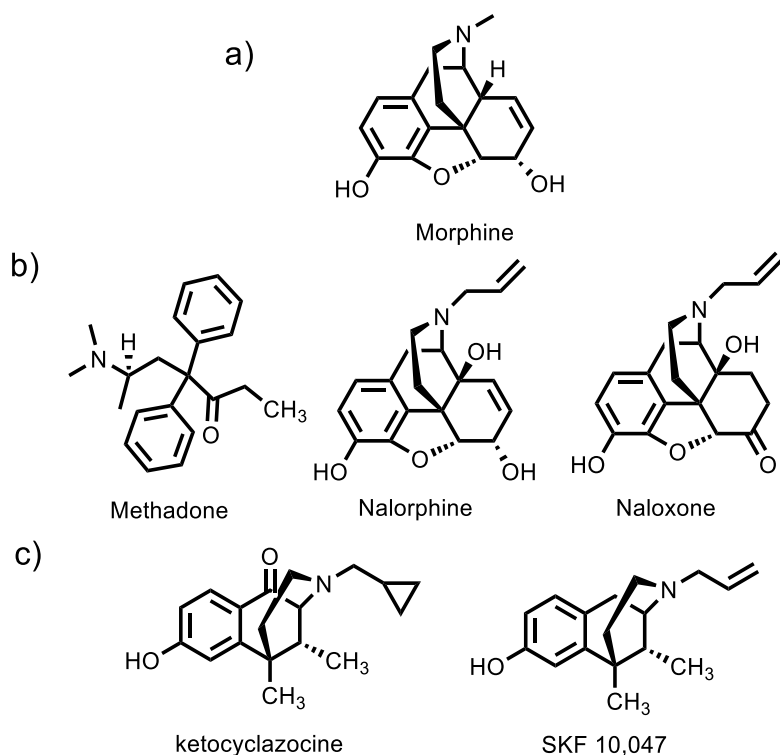


Figure 2.1 Structures of opioid ligands; also shown is the prototypical ligand for the sigma receptors.

## 2.2 Opioid receptors

In 1954, Beckett and Casy proposed the involvement of opioid receptors in mediating opioid effects.<sup>7</sup> As of the 1960's it was becoming increasingly apparent that the aforementioned pharmacological profiles could only be rationalized by the effects of the ligands on multiple opioid receptors, as proposed by thought leaders such as Portoghese<sup>8</sup> and Martin.<sup>9</sup> Following the discovery of opioid binding sites in the mammalian brain,<sup>10</sup> pharmacological studies pointed to multiple opioid receptors.<sup>11-13</sup> However, it was not until the 1970's that Martin and co-workers classified multiple opioid receptors.<sup>14</sup> The receptors were named after the opioid ligands used in the study;  $\mu$  (morphine),  $\kappa$  (ketocyclazocine) and  $\sigma$  (SKF 10,047, *N*-allylnorcyclazocine, Figure 2.1c). The  $\sigma$  receptor, proposed as an opioid receptor by Martin *et al*,<sup>14</sup> was later shown to differ in its pharmacological profile from the  $\mu$  (mu, MOR),  $\kappa$  (kappa, KOR), and  $\delta$  opioid receptor (delta, DOR).<sup>15, 16</sup>



The discovery of endogenous ligands for the opioid receptors in the 1970's marked a major advancement in opioid research. First, the discovery of the enkephalins,<sup>17</sup> endogenous ligands for a distinct receptor, concomitantly led to the proposal of the DOR.<sup>18</sup> The pentapeptides Tyr-Gly-Gly-Phe-Met (Met-enkephalin) and Tyr-Gly-Gly-Phe-Leu (Leu-enkephalin) were identified in brain extracts, and their effects on the guinea pig ileum could be reversed by naloxone.<sup>17, 19, 20</sup> Shortly thereafter,  $\beta$ -endorphin<sup>21</sup> and dynorphin ( $\kappa$ ),<sup>22</sup> both bearing structural similarities to the enkephalins, were identified (see Table 2.1 for structures of endogenous opioid peptides). New endogenous ligands for MOR were later discovered in the 1990's by Zadina and co-workers who isolated and synthesized these endogenous agonists, endomorphin- 1 and -2 (Table 2.1).<sup>23</sup>

Table 2.1 Endogenous opioid receptor and related peptides.

Endogenous peptides	Sequence
<b>Proenkephalin<sup>a</sup></b>	
Leu-enkephalin	Tyr-Gly-Gly-Phe-Leu
Met-enkephalin	Tyr-Gly-Gly-Phe-Met
Met-enkephalin-Arg <sup>6</sup> -Phe <sup>7</sup>	Tyr-Gly-Gly-Phe-Met-Arg-Phe
Met-enkephalin-Arg <sup>6</sup> -Gly <sup>7</sup> -Leu <sup>8</sup>	Tyr-Gly-Gly-Phe-Met-Arg-Gly-Leu
<b>Prodynorphin<sup>a</sup></b>	
Dynorphin A	Tyr-Gly-Gly-Phe-Leu-Arg-Arg-Ile-Arg-Pro-Lys-Leu-Lys-Trp-Asp-Asn-Gln
Dynorphin B	Tyr-Gly-Gly-Phe-Leu-Arg-Arg-Gln-Phe-Lys-Val-Val-Thr
$\alpha$ -Neoendorphin	Tyr-Gly-Gly-Phe-Leu-Arg-Lys-Tyr-Arg-Pro-Lys
$\beta$ -Neoendorphin	Tyr-Gly-Gly-Phe-Leu-Arg-Lys-Tyr-Arg-Pro
<b>Pro-opiomelanocortin<sup>a</sup></b>	
$\beta$ -Endorphin (human)	Tyr-Gly-Gly-Phe-Met-Thr-Ser-Glu-Lys-Ser-Gln-Thr-Pro-Leu-Val-Thr-Leu-Phe-Lys-Asn-Ala-Ile-Ile-Lys-Asn-Ala-Tyr-Lys-Lys-Gly-Glu
<b>Endomorphins<sup>b</sup></b>	
Endomorphin-1	Tyr-Pro-Trp-Phe-NH <sub>2</sub>
Endomorphin-2	Tyr-Pro-Phe-Phe-NH <sub>2</sub>
<b>Nociceptin and related peptide</b>	
Nociceptin/orphanin FQ	Phe-Gly-Gly-Phe-Thr-Gly-Ala-Arg-Lys-Ser-Ala-Arg-Lys-Leu-Ala-Asn-Gln
Orphanin FQ2	Phe-Ser-Glu-Phe-Met-Arg-Gln-Tyr-Leu-Val-Leu-Ser-Met-Gln-Ser-Ser-Gln
<sup>a</sup> Precursor protein of corresponding opioid peptides <sup>b</sup> Precursor not known	

Ultimately, the definitive demonstration of the three opioid receptors, MOR, KOR, and DOR, came from molecular biology. Advances in molecular biology led to the cloning of the

MOR, DOR, and KOR in the early 1990's, clearly establishing the existence of distinct MOR, KOR and DOR that share about 60% sequence homology.<sup>24-28</sup> In 1994 a related receptor, nociceptin/orphanin FQ (NOPR), also referred to as the opioid receptor like-1 (ORL-1) receptor, was identified. Following cloning of the NOPR receptor, a heptadecapeptide named nociceptin was identified as the endogenous ligand, as it caused hypersensitivity to pain *in vivo*.<sup>29, 30</sup> Nociceptin (Table 2.1) was also referred to as orphanin FQ where F and Q are the first and last residues in the heptadecapeptide.<sup>30</sup> Notably, the opioid receptor did not show appreciable affinity to opioid ligands, despite sharing ~60% sequence homology with the classical opioid receptors.<sup>31</sup>

### **2.2.1 Clinically used opioids**

Opioids invoke a variety of physiological responses that can be leveraged for therapeutic benefit. Opioids are used therapeutically primarily as analgesics (morphine and its analogs), but also as antidiarrheal agents (loperamide), and antitussive agents (codeine) (Figure 2.2). Additionally, opioid ligands such as methadone and buprenorphine (Figure 2.2) are used to treat opioid addiction. Agonists at the MOR are the most common therapy for chronic pain. Fentanyl (Figure 2.2) and fentanyl-related compounds, the 4-anilidopiperidines, which are potent agonists at MOR, are used as adjuvants to anesthesia.<sup>32</sup> KOR agonists induce analgesia while lacking the MOR agonist-related reinforcing effects; however, sedation and dysphoria have limited their utility.<sup>33</sup> Recently, the KOR-selective agonist nalfuramine hydrochloride (TRK-820, Figure 2.2) was approved in Japan as a treatment for severe itching related to liver disease and hemodialysis.

34

Opioid ligands with mixed pharmacological activity at the MOR and the KOR exhibit particular advantages with respect to addiction liability. Pentazocine, nalbuphine, and butorphanol (Figure 2.2) are mixed agonist/antagonists with limited abuse potential used as analgesics.<sup>1</sup> While

pentazocine and nalbuphine exhibit agonism at KOR and antagonism at MOR, butorphanol exhibits partial agonism at MOR and KOR. Buprenorphine has mixed pharmacology at three opioid receptors: partial MOR agonism, KOR antagonism and NOPR agonism.<sup>35-37</sup>

Buprenorphine is clinically approved to treat opioid dependence; the ceiling effect from partial agonism at the MOR mitigates respiratory depression associated with MOR agonism.<sup>38</sup> Abuse deterrent formulations of buprenorphine with naloxone have been developed to prevent its potential misuse (Figure 2.2).<sup>39</sup> The inclusion of naltrexone, another opioid antagonist, in buprenorphine formulations has been examined in humans to provide “functional KOR antagonism” which has shown efficacy in the treatment of opioid dependence.<sup>40-42</sup>

Opioid antagonists are clinically used to counter the effects of opioids and alleviate reinforcing behaviors. Naloxone is critical in the reversal of opioid overdose and post-operative sedation, while naltrexone is used to treat opioid dependence.<sup>1, 43</sup> Peripherally restricted antagonists methylnaltrexone bromide<sup>44</sup> and the recently approved naloxegol<sup>45</sup> are used as anti-constipation medications, while alvimopan<sup>46</sup> is used for post-operative recovery of gastrointestinal function (Figure 2.2). Opioid antagonists have shown promise in the treatment of compulsive disorders including gambling<sup>47</sup> and alcohol addiction; naltrexone and nalmefene (Figure 2.2) are used to treat alcohol dependence.<sup>48</sup> Nalmefene, a MOR and DOR antagonist and a partial agonist at KOR, was recently approved by European Medicines Agency.<sup>49</sup>

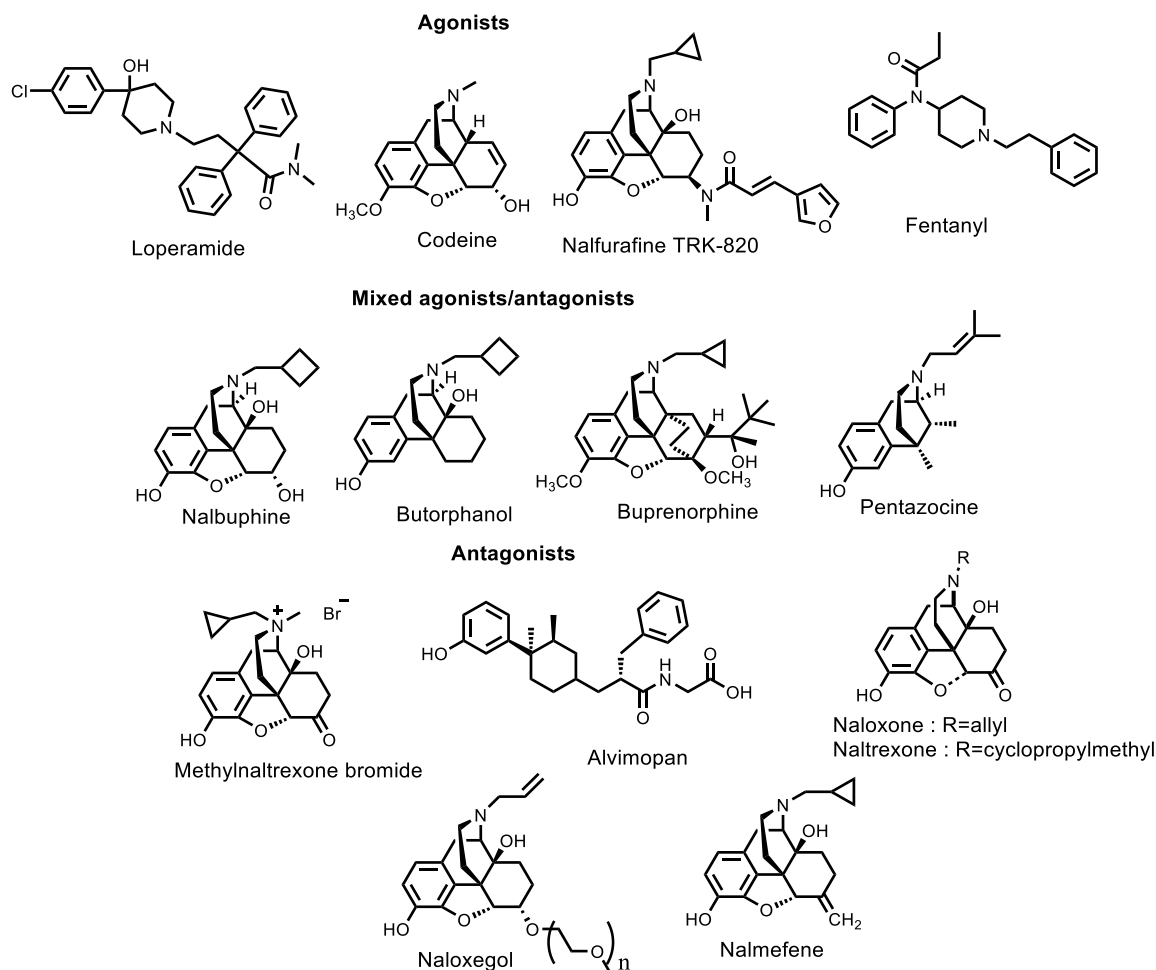


Figure 2.2. Opioid agonists and antagonists in clinical use discussed in text.

## 2.2.2 Opioid receptor signaling

The opioid receptors are G protein-coupled receptors (GPCR's), which comprise the largest receptor class in the human genome.<sup>50, 51</sup> As a result, GPCRs are important targets in medication development. Not surprisingly, a considerable percentage of clinically used medications, ~36%, target GPCR's.<sup>52</sup> Opioid receptors are coupled to G-proteins consisting of  $\alpha$ ,  $\beta$ , and  $\gamma$  subunits.<sup>53</sup> Activation of opioid receptors follows canonical GPCR signaling; ligand binding induces a conformational change in the receptor resulting in dissociation of the heterotrimeric G-protein complex and guanine-nucleotide exchange to give  $G_{GTP-\alpha}$ , and the  $G_{\beta\gamma}$  subunits.<sup>54, 55</sup> Opioid receptors are coupled to inhibitory G-proteins ( $G_{\alpha i}$ ); activation results in the

inhibition of adenylyl cyclase and calcium channels, and the activation of inwardly rectifying potassium channels.<sup>56, 57</sup> The heterotrimeric G-protein complex is reformed following GTP-hydrolysis which terminates the signal.<sup>58</sup>

A multitude of downstream signaling pathways have been associated with dissociated GTP- $\alpha$ ,  $\beta$ , and  $\gamma$  subunits following opioid receptor activation.<sup>59</sup> Over the last decade, G protein-coupled receptor kinases (GRKs) and  $\beta$ -arrestins, initially discovered and characterized for their mechanism of GPCR signal termination, have been shown to also transduce GPCR signals.<sup>60</sup> GPCRs show arrestin-dependent signaling following receptor phosphorylation, resulting in mitogen activated protein kinase (MAPK) signaling. MAP kinases phosphorylate a number of targets including cytosolic targets and transcription factors in the nucleus.<sup>60</sup>

Among the three MAP kinase families, a number of kinases are well characterized: extracellular signal related kinases 1/2 (ERK1/2), c-Jun-N-terminal kinases (JNK1-3), and p38-MAP kinases ( $\alpha$ ,  $\beta$ ,  $\gamma$ ,  $\delta$ ).<sup>61</sup> With respect to opioid receptors the ERK 1/2 subfamily is the best characterized; both  $\beta$ -arrestin dependent and G-protein activation cause ERK 1/2 activation.<sup>62</sup> Of note, aversion as a result of KOR activation, which limited the therapeutic utility of KOR agonists, has been linked to p38-MAPK signaling.<sup>62, 63</sup> Additionally, c-Jun-N-terminal kinase (JNK) signaling, extensively studied by Chavkin and co-workers, has been linked to the long lasting effects of KOR selective antagonists, norbinaltorphimine (norBNI) and JDTic (Figure 2.3).<sup>62, 64</sup>

### **2.2.3 Ligands used for *in vitro* studies of opioid receptors**

Since cloning of the opioid receptors in the early 1990's, cell-based assays with cloned receptors are extensively used for *in vitro* evaluation of opioid ligands.<sup>1</sup> Cell lines, such as chinese hamster ovary (CHO) cells, expressing one opioid receptor are broadly used for *in vitro* evaluation

of opioid ligands. This involves both radioligand binding assays to determine receptor affinity and selectivity, and functional assays to determine efficacy and potency.

The radioligand: [<sup>3</sup>H]DAMGO ([D-Ala<sup>2</sup>,MePhe<sup>4</sup>,glyol]enkephalin), [<sup>3</sup>H]DPDPE(*cyclo*[D-Pen<sup>2</sup>,D-Pen<sup>5</sup>]enkephalin), and [<sup>3</sup>H]U69593 (Figure 2.3) for  $\mu$ ,  $\delta$ , and  $\kappa$  receptors, respectively, are routinely used for the binding assays. Functional assays related to signaling and cAMP production, such as the [<sup>35</sup>S]GTP $\gamma$ S assay, measure efficacy and potency of opioid agonists in [<sup>35</sup>S]GTP $\gamma$ S binding, an indication of opioid receptors activation.<sup>65</sup> Given the coupling of opioid receptors to adenylyl cyclase via G<sub>i</sub>, inhibition of adenylyl cyclase activity resulting in reduced cAMP production is used to measure agonist activity.<sup>66</sup>

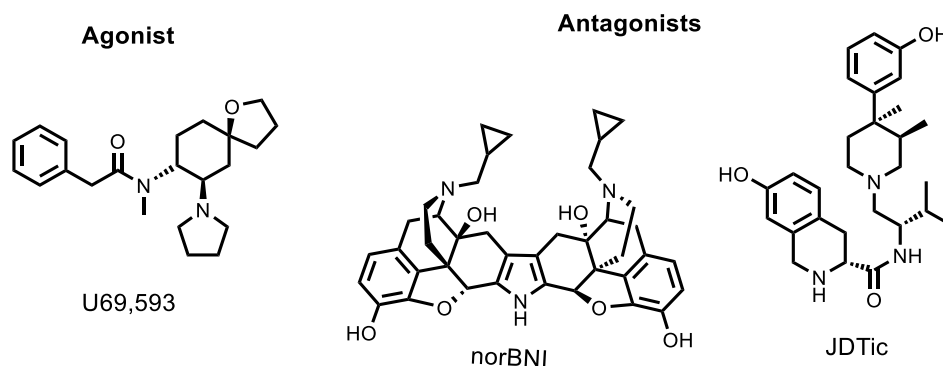


Figure 2.3 Structure of opioid ligands discussed in text.

## 2.2.4 Opioid receptor structures

Opioid receptors, consisting of 7 transmembrane regions (7TM), an extracellular N-terminus, intracellular C-terminus, extracellular and intracellular loops, are members of the rhodopsin family of GPCRs. Prior to the elucidation of high resolution opioid receptor crystal structures, receptor chimera studies and site-directed mutagenesis were important in elucidating the molecular basis for observed differences in the affinity of ligand binding between the opioid receptors. Receptor chimera studies elucidated regions of the receptors that were responsible for selectivity and discriminating ligands, while site-directed mutagenesis studies highlighted the

relative importance of specific residues. For instance, receptor chimera studies showed the importance of the KOR EL2 for the affinity of the endogenous ligand dynorphin A.<sup>67, 68</sup> More recently, Danielsson and co-workers inserted EL2 of KOR in a soluble  $\beta$ -barrel and used NMR paramagnetic relaxation data to demonstrate direct binding of dynorphin A to EL2.<sup>69</sup> Site-directed mutagenesis studies on the other hand established important residues for ligand recognition such as Glu297, Ser 310, Tyr 312 and Tyr 313 in the KOR.<sup>70</sup>

Opioid receptors share the highest sequence homology in the 2<sup>nd</sup>, 3<sup>rd</sup>, and 7<sup>th</sup> TM regions (Figure 2.4).<sup>1</sup> The four receptors, MOR, KOR, DOR, and NOPR share ~60% sequence homology with a conserved Asp residue in TM3, common in all aminergic GPCRs.<sup>71</sup> The crystal structures of all four opioid receptors were solved in 2012, thereby providing structural information to further explain opioid pharmacology. The mouse MOR and DOR crystal structures were resolved by Kobilka and co-workers,<sup>72, 73</sup> while the human KOR and NOPR receptor structures were resolved by Stevens and co-workers.<sup>31, 74</sup> A considerable amount of molecular engineering was required to crystallize the membrane-bound receptors including thermostabilizing mutations. Additional innovative approaches included truncation of the flexible N- and C-termini of the receptors, T4-lysozyme fusion for the KOR, MOR and DOR, and incorporation of apocytochrome b<sub>562</sub>RIL for the NOPR to stabilize the receptor structures.<sup>75</sup> Notably, the engineered receptors were functional and responded to selective agonists with only modest changes in affinity. MOR, DOR, and KOR receptors were crystallized as dimers, highlighting the ongoing discussions on the existence of receptor dimers *in vivo*;<sup>76</sup> however, the receptors were purified as monomers, and dimerization could be an artifact of the crystallization conditions.<sup>75</sup>

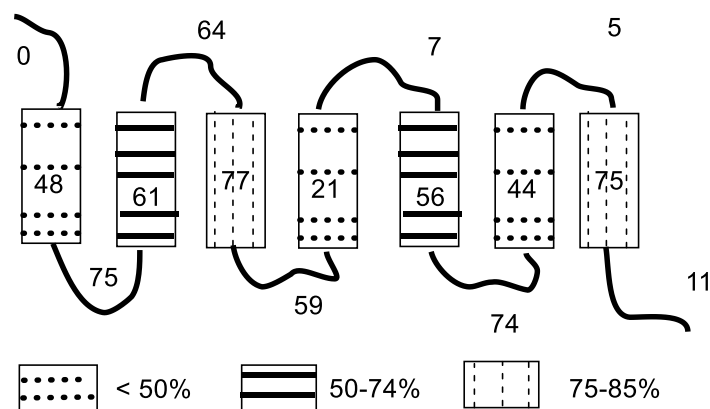


Figure 2.4 Schematic of the protein structure of the MOR, DOR and KOR showing the percentage of identical residues within the respective segments. Transmembrane helices are indicated by rectangles (from ref<sup>1</sup>).

Notably, all four receptors were crystallized in the inactive state with the respective antagonists;  $\beta$ -funaltrexamine for MOR, naltrindole for DOR, JDTic for KOR, and a peptide mimetic for NOPR.<sup>31, 72-74</sup> The crystal structures highlighted observations from previous pharmacological studies using chimeric receptors and site directed mutagenesis studies, particularly concerning ligand recognition. All receptor structures were characterized by a central ligand binding pocket encircled by transmembrane (TM) helices.<sup>75</sup> Conserved residues include Pro residues resulting in bends in most of the TM helices (TM2, TM4, TM5, TM6, and TM7) and cysteine residues forming a disulfide bridge between extracellular loop 2 (EL2) and the end of TM3. In addition, a common  $\beta$ -hairpin loop in EL2 allows access to the ligand binding pocket. More diversity was observed in extracellular loops where EL2 of KOR and NOPR had more acidic residues, Asp and Glu, compared to MOR and DOR, which correlates with the higher proportion of basic residues in the endogenous ligands dynorphin (KOR) and nociceptin (NOPR). Sequence conservation among the EL of the receptors was lowest in EL3 located between TM6 and TM7 (EL3 of KOR was however not resolved in the crystal structure).<sup>77</sup>

Ligand binding interactions included the conserved<sup>3,32</sup> Asp residue in TM3, [Asp 147<sup>3,32</sup> (MOR), Asp 128<sup>3,32</sup> (DOR), Asp 138<sup>3,32</sup> (KOR), and Asp 130<sup>3,32</sup> (NOPR)], which is involved in



charge-charge interactions with an amine in the ligands (superscripts show position of the residue as per Ballesteros-Weinstein numbering).<sup>78</sup> This conserved Asp occurs in all aminergic receptors,<sup>71</sup> and the ionic interaction had been proposed in the early 1950's by Beckett and Casy in their three binding site model for opioid receptor binding.<sup>7</sup> A conserved His in TM6, thought to be involved in a hydrogen bond with the phenol in opioids,<sup>79</sup> was observed in all receptors except the NOPR where it is replaced with a Gln residue. Conserved residues within 4Å of the ligand binding site in all four receptors were Asp<sup>3.32</sup>, Tyr<sup>3.33</sup>, Met<sup>3.36</sup>, Trp<sup>6.48</sup>, and Tyr<sup>7.43</sup> while divergent residues were observed around the binding pocket entrance surrounded by TM2, TM3 and TM7, suggesting a selectivity filter.<sup>77</sup>

JDTic in the KOR crystal structure makes a number of important interactions at the orthosteric binding site important for affinity. JDTic was observed in the binding pocket, capped by the EL2 β-hairpin, fixed in a V-shape conformation.<sup>74</sup> A salt bridge between the piperidine and isoquinoline protonated amines and Asp 138<sup>3.32</sup> anchors JDTic in the binding pocket. Hydrophobic contacts with Val 108<sup>2.53</sup>, Val 118<sup>2.63</sup>, Ile 294<sup>6.65</sup>, and a hydrophobic/polar interaction with Tyr 312<sup>7.35</sup> are unique to KOR contributing to selectivity at KOR, consistent with mutagenesis and SAR studies.<sup>80</sup> Additional contacts of particular interest include a salt bridge with Glu 297<sup>6.58</sup> and the hydrophobic contact of the isopropyl group in JDTic and Trp 287<sup>6.48</sup> (Figure 2.5).<sup>81</sup>

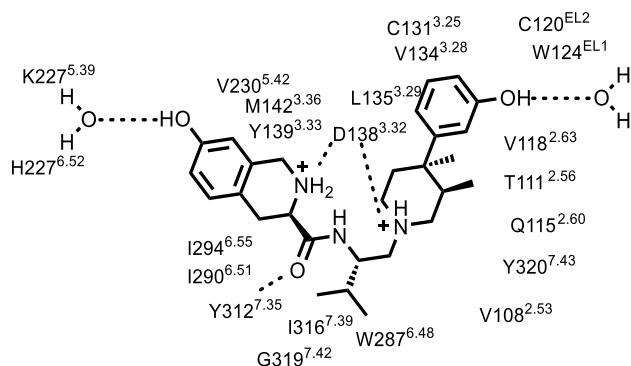


Figure 2.5 Interactions of JDTic in the human KOR ligand binding pocket.<sup>74</sup>

More recently, further studies in opioid pharmacology have leveraged the structural information from opioid receptor crystal structures, mutagenesis, and molecular modeling to rationally design chemogenetic tools that allow spatiotemporal control of neuronal activity.<sup>82</sup> In one particularly interesting study, Vardy *et al* mutated the conserved Asp residue in TM3 to abolish binding of endogenous KOR agonists.<sup>83</sup> The D138N mutant receptor was named kappa opioid receptor DREADD (Designer Receptor Exclusively Activated by Designer Drug) or KORD. KORD showed no response to endogenous opioids, but was activated by salvinorin B (Figure 2.6), an inactive metabolite of salvinorin A. Further studies with KORD indicated neuronal silencing *in vivo*.<sup>83, 84</sup> Chemogenetic tools such as KORD compliment tools such as optogenetics in understanding opioid pharmacology. Chemogenetic manipulation is limited however by the properties of the ligand; for instance, pharmacokinetic properties and the limited solubility of salvinorin B are important considerations in experimental design.<sup>83</sup> Overall, the mutant receptor provides a novel tool to study neuronal signaling.

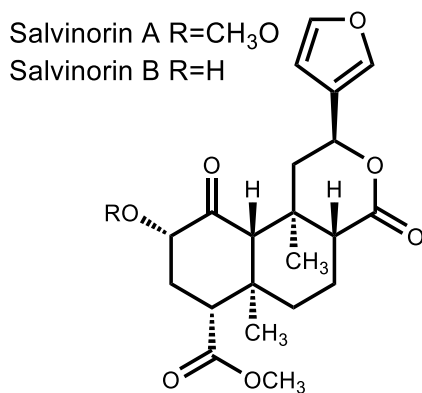


Figure 2.6 Non-nitrogenous KOR agonist salvinorin A and the metabolite salvinorin B.

Additional structures of the opioid receptors have been reported since 2012. These include a nanobody-stabilized human KOR in its active state crystallized with the epoxymorphinan opioid agonist MP1104,<sup>85</sup> a nanobody-stabilized mouse MOR in its active state crystallized with the

morphinan agonist BU72,<sup>86</sup> and the human DOR crystallized with naltrindole.<sup>87</sup> Moreover, the first structures of a peptide in complex with opioid receptors were reported. These included an X-ray structure of a bifunctional DOR antagonist and MOR agonist tetrapeptide, dimethyl tyrosine(Dmt)-Tic-Phe-Phe-NH<sub>2</sub>, with the human DOR<sup>88</sup> and an NMR-based structure of dynorphin bound to the human KOR.<sup>89</sup> Comparison of the active<sup>85, 86</sup> and the inactive<sup>73, 74</sup> crystal opioid receptor structures revealed global conformational changes indicating a general activation mechanism that involves contraction of the helical bundle on the extracellular face to allow opening of the helical bundle on the intracellular face.<sup>85</sup>

The DOR crystal structure with naltrindole, at a 1.8 Å resolution represents the highest resolution opioid structure to date. This structure shows the allosteric sodium site offering insights into opioid receptor signaling.<sup>87</sup> Notably, sodium ions are known for negative allosteric modulation of opioid receptors, decreasing the affinity of agonists at the orthosteric site.<sup>90</sup>

Elucidation of the crystal structures of the opioid receptors opened up the opportunity for structure-guided drug design efforts.<sup>77, 91</sup> For instance, virtual screening has led to a number of novel ligands at opioid receptors.<sup>92, 93</sup> The crystal structures are also an avenue to probe ligand-dependent signaling by looking at receptor function at the molecular level. This is particularly important in the context of ligand-induced conformations resulting in ligand-dependent cellular signaling.<sup>94</sup> For instance, Vardy *et al.* examined the binding modes of different structural classes of KOR agonists, showing how the different chemotypes stabilized corresponding receptor conformations.<sup>81</sup> Multiple chemotypes of KOR agonists have been developed to date; Roth and co-workers demonstrated ligand-dependent signaling based on chemotype, suggesting differing binding modes in the KOR.<sup>95</sup>

### 2.2.5 Ligand-directed signaling

Tolerance and dependence are among the drawbacks of MOR agonists such as morphine.<sup>96-98</sup> Bohn *et al.* showed that mice lacking  $\beta$ -arrestin-2 showed enhanced antinociception following administration of morphine.<sup>99, 100</sup> Bohn *et al.* reported that  $\beta$ -Arrestin-2 knock out mice did not show receptor desensitization following chronic morphine treatment, suggesting the involvement of  $\beta$ -arrestin-2 in developing tolerance. Dependence however, was not affected<sup>100</sup> as the characteristic upregulation of adenylyl cyclase<sup>101</sup> was not prevented following chronic morphine administration.

$\beta$ -Arrestin signaling is a non-canonical GPCR signaling pathway that has gained prominence in recent years because of its capacity to affect the side effect profile of drugs targeting GPCRs.<sup>102</sup> For a long time,  $\beta$ -arrestins were only implicated in GPCR desensitization by binding to the phosphorylated receptor thereby terminating GPCR signaling and directing it to clathrin-coated pits.<sup>103</sup> However, an increasing body of research has shown that  $\beta$ -arrestin signaling is distinct from canonical GPCR signaling involving G proteins, spurring the development of a new type of potential therapeutic targeting GPCRs.<sup>104, 105</sup> This non-canonical GPCR signaling kinase appears to involve ERK1/2 and JNK3 MAP kinases.<sup>103</sup> GPCRs can adopt different conformations, resulting in distinct downstream signaling depending on the ligand.<sup>106</sup> This ligand bias, also termed functional selectivity or ligand-directed signaling, has become an approach to design drugs with fewer side effects.<sup>107</sup> Biased ligands can differentiate between canonical and non-canonical signaling (Figure 2.7) involving either G-protein or  $\beta$ -arrestin signaling.<sup>94</sup>

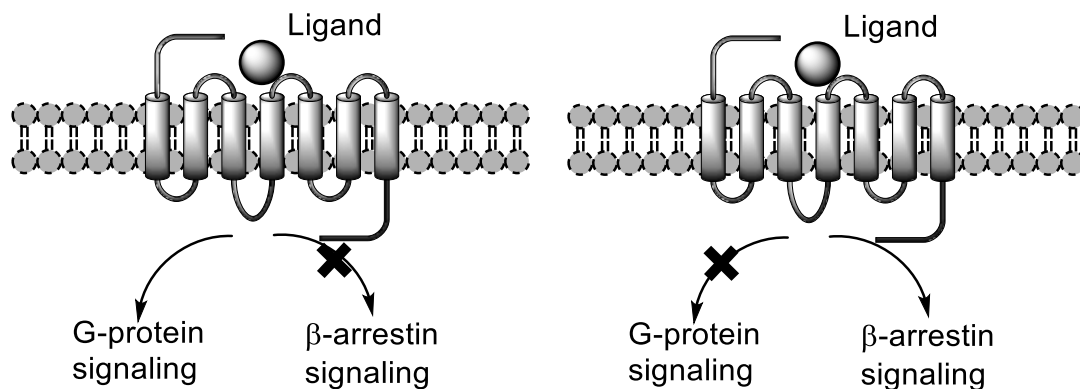


Figure 2.7 Schematic showing ligand-biased signaling at GPCRs.<sup>108</sup>

Ligand bias has gained prominence because of the potential to avert side effects that limit the therapeutic utility of opioid agonists. Recent reports on biased ligands at opioid receptors document the progress toward separation of therapeutically relevant effects from unwanted side effects.<sup>109, 110</sup> Recently, a G-protein-biased MOR agonist TRV-130 exhibited analgesia with reduced respiratory depression and constipation than morphine and in clinical trials for acute pain management.<sup>111, 112</sup> The dynorphin/KOR system has been targeted for the treatment of pain and mood disorders because it does not potentiate MOR related side effects such as reward and respiratory depression. However, side effects such as dysphoria and sedation have limited clinical use of centrally acting KOR ligands.<sup>113, 114</sup> Functional selectivity in downstream signaling has been reported for a number of KOR ligands. For example, the activation of ERK1/2 differed after treatment with KOR agonists U69,593 and MOM salvinorin B, whereas U69,593 activates astrocyte proliferation while 2-methoxymethyl(MOM) salvinorin B does not.<sup>115</sup> Another KOR agonist, 6'-guanidinonaltrindole (6'-GNTI), preferentially activated G-protein signaling over  $\beta$ -arrestin2 recruitment, but did not result in phosphorylation of ERK1/2.<sup>109</sup>  $\beta$ -Arrestin-mediated signaling has been associated with dysphoria, and therefore G-protein biased KOR ligands are desirable as analgesics.<sup>116</sup> Increasing reports describe KOR agonists with G-protein biased signaling as desirable analgesics; these agonists include recently KOR discovered chemotypes

such as the triazoles (Figure 2.8).<sup>117</sup> In recent preclinical studies, Brust *et al.* reported a functionally selective triazole KOR agonist that induced analgesia and antipruritic effects without KOR-associated liabilities such as dysphoria and sedation.<sup>117</sup>

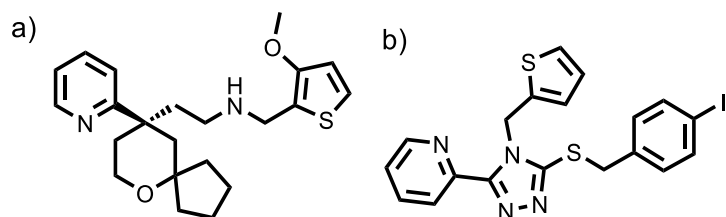


Figure 2.8 Structure of G-protein biased a) TRV-130<sup>111</sup> and b) the triazole chemotype of KOR agonist.<sup>116</sup>

### 2.3 Significance of the KOR

Wide expression of the KOR in brain areas associated with reward pathways, mood regulation, and cognitive function is well documented in both rat and human brains.<sup>118, 119</sup> These brain areas include the ventral tegmental area, nucleus accumbens, prefrontal cortex, substantia nigra, striatum, hippocampus and hypothalamus. KOR ligands, both agonists and antagonists, have been pursued for their therapeutic effects in pain, drug addiction, and mood disorders. KOR ligands have also shown promise as anti-angiogenic agents<sup>120</sup> and to inhibit HIV-1 expression in microglial cells.<sup>121</sup>

Activation of KOR notably produces analgesic effects without the undesirable side effects of MOR activation, including addiction liability and respiratory depression.<sup>122</sup> However, KOR agonists produce dysphoria that has limited their clinical use.<sup>123</sup> KOR and MOR were shown to have opposite effects, with KOR showing aversive effects whereas MOR showed positive reinforcing effects in a conditioned place preference (CPP) assay following treatment with the respective receptor agonists.<sup>124</sup>

KOR activation results in dysphoria, psychotomimetic effects and anxiety-like effects while MOR activation elevates the mood. The opposing effects were shown to emanate from modulation of dopamine release in the nucleus accumbens; Shippenberg and coworkers demonstrated modulation of dopamine release at dopaminergic neurons as a result of stimulating the KOR and MOR.<sup>125</sup> MOR activation by agonists, such as DAMGO and  $\beta$ -endorphin, in the ventral tegmental area elevated the mood. On the other hand, KOR activation by KOR agonists, such as dynorphin and U-69593, in the nucleus accumbens resulted in aversion. Blockade of the MOR by antagonists reduced dopamine release, whereas blockade of the KOR by norBNI increased dopamine levels.<sup>125</sup>

Further studies have demonstrated the involvement of the dopamine reward system in both drug addiction and mood disorders.<sup>126-128</sup> Notably, drugs of abuse increase dopamine levels in the nucleus accumbens.<sup>129</sup> Given the opposing effects of MOR and KOR in modulation of dopamine release, KOR agonists have been used to counter elevated dopamine levels in drug abuse treatment. Ironically, however, chronic administration of KOR agonists increases drug intake by the induction of stress.<sup>130</sup>

KOR antagonists, on the other hand, are beneficial in preventing relapse to drug seeking behavior<sup>41, 130, 131</sup> and have shown therapeutic promise in stress-induced dysphoria.<sup>132-134</sup> Additional reports have highlighted the utility of KOR antagonists in preventing reinstatement of drug seeking behavior induced by stress.<sup>135, 136</sup>

KOR activation in acute and chronic stress plays an important role in the behavioral response to the stressor. In acute stress, KOR activation can provide the necessary motivation to overcome threats; in chronic stress, however, KOR activation can precipitate adverse behaviors such as drug-seeking. A number of studies have demonstrated that increased stress precipitates

relapse of drug use in humans.<sup>137</sup> In animal models, depressive effects such as immobility and social defeat behavior have been observed following dynorphin release after chronic stress tests such as the forced-swim test (FST).<sup>138</sup> McLaughlin *et al.* showed that repeated forced-swim stress significantly potentiated the preference of mice for cocaine in the conditioned place preference (CPP) assay; blockade of the KOR system blocked the potentiation of cocaine-CPP.<sup>139</sup> Additionally, KOR agonists potentiated cocaine-CPP in a similar fashion to forced-swim stress, mice lacking KOR did show potentiation of cocaine-CPP in response to stress.<sup>140</sup> Of note, a growing body of evidence on depression and the KOR has demonstrated profound effects of KOR ligands on motivation and mood, thereby increasing the interest in KOR antagonists as potential therapeutics in mood disorders.<sup>141</sup>

### **2.3.1 KOR selective agonists**

The KOR is activated by a structurally diverse group of peptidic and non-peptidic ligands. Early studies of the KOR utilized less selective KOR ligands such as the benzomorphan derivative ketocyclazocine (Figure 2.1c). Increasingly KOR selective ligands include the arylacetamides U50,488, U69,593 and enandoline (Figure 2.9); U50,488 and U69,593 are used extensively to characterize opioid receptors.<sup>142-144</sup> Notably, modifications of U50,488 to include a spiroether resulted in the more selective U69,593;<sup>145</sup> modifying the phenyl ring in U69,593 to a benzofuran further enhanced the potency and selectivity to give enandoline (CI-977).<sup>144</sup>



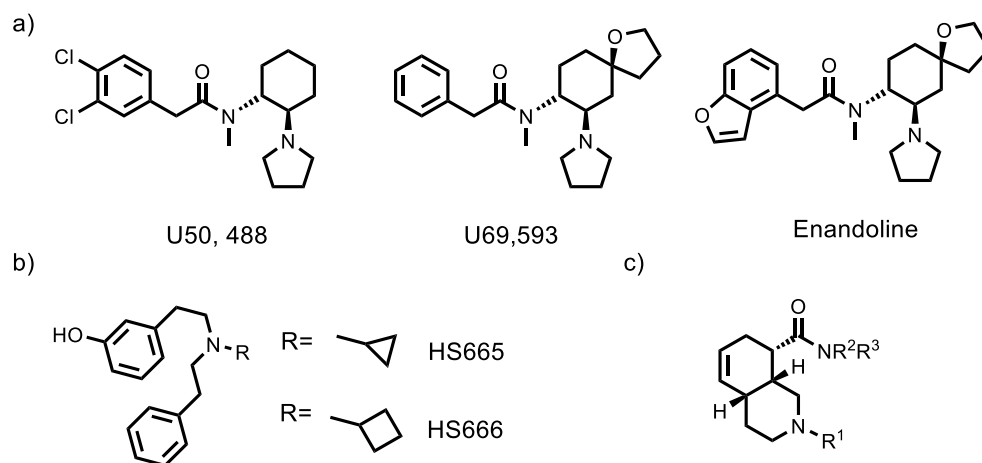


Figure 2.9 Structures of non-peptidic KOR agonists discussed in text a) arylacetamides b) diphenylethylamines, and c) octahydroquinoline carboxamides.

More recently, selective KOR agonists of different classes including neoclerodane diterpenes (Salvinorin A, Figure 2.6), diphenylethylamines (HS665, Figure 2.9b), and octahydroisoquinoline carboxamides (Figure 2.9c) derivatives have been developed.<sup>146-148</sup> Of note, the undesirable side effect profile of KOR agonists limits their clinical utility (see section 2.3). However, preclinical studies of promising analogs with a reduced side effect profile such as analogs of Salvinorin A (Figure 2.6), the first non-nitrogenous opioid receptor agonist, have been pursued.<sup>149, 150</sup> Simonson *et al* reported that the Sal A analog, Mesyl Sal B, had a longer duration of action than Sal A and thus holds potential for further development and clinical utility.<sup>151</sup> Brain-penetrant KOR ligands with bias towards G-protein signaling over  $\beta$ -arrestin signaling have also shown promise. Spetea *et al* reported reduced side effects due to G-protein biased signaling of the diphenylethylamine HS666 (Figure 2.9b), a partial agonist at KOR.<sup>152</sup>

KOR agonists that do not penetrate the BBB, and thus avoid centrally mediated side effects such as sedation and dysphoria, have been examined in both preclinical and clinical studies. These include ADL 10-1010 and asimadoline (Figure 2.10a), which has been investigated for a number of indications including irritable bowel syndrome<sup>153</sup> and pruritus.<sup>154</sup> More recently, a clinical trial

of asimadoline was conducted in pruritus associated with atopic dermatitis.<sup>155</sup> Additional peripherally selective KOR agonists include the peptidic FE200665 (now known as CR665) and FE200666, both of which are all D-tetrapeptides. (Figure 2.10b) that are unrelated to Dyn A. CR665 has been examined in clinical trials for postoperative pain<sup>33</sup> while a second generation analog, CR845 (Figure 2.10b), that is orally available has been examined in Phase 2 studies in acute postoperative pain, chronic pain and pruritus.<sup>156</sup> Ongoing studies include a Phase 3 clinical trial to evaluate IV CR845 in hemodialysis patients with moderate to severe pruritus.<sup>157</sup>

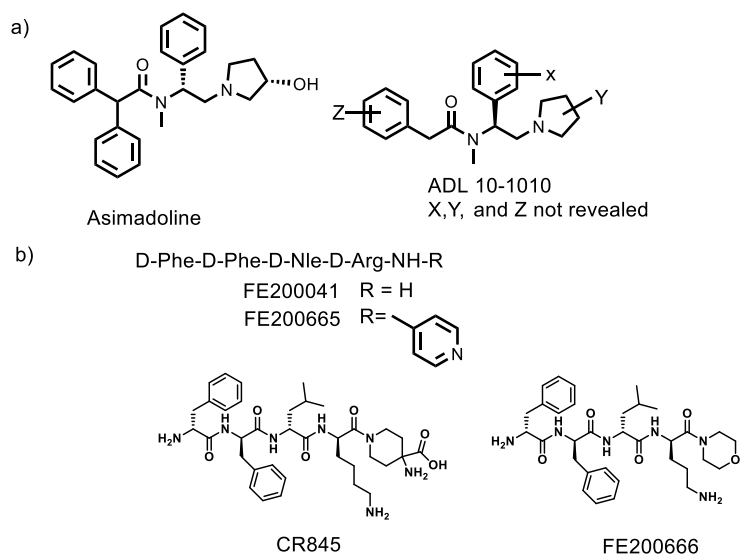


Figure 2.10 Structures of peripherally restricted a) non-peptidic and b) peptidic KOR agonists.

Majority of peptidic KOR selective ligands are based on the endogenous KOR ligand Dyn A. Modifications to Dyn A resulting in KOR selective agonists include N-terminal alkylation, substitutions at position 3, and modifications to increase metabolic stability.<sup>33</sup> N-terminal alkylation of [D-Pro<sup>10</sup>]Dyn A(1-11) with allyl, cyclopropylmethyl(CPM) or benzyl groups enhanced KOR selectivity.<sup>158</sup> Of note, the *N*-allyl and *N*-CPM analogs displayed potent KOR agonist activity while the *N*-benzyl analog displayed partial KOR agonist activity.<sup>158, 159</sup> KOR

selectivity was also enhanced considerably by Ala or D-Ala substitutions of position 3 in Dyn A(1-11) amide.<sup>160</sup>

In Dyn A(1-13), N-terminal (e.g. N-MeTyr) and C-terminal modifications (e.g. C-terminal amide) resulted in increased metabolic stability.<sup>33</sup> Further modifications to improve metabolic stability include D-amino acid substitutions such as D-Ala<sup>2</sup>, D-Ala<sup>8</sup>, and D-Pro<sup>10,161</sup> the D-Ala<sup>2</sup> substitution however decreased KOR selectivity.<sup>162</sup> Combinations of modifications to Dyn A(1-8) resulted in E-2078 and SK-9709 (Figure 2.11) with increased metabolic stability which were studied *in vivo*.<sup>163, 164</sup> Of note, SK-9709 has a reduced amide bond between Arg<sup>6</sup>-Arg<sup>7</sup> and displayed a 3-fold lower affinity toward KOR, but was 15-fold more selective for KOR over MOR compared to E-2078.<sup>163</sup>

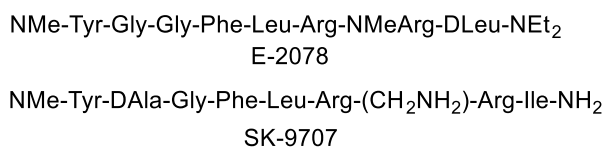


Figure 2.11 Structures of Dyn A-based KOR agonists with increased metabolic stability studied *in vivo*.

## 2.3.2 KOR selective antagonists

### 2.3.2.1 Non-peptidic KOR selective antagonists

KOR antagonists are also of varied chemical classes and are being pursued for their potential therapeutic utility in neuropsychiatric disorders, stress-related conditions and addiction.<sup>151</sup> Initial studies of KOR antagonists focused on morphinan related compounds. In the 1980's Portoghese and co-workers reported 1,8-bis( $\beta$ -naltrexamino)-3,6-dioxaoctane (TENA),<sup>165</sup> a modestly selective KOR antagonist that was 4- and 2.5-fold selective for MOR and DOR, respectively. Portoghese and co-workers later reported norbinaltrophimine (norBNI) as the first potent and highly selective KOR antagonist (Figure 2.12); norBNI was 520- and 580-fold selective

over MOR and DOR, respectively.<sup>166</sup> Subsequently, the same group reported the naltrindole-based 5'-guanidinonaltrindole (GNTI) with increased selectivity and potency than norBNI. Interestingly however, 6'-guanidinonaltrindole (6'-GNTI, Figure 2.12) displayed KOR agonist activity.<sup>167</sup> In spite of the utility of norBNI and 5'-GNTI as pharmacological tools, they exhibit long lasting KOR antagonism lasting weeks which complicates their use.<sup>168, 169</sup>

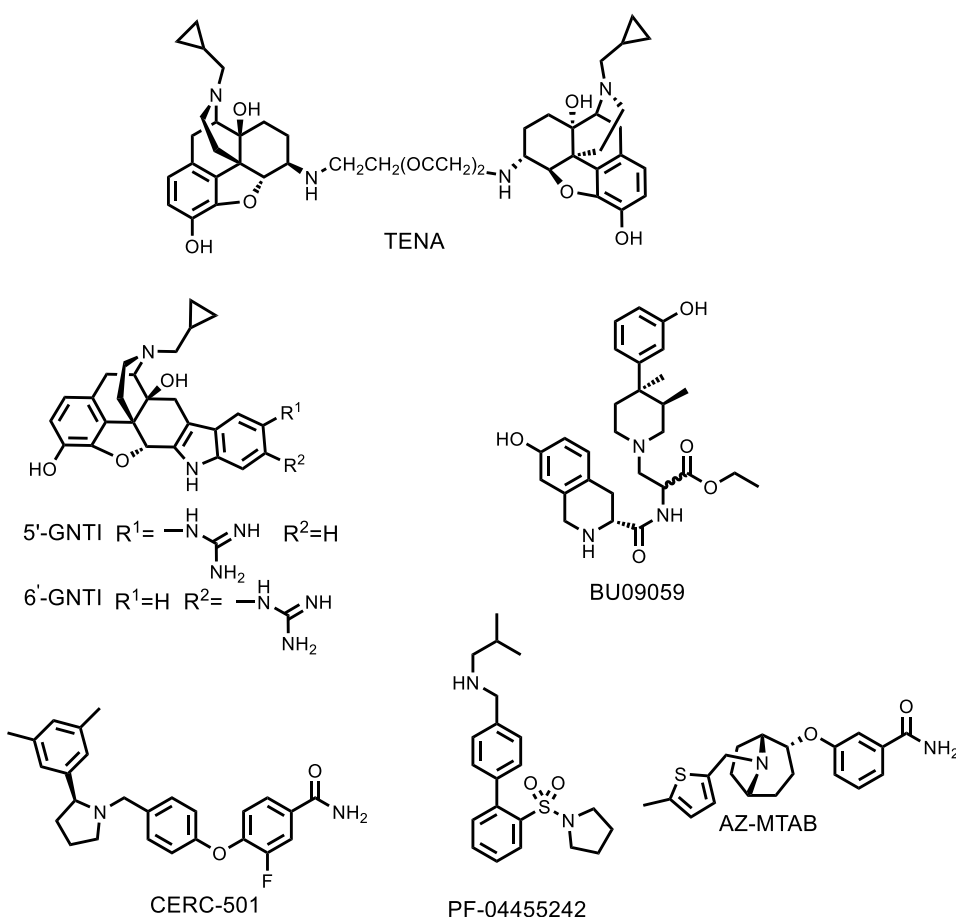


Figure 2.12 Non-peptidic KOR antagonists.

In 2001 Thomas *et al.* reported the highly potent and KOR selective antagonist *trans*-3,4-dimethyl-4-(3-hydroxyphenyl)piperidine derivative JD<sub>T</sub>ic (Figure 2.5).<sup>170</sup> JD<sub>T</sub>ic is more selective for KOR than norBNI and was recently used to elucidate the crystal structure of the human KOR.<sup>74</sup> *In vivo* evaluation of JD<sub>T</sub>ic in alcohol,<sup>171</sup> cocaine,<sup>135</sup> and opioid dependence<sup>172</sup> indicated promising

results pointing to its potential as a therapeutic. In 2014 JDtic entered clinical trials, but was withdrawn due to precipitation of non-sustained ventricular tachycardia (NSVT).<sup>173</sup> Carroll and co-workers at the Research Triangle Institute have reported a number of JDtic analogs to improve properties such as blood-brain barrier penetration, onset, and duration of action that characterize JDtic.<sup>134, 174</sup> Extensive modification of JDtic has been pursued to improve the drug-like properties of JDtic, but with limited success in obtaining analogs that retain the affinity and selectivity of JDtic.

In 2014 Bailey and co-workers reported a promising KOR antagonist, BU09059 (Figure 2.12), with a metabolically labile ethyl ester that retained the affinity and selectivity of JDtic and displayed improved pharmacodynamic properties.<sup>175</sup> Notably, BU09059 did not exhibit extended effects lasting weeks following single administration; reduced KOR antagonism was observed after 7 and 14 days. Further JDtic analogs to improve ADME properties have been reported by Perrio and co-workers who investigated O- and N-fluoroalkyl substitutions on the tetrahydroisoquinoline of JDtic.<sup>176</sup> N-Alkylation of the isoquinoline nitrogen retained affinity at KOR and displayed increased selectivity for KOR compared to JDtic;<sup>176</sup> however, functional and *in vivo* evaluation have yet to be reported.

Other scaffolds that have shown promise to provide selective KOR antagonists include biarylsulfonamides and aminobenzyloxyamides. The biarylsulfonamide PF-04455242 (Figure 2.11), developed by Pfizer, displayed a shorter duration of action than JDtic following *in vivo* evaluation in the warm water tail withdrawal assay and receptor occupancy studies.<sup>177-179</sup> PF-04455242 entered clinical trials<sup>180</sup> but was unfortunately withdrawn due to toxicological concerns in animals following a three month exposure to the compound.

CERC-501 (formerly LY2456302) is a potent aminobenzoyloxyarylamide KOR antagonist that was discovered by Eli Lilly while developing a radiotracer for receptor occupancy studies.<sup>181</sup> Following oral dosing, CERC-501 lowered self-administration of alcohol in animal models of chronic alcoholism and reduced immobility in animal models of depression. CERC-501 advanced into clinical trials for mood and anxiety spectrum disorders<sup>182</sup> as well as stress precipitated smoking lapse.<sup>183</sup>

Another KOR selective aminobenzoyloxyarylamide, AZ-MTAB (Figure 2.11), was developed by AstraZeneca following virtual screening and extensive SAR to improve KOR activity and selectivity.<sup>184,185</sup> AZ-MTAB dose-dependently inhibited diuresis induced by U50,488. Additionally, AZ-MTAB exhibited promising anxiolytic activity, similar to CERC-501, in the elevated plus-maze (EPM) model in rats.<sup>174</sup> Poor oral availability and hERG activity among other factors prevented development of AZ-MTAB.

### 2.3.2.2 Peptidic KOR selective antagonists

Peptidic KOR antagonists include linear and cyclic peptide analogs, the majority of which are analogs of the KOR endogenous ligand Dyn A. Dyn A-based KOR antagonists have been obtained following modifications in the N-terminus “message” sequence as well as in the C-terminal “address” sequence. These include dynantin, Pro<sup>3</sup> derivatives of Dyn A(1-11)NH<sub>2</sub>, [N,N-diallyl-Tyr<sup>1</sup>,D-Pro<sup>10</sup>]Dyn A(1-11), JVA-901 (venorphin), cyclodyn, arodyn, and zyklusin (Figure 2.13).<sup>33</sup> Cyclodyn, a cyclic analog based on JVA-901, is constrained in the “message” sequence, whereas zyklusin is constrained in the “address” sequence. Zyklusin and the acetylated dyn A derivative arodyn have displayed promising activity *in vivo*.<sup>136,186</sup>

*N,N*-diallyl-Tyr-Gly-Gly-Phe-Leu-Arg-Arg-Ile-Arg-D-Pro-Lys

[*N,N*-diallyl-Tyr<sup>1</sup>, D-Pro<sup>10</sup>]Dyn A(1-11)

Ac-Tyr-Lys-Trp-Trp-Leu-Arg-Arg-DAla-Arg-Pro-Lys-NH<sub>2</sub>

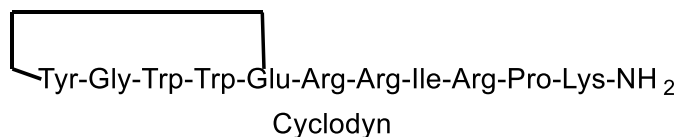
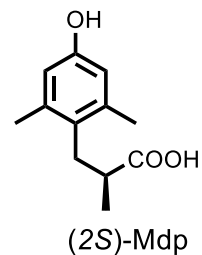
JVA 901 (Venorphin)

Tyr-Gly-D-Pro-Phe-Leu-Arg-Arg-Ile-Arg-Pro-Lys-NH<sub>2</sub>

[D-Pro<sup>3</sup>]Dyn A(1-11)NH<sub>2</sub>

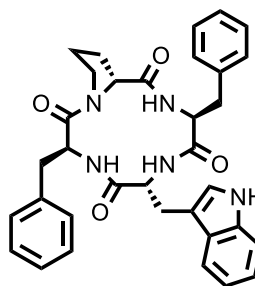
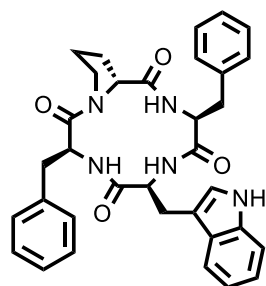
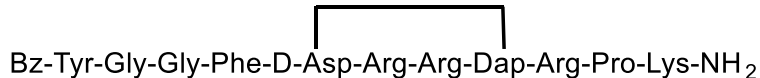
(2*S*)-Mdp-Gly-Gly-Phe-Leu-Arg-Arg-Ile-Arg-Pro-Lys-NH<sub>2</sub>

[(2*S*)-Mdp<sup>1</sup>]Dyn A(1-11)NH<sub>2</sub> (Dynantin)



Ac-Phe-Phe-Phe-Arg-Leu-Arg-Arg-D-Ala-Arg-Pro-Lys-NH<sub>2</sub>

Arodyn



\* Mixed agonist/antagonist

Figure 2.13 Peptidic KOR antagonists.

Arodyn (Figure 2.13) is a potent and selective KOR antagonist developed in the Aldrich laboratory that dose dependently antagonized U50,488 *in vivo* and attenuated stress-induced reinstatement, but not cocaine primed drug seeking behavior in the CPP assay.<sup>187, 188</sup> The Aldrich

laboratory reported initial SAR study of arodyn including alanine scan analogs, and N-MePhe<sup>1</sup> derivatives.<sup>189</sup> Alanine scan results suggested that while basic residues Arg<sup>6</sup> and Arg<sup>7</sup> were important for binding to KOR, basic residues in positions 4, 9 and 11 also made contributions to binding affinity.<sup>190</sup> Among these initial arodyn analogs [NMePhe<sup>1</sup>]arodyn displayed the highest KOR affinity ( $K_i=4.56$  nM) and higher selectivity ( $\kappa/\mu/\delta=1/1100/>2170$ ) compared to arodyn ( $\kappa/\mu/\delta=1/174/583$ ). Interestingly, [Tyr<sup>1</sup>]arodyn displayed inverse agonist activity. Cyclic derivatives of arodyn were prepared using ring closing metathesis between Tyr(All) residues in the “message” sequence.<sup>191</sup> Despite their reduced selectivities towards MOR and DOR compared to arodyn, the cyclic analogs displayed potent KOR antagonism ( $K_B=3.25$  and  $27.2$  nM) comparable to arodyn ( $K_B=17$  nM).

Zyklophin (Figure 2.13), also developed in the Aldrich laboratory, is a potent ( $K_i=30$  nM) and selective ( $\kappa/\mu/\delta=1/194/>330$ ) KOR antagonist cyclized between the 5<sup>th</sup> and 8<sup>th</sup> residues.<sup>192</sup> In contrast to arodyn, which is rapidly metabolized, the metabolic stability of zyklophin facilitated systemic administration.<sup>136</sup> Importantly, systemically administered zyklophin antagonized centrally administered KOR agonist U50488 and displayed short-acting antagonism lasting 12-18h, in contrast to long-lasting antagonism of prototypical KOR antagonist norBNI and JDtic. Similar to arodyn, zyklophin prevented stress-induced reinstatement of cocaine abuse. SAR analysis of zyklophin revealed that Arg<sup>7</sup> is important for KOR antagonism, and residues Phe<sup>4</sup> and Arg<sup>6</sup> contribute to KOR binding affinity.<sup>193</sup> Interestingly however, Tyr<sup>1</sup> was not important for KOR binding, unlike in Dyn (1–11)NH<sub>2</sub>. Variations in the lactam ring size resulted in 2-4-fold variations in KOR affinity and larger ring sizes did not lead to considerable losses affinity. Additionally, N-terminally substituted analogs were evaluated and were well tolerated at KOR; *N*-phenethyl and *N*-cyclopropylmethyl derivatives exhibited the highest KOR affinity and had higher



KOR vs. MOR selectivities compared to zyklophin. Following Dyn A(1-13) stimulation in the [<sup>35</sup>S]GTPγS assay, the *N*-benzyl-Phe<sup>1</sup> and *N*-cyclopropylmethyl analogs displayed KOR antagonist potencies that were 11- and 28- fold respectively more potent than zyklophin.

The natural product CJ-15,208, (*cyclo*[Phe-D-Pro-Phe-Trp]), which is unrelated to Dyn A, has displayed KOR antagonism *in vitro* (Figure 2.13). The macrocyclic tetrapeptide CJ-15,208, isolated from the fungus *Ctenomyces serratus*, displayed moderate selectivity for the KOR ( $\kappa/\mu/\delta=1/6/55$ ) and displayed KOR antagonism in a smooth muscle assay.<sup>194</sup> Interestingly, Aldrich and coworkers synthesized CJ-15,208 and its D-Trp isomer and demonstrated that CJ-15,208 exhibits mixed agonist/antagonist activity *in vivo*.<sup>195</sup> Further, CJ-15,208 inhibited cocaine and stress-induced reinstatement following oral administration in a dose and time dependent manner.<sup>196</sup>

The D-Trp isomer of CJ-15,208 displayed short acting KOR selective antagonism lasting less than 18 h and minimal MOR agonism following intracerebrovascular administration.<sup>195</sup> Short-acting KOR antagonism was also observed following oral administration.<sup>196</sup> The D-Trp isomer inhibited stress- but not cocaine-induced reinstatement of extinguished cocaine seeking behavior, consistent with its KOR antagonist activity.<sup>195, 196</sup> The promising oral activity of CJ-15,208 and its D-Trp isomer highlights their therapeutic potential in drug abuse treatments, particularly in relapse. Furthermore, the finite duration of action adds to their promise as lead compounds for substance abuse treatments.

SAR studies on CJ-15,208 and [D-Trp]CJ-15,208 have been pursued by Aldrich and coworkers as well as Dolle and co-workers.<sup>197-199</sup> In an *in vivo* antinociceptive assay, the alanine scan of CJ-15,208 analogs displayed KOR antagonist behavior but also displayed MOR agonist activity in contrast to the parent peptide.<sup>198</sup> Similarly, alanine scan analogs of [D-Trp]CJ-15,208 displayed

activity that was different from the parent peptide, exhibiting potent agonist activity *in vivo*.<sup>199</sup> Notably, treatment with one analog that displayed KOR agonist and antagonist behavior *in vivo* prevented both stress- and cocaine induced reinstatement of cocaine seeking in a time-dependent manner in a CPP assay. KOR selective CJ-15,208 and [D-Trp]CJ-15,208 analogs have been elusive; nevertheless, the unusual behavior of these macrocyclic peptides and their analogs presents an intriguing area for further study in peptide-based analgesics or substance abuse therapy.

## 2.4 Conclusions

Increasing studies since the discovery of opioid receptors have led to the discovery of selective ligands to further understand opioid pharmacology. KOR ligands have gathered increasing interest due to their potential therapeutic effects in pain, drug addiction, and mood disorders. Several KOR ligands with mixed activity involving KOR are used in the clinic, while others are in clinical development. Extensive studies on analogs of Dyn A, the endogenous peptidic ligand for KOR, have resulted in the identification of various ligands, both agonists and antagonists. Both non-peptidic and peptidic KOR antagonists are being developed for potential therapeutic application in substance abuse and mood disorders. While classical non-peptidic KOR antagonists have a long duration of action, peptidic ligands are promising due to their finite duration of action. Peptides can however be rapidly metabolized leading to challenges in their delivery. To this effect, a variety of modifications, including the incorporation of D-amino acid residues and cyclization, have been applied to peptides to enhance their potential therapeutic utility.

## 2.5 References

1. Aldrich, J. V.; Vigil-Cruz, S. C.; Abraham, D. J. Narcotic Analgesics. In *Burger's Medicinal Chemistry and Drug Discovery*, John Wiley & Sons, Inc.: 2003.

2. Waldhoer, M.; Bartlett, S. E.; Whistler, J. L. Opioid receptors. *Annu Rev Biochem* **2004**, *73*, 953-990.
3. Trang, T.; Al-Hasani, R.; Salvemini, D.; Salter, M. W.; Gutstein, H.; Cahill, C. M. Pain and Poppies: The Good, the Bad, and the Ugly of Opioid Analgesics. *J Neurosci* **2015**, *35*, 13879-13888.
4. Brownstein, M. J. A brief history of opiates, opioid peptides, and opioid receptors. *Proc Natl Acad Sci U.S.A.* **1993**, *90*, 5391-5393.
5. Pasternak, G. W.; Pan, Y.-X. Mu Opioids and Their Receptors: Evolution of a Concept. *Pharmacol Rev* **2013**, *65*, 1257-1317.
6. Scott, C. C.; Chen, K. K. The action of 1,1-diphenyl-1 (dimethylaminoisopropyl) butanone-2, a potent analgesic agent. *J Pharmacol Exp Ther* **1946**, *87*, 63-71.
7. Beckett, A. H.; Casy, A. F. Synthetic Analgesics: Stereochemical Considerations. *J Pharm Pharmacol* **1954**, *6*, 986-1001.
8. Portoghese, P. S. Stereochemical factors and receptor interactions associated with narcotic analgesics. *J Pharm Sci* **1966**, *55*, 865-887.
9. Martin, W. R. Opioid antagonists. *Pharmacol Rev* **1967**, *19*, 463-521.
10. Pert, C. B.; Snyder, S. H. Opiate receptor: demonstration in nervous tissue. *Science* **1973**, *179*, 1011-1014.
11. Lord, J. A. H.; Waterfield, A. A.; Hughes, J.; Kosterlitz, H. W. Endogenous opioid peptides: multiple agonists and receptors. *Nature* **1977**, *267*, 495-499.
12. Chang, K. J.; Cuatrecasas, P. Multiple opiate receptors. Enkephalins and morphine bind to receptors of different specificity. *J Biol Chem* **1979**, *254*, 2610-2618.
13. Chang, K. J.; Cooper, B. R.; Hazum, E.; Cuatrecasas, P. Multiple opiate receptors: different regional distribution in the brain and differential binding of opiates and opioid peptides. *Mol Pharmacol* **1979**, *16*, 91-104.
14. Martin, W. R.; Eades, C. G.; Thompson, J. A.; Huppler, R. E.; Gilbert, P. E. The effects of morphine- and nalorphine- like drugs in the nondependent and morphine-dependent chronic spinal dog. *J Pharmacol Exp Ther* **1976**, *197*, 517-532.
15. Tam, S. W. Naloxone-inaccessible sigma receptor in rat central nervous system. *Proc Natl Acad Sci U.S.A.* **1983**, *80*, 6703-6707.

16. Zukin, S. R.; Tempel, A.; Gardner, E. L.; Zukin, R. S. Interaction of [3H](–)-SKF-10,047 with Brain  $\sigma$  Receptors: Characterization and Autoradiographic Visualization. *J Neurochem* **1986**, 46, 1032-1041.
17. Hughes, J.; Smith, T. W.; Kosterlitz, H. W.; Fothergill, L. A.; Morgan, B. A.; Morris, H. R. Identification of two related pentapeptides from the brain with potent opiate agonist activity. *Nature* **1975**, 258, 577-580.
18. Lord, J. A.; Waterfield, A. A.; Hughes, J.; Kosterlitz, H. W. Endogenous opioid peptides: multiple agonists and receptors. *Nature* **1977**, 267, 495-499.
19. Simantov, R.; Snyder, S. H. Morphine-like peptides in mammalian brain: isolation, structure elucidation, and interactions with the opiate receptor. *Proc Natl Acad Sci* **1976**, 73, 2515-2519.
20. Pasternak, G. W.; Simantov, R.; Snyder, S. H. Characterization of an endogenous morphine-like factor(enkephalin) in mammalian brain. *Mol Pharmacol* **1976**, 12, 504-513.
21. Loh, H. H.; Tseng, L. F.; Wei, E.; Li, C. H. beta-endorphin is a potent analgesic agent. *Proc Natl Acad Sci U.S.A.* **1976**, 73, 2895-2898.
22. Goldstein, A.; Tachibana, S.; Lowney, L. I.; Hunkapiller, M.; Hood, L. Dynorphin-(1-13), an extraordinarily potent opioid peptide. *Proc Natl Acad Sci* **1979**, 76, 6666-6670.
23. Zadina, J. E.; Hackler, L.; Ge, L. J.; Kastin, A. J. A potent and selective endogenous agonist for the mu-opiate receptor. *Nature* **1997**, 386, 499-502.
24. Kieffer, B. L.; Befort, K.; Gaveriaux-Ruff, C.; Hirth, C. G. The delta-opioid receptor: isolation of a cDNA by expression cloning and pharmacological characterization. *Proc Natl Acad Sci* **1992**, 89, 12048-12052.
25. Chen, Y.; Mestek, A.; Liu, J.; Hurley, J. A.; Yu, L. Molecular cloning and functional expression of a mu-opioid receptor from rat brain. *Mol Pharmacol* **1993**, 44, 8-12.
26. Wang, J. B.; Imai, Y.; Eppler, C. M.; Gregor, P.; Spivak, C. E.; Uhl, G. R. mu opiate receptor: cDNA cloning and expression. *Proc Natl Acad Sci* **1993**, 90, 10230-10234.
27. Evans, C. J.; Keith, D. E., Jr.; Morrison, H.; Magendzo, K.; Edwards, R. H. Cloning of a delta opioid receptor by functional expression. *Science* **1992**, 258, 1952-1955.
28. Zhu, J.; Chen, C.; Xue, J. C.; Kunapuli, S.; DeRiel, J. K.; Liu-Chen, L. Y. Cloning of a human kappa opioid receptor from the brain. *Life Sci* **1995**, 56, P1201-207.

29. Meunier, J.-C.; Mollereau, C.; Toll, L.; Suaudeau, C.; Moisand, C.; Alvinerie, P.; Butour, J.-L.; Guillemot, J.-C.; Ferrara, P.; Monsarrat, B.; Mazarguil, H.; Vassart, G.; Parmentier, M.; Costentin, J. Isolation and structure of the endogenous agonist of opioid receptor-like ORL1 receptor. *Nature* **1995**, *377*, 532-535.
30. Reinscheid, R. K.; Nothacker, H. P.; Bourson, A.; Ardati, A.; Henningsen, R. A.; Buzow, J. R.; Grandy, D. K.; Langen, H.; Monsma, F. J., Jr.; Civelli, O. Orphanin FQ: a neuropeptide that activates an opioidlike G protein-coupled receptor. *Science* **1995**, *270*, 792-794.
31. Thompson, A. A.; Liu, W.; Chun, E.; Katritch, V.; Wu, H.; Vardy, E.; Huang, X.-P.; Trapella, C.; Guerrini, R.; Calo, G.; Roth, B. L.; Cherezov, V.; Stevens, R. C. Structure of the nociceptin/orphanin FQ receptor in complex with a peptide mimetic. *Nature* **2012**, *485*, 395-399.
32. McLeod, D. C.; Reitz, J. A. Alfentanil in Anesthesia and Analgesia. *Drug Intell Clin Pharm* **1986**, *20*, 335-341.
33. Aldrich, J. V.; McLaughlin, J. P. Peptide kappa opioid receptor ligands: potential for drug development. *AAPS J* **2009**, *11*, 312-322.
34. Kamimura, K.; Yokoo, T.; Kamimura, H.; Sakamaki, A.; Abe, S.; Tsuchiya, A.; Takamura, M.; Kawai, H.; Yamagiwa, S.; Terai, S. Long-term efficacy and safety of nalfurafine hydrochloride on pruritus in chronic liver disease patients: Patient-reported outcome based analyses. *PloS one* **2017**, *12*, e0178991.
35. Dum, J. E.; Herz, A. In vivo receptor binding of the opiate partial agonist, buprenorphine, correlated with its agonistic and antagonistic actions. *Br J Pharmacol* **1981**, *74*, 627-633.
36. Romero, D. V.; Partilla, J. S.; Zheng, Q. X.; Heyliger, S. O.; Ni, Q.; Rice, K. C.; Lai, J.; Rothman, R. B. Opioid peptide receptor studies. 12. Buprenorphine is a potent and selective mu/kappa antagonist in the [35S]-GTP-gamma-S functional binding assay. *Synapse* **1999**, *34*, 83-94.
37. Bloms-Funke, P.; Gillen, C.; Schuettler, A. J.; Wnendt, S. Agonistic effects of the opioid buprenorphine on the nociceptin/OFQ receptor. *Peptides* **2000**, *21*, 1141-1146.
38. Walsh, S. L.; Preston, K. L.; Stitzer, M. L.; Cone, E. J.; Bigelow, G. E. Clinical pharmacology of buprenorphine: ceiling effects at high doses. *Clin Pharmacol Ther* **1994**, *55*, 569-580.

39. Orman, J. S.; Keating, G. M. Spotlight on buprenorphine/naloxone in the treatment of opioid dependence. *CNS drugs* **2009**, *23*, 899-902.
40. Rothman, R. B.; Gorelick, D. A.; Heishman, S. J.; Eichmiller, P. R.; Hill, B. H.; Norbeck, J.; Liberto, J. G. An open-label study of a functional opioid kappa antagonist in the treatment of opioid dependence. *J Subst Abuse Treat* **2000**, *18*, 277-281.
41. Gerra, G.; Fantoma, A.; Zaimovic, A. Naltrexone and buprenorphine combination in the treatment of opioid dependence. *J Psychopharmacol* **2006**, *20*, 806-814.
42. Ling, W.; Hillhouse, M. P.; Saxon, A. J.; Mooney, L. J.; Thomas, C. M.; Ang, A.; Matthews, A. G.; Hasson, A.; Annon, J.; Sparenborg, S.; Liu, D. S.; McCormack, J.; Church, S.; Swafford, W.; Drexler, K.; Schuman, C.; Ross, S.; Wiest, K.; Korthis, P. T.; Lawson, W.; Brigham, G. S.; Knox, P. C.; Dawes, M.; Rotrosen, J. Buprenorphine + naloxone plus naltrexone for the treatment of cocaine dependence: the Cocaine Use Reduction with Buprenorphine (CURB) study. *Addiction* **2016**, *111*, 1416-1427.
43. Dahan, A.; Aarts, L.; Smith, T. W. Incidence, Reversal, and Prevention of Opioid-induced Respiratory Depression. *Anesthesiology* **2010**, *112*, 226-238.
44. Bader, S.; Dürk, T.; Becker, G. Methyl naltrexone for the treatment of opioid-induced constipation. *Expert Rev Gastroenterol Hepatol* **2013**, *7*, 13-26.
45. Tack, J.; Lappalainen, J.; Diva, U.; Tummala, R.; Sostek, M. Efficacy and safety of naloxegol in patients with opioid-induced constipation and laxative-inadequate response. *United European Gastroenterol J* **2015**, *3*, 471-480.
46. Sultan, S.; Coles, B.; Dahm, P. Alvimopan for recovery of bowel function after radical cystectomy. *Cochrane Database Syst Rev* **2017**, *5*, Cd012111.
47. Grant, J. E.; Kim, S. W.; Hartman, B. K. A double-blind, placebo-controlled study of the opiate antagonist naltrexone in the treatment of pathological gambling urges. *J Clin Psychiatry* **2008**, *69*, 783-789.
48. Soyka, M.; Friede, M.; Schnitker, J. Comparing Nalmefene and Naltrexone in Alcohol Dependence: Are there any Differences? Results from an Indirect Meta-Analysis. *Pharmacopsychiatry* **2016**, *49*, 66-75.
49. Soyka, M. Nalmefene for the treatment of alcohol use disorders: recent data and clinical potential. *Expert Opin Pharmacother* **2016**, *17*, 619-626.

50. Lagerstrom, M. C.; Schioth, H. B. Structural diversity of G protein-coupled receptors and significance for drug discovery. *Nat Rev Drug Discov* **2008**, *7*, 339-357.
51. Fredriksson, R.; Lagerstrom, M. C.; Lundin, L. G.; Schioth, H. B. The G-protein-coupled receptors in the human genome form five main families. Phylogenetic analysis, paralogon groups, and fingerprints. *Mol Pharmacol* **2003**, *63*, 1256-1272.
52. Rask-Andersen, M.; Almén, M. S.; Schiöth, H. B. Trends in the exploitation of novel drug targets. *Nat Rev Drug Discov* **2011**, *10*, 579-590.
53. Gether, U. Uncovering molecular mechanisms involved in activation of G protein-coupled receptors. *Endocr Rev* **2000**, *21*, 90-113.
54. Hepler, J. R.; Gilman, A. G. G proteins. *Trends Biochem Sci* **1992**, *17*, 383-387.
55. Oldham, W. M.; Hamm, H. E. Heterotrimeric G protein activation by G-protein-coupled receptors. *Nat Rev Mol Cell Biol* **2008**, *9*, 60-71.
56. Satoh, M.; Minami, M. Molecular pharmacology of the opioid receptors. *Pharmacol Ther* **1995**, *68*, 343-364.
57. Wickman, K. D.; Clapham, D. E. G-protein regulation of ion channels. *Curr Opin Neurobiol* **1995**, *5*, 278-285.
58. Bourne, H. R.; Sanders, D. A.; McCormick, F. The GTPase superfamily: conserved structure and molecular mechanism. *Nature* **1991**, *349*, 117-127.
59. Hamm, H. E. The Many Faces of G Protein Signaling. *J Biol Chem* **1998**, *273*, 669-672.
60. Lefkowitz, R. J.; Shenoy, S. K. Transduction of Receptor Signals by  $\beta$ -Arrestins. *Science* **2005**, *308*, 512-517.
61. Lu, Z.; Xu, S. ERK1/2 MAP kinases in cell survival and apoptosis. *IUBMB Life* **2006**, *58*, 621-631.
62. Bruchas, M. R.; Chavkin, C. Kinase cascades and ligand-directed signaling at the kappa opioid receptor. *Psychopharmacology* **2010**, *210*, 137-147.
63. Ehrlich, J. M.; Messinger, D. I.; Knakal, C. R.; Kuhar, J. R.; Schattauer, S. S.; Bruchas, M. R.; Zweifel, L. S.; Kieffer, B. L.; Phillips, P. E.; Chavkin, C. Kappa Opioid Receptor-Induced Aversion Requires p38 MAPK Activation in VTA Dopamine Neurons. *J Neurosci* **2015**, *35*, 12917-12931.

64. Bruchas, M. R.; Yang, T.; Schreiber, S.; DeFino, M.; Kwan, S. C.; Li, S.; Chavkin, C. Long-acting  $\kappa$  Opioid Antagonists Disrupt Receptor Signaling and Produce Noncompetitive Effects by Activating c-Jun N-terminal Kinase. *J Biol Chem* **2007**, 282, 29803-29811.
65. Zhu, J.; Luo, L. Y.; Li, J. G.; Chen, C.; Liu-Chen, L. Y. Activation of the cloned human kappa opioid receptor by agonists enhances [35S]GTPgammaS binding to membranes: determination of potencies and efficacies of ligands. *J Pharmacol Exp Ther* **1997**, 282, 676-684.
66. Blume, A. J.; Lichtshtein, D.; Boone, G. Coupling of opiate receptors to adenylate cyclase: requirement for Na<sup>+</sup> and GTP. *Proc Natl Acad Sci* **1979**, 76, 5626-5630.
67. Wang, J. B.; Johnson, P. S.; Wu, J. M.; Wang, W. F.; Uhl, G. R. Human kappa opiate receptor second extracellular loop elevates dynorphin's affinity for human mu/kappa chimeras. *J Biol Chem* **1994**, 269, 25966-25969.
68. Meng, F.; Hoversten, M. T.; Thompson, R. C.; Taylor, L.; Watson, S. J.; Akil, H. A chimeric study of the molecular basis of affinity and selectivity of the kappa and the delta opioid receptors. Potential role of extracellular domains. *J Biol Chem* **1995**, 270, 12730-12736.
69. Bjorneras, J.; Kurnik, M.; Oliveberg, M.; Graslund, A.; Maler, L.; Danielsson, J. Direct detection of neuropeptide dynorphin A binding to the second extracellular loop of the kappa opioid receptor using a soluble protein scaffold. *Febs J* **2014**, 281, 814-824.
70. Seki, T.; Minami, M.; Nakagawa, T.; Ienaga, Y.; Morisada, A.; Satoh, M. DAMGO recognizes four residues in the third extracellular loop to discriminate between mu- and kappa-opioid receptors. *Eur J Pharmacol* **1998**, 350, 301-310.
71. Michino, M.; Beuming, T.; Donthamsetti, P.; Newman, A. H.; Javitch, J. A.; Shi, L. What Can Crystal Structures of Aminergic Receptors Tell Us about Designing Subtype-Selective Ligands? *Pharmacol Rev* **2015**, 67, 198-213.
72. Granier, S.; Manglik, A.; Kruse, A. C.; Kobilka, T. S.; Thian, F. S.; Weis, W. I.; Kobilka, B. K. Structure of the  $\delta$ -opioid receptor bound to naltrindole. *Nature* **2012**, 485, 400-404.
73. Manglik, A.; Kruse, A. C.; Kobilka, T. S.; Thian, F. S.; Mathiesen, J. M.; Sunahara, R. K.; Pardo, L.; Weis, W. I.; Kobilka, B. K.; Granier, S. Crystal structure of the  $\mu$ -opioid receptor bound to a morphinan antagonist. *Nature* **2012**, 485, 321-326.
74. Wu, H.; Wacker, D.; Mileni, M.; Katritch, V.; Han, G. W.; Vardy, E.; Liu, W.; Thompson, A. A.; Huang, X.-P.; Carroll, F. I.; Mascarella, S. W.; Westkaemper, R. B.; Mosier,



P. D.; Roth, B. L.; Cherezov, V.; Stevens, R. C. Structure of the human kappa-opioid receptor in complex with JDTic. *Nature* **2012**, 485, 327-332.

75. Cox, B. M. Recent Developments in the Study of Opioid Receptors. *Mol Pharmacol* **2013**, 83, 723.

76. Massotte, D. In vivo opioid receptor heteromerization: where do we stand? *Br J Pharmacol* **2015**, 172, 420-434.

77. Filizola, M.; Devi, L. A. Grand opening of structure-guided design for novel opioids. *Trends Pharmacol. Sci.* **2013**, 34, 6-12.

78. Ballesteros, J. A.; Weinstein, H. Integrated methods for the construction of three-dimensional models and computational probing of structure-function relations in G protein-coupled receptors. In *Methods in Neurosciences*, Stuart, C. S., Ed. Academic Press: 1995; Vol. Volume 25, pp 366-428.

79. Kane, B. E.; Svensson, B.; Ferguson, D. M. Molecular Recognition of Opioid Receptor Ligands. In *Drug Addiction: From Basic Research to Therapy*, Rapaka, R. S.; Sadée, W., Eds. Springer New York: New York, NY, 2008; pp 585-608.

80. Martinez-Mayorga, K.; Byler, K. G.; Yongye, A. B.; Giulianotti, M. A.; Dooley, C. T.; Houghten, R. A. Ligand/kappa-Opioid Receptor Interactions: Insights From the X-ray Crystal Structure. *Eur J Med Chem* **2013**, 66, 114-121.

81. Vardy, E.; Mosier, P. D.; Frankowski, K. J.; Wu, H.; Katritch, V.; Westkaemper, R. B.; Aubé, J.; Stevens, R. C.; Roth, B. L. Chemotype-selective Modes of Action of  $\kappa$ -Opioid Receptor Agonists. *J Biol Chem* **2013**, 288, 34470-34483.

82. Bruchas, M. R.; Roth, B. L. New Technologies for Elucidating Opioid Receptor Function. *Trends Pharmacol Sci* **2016**, 37, 279-289.

83. Vardy, E.; Robinson, J. E.; Li, C.; Olsen, R. H.; DiBerto, J. F.; Giguere, P. M.; Sassano, F. M.; Huang, X. P.; Zhu, H.; Urban, D. J.; White, K. L.; Rittiner, J. E.; Crowley, N. A.; Pleil, K. E.; Mazzone, C. M.; Mosier, P. D.; Song, J.; Kash, T. L.; Malanga, C. J.; Krashes, M. J.; Roth, B. L. A New DREADD Facilitates the Multiplexed Chemogenetic Interrogation of Behavior. *Neuron* **2015**, 86, 936-946.

84. Marchant, N. J.; Whitaker, L. R.; Bossert, J. M.; Harvey, B. K.; Hope, B. T.; Kaganovsky, K.; Adhikary, S.; Prisinzano, T. E.; Vardy, E.; Roth, B. L.; Shaham, Y. Behavioral

and Physiological Effects of a Novel Kappa-Opioid Receptor-Based DREADD in Rats.

*Neuropsychopharmacology* **2016**, 41, 402-409.

85. Che, T.; Majumdar, S.; Zaidi, S. A.; Ondachi, P.; McCorvy, J. D.; Wang, S.; Mosier, P. D.; Uprety, R.; Vardy, E.; Krumm, B. E.; Han, G. W.; Lee, M.-Y.; Pardon, E.; Steyaert, J.; Huang, X.-P.; Strachan, R. T.; Tribo, A. R.; Pasternak, G. W.; Carroll, F. I.; Stevens, R. C.; Cherezov, V.; Katritch, V.; Wacker, D.; Roth, B. L. Structure of the Nanobody-Stabilized Active State of the Kappa Opioid Receptor. *Cell* **172**, 55-67

86. Huang, W.; Manglik, A.; Venkatakrisnan, A. J.; Laeremans, T.; Feinberg, E. N.; Sanborn, A. L.; Kato, H. E.; Livingston, K. E.; Thorsen, T. S.; Kling, R. C.; Granier, S.; Gmeiner, P.; Husbands, S. M.; Traynor, J. R.; Weis, W. I.; Steyaert, J.; Dror, R. O.; Kobilka, B. K. Structural insights into mu-opioid receptor activation. *Nature* **2015**, 524, 315-321.

87. Fenalti, G.; Giguere, P. M.; Katritch, V.; Huang, X.-P.; Thompson, A. A.; Cherezov, V.; Roth, B. L.; Stevens, R. C. Molecular control of delta-opioid receptor signalling. *Nature* **2014**, 506, 191-196.

88. Fenalti, G.; Zatsopin, N. A.; Betti, C.; Giguere, P.; Han, G. W.; Ishchenko, A.; Liu, W.; Guillemyn, K.; Zhang, H.; James, D.; Wang, D.; Weierstall, U.; Spence, J. C. H.; Boutet, S.; Messerschmidt, M.; Williams, G. J.; Gati, C.; Yefanov, O. M.; White, T. A.; Oberthuer, D.; Metz, M.; Yoon, C. H.; Barty, A.; Chapman, H. N.; Basu, S.; Coe, J.; Conrad, C. E.; Fromme, R.; Fromme, P.; Tourwé, D.; Schiller, P. W.; Roth, B. L.; Ballet, S.; Katritch, V.; Stevens, R. C.; Cherezov, V. Structural basis for bifunctional peptide recognition at human  $\delta$ -opioid receptor. *Nat Struct Mol Biol* **2015**, 22, 265-268.

89. O'Connor, C.; White, K. L.; Doncescu, N.; Didenko, T.; Roth, B. L.; Czaplicki, G.; Stevens, R. C.; Wüthrich, K.; Milon, A. NMR structure and dynamics of the agonist dynorphin peptide bound to the human kappa opioid receptor. *Proc Natl Acad Sci* **2015**, 112, 11852-11857.

90. Pert, C. B.; Pasternak, G.; Snyder, S. H. Opiate agonists and antagonists discriminated by receptor binding in brain. *Science* **1973**, 182, 1359-1361.

91. Daga, P. R.; Polgar, W. E.; Zaveri, N. T. Structure-based virtual screening of the nociceptin receptor: hybrid docking and shape-based approaches for improved hit identification. *J Chem Inf Model* **2014**, 54, 2732-2743.

92. Kaserer, T.; Lantero, A.; Schmidhammer, H.; Spetea, M.; Schuster, D.  $\mu$  Opioid receptor: novel antagonists and structural modeling. *Sci Rep* **2016**, *6*, 21548.
93. Negri, A.; Rives, M. L.; Caspers, M. J.; Prisinzano, T. E.; Javitch, J. A.; Filizola, M. Discovery of a novel selective kappa-opioid receptor agonist using crystal structure-based virtual screening. *J Chem Inf Model* **2013**, *53*, 521-526.
94. Urban, J. D.; Clarke, W. P.; von Zastrow, M.; Nichols, D. E.; Kobilka, B.; Weinstein, H.; Javitch, J. A.; Roth, B. L.; Christopoulos, A.; Sexton, P. M.; Miller, K. J.; Spedding, M.; Mailman, R. B. Functional Selectivity and Classical Concepts of Quantitative Pharmacology. *J Pharm Exp Ther* **2007**, *320*, 1-13.
95. White, K. L.; Scopton, A. P.; Rives, M.-L.; Bikbulatov, R. V.; Polepally, P. R.; Brown, P. J.; Kenakin, T.; Javitch, J. A.; Zjawiony, J. K.; Roth, B. L. Identification of Novel Functionally Selective Kappa Opioid Receptor Scaffolds. *Mol Pharmacol* **2014**, *85*, 83-90.
96. DeLander, G. E.; Portoghese, P. S.; Takemori, A. E. Role of spinal mu opioid receptors in the development of morphine tolerance and dependence. *J Pharmacol Exp Ther* **1984**, *231*, 91-96.
97. Collin, E.; Cesselin, F. Neurobiological mechanisms of opioid tolerance and dependence. *Clin Neuropharmacol* **1991**, *14*, 465-488.
98. Williams, J. T.; Ingram, S. L.; Henderson, G.; Chavkin, C.; von Zastrow, M.; Schulz, S.; Koch, T.; Evans, C. J.; Christie, M. J. Regulation of mu-opioid receptors: desensitization, phosphorylation, internalization, and tolerance. *Pharmacol Rev* **2013**, *65*, 223-254.
99. Bohn, L. M.; Lefkowitz, R. J.; Gainetdinov, R. R.; Peppel, K.; Caron, M. G.; Lin, F. T. Enhanced morphine analgesia in mice lacking beta-arrestin 2. *Science* **1999**, *286*, 2495-2498.
100. Bohn, L. M.; Gainetdinov, R. R.; Lin, F.-T.; Lefkowitz, R. J.; Caron, M. G. Mu-Opioid receptor desensitization by Beta-arrestin-2 determines morphine tolerance but not dependence. *Nature* **2000**, *408*, 720-723.
101. Gintzler, A. R.; Chakrabarti, S. Opioid tolerance and the emergence of new opioid receptor-coupled signaling. *Mol Neurobiol* **2000**, *21*, 21-33.
102. Violin, J. D.; Lefkowitz, R. J. Beta-arrestin-biased ligands at seven-transmembrane receptors. *Trends Pharmacol Sci* **2007**, *28*, 416-422.
103. Luttrell, L. M.; Lefkowitz, R. J. The role of  $\beta$ -arrestins in the termination and transduction of G-protein-coupled receptor signals. *J Cell Sci* **2002**, *115*, 455-465.

104. Rajagopal, S.; Rajagopal, K.; Lefkowitz, R. J. Teaching old receptors new tricks: biasing seven-transmembrane receptors. *Nat Rev Drug Discov* **2010**, *9*, 373-386.
105. Correll, C. C.; McKittrick, B. A. Biased Ligand Modulation of Seven Transmembrane Receptors (7TMRs): Functional Implications for Drug Discovery. *J Med Chem* **2014**, *57*, 6887-6896.
106. Shukla, A. K.; Violin, J. D.; Whalen, E. J.; Gesty-Palmer, D.; Shenoy, S. K.; Lefkowitz, R. J. Distinct conformational changes in beta-arrestin report biased agonism at seven-transmembrane receptors. *Proc Natl Acad Sci* **2008**, *105*, 9988-9993.
107. Reiter, E.; Ahn, S.; Shukla, A. K.; Lefkowitz, R. J. Molecular mechanism of beta-arrestin-biased agonism at seven-transmembrane receptors. *Annu Rev Pharmacol Toxicol* **2012**, *52*, 179-197.
108. Correll, C. C.; McKittrick, B. A. Biased ligand modulation of seven transmembrane receptors (7TMRs): functional implications for drug discovery. *J Med Chem* **2014**, *57*, 6887-6896.
109. Schmid, C. L.; Streicher, J. M.; Groer, C. E.; Munro, T. A.; Zhou, L.; Bohn, L. M. Functional Selectivity of 6'-Guanidinotrindole (6'-GNTI) at  $\kappa$ -Opioid Receptors in Striatal Neurons. *J Biol Chem* **2013**, *288*, 22387-22398.
110. Crowley, R. S.; Riley, A. P.; Sherwood, A. M.; Groer, C. E.; Shivaperumal, N.; Biscaia, M.; Paton, K.; Schneider, S.; Provasi, D.; Kivell, B. M.; Filizola, M.; Prisinzano, T. E. Synthetic Studies of Neoclerodane Diterpenes from *Salvia divinorum*: Identification of a Potent and Centrally Acting  $\mu$  Opioid Analgesic with Reduced Abuse Liability. *J Med Chem* **2016**, *59*, 11027-11038.
111. Schneider, S.; Provasi, D.; Filizola, M. How Oliceridine (TRV-130) Binds and Stabilizes a  $\mu$ -Opioid Receptor Conformational State That Selectively Triggers G Protein Signaling Pathways. *Biochemistry* **2016**, *55*, 6456-6466.
112. Singla, N.; Minkowitz, H. S.; Soergel, D. G.; Burt, D. A.; Subach, R. A.; Salamea, M. Y.; Fossler, M. J.; Skobieranda, F. A randomized, Phase IIb study investigating oliceridine (TRV130), a novel  $\mu$ -receptor G-protein pathway selective ( $\mu$ -GPS) modulator, for the management of moderate to severe acute pain following abdominoplasty. *J Pain Res* **2017**, *10*, 2413-2424.

113. Walsh, S. L.; Geter-Douglas, B.; Strain, E. C.; Bigelow, G. E. Enadoline and Butorphanol: Evaluation of  $\kappa$ -Agonists on Cocaine Pharmacodynamics and Cocaine Self-Administration in Humans. *J Pharm Exp Ther* **2001**, 299, 147-158.
114. Pfeiffer, A.; Brantl, V.; Herz, A.; Emrich, H. Psychotomimesis mediated by kappa opiate receptors. *Science* **1986**, 233, 774-776.
115. McLennan, G. P.; Kiss, A.; Miyatake, M.; Belcheva, M. M.; Chambers, K. T.; Pozek, J. J.; Mohabbat, Y.; Moyer, R. A.; Bohn, L. M.; Coscia, C. J. Kappa opioids promote the proliferation of astrocytes via Gbetagamma and beta-arrestin 2-dependent MAPK-mediated pathways. *J Neurochem* **2008**, 107, 1753-1765.
116. Zhou, L.; Lovell, K. M.; Frankowski, K. J.; Slauson, S. R.; Phillips, A. M.; Streicher, J. M.; Stahl, E.; Schmid, C. L.; Hodder, P.; Madoux, F.; Cameron, M. D.; Prisinzano, T. E.; Aubé, J.; Bohn, L. M. Development of Functionally Selective, Small Molecule Agonists at Kappa Opioid Receptors. *J Biol Chem* **2013**, 288, 36703-36716.
117. Brust, T. F.; Morgenweck, J.; Kim, S. A.; Rose, J. H.; Locke, J. L.; Schmid, C. L.; Zhou, L.; Stahl, E. L.; Cameron, M. D.; Scarry, S. M.; Aubé, J.; Jones, S. R.; Martin, T. J.; Bohn, L. M. Biased agonists of the kappa opioid receptor suppress pain and itch without causing sedation or dysphoria. *Sci Signal* **2016**, 9, ra117
118. Simonin, F.; Gavériaux-Ruff, C.; Befort, K.; Matthes, H.; Lannes, B.; Micheletti, G.; Mattéi, M. G.; Charron, G.; Bloch, B.; Kieffer, B. kappa-Opioid receptor in humans: cDNA and genomic cloning, chromosomal assignment, functional expression, pharmacology, and expression pattern in the central nervous system. *Proc Natl Acad Sci U.S.A.* **1995**, 92, 7006-7010.
119. Shirayama, Y.; Ishida, H.; Iwata, M.; Hazama, G. I.; Kawahara, R.; Duman, R. S. Stress increases dynorphin immunoreactivity in limbic brain regions and dynorphin antagonism produces antidepressant-like effects. *J Neurochem* **2004**, 90, 1258-1268.
120. Yamamizu, K.; Hamada, Y.; Narita, M.  $\kappa$  Opioid receptor ligands regulate angiogenesis in development and in tumours. *Br J Pharmacol* **2015**, 172, 268-276.
121. Gekker, G.; Hu, S.; Wentland, M. P.; Bidlack, J. M.; Lokensgard, J. R.; Peterson, P. K.  $\kappa$ -Opioid Receptor Ligands Inhibit Cocaine-Induced HIV-1 Expression in Microglial Cells. *J Pharm Exp Ther* **2004**, 309, 600-606.

122. Vanderah, T. W. Delta and kappa opioid receptors as suitable drug targets for pain. *Clin J Pain* **2010**, 26 Suppl 10, S10-15.
123. Land, B. B.; Bruchas, M. R.; Schattaer, S.; Giardino, W. J.; Aita, M.; Messinger, D.; Hnasko, T. S.; Palmiter, R. D.; Chavkin, C. Activation of the kappa opioid receptor in the dorsal raphe nucleus mediates the aversive effects of stress and reinstates drug seeking. *Proc Natl Acad Sci* **2009**, 106, 19168-19173.
124. Shippenberg, T. S.; Herz, A. Differential effects of mu and kappa opioid systems on motivational processes. *NIDA Res Monogr* **1986**, 75, 563-566.
125. Spanagel, R.; Herz, A.; Shippenberg, T. S. Opposing tonically active endogenous opioid systems modulate the mesolimbic dopaminergic pathway. *Proc Natl Acad Sci* **1992**, 89, 2046-2050.
126. Nestler, E. J.; Carlezon, W. A., Jr. The mesolimbic dopamine reward circuit in depression. *Biol Psychiatry* **2006**, 59, 1151-1159.
127. Chefer, V. I.; Backman, C. M.; Gigante, E. D.; Shippenberg, T. S. Kappa opioid receptors on dopaminergic neurons are necessary for kappa-mediated place aversion. *Neuropsychopharmacology* **2013**, 38, 2623-2631.
128. del Rosario Capriles, N.; Cancela, L. M. Motivational effects mu- and kappa-opioid agonists following acute and chronic restraint stress: involvement of dopamine D(1) and D(2) receptors. *Behav Brain Res* **2002**, 132, 159-169.
129. Di Chiara, G.; Imperato, A. Drugs abused by humans preferentially increase synaptic dopamine concentrations in the mesolimbic system of freely moving rats. *Proc Natl Acad Sci* **1988**, 85, 5274-5278.
130. Wee, S.; Koob, G. F. The role of the dynorphin- $\kappa$  opioid system in the reinforcing effects of drugs of abuse. *Psychopharmacology* **2010**, 210, 121-135.
131. Aldrich, J. V.; Senadheera, S. N.; Ross, N. C.; Ganno, M. L.; Eans, S. O.; McLaughlin, J. P. The Macrocyclic Peptide Natural Product CJ-15,208 Is Orally Active and Prevents Reinstatement of Extinguished Cocaine-Seeking Behavior. *J Nat Prod* **2013**, 76, 433-438.
132. Land, B. B.; Bruchas, M. R.; Lemos, J. C.; Xu, M.; Melief, E. J.; Chavkin, C. The dysphoric component of stress is encoded by activation of the dynorphin kappa-opioid system. *J Neurosci* **2008**, 28, 407-414.

133. Bruchas, M. R.; Land, B. B.; Chavkin, C. The dynorphin/kappa opioid system as a modulator of stress-induced and pro-addictive behaviors. *Brain research* **2010**, 1314, 44-55.
134. Carroll, F. I.; Carlezon, W. A., Jr. Development of kappa opioid receptor antagonists. *J Med Chem* **2013**, 56, 2178-2195.
135. Beardsley, P. M.; Howard, J. L.; Shelton, K. L.; Carroll, F. I. Differential effects of the novel kappa opioid receptor antagonist, JD1c, on reinstatement of cocaine-seeking induced by footshock stressors vs cocaine primes and its antidepressant-like effects in rats. *Psychopharmacology (Berl)* **2005**, 183, 118-126.
136. Aldrich, J. V.; Patkar, K. A.; McLaughlin, J. P. Zyklophin, a systemically active selective kappa opioid receptor peptide antagonist with short duration of action. *Proc Natl Acad Sci* **2009**, 106, 18396-18401.
137. Epstein, D. H.; Preston, K. L. The reinstatement model and relapse prevention: a clinical perspective. *Psychopharmacology (Berl)* **2003**, 168, 31-41.
138. McLaughlin, J. P.; Li, S.; Valdez, J.; Chavkin, T. A.; Chavkin, C. Social Defeat Stress-Induced Behavioral Responses are Mediated by the Endogenous Kappa Opioid System. *Neuropsychopharmacology* **2006**, 31, 1241-1248.
139. McLaughlin, J. P.; Marton-Popovici, M.; Chavkin, C. Kappa opioid receptor antagonism and prodynorphin gene disruption block stress-induced behavioral responses. *J Neurosci* **2003**, 23, 5674-5683.
140. McLaughlin, J. P.; Land, B. B.; Li, S.; Pintar, J. E.; Chavkin, C. Prior Activation of Kappa Opioid Receptors by U50,488 Mimics Repeated Forced Swim Stress to Potentiate Cocaine Place Preference Conditioning. *Neuropsychopharmacology* **2006**, 31, 787-794.
141. Van't Veer, A.; Carlezon, W. A., Jr. Role of kappa-opioid receptors in stress and anxiety-related behavior. *Psychopharmacology (Berl)* **2013**, 229, 435-452.
142. Szmuszkowicz, J.; Von Voigtlander, P. F. Benzeneacetamide amines: structurally novel non-mu opioids. *J Med Chem* **1982**, 25, 1125-1126.
143. Halfpenny, P. R.; Horwell, D. C.; Hughes, J.; Hunter, J. C.; Rees, D. C. Highly selective kappa-opioid analgesics. 3. Synthesis and structure-activity relationships of novel N-[2-(1-pyrrolidinyl)-4- or -5-substituted-cyclohexyl]arylamide derivatives. *J Med Chem* **1990**, 33, 286-291.

144. Hunter, J. C.; Leighton, G. E.; Meecham, K. G.; Boyle, S. J.; Horwell, D. C.; Rees, D. C.; Hughes, J. CI-977, a novel and selective agonist for the kappa-opioid receptor. *Br J Pharmacol* **1990**, 101, 183-189.
145. Lahti, R. A.; Mickelson, M. M.; McCall, J. M.; Von Voigtlander, P. F. [3H]U-69593 a highly selective ligand for the opioid kappa receptor. *Eur J Pharmacol* **1985**, 109, 281-284.
146. Kivell, B. M.; Ewald, A. W.; Prisinzano, T. E. Salvinorin A analogs and other kappa-opioid receptor compounds as treatments for cocaine abuse. *Adv Pharmacol* **2014**, 69, 481-511.
147. Guerrieri, E.; Mallareddy, J. R.; Toth, G.; Schmidhammer, H.; Spetea, M. Synthesis and pharmacological evaluation of [(3)H]HS665, a novel, highly selective radioligand for the kappa opioid receptor. *ACS Chem Neurosci* **2015**, 6, 456-463.
148. Frankowski, K. J.; Ghosh, P.; Setola, V.; Tran, T. B.; Roth, B. L.; Aube, J. N-Alkyl-octahydroisoquinolin-1-one-8-carboxamides: a Novel Class of Selective, Nonbasic, Nitrogen-Containing kappa-Opioid Receptor Ligands. *ACS Med Chem Lett* **2010**, 1, 189-193.
149. Roth, B. L.; Baner, K.; Westkaemper, R.; Siebert, D.; Rice, K. C.; Steinberg, S.; Ernsberger, P.; Rothman, R. B. Salvinorin A: a potent naturally occurring nonnitrogenous kappa opioid selective agonist. *Proc Natl Acad Sci* **2002**, 99, 11934-11939.
150. Kivell, B. M.; Ewald, A. W. M.; Prisinzano, T. E. Chapter Twelve - Salvinorin A Analogs and Other Kappa-Opioid Receptor Compounds as Treatments for Cocaine Abuse. In *Advances in Pharmacology*, Dwoskin, L. P., Ed. Academic Press: 2014; Vol. 69, pp 481-511.
151. Simonson, B.; Morani, A. S.; Ewald, A. W. M.; Walker, L.; Kumar, N.; Simpson, D.; Miller, J. H.; Prisinzano, T. E.; Kivell, B. M. Pharmacology and anti-addiction effects of the novel  $\kappa$  opioid receptor agonist Mesyl Sal B, a potent and long-acting analogue of salvinorin A. *Br J Pharmacol* **2015**, 172, 515-531.
152. Spetea, M.; Eans, S. O.; Ganno, M. L.; Lantero, A.; Mairegger, M.; Toll, L.; Schmidhammer, H.; McLaughlin, J. P. Selective  $\kappa$  receptor partial agonist HS666 produces potent antinociception without inducing aversion after i.c.v. administration in mice. *Br J Pharmacol* **2017**, 174, 2444-2456.
153. Mangel, A. W.; Hicks, G. A. Asimadoline and its potential for the treatment of diarrhea-predominant irritable bowel syndrome: a review. *Clin Exp Gastroenterol* **2012**, 5, 1-10.
154. Tey, H. L.; Yosipovitch, G. Targeted treatment of pruritus - a look into the future. *Br J Dermatol* **2011**, 165, 5-17.



155. <http://clinicaltrials.gov> NCT02475447 (accessed Apr 10, 2018).
156. Cara Therapeutics. <http://www.caratherapeutics.com/pipeline-technology/kappa-opioid-receptor-agonists/> (accessed Apr 12, 2018).
157. <http://clinicaltrials.gov> NCT03281538 (accessed Apr 10, 2018).
158. Choi, H.; Murray, T. F.; DeLander, G. E.; Schmidt, W. K.; Aldrich, J. V. Synthesis and opioid activity of [D-Pro10]dynorphin A-(1-11) analogues with N-terminal alkyl substitution. *J Med Chem* **1997**, 40, 2733-2739.
159. Soderstrom, K.; Choi, H.; Berman, F. W.; Aldrich, J. V.; Murray, T. F. N-alkylated derivatives of [D-Pro10]dynorphin A-(1-11) are high affinity partial agonists at the cloned rat kappa-opioid receptor. *Eur J Pharmacol* **1997**, 338, 191-197.
160. Lung, F. D.; Meyer, J. P.; Lou, B. S.; Xiang, L.; Li, G.; Davis, P.; DeLeon, I. A.; Yamamura, H. I.; Porreca, F.; Hruby, V. J. Effects of modifications of residues in position 3 of dynorphin A(1-11)-NH<sub>2</sub> on kappa receptor selectivity and potency. *J Med Chem* **1996**, 39, 2456-2460.
161. Lemaire, S.; Lafrance, L.; Dumont, M. Synthesis and biological activity of dynorphin-(1-13) and analogs substituted in positions 8 and 10. *Int J Pept Protein Res* **1986**, 27, 300-305.
162. Chavkin, C.; Goldstein, A. Specific receptor for the opioid peptide dynorphin: structure-activity relationships. *Proc Natl Acad Sci* **1981**, 78, 6543-6547.
163. Hiramatsu, M.; Inoue, K.; Ambo, A.; Sasaki, Y.; Kameyama, T. Long-lasting antinociceptive effects of a novel dynorphin analogue, Tyr-D-Ala-Phe-Leu-Arg psi (CH<sub>2</sub>)NH Arg-NH<sub>2</sub>, in mice. *Br J Pharmacol* **2001**, 132, 1948-1956.
164. Butelman, E. R.; Ball, J. W.; Kreek, M. J. Peripheral selectivity and apparent efficacy of dynorphins: comparison to non-peptidic kappa-opioid agonists in rhesus monkeys. *Psychoneuroendocrinology* **2004**, 29, 307-326.
165. Erez, M.; Takemori, A. E.; Portoghese, P. S. Narcotic antagonistic potency of bivalent ligands which contain .beta.-naltrexamine. Evidence for simultaneous occupation of proximal recognition sites. *J Med Chem* **1982**, 25, 847-849.
166. Portoghese, P. S.; Lipkowski, A. W.; Takemori, A. E. Bimorphinans as highly selective, potent .kappa. opioid receptor antagonists. *J Med Chem* **1987**, 30, 238-239.

167. Sharma, S. K.; Jones, R. M.; Metzger, T. G.; Ferguson, D. M.; Portoghese, P. S. Transformation of a kappa-opioid receptor antagonist to a kappa-agonist by transfer of a guanidinium group from the 5'- to 6'-position of naltrindole. *J Med Chem* **2001**, 44, 2073-2079.
168. Munro, T. A.; Berry, L. M.; Van't Veer, A.; Béguin, C.; Carroll, F. I.; Zhao, Z.; Carlezon, W. A.; Cohen, B. M. Long-acting  $\kappa$  opioid antagonists nor-BNI, GNTI and JDtic: pharmacokinetics in mice and lipophilicity. *BMC Pharmacol* **2012**, 12, 5.
169. Carroll, F. I.; Carlezon, W. A. Development of Kappa Opioid Receptor Antagonists. *J Med Chem* **2013**, 56, 2178-2195.
170. Thomas, J. B.; Atkinson, R. N.; Rothman, R. B.; Fix, S. E.; Mascarella, S. W.; Vinson, N. A.; Xu, H.; Dersch, C. M.; Lu, Y.; Cantrell, B. E.; Zimmerman, D. M.; Carroll, F. I. Identification of the first trans-(3R,4R)- dimethyl-4-(3-hydroxyphenyl)piperidine derivative to possess highly potent and selective opioid kappa receptor antagonist activity. *J Med Chem* **2001**, 44, 2687-2690.
171. Schank, J. R.; Goldstein, A. L.; Rowe, K. E.; King, C. E.; Marusich, J. A.; Wiley, J. L.; Carroll, F. I.; Thorsell, A.; Heilig, M. The kappa opioid receptor antagonist JDtic attenuates alcohol seeking and withdrawal anxiety. *Addict Biol* **2012**, 17, 634-647.
172. Carroll, F. I.; Harris, L. S.; Aceto, M. D. Effects of JDtic, a selective  $\kappa$ -opioid receptor antagonist, on the development and expression of physical dependence on morphine using a rat continuous-infusion model. *Eur J Pharmacol* **2005**, 524, 89-94.
173. Chavkin, C.; Martinez, D. Kappa Antagonist JDtic in Phase 1 Clinical Trial. *Neuropsychopharmacology* **2015**, 40, 2057-2058.
174. Helal, M. A.; Habib, E. S.; Chittiboyina, A. G. Selective kappa opioid antagonists for treatment of addiction, are we there yet? *Eur J Med Chem* **2017**, 141, 632-647.
175. Casal-Dominguez, J. J.; Furkert, D.; Ostovar, M.; Teintang, L.; Clark, M. J.; Traynor, J. R.; Husbands, S. M.; Bailey, S. J. Characterization of BU09059: A Novel Potent Selective  $\kappa$ -Receptor Antagonist. *ACS Chem Neurosci* **2014**, 5, 177-184.
176. Schmitt, S.; Colloc'h, N.; Perrio, C. Novel fluoroalkyl derivatives of selective kappa opioid receptor antagonist JDtic: Design, synthesis, pharmacology and molecular modeling studies. *Eur J Med Chem* **2015**, 90, 742-750.
177. Verhoest, P. R.; Basak, A. S.; Parikh, V.; Hayward, M.; Kauffman, G. W.; Paradis, V.; McHardy, S. F.; McLean, S.; Grimwood, S.; Schmidt, A. W.; Vanase-Frawley, M.; Freeman, J.;

Van Deusen, J.; Cox, L.; Wong, D.; Liras, S. Design and discovery of a selective small molecule kappa opioid antagonist (2-methyl-N-((2'-(pyrrolidin-1-ylsulfonyl)biphenyl-4-yl)methyl)propan-1-amine, PF-4455242). *J Med Chem* **2011**, *54*, 5868-5877.

178. Grimwood, S.; Lu, Y.; Schmidt, A. W.; Vanase-Frawley, M. A.; Sawant-Basak, A.; Miller, E.; McLean, S.; Freeman, J.; Wong, S.; McLaughlin, J. P.; Verhoest, P. R.

Pharmacological characterization of 2-methyl-N-((2'-(pyrrolidin-1-ylsulfonyl)biphenyl-4-yl)methyl)propan-1-amine (PF-04455242), a high-affinity antagonist selective for kappa-opioid receptors. *J Pharmacol Exp Ther* **2011**, *339*, 555-566.

179. Melief, E. J.; Miyatake, M.; Carroll, F. I.; Beguin, C.; Carlezon, W. A., Jr.; Cohen, B. M.; Grimwood, S.; Mitch, C. H.; Rorick-Kehn, L.; Chavkin, C. Duration of action of a broad range of selective kappa-opioid receptor antagonists is positively correlated with c-Jun N-terminal kinase-1 activation. *Mol Pharmacol* **2011**, *80*, 920-929.

180. <https://clinicaltrials.gov> NCT00939887 (accessed Apr 10, 2018).

181. Mitch, C. H.; Quimby, S. J.; Diaz, N.; Pedregal, C.; de la Torre, M. G.; Jimenez, A.; Shi, Q.; Canada, E. J.; Kahl, S. D.; Statnick, M. A.; McKinzie, D. L.; Benesh, D. R.; Rash, K. S.; Barth, V. N. Discovery of aminobenzyloxyarylamides as kappa opioid receptor selective antagonists: application to preclinical development of a kappa opioid receptor antagonist receptor occupancy tracer. *J Med Chem* **2011**, *54*, 8000-8012.

182. <http://clinicaltrials.gov> NCT02218736 (accessed Apr 10, 2018).

183. <https://clinicaltrials.gov> NCT02800928 (accessed Apr 10, 2018).

184. Brugel, T. A.; Smith, R. W.; Balestra, M.; Becker, C.; Daniels, T.; Hoerter, T. N.; Koether, G. M.; Throner, S. R.; Panko, L. M.; Folmer, J. J.; Cacciola, J.; Hunter, A. M.; Liu, R.; Edwards, P. D.; Brown, D. G.; Gordon, J.; Ledonne, N. C.; Pietras, M.; Schroeder, P.; Sygowski, L. A.; Hirata, L. T.; Zacco, A.; Peters, M. F. Discovery of 8-azabicyclo[3.2.1]octan-3-yloxy-benzamides as selective antagonists of the kappa opioid receptor. Part 1. *Bioorg Med Chem Lett* **2010**, *20*, 5847-5852.

185. Brugel, T. A.; Smith, R. W.; Balestra, M.; Becker, C.; Daniels, T.; Koether, G. M.; Throner, S. R.; Panko, L. M.; Brown, D. G.; Liu, R.; Gordon, J.; Peters, M. F. SAR development of a series of 8-azabicyclo[3.2.1]octan-3-yloxy-benzamides as kappa opioid receptor antagonists. Part 2. *Bioorg Med Chem Lett* **2010**, *20*, 5405-5410.

186. Carey, A. N.; Borozny, K.; Aldrich, J. V.; McLaughlin, J. P. Reinstatement of cocaine place-conditioning prevented by the peptide kappa-opioid receptor antagonist arodyn. *Eur J Pharmacol* **2007**, 569, 84-89.
187. Bennett, M. A.; Murray, T. F.; Aldrich, J. V. Identification of Arodyn, a Novel Acetylated Dynorphin A-(1-11) Analogue, as a  $\kappa$  Opioid Receptor Antagonist. *J Med Chem* **2002**, 45, 5617-5619.
188. Carey, A. N.; Borozny, K.; Aldrich, J. V.; McLaughlin, J. P. Reinstatement of Cocaine Place-Conditioning Prevented by the Peptide kappa-Opioid Receptor Antagonist Arodyn. *Eur J Pharmacol* **2007**, 569, 84-89.
189. Bennett, M. A.; Murray, T. F.; Aldrich, J. V. Structure-activity relationships of arodyn, a novel acetylated kappa opioid receptor antagonist. *J Pept Sci* **2005**, 65, 322-332.
190. Bennett, M. A.; Murray, T. F.; Aldrich, J. V. Structure-activity relationships of arodyn, a novel acetylated kappa opioid receptor antagonist. *J Pept Res* **2005**, 65, 322-332.
191. Fang, W.-J.; Murray, T. F.; Aldrich, J. V. Design, synthesis, and opioid activity of arodyn analogs cyclized by ring-closing metathesis involving Tyr(allyl). *Bioorg Med Chem* **2018**, 26, 1157-1161.
192. Patkar, K. A.; Murray, T. F.; Aldrich, J. V. The effects of C-terminal modifications on the opioid activity of [N-benzylTyr(1)]dynorphin A-(1-11) analogues. *J Med Chem* **2009**, 52, 6814-6821.
193. Joshi, A. A.; Murray, T. F.; Aldrich, J. V. Structure-Activity Relationships of the Peptide Kappa Opioid Receptor Antagonist Zyklophin. *J Med Chem* **2015**, 58, 8783-8795.
194. Saito, T.; Hirai, H.; Kim, Y. J.; Kojima, Y.; Matsunaga, Y.; Nishida, H.; Sakakibara, T.; Suga, O.; Sujaku, T.; Kojima, N. CJ-15,208, a novel kappa opioid receptor antagonist from a fungus, *Ctenomyces serratus* ATCC15502. *J Antibiot* **2002**, 55, 847-854.
195. Ross, N. C.; Reilley, K. J.; Murray, T. F.; Aldrich, J. V.; McLaughlin, J. P. Novel opioid cyclic tetrapeptides: Trp isomers of CJ-15,208 exhibit distinct opioid receptor agonism and short-acting kappa opioid receptor antagonism. *Br J Pharmacol* **2012**, 165, 1097-1108.
196. Eans, S. O.; Ganno, M. L.; Reilley, K. J.; Patkar, K. A.; Senadheera, S. N.; Aldrich, J. V.; McLaughlin, J. P. The macrocyclic tetrapeptide [D-Trp]CJ-15,208 produces short-acting kappa opioid receptor antagonism in the CNS after oral administration. *Br J Pharmacol* **2013**, 169, 426-436.

197. Dolle, R. E.; Michaut, M.; Martinez-Teipel, B.; Seida, P. R.; Ajello, C. W.; Muller, A. L.; DeHaven, R. N.; Carroll, P. J. Nascent structure–activity relationship study of a diastereomeric series of kappa opioid receptor antagonists derived from CJ-15,208. *Bioorg Med Chem* **2009**, *19*, 3647-3650.
198. Aldrich, J. V.; Kulkarni, S. S.; Senadheera, S. N.; Ross, N. C.; Reilley, K. J.; Eans, S. O.; Ganno, M. L.; Murray, T. F.; McLaughlin, J. P. Unexpected Opioid Activity Profiles of Analogues of the Novel Peptide Kappa Opioid Receptor Ligand CJ-15,208. *ChemMedChem* **2011**, *6*, 1739-1745.
199. Aldrich, J. V.; Senadheera, S. N.; Ross, N. C.; Reilley, K. A.; Ganno, M. L.; Eans, S. E.; Murray, T. F.; McLaughlin, J. P. Alanine analogues of [D-Trp]CJ-15,208: novel opioid activity profiles and prevention of drug- and stress-induced reinstatement of cocaine-seeking behaviour. *Br J Pharmacol* **2014**, *171*, 3212-3222.

**Chapter 3 - Literature review: challenges and opportunities for ring closing metathesis in peptide cyclization**

### 3.1 Introduction

Interest in peptides has surged in recent years<sup>1-3</sup> alongside increasing interest in cyclic peptides<sup>4,5</sup> which can effectively modulate difficult targets such as protein-protein interactions.<sup>6,7</sup> Peptides as a class are conformationally flexible and a large body of work has focused on restricting their flexibility. Accordingly, tools for conformational control have emerged as useful approaches to leverage the unique properties of peptides to modulate biological targets.<sup>8-10</sup> Various strategies to confer conformational constraint have been broadly applied to overcome disorder in linear peptides and thus stabilize the bioactive structure or a particular secondary structure.<sup>9, 11</sup> These strategies include: cyclization, incorporating rigid building blocks and rigid peptide bond isosteres, which also reduce peptide degradation by proteases and improve physicochemical properties.<sup>12-14</sup>

In addition to enhancing metabolic stability, cyclization can increase cell permeability and stabilize the bioactive conformation of peptides.<sup>15-21</sup> Notably, the cyclization strategy can mimic naturally occurring cyclic motifs in highly potent ligands that are resistant to thermal and proteolytic degradation, such as cyclotides<sup>22, 23</sup> and the fungal toxin  $\alpha$ -amanitin.<sup>24, 25</sup> Examples of naturally occurring and clinically relevant cyclic peptides include: ziconotide, vancomycin, and cyclosporine (Figure 3.1).<sup>4</sup>

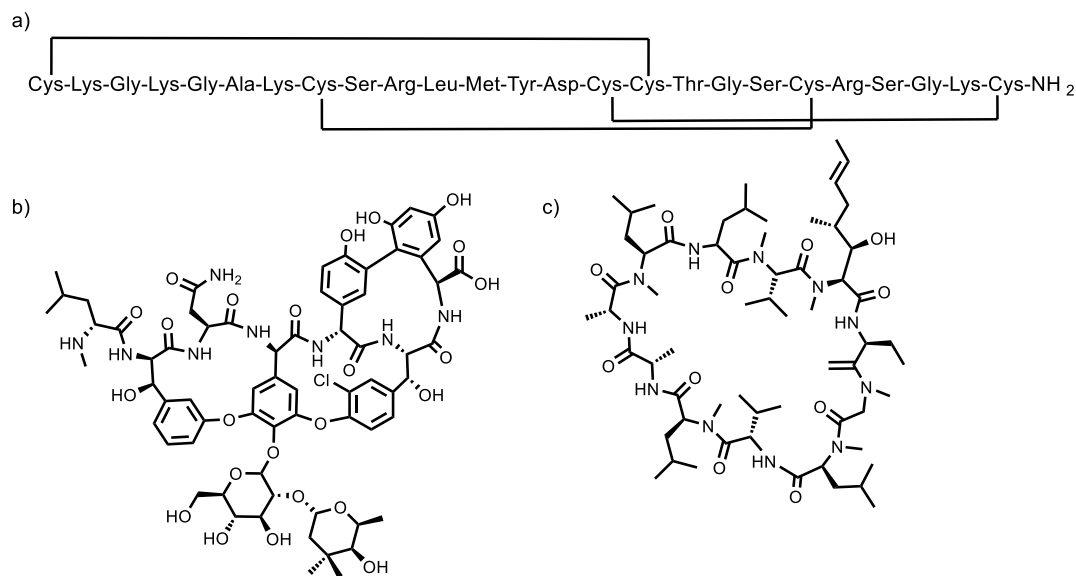


Figure 3.1 Therapeutically relevant cyclic peptides a) ziconotide b) vancomycin, and c) cyclosporine.

Peptides can be cyclized from either termini or from the side chains to generate a variety of cyclization motifs such as: head to tail, end (head/tail) to side chain, and side chain to side chain (Figure 3.2).<sup>9</sup> Notably, the cyclic constraint can consist of only peptide bonds (homodetic) or comprise of different functional groups (heterodetic).<sup>4</sup> Early cyclization strategies predominantly focused on stabilizing secondary structures utilizing chemistries such as lactam and disulfide bridges in addition to lactones (Figure 3.3a-c).<sup>9</sup> More recently, hydrocarbon linkages have become established approaches for peptide cyclization (Figure 3.3d).

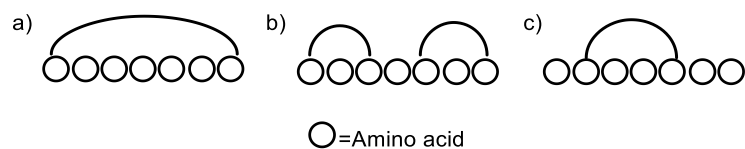


Figure 3.2 Cyclization motifs for peptide cyclization a) head to tail b) end (head/tail) to side chain, and c) side chain to side chain.

An increasing variety of linkages continue to be explored including: triazole, amine, ureido and guanine linkages, which have been extensively reviewed (Figure 3.3).<sup>9, 26</sup> Of note, hydrocarbon linkages using ring closing metathesis have made wide ranging impact in peptide



stapling to stabilize alpha helical structures leading to the development of effective cell permeable inhibitors of protein-protein interactions.<sup>27</sup> Grubbs and coworkers pioneered the use of hydrocarbon peptides by replacing a disulfide with a hydrocarbon crosslink.<sup>28, 29</sup>

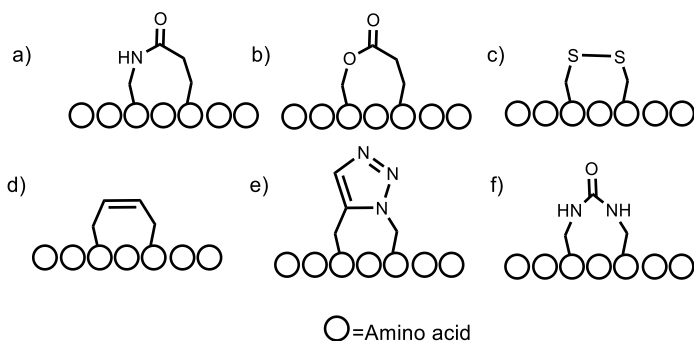


Figure 3.3 Representative peptide cyclization chemistries showing a) lactam, b) lactone, c) disulfide, d) alkene, e) triazole, and f) ureido cyclizations.

Hydrocarbon linkers confer resistance to metabolic degradation, a restrictive attribute of peptide therapeutics that limits *in vivo* administration, due to their non-native character.<sup>5</sup> Conversely, amide, disulfide or thioether linkages can be proteolytically or oxidatively metabolized. Walensky and coworkers demonstrated the enhanced proteolytic stability of singly and doubly stapled analogs of enfuvirtide and exanetide, both lengthy peptides used as drugs in HIV and diabetes, respectively.<sup>30</sup> Hydrocarbon stapling was also applied in the synthesis of proteolytically stable HIV-1 immunogens for HIV vaccines.<sup>31</sup> In addition to proteolytic stability, hydrocarbon stapling is reported to enhance cell penetration, which makes them particularly useful for drugging intracellular targets.<sup>32, 33, 34</sup> Notably, peptide stapling alone does not confer permeability as other factors such as sequence optimization are particularly important considerations.<sup>33, 34</sup>

An additional characteristic of hydrocarbon linkers is the difference in dihedral angle geometry of the linkage relative to typical linkages such as disulfides. Disulfide linkages with a dihedral angle of approximately  $\pm 90^\circ$  differ from lactam linkages which can be  $0^\circ$  (*cis*) or  $180^\circ$

(*trans*) amide bonds. Ring closing metathesis results in either *cis* or *trans* olefins which may be separated unlike lactam linkages where the amide bond bridge is generally in the *trans* configuration.

Of note, interactions between the cyclic bridge and the protein target can potentially contribute to the affinity to the target; for instance, stabilizing hydrophobic contacts were observed between the hydrocarbon bridge and the MCL-1 binding interface.<sup>35</sup> However, in the constraint of human tumor susceptibility gene 101 protein (Tsg101) binding peptides, cyclization resulted in mixed results where some cyclic analogs significantly lost affinity while some retained affinity for the target similar to the wild type peptide.<sup>36</sup> Similar results have been reported where optimization of the ring size, ring linkage, and ring configuration all factor into affinity for the target.<sup>18</sup>

### **3.1.1 Solution phase and solid phase cyclization of peptides**

Cyclization of peptides can be performed in solution or on-resin during solid-phase peptide synthesis (SPPS,<sup>37</sup> Figure 3.4). Notably, each cyclization strategy has advantages and disadvantages relating to among other factors: compatibility with SPSS, efficiency of the ring closing reaction, sequence-dependent effects, and compatibility with amino acid functional groups. Unnatural amino acids are required for a number of cyclization strategies some of which utilize orthogonal protection and selective deprotection to facilitate cyclization of the peptide. The growing demand for peptides has spurred advances in SPPS, including increasingly modified building blocks, incorporation of mechanical strength and sufficient swelling in common solvents that facilitate access to active sites on the solid support.<sup>38</sup>

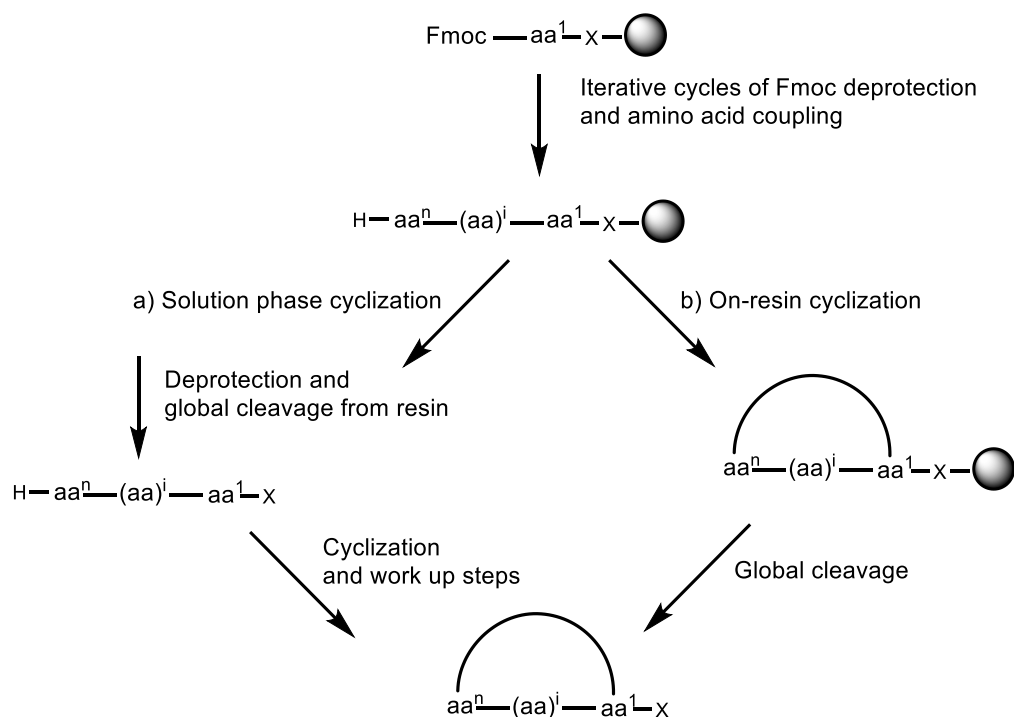


Figure 3.4 Solid phase peptide synthesis using the Fmoc strategy showing a) solution phase and b) on-resin cyclization.

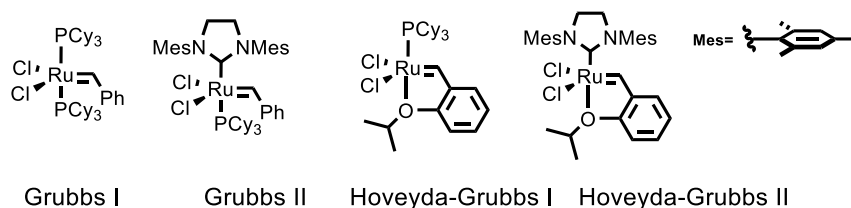
On-resin cyclization is a useful and expedient route to access cyclic peptides given the fewer purification steps required. In a comparative study of solution phase and on-resin cyclization of a 22-residue peptide, Andreu and coworkers observed that while solution phase cyclization consistently gave higher yields, global yields from on-resin cyclization were comparable factoring in the necessary purification steps.<sup>39</sup> In a similar study by the same group, on-resin cyclization of a 15-residue peptide showed greater results compared to solution phase cyclization.<sup>40</sup> Solution-phase cyclization requires high-dilution strategies to avoid oligomerization<sup>41</sup>, but on-resin cyclization does not. An additional advantage to on-resin cyclization is the pseudodilution effect<sup>42-44</sup> due to attaching the peptide to an insoluble solid support thereby favoring the intramolecular reaction over the intermolecular reaction. Accordingly, on-resin cyclization of peptides has increased in the recent past including strategies such as ring closing metathesis, intramolecular

nucleophilic substitution reactions ( $S_N2$  or  $S_NAr$ ), thiol-ene cyclization, Cu (I) catalyzed azide-alkyne cycloaddition, and transition metal catalyzed coupling reactions.<sup>45</sup>

### 3.2 Ring closing metathesis (RCM) of peptides

Olefin metathesis facilitates the construction of C-C bonds and is widely applied due to the mild condition requirement for the transformation, functional group tolerance, high catalytic activity, and stability of commercially available Ru-alkylidene catalysts<sup>46</sup> (Figure 3.5a). Consequently, olefin metathesis has been applied in molecules with multiple functional groups, including peptides, to generate hydrocarbon crosslinks via ring closing metathesis (RCM) and ring closing alkyne metathesis. RCM proceeds through a catalytic cycle that involves metallacyclobutane intermediates (Figure 3.5b); release of ethylene gas drives the reaction forward.<sup>47, 48</sup>

a)



b)

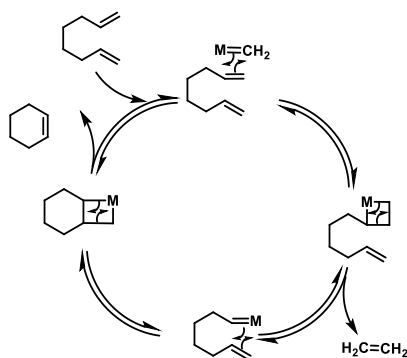


Figure 3.5 a) Structures of ruthenium-based Grubbs catalyst developed by altering the ligands around the metal center to tune catalyst activity and the stability of 1<sup>st</sup> and 2<sup>nd</sup> generation catalysts and b) a representative mechanism of RCM.

RCM has been used to enhance various secondary structures such as alpha helices and  $\beta$ -turns as well as to replace disulfide bonds with dicarba mimics. Typically, selected residues on the peptide that are not critical to binding are substituted by alkene containing non-natural amino acids, such as allyl glycine, to facilitate RCM (Figure 3.6a). Grubbs and coworkers used allyl glycine in the seminal RCM on peptides to mimic a cystine stabilized  $\beta$ -turn.<sup>28</sup> Other RCM precursors residues include  $\alpha,\alpha$  disubstituted alkenyl amino acids, allyl serine and cysteine residues, and allyl tyrosine residues (Figure 3.6b). Notably,  $\alpha$ -methyl,  $\alpha$ -alkenyl amino acids which have been extensively used in stapled peptides to reinforce an alpha helical structure.<sup>49</sup> RCM has also been applied to stabilize alpha helical conformation in hydrogen bond surrogates where the hydrocarbon cross link is formed between olefins at the N-terminus and an N-alkylated residue resulting in an end-capped alpha helix (Figure 3.6c).<sup>50, 51</sup> Interestingly, Grossman and coworkers have more recently applied RCM to stabilize irregular secondary structures involved in protein-protein interactions, thereby expanding the utility of RCM in molecular recognition applications.<sup>52</sup>

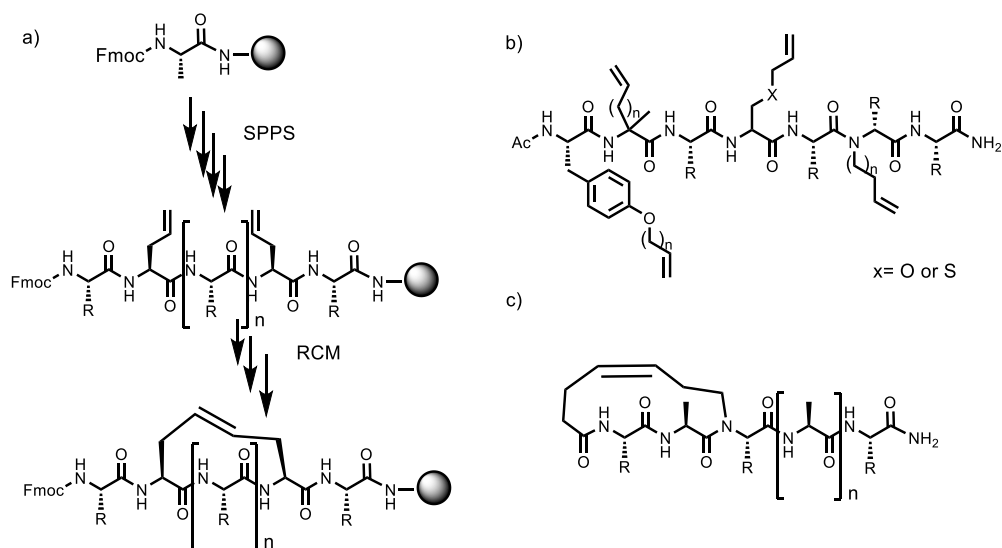


Figure 3.6. a) General scheme for ring closing metathesis of a resin-bound peptide following incorporation of allyl glycine residues b) a representative example of alkene precursors on a peptidic substrate, and c) structure of a hydrogen bond surrogate

Hydrocarbon crosslinks have been used as cystine bridge replacements in a variety of peptides such as oxytocin analogs. Vederas and coworkers studied hydrocarbon crosslinks of oxytocin highlighting the effect of olefin geometry, ring size, and olefin saturation on biological activity.<sup>53</sup> Initial studies indicated that a *cis* isomer was more potent than the *trans* isomer although less active than the parent peptide while saturated analogs were less potent than the parent peptide. Further studies on oxytocin analogs and antagonists indicated that a 20-membered ring was more active than peptides with larger rings; notably, the 22-membered ring peptide was inactive. Robinson and coworkers reported that unsaturated analogs are more active thereby emphasizing advantage of conformational restriction relative to the native S-S bond.

Despite the widespread utility of RCM, challenges remain in cyclization using Grubbs catalysts. Evidently, it is difficult to find general conditions that guarantee successful RCM due to a multitude of parameters influencing the process.<sup>54,55</sup> Additionally, competing reactions including olefin isomerization limit RCM efficiency;<sup>56,57</sup> olefin isomerization due to catalyst degradation products such as ruthenium hydrides can result in unwanted side products.<sup>58-60</sup> Schroeder and coworkers reported high degrees of olefin isomerization during olefin metathesis resulting in CH<sub>2</sub> insertions and deletions while<sup>61</sup> Liskamp and coworkers have reported significant olefin isomerization of peptidic substrates during RCM.<sup>62, 63</sup> Interestingly, ring contraction products could result from RCM of isomerized olefins (Figure 3.7). For instance, Larhed and coworkers observed olefin isomerization and ring contraction products during RCM of macrocyclic HIV-1 protease inhibitors.<sup>64</sup> Olefin isomerization and ring contraction products were also reported by Hanson *et al.* in the synthesis of dolabelide C.<sup>65</sup>

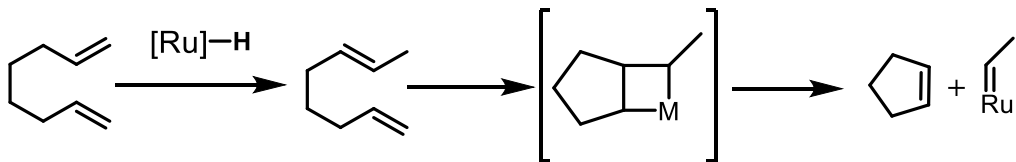


Figure 3.7 Proposed mechanism of formation of ring contraction products following olefin isomerization during RCM.

Furthermore, on-resin RCM is influenced by the choice of solid support, solvent, catalyst and alkene precursor. It is therefore not surprising that considerable challenges have been reported during on-resin peptide RCM. In another example, Bergman *et al* reported that a 4:1 mixture of trifluoroethanol (TFE) and dichloromethane (DCM) facilitated RCM between O-allyl serine residues in a  $\beta^3$ -peptide following extensive screening of commonly used solvents in RCM.<sup>66</sup> Additionally, the amount of catalyst required for sufficient conversion was dependent on the solid-support used for SPPS. Further examples and several strategies to improve peptide RCM, include using solvent mixtures, additives, and microwave, heating have been reported (Table 3.1).

Robinson and coworkers have documented challenges in peptide RCM that limit efficient cyclization including sequence dependence of the linear precursor and peptide aggregation on the solid support.<sup>67</sup> For difficult substrates, chemical modification is required; pseudoproline insertion facilitated RCM of a human growth hormone fragment after microwave heating and addition of chaotropic salts to disrupt peptide aggregation failed to promote cyclization.<sup>68</sup> Pseudoproline insertion induces a *cis* amide bond that allows reacting termini to localize favorably thereby promoting RCM.

Similarly, Kessler and coworkers used reversible backbone protection of a serine residue to promote RCM of a decapeptide that only cyclized with the turn-inducing insertion.<sup>69</sup> Characterization of the olefin tether, typically done using <sup>1</sup>H-NMR, also presents non-trivial

challenges; Robinson and coworkers highlight difficulties in determination of geometrical isomers due to poor resolution of olefin peaks which led them to develop the use of  $^{13}\text{C}$  NMR for geometrical assignments.<sup>70</sup> Similarly, Liskamp and coworkers reported difficulties in structural characterization of the olefins following RCM to mimic the bicyclic vancomycin structure.<sup>63</sup>

Table 3.1 Selected RCM conditions for synthesis of cyclic peptides and corresponding reaction conditions illustrating various reaction optimization and synthetic challenges

Entry	Peptidic substrate	RCM conditions <sup>a</sup>	Comments
1	Human growth hormone analog <sup>68</sup>	20 mol% G II DCM, LiCl in DMF, 100 °C, $\mu\text{W}$ , 1h	Peptide contained a turn inducing pseudoproline residue; chaotropic salt and $\mu\text{W}$ heating used to promote RCM
2	Decapeptide epitope <sup>69</sup>	>Stoichiometric G I, DCM, 40 °C, 12h	Reversible backbone protection (Ser( $\Psi^{\text{Me,Me}}$ pro) to induce a favorable conformation for RCM
3	Cyclic peptoids <sup>71</sup>	2 mol% Grubbs catalysts, DCM, 40 °C, 2 h or 1,2-dichlorobenzene, 300 W $\mu\text{W}$ , 2 min	RCM efficiency dependent on type of Grubbs catalyst used and length of alkenyl precursor
4	Cyclic dipeptides <sup>62</sup>	10 mol% G I, 1,1,2-trichloroethane (TCE), additives, 16h	Screening of additives to suppress olefin migration in amide backbone cyclized peptides, length of alkenyl precursor did not affect olefin migration
5	Vancomycin bicyclic ring mimic <sup>63</sup>	Stoichiometric G II, TCE/DMF, hydride scavengers, 80 °C, 10 min	Addition of hydride scavengers to minimize olefin isomerization during RCM between aryl-allyl and <i>O</i> -allyl substrates; complex characterization of olefins in bicyclic structure
6	Macrocyclic $\beta$ -strand <sup>72</sup>	10 mol% G II (10 mM) TCE, additives, various thermal and $\mu\text{W}$ conditions	Additives including Lewis acids were explored to improve RCM efficiency. Multiple additions of catalyst were explored.
7	Macrocyclic HIV-1 protease inhibitors <sup>64</sup>	20 mol% G II DCM, 130 °C, $\mu\text{W}$ , 1h	Olefin migration and ring contraction following RCM
8	$\beta^3$ -peptide <sup>66</sup>	20-35 mol % HG II, trifluoroethanol (TFE)/DCM 4:1, rt, 48h	RCM efficiency was highly solvent dependent; catalyst loading dependent on resin suggesting catalyst sequestration
9	Hydrogen bond surrogates <sup>73</sup>	10 mol% various catalysts and conditions under thermal and $\mu\text{W}$ heating	RCM efficiency dependent on solvent, temperature, and catalyst used. Differences in G II and HG II catalyst activity under $\mu\text{W}$ heating

<sup>a</sup>Grubbs 1<sup>st</sup> generation catalyst (G I), Grubbs 2<sup>nd</sup> generation catalyst (G II), Hoveyda-Grubbs 2<sup>nd</sup> generation catalyst (HG II)



Control of olefin geometry has been a considerable challenge in ring closing metathesis, giving mixtures of *E* and *Z* isomers which can be difficult to separate. Separation of geometrical isomers is particularly important due to differences in biological activity which are commonly observed between *cis* and *trans* isomers.<sup>53,74</sup> A number of approaches have been devised to address the geometry of olefin metathesis such as selective enrichment via ethenolysis<sup>75</sup> and development of stereoselective catalysts.<sup>76</sup> Grubbs and coworkers explored the use of a *Z*-selective catalyst on peptidic substrates highlighting that the type of olefin and amino acid side chain significantly influenced the catalyst activity.<sup>77</sup> Additionally, noteworthy differences in cyclization based upon the solid support used for on-resin RCM were observed. Strikingly, preorganization of the peptide hindered *Z*-selective RCM instead resulting in the *E*- isomer, thereby indicating the effect of substrate bias on peptide RCM.

Given the challenges of on-resin RCM, alternative approaches such as using aqueous media have been explored to potentially address issues such as peptide aggregation on-resin. One such approach is RCM of peptides in aqueous media. Vederas and coworkers probed the use of detergents and *tert*-butanol to solubilize ruthenium based catalysts, but found mixed results depending on the alkene precursor following aqueous RCM.<sup>78</sup> More recently, Donahue and coworkers demonstrated RCM of a DNA-bound peptide in aqueous media where they used MgCl<sub>2</sub> to limit Ru-induced decomposition of DNA.<sup>79</sup> This seminal work highlights the challenges of peptide RCM, but also the opportunities to broaden the utility of olefin metathesis in constraining peptides.

### **3.2.1 Polycyclic ligands and RCM**

Polycyclic peptides have garnered increasing interest given the success of conformationally constrained peptides such as vancomycin and cyclosporine, which have had

demonstrable clinical success. Given the advantages of monocyclic peptides, the additional conformational constraint and metabolic stability of polycyclic peptides can potentially enhance target binding affinities and selectivities to antibody-like levels.<sup>80</sup> This is especially important in the context of undruggable targets such as protein-protein interactions. For instance, a remarkable improvement in potency and selectivity was observed upon conversion of the monocyclic undecapeptide growth factor receptor-bound protein 2 (Grb2) Src homology 2 (SH2) domain peptide inhibitor into a bicyclic peptide.<sup>81</sup> In this example, bicyclization resulted in a 60-fold increase in potency and 200-fold increased selectivity for the Grb2 SH2 domain. Walensky and coworkers have also reported benefits of additional constraints; double stapling not only improved metabolic stability but also enhance biological activity of enfuvirtide, an HIV fusion inhibitor.<sup>30</sup> Similarly, improved proteolytic stability and cell penetration was observed in a doubly stapled “stitched peptide” with a contiguous alkene bridge (Figure 3.8a).<sup>82</sup>

Rhodes and Pei have extensively reviewed progress in the synthesis of bicyclic peptides, and highlight multiple synthetic approaches as well as the increasing utility of these constrained motifs.<sup>80</sup> Indeed, multiple cyclization strategies can be combined to generate polycyclic peptides as has been reported for HDAC inhibitors<sup>83</sup> (Figure 3.8b) and is observed in the natural product HDAC inhibitor romidepsin (Figure 3.8c), which is clinically approved to treat cutaneous and peripheral T-cell lymphoma.<sup>84</sup> The combination of multiple cyclization approaches increases the diversity of polycyclic peptides. Additionally, polycyclization facilitates attachment of multiple pharmacophores; Lian *et al* reported a bicyclic peptide that targets peptidyl-prolyl *cis-trans* isomerase (Pin1) that is fused with a cyclic cell penetrating peptide (Figure 3.8d).<sup>85</sup>

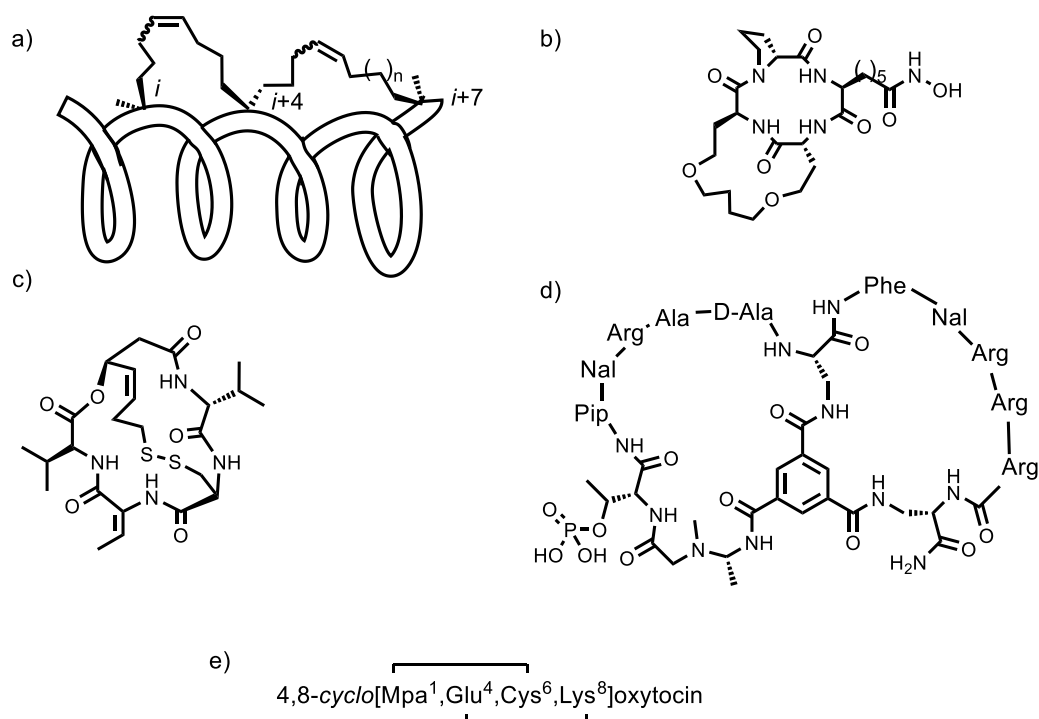


Figure 3.8. Representative polycyclic peptides: a) schematic structure showing a stitched peptide with contiguous alkene bridging, b) bicyclic HDAC inhibitor, c) romidepsin, d) a Pin 1 inhibitor fused with a cell penetrating peptide, and e) a bicyclic oxytocin analog. Pip = pipecolic acid, Nal = naphthylalanine.

Combinatorial library screens and rational design have resulted in the discovery of bicyclic ligands.<sup>80</sup> Heinis *et al* screened a phage display library of bicyclic peptides resulting in a potent human plasma kallikrein inhibitor.<sup>86</sup> Using rational design Hruby and coworkers generated bicyclic ligands from monocyclic lead peptides. Hruby and coworkers synthesized a bicyclic oxytocin receptor antagonist that demonstrated both *in vitro* ( $pA_2=8.2$ ) and *in vivo* ( $pA_2=6.45$ ) potency (Figure 3.8e).<sup>87</sup> Notably, no bicyclic ligands for the opioid receptors have been reported though dynorphin analogs are reported, though dynorphin analogs offer the necessary size to allow modifications resulting in a polycyclic ligand.<sup>88</sup>

Generally, synthesis of polycyclic peptides is challenging because of the multiple orthogonal protection strategies that are necessary to prevent unwanted isomers. For instance, cysteine scrambling is a prominent concern during the synthesis of peptides with multiple cysteine

bridges such as conotoxins.<sup>89</sup> Accordingly, multiple strategies have been pursued to achieve regioselectivity in the synthesis of polycyclic peptides via RCM. Sequential ring closure was employed during synthesis of the lantibiotic analog, lantacin 3147 A2 (Figure 3.9a)<sup>90</sup>, while a preorganization-based strategy was used for the synthesis of a nisin analog mimic bearing an interlocked alkene bridge (Figure 3.9b).<sup>91</sup> Notably, preorganization can allow facile bicyclization and separation of *cis/trans* isomers as was observed by Rijkers and coworkers.<sup>91</sup> However, in the absence of preorganization, cyclization and separation of *cis/trans* isomers in polycyclic peptides with alkene bridges is challenging.<sup>63 67</sup>

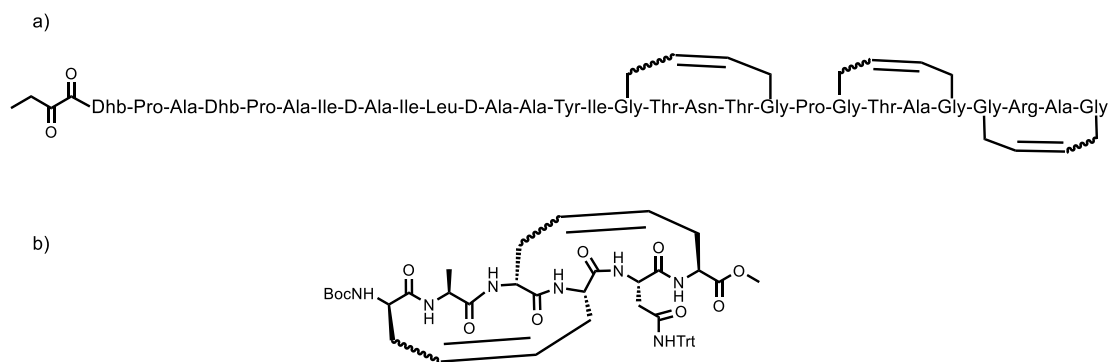


Figure 3.9 Structure of polycyclic peptides synthesized through RCM a) lantacin 3147 A2 synthesized by sequential RCM and b) the carbon-bridged nisin DE ring mimic synthesized in one-step. Dhb= didehydroaminobutyric acid.

Other strategies to achieve regioselectivity during formation of polycyclic alkene bridged peptides include using alkene precursors with varying activity towards the catalysts and using orthogonal metathesis catalysts.<sup>67</sup> Robinson and coworkers leveraged the reduced metathesis reactivity of prenyl glycine to selectively form alkene bridges between AllGly residues during the synthesis of the  $\alpha$ -conotoxin Rg1A analog (Figure 3.10). Notably, cross metathesis and asymmetric hydrogenation were employed to facilitate ring closing metathesis of the metathesis inactive prenyl glycine.<sup>92</sup> Besides regioselectivity, undesired side reactions also present a challenge in the synthesis of polycyclic peptides that limits the scaffolds accessible through

sequential RCM. For instance, Bird and Walensky observed that side reactions are dependent on ring size and distance and therefore optimized these parameters to limit side reactions.<sup>49</sup>

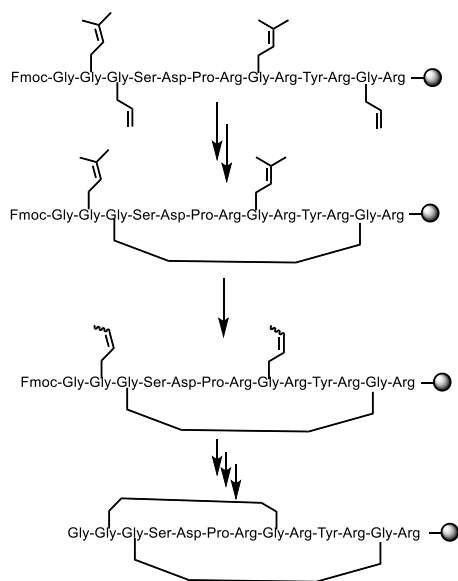


Figure 3.10 A representative schematic of the regioselective synthesis of the  $\alpha$ -conotoxin Rg1A analog where prenyl glycine residues were used to prevent unwanted cyclization during RCM.

In contrast to the strategy above that leveraged sequential ring closure to achieve regioselectivity, RCM and ring closing alkyne metathesis (RCAM) can simultaneously facilitate a one-pot synthesis due to the orthogonal nature of the two transformations. This strategy was employed by Cromm *et al.* who demonstrated regioselective ring closure in a one-pot reaction to generate a bicyclic peptide targeting the GTPase (Figure 3.10).<sup>93</sup> Cromm *et al.* prepared the bicyclic GTPase Rab8 inhibitor in one step using Grubbs first generation catalyst (G I) for RCM and molybdenum based catalyst (Figure 3.11) for RCAM. Notably, the less reactive Ru-catalyst G I was used to promote RCM rather than later generations of Grubbs catalysts because the increased reactivity of later generations of catalysts could also promote RCAM.<sup>67</sup>

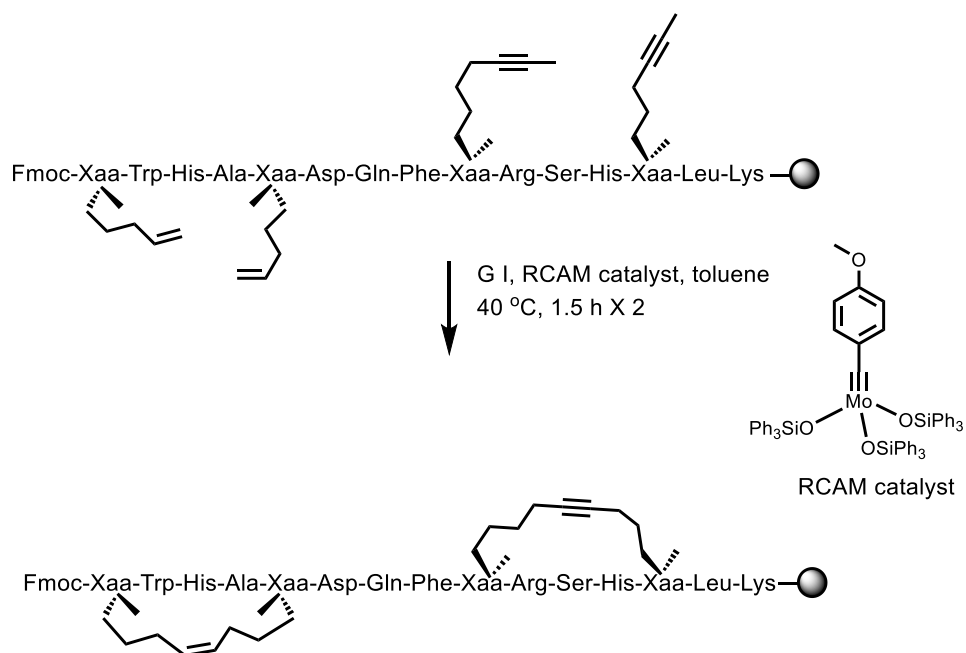


Figure 3.11 One-pot bicyclization of the GTPase Rab8 inhibitor using G I and the molybdenum based RCAM catalyst.

### 3.2.2 RCM and opioid peptides

Opioid peptides have been cyclized using a variety of cyclization approaches including disulfide, lactam, and ring closing metathesis approaches. These cyclic opioid peptides have been extensively reviewed by Remesic *et al*<sup>88</sup> as well as by Janecka and coworkers.<sup>26</sup> Similarly, ring closing metathesis of opioid peptides has been briefly reviewed by Jacobsen and coworkers.<sup>94</sup> Opioid peptide ligands generally consist of short peptides (enkephalins and dermorphins) preferentially active at  $\mu$  and  $\delta$  opioid receptors, and longer peptides (dynorphins) preferentially active at the  $\kappa$  opioid receptor. Endorphins and enkephalins are pentapeptides while dermorphin is a heptapeptide; undecapeptide peptide analogs of the heptadecapeptide dynorphin A consisting of the first 11 residues are typically used as  $\kappa$  opioid receptor ligands. This discussion will highlight cyclization of opioid peptides by ring closing metathesis with a focus on cyclic  $\kappa$  opioid receptor ligands.

The groups of Schiller<sup>95</sup> and Hruby<sup>96</sup> have reported RCM of short opioid peptides while the Aldrich group has reported RCM of dynorphin A (1-11)<sup>97</sup> (Figure 3.12). Cyclization of short peptides by RCM introduced a conformational constraint in the “message” region that binds and activates the receptor while cyclization of dynorphin analogs examined cyclization at the “message” and C-terminal “address” segment that enhances potency for a particular receptor (Figure 3.13).<sup>98</sup> The “message” region contains the opioid receptor pharmacophoric residues, Tyr and Phe, separated by Gly spacers. Both Schiller and Hruby and their coworkers prepared cyclic enkephalins where the disulfide bridge in H-Tyr-*c*[D-Cys-Gly-Phe-D-Cys] was replaced by a dicarba bridge. In contrast to cyclic C-terminal amide analogs prepared by Schiller and coworkers, Hruby and coworkers synthesized cyclic enkephalin analogs with a C-terminal acid (Figure 3.12a). The analogs were cyclized in a side chain to side chain motif using D/L-allylglycine (AllGly) and retained affinity at both  $\mu$  and  $\delta$  opioid receptors (Figure 3.12a). As expected, all cyclic analogs exhibited selectivity for the  $\mu$  and  $\delta$  opioid receptors over the  $\kappa$  opioid receptors. Additionally, considerable differences were observed between *cis* and *trans* isomers as well as saturated analogs.

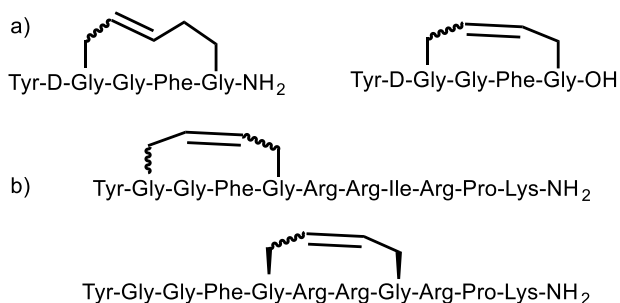


Figure 3.12 Representative examples of opioid peptides cyclized by RCM. A) cyclic enkephalin analogs, and b) cyclic dynorphin A analogs.

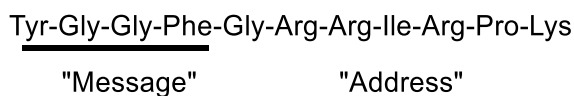


Figure 3.13 “Message” and “address”<sup>99</sup> regions of opioid peptides illustrated in dynorphin A (1-11).

Aldrich and coworkers explored RCM of dynorphin analogs as well the effect of stereochemistry at position 2 on opioid receptor binding.<sup>97</sup> A mixed solvent system was used for the RCM reactions for compatibility with the resin and the reaction gave reasonable yields (56-74%, Figure 3.14). Cyclization was performed between AllGly residues at position 2 and 5, or 5 and 8 whose modification is tolerated by the  $\kappa$  opioid receptor (KOR). Notably, RCM results in a hydrophobic tether that maintains the hydrophobic nature of the residues at these positions. Whereas cyclizations involving D-AllGly at residues 2 and 5 retained high affinity for all three opioid receptors, they exhibited minimal selectivity for KOR over  $\mu$  (MOR) and  $\delta$  opioid receptors (DOR) (Table 3.2). Cyclizations involving L-AllGly at residues 2 and 5 showed lower affinity but exhibited higher selectivity for KOR compare with the parent peptide Dyn A (1-11)NH<sub>2</sub>. Cyclizations involving AllGly at residues 5 and 8 displayed intermediate affinities but higher selectivity for KOR than the parent peptide. The *trans* isomer in cyclizations involving L-AllGly at positions 2 and 5 or 5 and 8 displayed higher KOR binding affinity than the *cis* isomer, indicating the effect of olefin geometry on KOR binding affinity (Table 3.2).

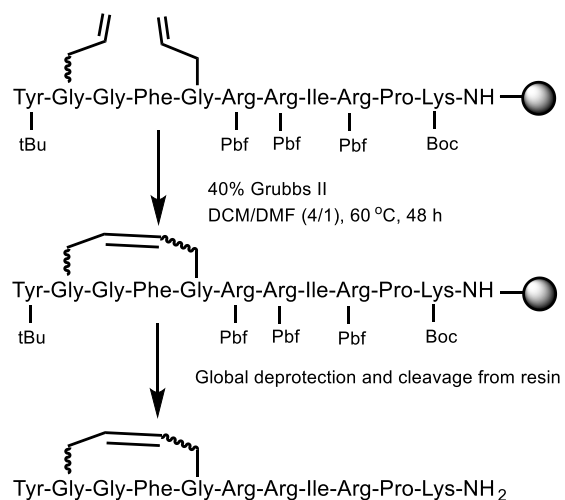


Figure 3.14 Schematic representation showing RCM of dynorphin A analogs.



Table 3.2 Binding affinities of Dyn A analogs cyclized by RCM.

Compound		K <sub>i</sub> (nM ± SEM)			K <sub>i</sub> ratio KOR/ MOR/ DOR
		KOR	MOR	DOR	
Dyn A(1-11)NH <sub>2</sub> <sup>a</sup>		0.57 ± 0.01	1.85 ± 0.52	6.81 ± 1.01	1/3/11
cyclo[Ala <sup>2</sup> (-CH=CH-)Ala <sup>5</sup> ]Dyn A(1-11)NH <sub>2</sub> <sup>b</sup>	<i>cis</i>	87.2 ± 6.9	763 ± 35	7670 ± 1030	1/8.8/88
	<i>trans</i>	9.46 ± 1.80	180 ± 10	1130 ± 98	1/19/119
cyclo[D-Ala <sup>2</sup> (-CH=CH-)Ala <sup>5</sup> ]Dyn A(1-11)NH <sub>2</sub> <sup>b</sup>	<i>cis</i>	0.84 ± 0.10	2.33 ± 0.20	9.30 ± 1.00	1/2.8/11
	<i>trans</i>	1.38 ± 0.31	2.33 ± 0.22	7.17 ± 0.55	1/1.7/5.2
cyclo[Ala <sup>5</sup> (-CH=CH-)Ala <sup>8</sup> ]Dyn A-(1-11)NH <sub>2</sub> <sup>b</sup>	<i>cis</i>	10.9 ± 1.8	93.0 ± 6.0	1210 ± 90	1/8.5/111
	<i>trans</i>	2.46 ± 0.57	36.0 ± 2.1	460 ± 51	1/15/187

<sup>a</sup> From ref<sup>100</sup> ; <sup>b</sup> from ref<sup>74</sup>

### 3.2.2.1 RCM of KOR antagonists

Previous conformationally constrained antagonists at the KOR have included lactam cyclizations (Figure 3.15).<sup>101, 102 103 104</sup> The kappa opioid antagonist arodyn (Figure 3.16) is a relatively potent (K<sub>i</sub> = 10 nM) and selective ( $\kappa/\mu/\delta$ )=1/174/583) peptide ligand that was shown to block stress induced reinstatement of cocaine-seeking *in vivo* after intracerebrovascular administration.<sup>105</sup> However, arodyn is rapidly metabolized which prevented evaluation following systemic administration. Cyclization of arodyn via lactam or alkene bridges has been explored to introduce conformation rigidity in this lead peptide KOR antagonist (Figure 3.16).<sup>106</sup> Cyclization was explored between residues 2 and , or 5 and 8, residues that showed minimal contribution to KOR affinity in an alanine scan.<sup>107</sup> Most of the cyclic analogs initially prepared exhibited low KOR affinity.<sup>106</sup>

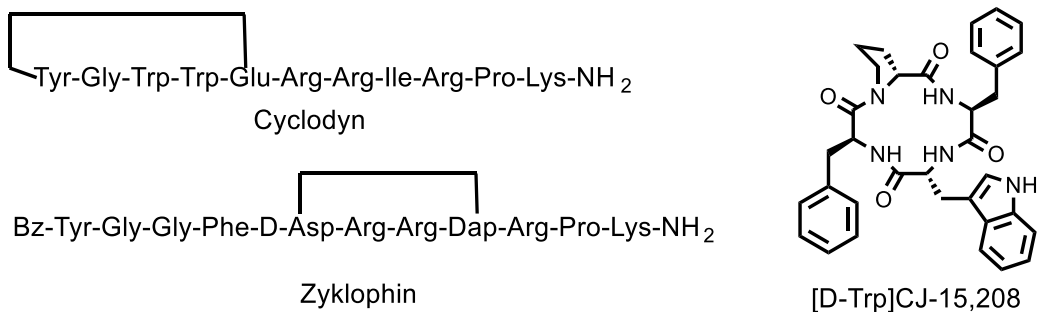


Figure 3.15 Structures of cyclic kappa opioid receptor antagonists.

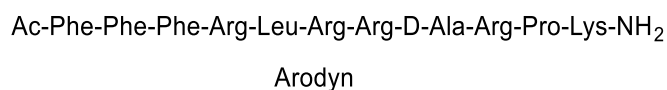


Figure 3.16 Structure of arodyn.

RCM was employed to synthesize alkene bridged arodyn analogs, both head to side chain and side chain to side chain cyclization motifs were explored, but synthetic challenges did not permit the synthesis of several analogs.<sup>106</sup> Generally, side chain to side chain cyclizations involving AllGly at residues 2, 5, and 8 resulted in high yields (70-90%), but the head to side chain cyclizations were generally unsuccessful likely due to unfavorable conformations of the olefin precursors in the linear peptides. Cyclization was only successful for one head to side chain analog after N-methylation of the N-terminus; in this case an N-terminal Alloc group was used to prevent a side reaction related to N-methylation (Figure 3.17).<sup>108</sup>

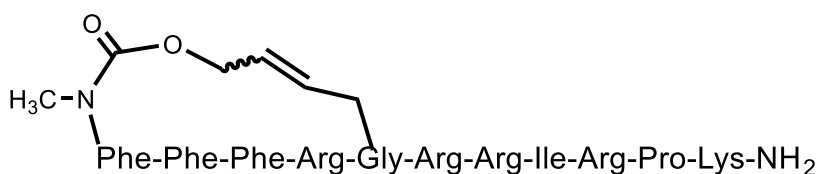


Figure 3.17 Structure of the cyclic N-methylated arodyn analog. N-Methylation facilitated head to side chain cyclization.

To introduce cyclizations in the N-terminal segment that maintain aromatic character, Tyr(All) residues were incorporated into arodyn to constrain relatively important residues. However, a side reaction leading to the loss of the allyl group compromised the yields of side chain to side chain cyclizations involving aromatic residues (Figure 3.18).<sup>106, 109</sup> Reaction product mixtures contained mixtures of mono and bis-desallyl products, indicating that the side reaction competed with cyclization and suggesting that the reacting olefins did not orient favorably for cyclization. Varying receptor affinities were observed for cyclized arodyn analogs.<sup>109</sup> Cyclization between Tyr(All)<sup>3</sup> and AllGly<sup>5</sup> displayed a 40-fold loss in affinity for KOR while cyclization between adjacent aromatic residues was better tolerated at KOR. (*cyclo*[Tyr<sup>2</sup>(CH<sub>2</sub>-CH=CH-CH<sub>2</sub>)Tyr<sup>3</sup>,Ile<sup>8</sup>]arodyn displayed a 5.5 fold loss in affinity ( $K_i = 55$  nM) for KOR compared to arodyn (Figure 3.18) while (*cyclo*[Tyr<sup>1</sup>(CH<sub>2</sub>-CH=CH-CH<sub>2</sub>)Tyr<sup>2</sup>,Ile<sup>8</sup>]arodyn displayed a 7-fold loss in affinity ( $K_i = 71.7$  nM) for KOR.<sup>109</sup> It should be noted however that this analog contained Ile<sup>8</sup> in place of D-Ala<sup>8</sup>. Incorporation of D-Ala<sup>8</sup> could enhance affinity to the KOR. Sequence dependent effects were most evident for *cyclo*[Tyr<sup>1</sup>(CH<sub>2</sub>-CH=CH-CH<sub>2</sub>)Tyr<sup>3</sup>,Ile<sup>8</sup>], *cyclo*<sup>5</sup>[Tyr<sup>1</sup>(CH<sub>2</sub>-CH=CH)Ala<sup>5</sup>,Ile<sup>8</sup>], and *cyclo*<sup>5</sup>[Tyr<sup>2</sup>(CH<sub>2</sub>-CH=CH)Ala<sup>5</sup>,Ile<sup>8</sup>] where cyclizations were unsuccessful resulting in des-allyl products.

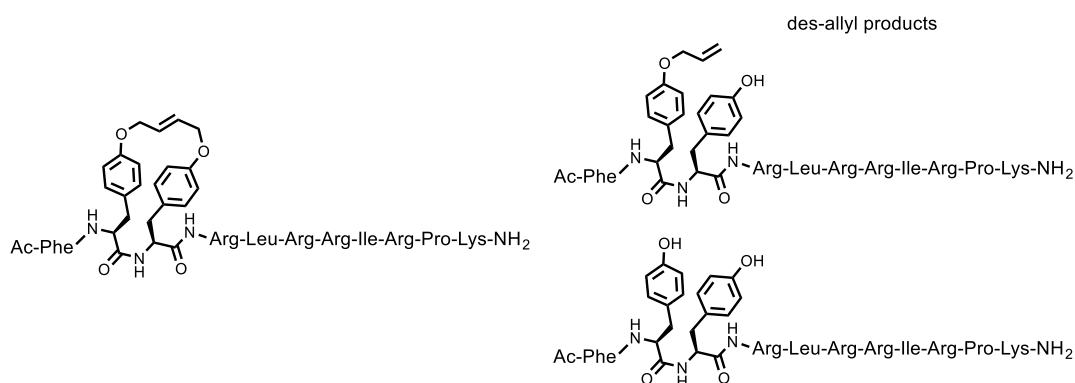


Figure 3.18 Representative structures of a cyclic arodyn analog, *cyclo*<sup>2,3</sup>[Tyr<sup>2</sup>(CH<sub>2</sub>-CH=CH-CH<sub>2</sub>)Tyr<sup>3</sup>,Ile<sup>8</sup>]arodyn, and the des-allyl products from a side reaction during RCM.

### 3.3 Conclusion

Cyclic peptides have a growing prominence, especially with respect to probing biological function. Ring closing metathesis, which involves the exchange of intramolecular olefins to generate carbon-carbon bonds catalyzed by Grubb's catalysts<sup>46</sup> (Figure 3.5a), is one approach that has had wide impact in peptide cyclization. The resulting ethylene bridge has become increasingly valuable in constraining peptides and peptidomimetics, as demonstrated by reports of increased metabolic stability and bioactivity of cyclic ligands.<sup>27, 110, 111</sup> Despite challenges in peptide RCM (Table 3.1), new developments in peptide stapling technology through development of stable catalysts and modified reaction conditions for different substrates increase the utility of ring closing metathesis.

### 3.4 References

1. Craik, D. J.; Fairlie, D. P.; Liras, S.; Price, D. The future of peptide-based drugs. *Chem Biol Drug Des* **2013**, 81, 136-147.
2. Vlieghe, P.; Lisowski, V.; Martinez, J.; Khrestchatsky, M. Synthetic therapeutic peptides: science and market. *Drug Discov Today* **2010**, 15, 40-56.
3. Henninot, A.; Collins, J. C.; Nuss, J. M. The Current State of Peptide Drug Discovery: Back to the Future? *J Med Chem* **2017**, 1382-1414.
4. Tapeinou, A.; Matsoukas, M.-T.; Simal, C.; Tselios, T. Review Cyclic Peptides on a Merry-Go-Round; Towards Drug Design. *Biopolymers* **2015**, 104, 453-461.
5. Chang, Y. S.; Graves, B.; Guerlavais, V.; Tovar, C.; Packman, K.; To, K.-H.; Olson, K. A.; Kesavan, K.; Gangurde, P.; Mukherjee, A.; Baker, T.; Darlak, K.; Elkin, C.; Filipovic, Z.; Qureshi, F. Z.; Cai, H.; Berry, P.; Feyfant, E.; Shi, X. E.; Horstick, J.; Annis, D. A.; Manning, A. M.; Fotouhi, N.; Nash, H.; Vassilev, L. T.; Sawyer, T. K. Stapled  $\alpha$ -helical peptide drug development: A potent dual inhibitor of MDM2 and MDMX for p53-dependent cancer therapy. *Proc Natl Acad Sci* **2013**, 110, E3445-E3454.
6. Sawyer, N.; Watkins, A. M.; Arora, P. S. Protein Domain Mimics as Modulators of Protein-Protein Interactions. *Acc Chem Res* **2017**, 50, 1313-1322.
7. Gao, M.; Cheng, K.; Yin, H. Targeting protein-protein interfaces using macrocyclic peptides. *Biopolymers* **2015**, 104, 310-316.

8. Bock, J. E.; Gavenonis, J.; Kritzer, J. A. Getting in Shape: Controlling Peptide Bioactivity and Bioavailability Using Conformational Constraints. *ACS Chem Biol* **2013**, *8*, 488-499.
9. White, C. J.; Yudin, A. K. Contemporary strategies for peptide macrocyclization. *Nat Chem* **2011**, *3*, 509-524.
10. Lau, Y. H.; de Andrade, P.; Wu, Y.; Spring, D. R. Peptide stapling techniques based on different macrocyclisation chemistries. *Chem Soc Rev* **2015**, *44*, 91-102.
11. Taylor, J. W. The synthesis and study of side-chain lactam-bridged peptides. *Biopolymers* **2002**, *66*, 49-75.
12. Vagner, J.; Qu, H.; Hruby, V. J. Peptidomimetics, a synthetic tool of drug discovery. *Curr Opin Chem Biol* **2008**, *12*, 292-296.
13. Xu, S.; Li, H.; Shao, X.; Fan, C.; Ericksen, B.; Liu, J.; Chi, C.; Wang, C. Critical Effect of Peptide Cyclization on the Potency of Peptide Inhibitors against Dengue Virus NS2B-NS3 Protease. *J Med Chem* **2012**, *55*, 6881-6887.
14. Aldrich, J. V. CHAPTER 7 Peptide Lead Optimization-Strategies and Tactics. In *Peptide-based Drug Discovery: Challenges and New Therapeutics*, The Royal Society of Chemistry: 2017; pp 192-222.
15. Dathe, M.; Nikolenko, H.; Klose, J.; Bienert, M. Cyclization Increases the Antimicrobial Activity and Selectivity of Arginine- and Tryptophan-Containing Hexapeptides. *Biochemistry* **2004**, *43*, 9140-9150.
16. Nam, N.-H.; Ye, G.; Sun, G.; Parang, K. Conformationally Constrained Peptide Analogues of pTyr-Glu-Glu-Ile as Inhibitors of the Src SH2 Domain Binding. *J Med Chem* **2004**, *47*, 3131-3141.
17. Khan, A. R.; Parrish, J. C.; Fraser, M. E.; Smith, W. W.; Bartlett, P. A.; James, M. N. G. Lowering the Entropic Barrier for Binding Conformationally Flexible Inhibitors to Enzymes. *Biochemistry* **1998**, *37*, 16839-16845.
18. Long, Y.-Q.; Lung, F.-D. T.; Roller, P. P. Global optimization of conformational constraint on non-phosphorylated cyclic peptide antagonists of the Grb2-SH2 domain. *Bioorg Med Chem* **2003**, *11*, 3929-3936.
19. Schafmeister, C. E.; Po, J.; Verdine, G. L. An All-Hydrocarbon Cross-Linking System for Enhancing the Helicity and Metabolic Stability of Peptides. *J Am Chem Soc* **2000**, *122*, 5891-5892.
20. Oba, M.; Kunitake, M.; Kato, T.; Ueda, A.; Tanaka, M. Enhanced and Prolonged Cell-Penetrating Abilities of Arginine-Rich Peptides by Introducing Cyclic  $\alpha,\alpha$ -Disubstituted  $\alpha$ -Amino Acids with Stapling. *Bioconjugate Chem* **2017**, *28*, 1801-1806.
21. Lautrette, G.; Touti, F.; Lee, H. G.; Dai, P.; Pentelute, B. L. Nitrogen Arylation for Macrocyclization of Unprotected Peptides. *J Am Chem Soc* **2016**, *138*, 8340-8343.

22. Craik, D. J.; Swedberg, J. E.; Mylne, J. S.; Cemazar, M. Cyclotides as a basis for drug design. *Expert Opin Drug Discov* **2012**, *7*, 179-194.
23. Colgrave, M. L.; Craik, D. J. Thermal, chemical, and enzymatic stability of the cyclotide kalata B1: the importance of the cyclic cystine knot. *Biochemistry* **2004**, *43*, 5965-5975.
24. Sgambelluri, R. M.; Epis, S.; Sasser, D.; Luo, H.; Angelos, E. R.; Walton, J. D. Profiling of Amatoxins and Phallotoxins in the Genus *Lepiota* by Liquid Chromatography Combined with UV Absorbance and Mass Spectrometry. *Toxins* **2014**, *6*, 2336-2347.
25. Gong, X. Q.; Nedialkov, Y. A.; Burton, Z. F.  $\alpha$ -Amanitin Blocks Translocation by Human RNA Polymerase II. *J Biol Chem* **2004**, *279*, 27422-27427.
26. Piekielna, J.; Perlikowska, R.; Gach, K.; Janecka, A. Cyclization in Opioid Peptides. *Curr Drug Targets* **2013**, *14*, 798-816.
27. Wachter, F.; Morgan, A. M.; Godes, M.; Mourtada, R.; Bird, G. H.; Walensky, L. D. Mechanistic validation of a clinical lead stapled peptide that reactivates p53 by dual HDM2 and HDMX targeting. *Oncogene* **2017**, *36*, 2184-2190.
28. Miller, S. J.; Blackwell, H. E.; Grubbs, R. H. Application of Ring-Closing Metathesis to the Synthesis of Rigidified Amino Acids and Peptides. *J Am Chem Soc* **1996**, *118*, 9606-9614.
29. Miller, S. J.; Grubbs, R. H. Synthesis of Conformationally Restricted Amino Acids and Peptides Employing Olefin Metathesis. *J Am Chem Soc* **1995**, *117*, 5855-5856.
30. Bird, G. H.; Madani, N.; Perry, A. F.; Princiotto, A. M.; Supko, J. G.; He, X.; Gavathiotis, E.; Sodroski, J. G.; Walensky, L. D. Hydrocarbon Double-Stapling Remedies the Proteolytic Instability of a Lengthy Peptide Therapeutic. *Proc Natl Acad Sci* **2010**, *107*, 14093-14098.
31. Bird, G. H.; Irimia, A.; Ofek, G.; Kwong, P. D.; Wilson, I. A.; Walensky, L. D. Stapled HIV-1 peptides recapitulate antigenic structures and engage broadly neutralizing antibodies. *Nat Struct Mol Biol* **2014**, *21*, 1058.
32. Verdine, G. L.; Hilinski, G. J. Stapled peptides for intracellular drug targets. *Methods Enzymol* **2012**, *503*, 3-33.
33. Chu, Q.; Moellering, R. E.; Hilinski, G. J.; Kim, Y.-W.; Grossmann, T. N.; Yeh, J. T. H.; Verdine, G. L. Towards understanding cell penetration by stapled peptides. *MedChemComm* **2015**, *6*, 111-119.
34. Cromm, P. M.; Spiegel, J.; Grossmann, T. N. Hydrocarbon Stapled Peptides as Modulators of Biological Function. *ACS Chem Biol* **2015**, *10*, 1362-1375.
35. Stewart, M. L.; Fire, E.; Keating, A. E.; Walensky, L. D. The MCL-1 BH3 helix is an exclusive MCL-1 inhibitor and apoptosis sensitizer. *Nat Chem Biol* **2010**, *6*, 595-601.

36. Liu, F.; Stephen, A. G.; Waheed, A. A.; Freed, E. O.; Fisher, R. J.; Burke Jr, T. R. Application of ring-closing metathesis macrocyclization to the development of Tsg101-binding antagonists. *Bioorg Med Chem Lett* **2010**, 20, 318-321.
37. Merrifield, R. B. Solid Phase Peptide Synthesis. I. The Synthesis of a Tetrapeptide. *J Am Chem Soc* **1963**, 85, 2149-2154.
38. Sabatino, G.; Papini, A. M. Advances in automatic, manual and microwave-assisted solid-phase peptide synthesis. *Curr Opin Drug Discov Devel* **2008**, 11, 762-770.
39. Camarero, J. A.; Cairo, J. J.; Giralt, E.; Andreu, D. Solution versus solid-phase cyclization strategies for large sidechain lactam-bridged peptides: a comparative study. *J Pept Sci* **1995**, 1, 241-250.
40. Valero, M. L.; Valero, M.; L. A comparative study of cyclization strategies applied to the synthesis of head-to-tail cyclic analogs of a viral epitope. *J Pept Sci* **53**, 56-67.
41. Malesevic, M.; Strijowski, U.; Bächle, D.; Sewald, N. An improved method for the solution cyclization of peptides under pseudo-high dilution conditions. *J Biotechnol* **2004**, 112, 73-77.
42. Scott, L. T.; Rebek, J.; Ovsyanko, L.; Sims, C. L. Organic chemistry on the solid phase. Site-site interactions on functionalized polystyrene. *J Am Chem Soc* **1977**, 99, 625-626.
43. Fan, Q.; Wang, T.; Dai, J.; Kuttner, J.; Hilt, G.; Gottfried, J. M.; Zhu, J. On-Surface Pseudo-High-Dilution Synthesis of Macrocycles: Principle and Mechanism. *ACS Nano* **2017**, 11, 5070-5079.
44. Mazur, S.; Jayalekshmy, P. Chemistry of polymer-bound o-benzyne. Frequency of encounter between substituents on crosslinked polystyrenes. *J Am Chem Soc* **1979**, 101, 677-683.
45. Wu, Z.-M.; Liu, S.-Z.; Cheng, X.-Z.; Ding, W.-Z.; Zhu, T.; Chen, B. Recent progress of on-resin cyclization for the synthesis of glycopeptidomimetics. *Chin Chem Lett* **2016**, 27, 1731-1739.
46. Vougioukalakis, G. C.; Grubbs, R. H. Ruthenium-Based Heterocyclic Carbene-Coordinated Olefin Metathesis Catalysts. *Chem Rev* **2010**, 110, 1746-1787.
47. Hans-Günther, S. Catalytic Ring-Closing Metathesis: A New, Powerful Technique for Carbon–Carbon Coupling in Organic Synthesis. *Angew Chem Int* **1995**, 34, 1833-1836.
48. van der Eide, E. F.; Piers, W. E. Mechanistic insights into the ruthenium-catalysed diene ring-closing metathesis reaction. *Nat Chem* **2010**, 2, 571.
49. Walensky, L. D.; Bird, G. H. Hydrocarbon-Stapled Peptides: Principles, Practice, and Progress. *J Med Chem* **2014**, 57, 6275-6288.
50. Patgiri, A.; Menzenski, M. Z.; Mahon, A. B.; Arora, P. S. Solid-phase synthesis of short [alpha]-helices stabilized by the hydrogen bond surrogate approach. *Nat. Protocols* **2010**, 5, 1857-1865.
51. Wang, D.; Chen, K.; Kulp Iii, J. L.; Arora, P. S. Evaluation of biologically relevant short alpha-helices stabilized by a main-chain hydrogen-bond surrogate. *J Am Chem Soc* **2006**, 128, 9248-9256.

52. Glas, A.; Grossmann, T. N. Constraining Peptide Conformations with the Help of Ring-Closing Metathesis. *Synlett* **2015**, 26, 1-5.
53. Stymiest, J. L.; Mitchell, B. F.; Wong, S.; Vederas, J. C. Synthesis of Biologically Active Dicarba Analogues of the Peptide Hormone Oxytocin Using Ring-Closing Metathesis. *Org Lett* **2003**, 5, 47-49.
54. Nelson, D. J.; Manzini, S.; Urbina-Blanco, C. A.; Nolan, S. P. Key processes in ruthenium-catalysed olefin metathesis. *Chem Commun* **2014**, 50, 10355-10375.
55. Hong, S. H.; Day, M. W.; Grubbs, R. H. Decomposition of a Key Intermediate in Ruthenium-Catalyzed Olefin Metathesis Reactions. *J Am Chem Soc* **2004**, 126, 7414-7415.
56. Martinez-Amezaga, M.; Delpiccolo, C.; Méndez, L.; Dragutan, I.; Dragutan, V.; Mata, E. Unprecedented Multifunctionality of Grubbs and Hoveyda–Grubbs Catalysts: Competitive Isomerization, Hydrogenation, Silylation and Metathesis Occurring in Solution and on Solid Phase. *Catalysts* **2017**, 7, 111.
57. Dinger, Maarten B.; Mol, Johannes C. Degradation of the Second-Generation Grubbs Metathesis Catalyst with Primary Alcohols and Oxygen – Isomerization and Hydrogenation Activities of Monocarbonyl Complexes. *Eur J Inorg Chem* **2003**, 2003, 2827-2833.
58. Schmidt, B. Catalysis at the Interface of Ruthenium Carbene and Ruthenium Hydride Chemistry: Organometallic Aspects and Applications to Organic Synthesis. *Eur J Org Chem* **2004**, 2004, 1865-1880.
59. Hong, S. H.; Sanders, D. P.; Lee, C. W.; Grubbs, R. H. Prevention of Undesirable Isomerization during Olefin Metathesis. *J Am Chem Soc* **2005**, 127, 17160-17161.
60. Engel, J.; Smit, W.; Foscatto, M.; Occhipinti, G.; Törnroos, K. W.; Jensen, V. R. Loss and Reformation of Ruthenium Alkylidene: Connecting Olefin Metathesis, Catalyst Deactivation, Regeneration, and Isomerization. *J Am Chem Soc* **2017**, 139, 16609-16619.
61. O'Doherty, I.; Yim, J. J.; Schmelz, E. A.; Schroeder, F. C. Synthesis of Caeliferins, Elicitors of Plant Immune Responses: Accessing Lipophilic Natural Products via Cross Metathesis. *Org Lett* **2011**, 13, 5900-5903.
62. Reichwein, John F.; Liskamp, Rob M. J. Synthesis of Cyclic Dipeptides by Ring-Closing Metathesis. *Eur J Org Chem* **2000**, 2000, 2335-2344.
63. ten Brink, H. T.; Rijkers, D. T.; Kemmink, J.; Hilbers, H. W.; Liskamp, R. M. Ring-closing metathesis for the synthesis of side chain knotted pentapeptides inspired by vancomycin. *Org Biomol Chem* **2004**, 2, 2658-2663.
64. De Rosa, M.; Unge, J.; Motwani, H. V.; Rosenquist, Å.; Vrang, L.; Wallberg, H.; Larhed, M. Synthesis of P1'-Functionalized Macrocyclic Transition-State Mimicking HIV-1 Protease Inhibitors Encompassing a Tertiary Alcohol. *J Med Chem* **2014**, 57, 6444-6457.



65. Hanson, P. R.; Chegondi, R.; Nguyen, J.; Thomas, C. D.; Waetzig, J. D.; Whitehead, A. Total Synthesis of Dolabelide C: A Phosphate-Mediated Approach. *J Org Chem* **2011**, 76, 4358-4370.
66. Bergman, Y. E.; Del Borgo, M. P.; Gopalan, R. D.; Jalal, S.; Unabia, S. E.; Ciampini, M.; Clayton, D. J.; Fletcher, J. M.; Mulder, R. J.; Wilce, J. A.; Aguilar, M.-I.; Perlmutter, P. Synthesis of Stapled  $\beta^3$ -Peptides through Ring-Closing Metathesis. *Org Lett* **2009**, 11, 4438-4440.
67. Gleeson, E. C.; Jackson, W. R.; Robinson, A. J. Ring-closing metathesis in peptides. *Tetrahedron Lett* **2016**, 57, 4325-4333.
68. van Lierop, B. J.; Whelan, A. N.; Andrikopoulos, S.; Mulder, R. J.; Jackson, W. R.; Robinson, A. J. Methods for Enhancing Ring Closing Metathesis Yield in Peptides: Synthesis of a Dicarba Human Growth Hormone Fragment. *Int J Pept Res* **2010**, 16, 133-144.
69. Schmiedeberg, N.; Kessler, H. Reversible Backbone Protection Enables Combinatorial Solid-Phase Ring-Closing Metathesis Reaction (RCM) in Peptides. *Org Lett* **2002**, 4, 59-62.
70. Gleeson, E. C.; Wang, Z. J.; Robinson, S. D.; Chhabra, S.; MacRaild, C. A.; Jackson, W. R.; Norton, R. S.; Robinson, A. J. Stereoselective synthesis and structural elucidation of dicarba peptides. *Chem Commun* **2016**, 52, 4446-4449.
71. Khan, S. N.; Kim, A.; Grubbs, R. H.; Kwon, Y.-U. Ring-Closing Metathesis Approaches for the Solid-Phase Synthesis of Cyclic Peptoids. *Org Lett* **2011**, 13, 1582-1585.
72. Abell, A. D.; Alexander, N. A.; Aitken, S. G.; Chen, H.; Coxon, J. M.; Jones, M. A.; McNabb, S. B.; Muscroft-Taylor, A. Synthesis of macrocyclic beta-strand templates by ring closing metathesis. *J Org Chem* **2009**, 74, 4354-4356.
73. Chapman, R. N.; Arora, P. S. Optimized synthesis of hydrogen-bond surrogate helices: surprising effects of microwave heating on the activity of Grubbs catalysts. *Org Lett* **2006**, 8, 5825-5828.
74. Fang, W.-J.; Cui, Y.; Murray, T. F.; Aldrich, J. V. Design, Synthesis, and Pharmacological Activities of Dynorphin A Analogs Cyclized by Ring-Closing Metathesis. *J Med Chem* **2009**, 52, 5619-5625.
75. Mangold, S. L.; Grubbs, R. H. Stereoselective synthesis of macrocyclic peptides via a dual olefin metathesis and ethenolysis approach. *Chem Sci* **2015**, 6, 4561-4569.
76. Montgomery, T. P.; Johns, A. M.; Grubbs, R. H. Recent Advancements in Stereoselective Olefin Metathesis Using Ruthenium Catalysts. *Catalysts* **2017**, 7, 87.
77. Mangold, S. L.; O'Leary, D. J.; Grubbs, R. H. Z-Selective Olefin Metathesis on Peptides: Investigation of Side-Chain Influence, Preorganization, and Guidelines in Substrate Selection. *J Am Chem Soc* **2014**, 136, 12469-12478.
78. Cochrane, S. A.; Huang, Z.; Vederas, J. C. Investigation of the ring-closing metathesis of peptides in water. *Org Biomol Chem* **2013**, 11, 630-639.

79. Lu, X.; Fan, L.; Phelps, C. B.; Davie, C. P.; Donahue, C. P. Ruthenium Promoted On-DNA Ring-Closing Metathesis and Cross-Metathesis. *Bioconjugate Chem* **2017**, *28*, 1625-1629.
80. Rhodes, C. A.; Pei, D. Bicyclic Peptides as Next-Generation Therapeutics. *Chem Eur J* **2017**, *23*, 12690-12703.
81. Quartararo, J. S.; Eshelman, M. R.; Peraro, L.; Yu, H.; Baleja, J. D.; Lin, Y. S.; Kritzer, J. A. A bicyclic peptide scaffold promotes phosphotyrosine mimicry and cellular uptake. *Bioorg Med Chem* **2014**, *22*, 6387-6391.
82. Hilinski, G. J.; Kim, Y.-W.; Hong, J.; Kutchukian, P. S.; Crenshaw, C. M.; Berkovitch, S. S.; Chang, A.; Ham, S.; Verdine, G. L. Stitched  $\alpha$ -Helical Peptides via Bis Ring-Closing Metathesis. *J Am Chem Soc* **2014**, *136*, 12314-12322.
83. Islam, M. N.; Islam, M. S.; Hoque, M. A.; Kato, T.; Nishino, N.; Ito, A.; Yoshida, M. Bicyclic tetrapeptides as potent HDAC inhibitors: Effect of aliphatic loop position and hydrophobicity on inhibitory activity. *Bioorg Med Chem* **2014**, *22*, 3862-3870.
84. Saijo, K.; Imamura, J.; Narita, K.; Oda, A.; Shimodaira, H.; Katoh, T.; Ishioka, C. Biochemical, biological and structural properties of romidepsin (FK228) and its analogs as novel HDAC/PI3K dual inhibitors. *Cancer Sci* **2015**, *106*, 208-215.
85. Lian, W.; Jiang, B.; Qian, Z.; Pei, D. Cell-permeable bicyclic peptide inhibitors against intracellular proteins. *J Am Chem Soc* **2014**, *136*, 9830-9833.
86. Heinis, C.; Rutherford, T.; Freund, S.; Winter, G. Phage-encoded combinatorial chemical libraries based on bicyclic peptides. *Nat Chem Biol* **2009**, *5*, 502-507.
87. Hill, P. S.; Smith, D. D.; Slaninova, J.; Hruby, V. J. Bicyclization of a weak oxytocin agonist produces a highly potent oxytocin antagonist. *J Am Chem Soc* **1990**, *112*, 3110-3113.
88. Remesic, M.; Lee, Y. S.; Victor, H. J. Cyclic Opioid Peptides. *Curr Med Chem* **2016**, *23*, 1288-1303.
89. Postma, T. M.; Albericio, F. N-chlorosuccinimide, an efficient peptide disulfide bond-forming reagent in aqueous solution. *RSC Advances* **2013**, *3*, 14277-14280.
90. Pattabiraman, V. R.; Stymiest, J. L.; Derksen, D. J.; Martin, N. I.; Vederas, J. C. Multiple On-Resin Olefin Metathesis to Form Ring-Expanded Analogues of the Lantibiotic Peptide, Lactacin 3147 A2. *Org Lett* **2007**, *9*, 699-702.
91. Slootweg, J. C.; Kemmink, J.; Liskamp, R. M. J.; Rijkers, D. T. S. Synthesis and structural characterization of the individual diastereoisomers of a cross-stapled alkene-bridged nisin DE-ring mimic. *Org Biomol Chem* **2013**, *11*, 7486-7496.

92. Robinson, A. J.; van Lierop, B. J.; Garland, R. D.; Teoh, E.; Elaridi, J.; Illesinghe, J. P.; Jackson, W. R. Regioselective formation of interlocked dicarba bridges in naturally occurring cyclic peptide toxins using olefin metathesis. *Chem Commun* **2009**, 4293-4295.
93. Cromm, P. M.; Schaubach, S.; Spiegel, J.; Furstner, A.; Grossmann, T. N.; Waldmann, H. Orthogonal ring-closing alkyne and olefin metathesis for the synthesis of small GTPase-targeting bicyclic peptides. *Nat Commun* **2016**, 7, 11300.
94. Jacobsen, Ø.; Klaveness, J.; Rongved, P. Structural and Pharmacological Effects of Ring-Closing Metathesis in Peptides. *Molecules* **2010**, 15, 6638-6677.
95. Berezowska, I.; Lemieux, C.; Chung, N. N.; Wilkes, B. C.; Schiller, P. W. Cyclic Opioid Peptide Agonists and Antagonists Obtained Via Ring-Closing Metathesis. *Chem Biol Drug Des* **2009**, 74, 329-334.
96. Mollica, A.; Guardiani, G.; Davis, P.; Ma, S.-W.; Porreca, F.; Lai, J.; Mannina, L.; Sobolev, A. P.; Hruby, V. J. Synthesis of Stable and Potent  $\delta/\mu$  Opioid Peptides: Analogues of H-Tyr-c[D-Cys-Gly-Phe-D-Cys]-OH by Ring-Closing Metathesis. *J Med Chem* **2007**, 50, 3138-3142.
97. Fang, W.-J.; Cui, Y.; Murray, T. F.; Aldrich, J. V. Design, Synthesis, and Pharmacological Activities of Dynorphin A Analogues Cyclized by Ring-Closing Metathesis. *J Med Chem* **2009**, 52, 5619-5625.
98. Chavkin, C.; Goldstein, A. Specific Receptor for the Opioid Peptide Dynorphin: Structure-Activity Relationships. *Proc Natl Acad Sci* **1981**, 78, 6543-6547.
99. Chavkin, C.; Goldstein, A. Specific receptor for the opioid peptide dynorphin: structure--activity relationships. *Proc Natl Acad Sci U.S.A.* **1981**, 78, 6543-6547.
100. Patkar, K. A.; Yan, X.; Murray, T. F.; Aldrich, J. V. [ $N\alpha$ -BenzylTyr,cyclo(d-Asp5,Dap8)]-dynorphin A-(1-11)NH<sub>2</sub> Cyclized in the "Address" Domain Is a Novel  $\kappa$ -Opioid Receptor Antagonist. *J Med Chem* **2005**, 48, 4500-4503.
101. Vig, B. S.; Murray, T. F.; Aldrich, J. V. A Novel N-Terminal Cyclic Dynorphin A Analogue cycloN<sub>5</sub>[Trp3,Trp4,Glu5] Dynorphin A-(1-11)NH<sub>2</sub> That Lacks the Basic N-Terminus. *J Med Chem* **2003**, 46, 1279-1282.
102. Aldrich, J. V.; Patkar, K. A.; McLaughlin, J. P. Zyklophin, a systemically active selective kappa opioid receptor peptide antagonist with short duration of action. *Proc Natl Acad Sci* **2009**, 106, 18396-18401.
103. Aldrich, J. V.; Senadheera, S. N.; Ross, N. C.; Ganno, M. L.; Eans, S. O.; McLaughlin, J. P. The macrocyclic peptide natural product CJ-15,208 is orally active and prevents reinstatement of extinguished cocaine-seeking behavior. *J Nat Prod* **2013**, 76, 433-438.

104. Joshi, A. A.; Murray, T. F.; Aldrich, J. V. Structure–Activity Relationships of the Peptide Kappa Opioid Receptor Antagonist Zyklophin. *J Med Chem* **2015**, *58*, 8783-8795.
105. Bennett, M. A.; Murray, T. F.; Aldrich, J. V. Identification of Arodyn, a Novel Acetylated Dynorphin A-(1–11) Analogue, as a  $\kappa$  Opioid Receptor Antagonist. *J Med Chem* **2002**, *45*, 5617-5619.
106. Fang, W. Design and Synthesis of Novel Linear and Cyclic Peptide Ligands for Kappa Opioid Receptors. University of Kansas, 2008.
107. Bennett, M. A.; Murray, T. F.; Aldrich, J. V. Structure–activity relationships of arodyn, a novel acetylated kappa opioid receptor antagonist\*,†. *J Pept Sci* **2005**, *65*, 322-332.
108. Fang, W. J.; Bennett, M. A.; Aldrich, J. V. Deletion of Ac-NMePhe(1) from [NMePhe(1)]arodyn under acidic conditions, part 1: effects of cleavage conditions and N-terminal functionality. *Biopolymers* **2011**, *96*, 97-102.
109. Fang, W.-J.; Murray, T. F.; Aldrich, J. V. Design, synthesis, and opioid activity of arodyn analogs cyclized by ring-closing metathesis involving Tyr(allyl). *Bioorg Med Chem* **2018**, *26*, 1157-1161.
110. Chang, Y. S.; Graves, B.; Guerlavais, V.; Tovar, C.; Packman, K.; To, K. H.; Olson, K. A.; Kesavan, K.; Gangurde, P.; Mukherjee, A.; Baker, T.; Darlak, K.; Elkin, C.; Filipovic, Z.; Qureshi, F. Z.; Cai, H.; Berry, P.; Feyfant, E.; Shi, X. E.; Horstick, J.; Annis, D. A.; Manning, A. M.; Fotouhi, N.; Nash, H.; Vassilev, L. T.; Sawyer, T. K. Stapled alpha-helical peptide drug development: a potent dual inhibitor of MDM2 and MDMX for p53-dependent cancer therapy. *Proc Natl Acad Sci* **2013**, *110*, E3445-3454.
111. Tsantrizos, Y. S. The design of a potent inhibitor of the hepatitis C virus NS3 protease: BILN 2061—From the NMR tube to the clinic. *Biopolymers* **2004**, *76*, 309-323.

**Chapter 4 - Suppression of desallyl side products in peptide ring closing metathesis involving Tyr(All): a model dipeptide study**

## 4.1 Introduction

Cyclization of peptides is a useful approach to probe ligand binding at biological targets. A cyclic constraint can potentially improve metabolic stability,<sup>1</sup> enhance affinity for a biological target by stabilizing the bioactive conformation<sup>2</sup> and/or improve membrane permeability.<sup>3,4</sup> Ring closing metathesis (RCM) is a widely used cyclization strategy in which intramolecular alkene precursors undergo olefin metathesis, resulting in a C-C double bond that reduces the conformational freedom of the product. Unlike standard peptide cyclization strategies such as disulfide and lactam linkages, RCM generates a non-native C-C bond with distinct geometry that is particularly stable.<sup>5</sup> The synthesis of cyclic peptides by RCM, on-resin and in solution, has increased extensively<sup>6,7</sup> due to the broad versatility of RCM.<sup>8-10</sup> In addition to the development of stable catalysts,<sup>11-14</sup> the rising utility of RCM in peptide modification is due, in part, to the increasing availability of non-natural alkene amino acid precursors as a result of their improved syntheses.<sup>15-17</sup> It is not surprising that a corresponding increase in the use of RCM in peptide and biological applications has been observed.<sup>18,19</sup>

Notably, peptide RCM generally features all-hydrocarbon RCM bridges utilizing amino acid residues such as  $\alpha$ -alkenyl and allylglycine residues.<sup>4,18,20,21</sup> Additionally, several studies have used heteroatom substituted allylic or homoallylic residues to increase the diversity of RCM bridges; these include allylserine, allylcysteine, and allyl tyrosine (Tyr(All)) residues.<sup>22-24</sup> Incorporation of these amino acids into the peptide sequence allows the formation of RCM bridges with distinct lengths and properties.

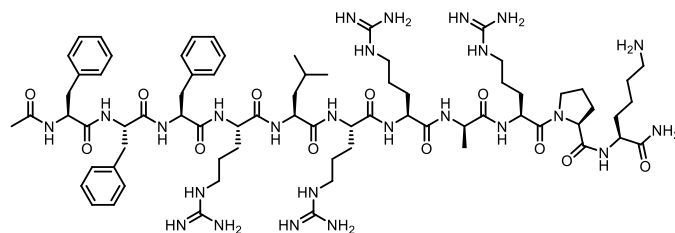
While the selectivity of RCM for alkenes in the presence of multiple functional groups is a significant advantage, particularly in peptide RCM, there are accompanying shortcomings. Chelation of the catalyst to polar functionalities in the peptide has been reported to decrease the

amount of catalyst available for productive metathesis.<sup>25</sup> Additionally, aggregation of the peptide on the solid support can be limiting.<sup>23</sup> Approaches that have been reported to enhance on-resin RCM include additives such as chaotropic salts or Lewis acids, and the use of microwave heating.<sup>26,27</sup> Sequence dependent effects also affect the efficiency of the cyclizations;<sup>28</sup> Robinson and co-workers reported that incorporation of a turn-inducing residue and microwave irradiation were required to facilitate RCM of a human growth hormone fragment.<sup>23</sup>

A number of reports describing additives, further development of catalysts, and optimization of reaction conditions to enhance olefin metathesis highlight its utility, but also its shortcomings.<sup>29-32</sup> Whereas ruthenium catalyzed olefin isomerization has been conveniently employed to synthesize various heterocyclic compounds<sup>33,34</sup> and complex natural products,<sup>35</sup> it can be a limiting factor in RCM cyclizations, particularly in isomerization-prone substrates such aryl-allyl groups<sup>36</sup> and heteroatom substituted allylic groups.<sup>37</sup> Despite the utility of RCM, side reactions, such as olefin isomerization,<sup>12,30</sup> can limit the utility of RCM in synthesizing the desired cyclic peptide derivatives.

This study stems from initial attempts to prepare constrained analogs of the novel acetylated dynorphin A (Dyn A) analog arodyn (Ac[Phe<sup>1,2,3</sup>,Arg<sup>4</sup>,D-Ala<sup>8</sup>]Dyn A(1-11)-NH<sub>2</sub>, Figure 4.1) with cyclizations involving aromatic residues.<sup>38</sup> Arodyn is a potent and selective kappa opioid receptor (KOR) antagonist which has high affinity ( $K_i = 10$  nM) and selectivity for KOR ( $K_i$  ratio ( $\kappa/\mu/\delta$ ) = 1/174/583).<sup>39</sup> KOR antagonists, used classically as pharmacological tools, have more recently shown potential for the treatment of depression and drug addiction.<sup>40</sup> Unlike cyclization of Dyn A analogs via RCM utilizing allylglycine residues,<sup>41</sup> attempts to cyclize the peptide via RCM of [Tyr(All)<sup>2,3</sup>,Ile<sup>8</sup>]arodyn resulted in a mixture including desallyl products<sup>38</sup> (Figure 4.2), thereby limiting the utility of RCM for cyclizations involving Tyr(All) residues. In

this study, we describe the optimization of methodology to enhance on-resin RCM between Tyr(All) residues and suppress desallyl product formation, which is presumably due to olefin isomerization.



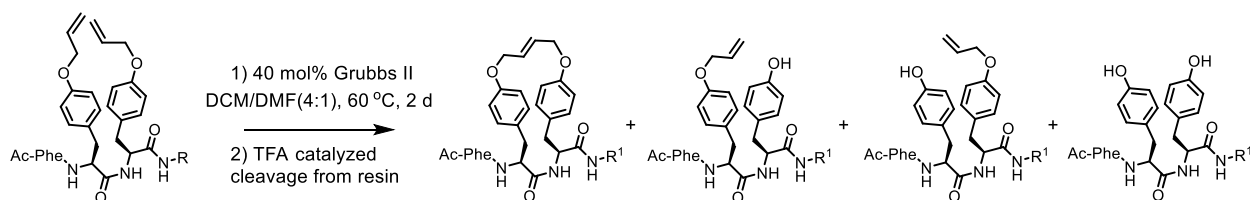
Ac-Phe-Phe-Phe-Arg-Leu-Arg-Arg-D-Ala-Arg-Pro-Lys-NH<sub>2</sub>

Arodyn

H-Tyr-Gly-Gly-Phe-Leu-Arg-Arg-Ile-Arg-Pro-Lys-OH

Dynorphin A(1-11)

Figure 4.1 Structure of arodyn and Dyn A(1-11), a fragment of the endogenous KOR ligand Dyn A.



R = Arg(Pbf)-Leu-Arg(Pbf)-Arg(Pbf)-Ile-Arg(Pbf)-Pro-Lys(Boc)-NH-resin

R<sup>1</sup> = Arg-Leu-Arg-Arg-Ile-Arg-Pro-Lys-NH<sub>2</sub>

Figure 4.2 Reaction mixture resulting from RCM of [Tyr(All)<sup>2,3</sup>,Ile<sup>8</sup>]arodyn.<sup>38</sup>

Olefin isomerization during RCM can compromise yields of the target macrocycle in isomerization-prone substrates. Undesirable olefin isomerization during metathesis is common in aryl-allyl groups as well as heteroatom substituted allylic groups.<sup>36,37</sup> Heteroatom substituted homoallylic groups are also susceptible to isomerization.<sup>37</sup> Olefin isomerization can result in ring



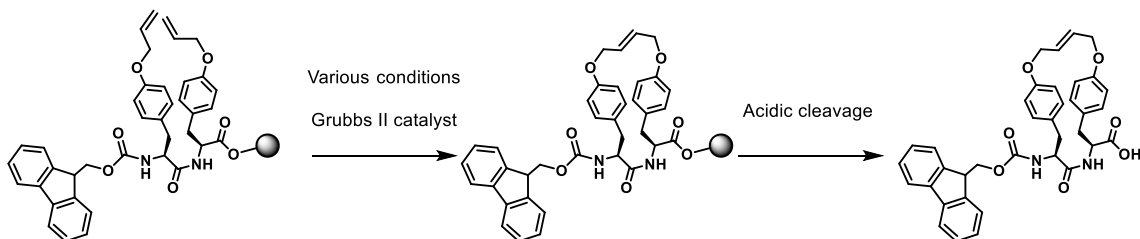
contraction<sup>42</sup> or deallylation,<sup>37,43</sup> thereby resulting in a complex mixture and reducing the RCM product yield.<sup>44</sup>

Olefin isomerization is reportedly caused by catalyst degradation products such as ruthenium hydrides.<sup>30,45</sup> A number of additives, including phenol,<sup>46</sup> 1,4-benzoquinone,<sup>30,47</sup> and copper (I) halides,<sup>43</sup> have been reported to substantially suppress olefin isomerization. Phenol and copper iodide are also reported to increase the rate of olefin metathesis.<sup>46,48</sup> However, while 1,4-benzoquinone suppresses olefin isomerization, it also suppresses the catalytic activity of Grubbs catalysts.<sup>36</sup> Although copper iodide retards ruthenium hydride formation,<sup>43</sup> it can be difficult to remove from reaction mixtures.<sup>49</sup>

On-resin RCM of peptides and peptidomimetics has particular advantages compared to solution phase RCM. Reactions on solid phase allow easy removal of reagent byproducts by filtration; on-resin RCM therefore allows cyclization of the resin-bound peptide and washing of impurities following SPPS without additional steps. Furthermore, pseudodilution on the solid phase favors the desired intramolecular cyclization and limits intermolecular cyclization.

In order to enhance RCM yields of the cyclic peptides, we used a model dipeptide Fmoc-Tyr(All)-Tyr(All) (Figure 4.3a) to explore conditions that minimize olefin isomerization and deallylation. The possible desallyl side products (Figure 4.3b) were synthesized so that the extent of deallylation during RCM could be easily monitored. Here, we present synthetic methodology optimized using this model dipeptide.

a)



b)

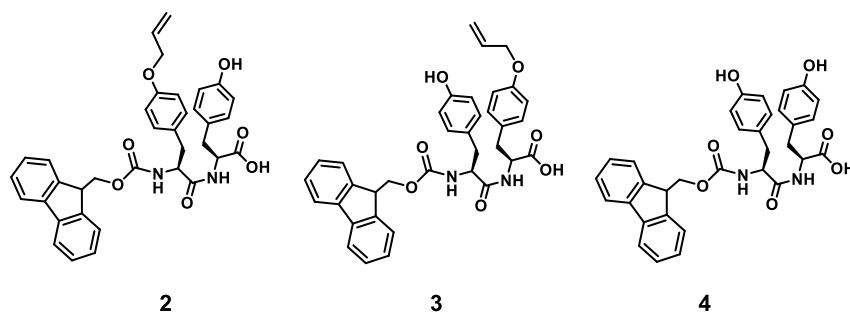


Figure 4.3 a) Model dipeptide RCM reaction and b) potential desallyl side products.

## 4.2 Results and discussion

While RCM between allylglycine residues in dynorphin analogs resulted in high RCM product yields,<sup>41</sup> RCM between Tyr(All) residues in arodyn and the model dipeptide using the same conditions resulted in low RCM product yields (Table 4.1). Products potentially due to unproductive metathesis, desallyl products, and oligomers reduced the RCM product as has been observed for Grubbs catalysts.<sup>50</sup> Additionally, the fraction of desallyl products varied with reaction temperature. Given concerns with higher catalyst loadings, including increased catalyst degradation products and higher isomerization,<sup>50</sup> we explored the use of a lower catalyst loading (15 mol%). In addition, we varied the catalyst concentration, temperature, and examined the inclusion of reported isomerization suppressants benzoquinone<sup>30</sup> and phenol.<sup>46</sup>

Table 4.1 Product profiles for RCM using 2<sup>nd</sup> generation Grubbs catalyst (G II).<sup>a</sup>

Entry	Substrate	Temp. (°C)	RCM pdt. (%)	Total desallyl pdt. (%)	SM <sup>b</sup> (%)
1	[Tyr(All) <sup>2,3</sup> ]arodyn <sup>c</sup>	60	32	31	- <sup>d</sup>
2	[Tyr(All) <sup>2,3</sup> ]arodyn <sup>c</sup>	40	18	44	-
3	Fmoc-Tyr(All)-Tyr(All) <sup>c</sup>	60	20	25	-
4	Fmoc-Tyr(All)-Tyr(All) <sup>c</sup>	40	-	18	16

<sup>a</sup>3 mM, 40 mol% G II 2 d, DCM/DMF (4:1); <sup>b</sup>SM: starting material; <sup>c</sup>additional side product peaks were observed in the product mixture (see Appendix 1); <sup>d</sup>- < 10%

Reaction temperature had a significant effect on the RCM product yield (Table 4.2 and Figure 4.4). High yields of desallyl products were observed at 60 °C at all of the 2<sup>nd</sup> generation Grubbs catalyst (G II) concentrations examined, which is consistent with catalyst degradation at elevated temperatures. The desired RCM product was only observed in appreciable yields at 40 °C, with the highest yields at 3 mM and 1 mM catalyst. Lowering the catalyst concentration further (0.3 mM) decreased the RCM product yield.

Table 4.2 Effect of temperature and catalyst concentration on model dipeptide RCM product yields.<sup>a</sup>

Entry	Temp. (°C)	[Cat.] (mM)	Yield (%) <sup>b,c</sup>		
			RCM pdt.	Total desallyl pdt.	SM <sup>d</sup>
1	60	3	- <sup>e</sup>	82	-
2	60	1	-	39	-
3	60	0.3	-	78	-
4	40	3	63	16	-
5	40	1	55	13	-
6	40	0.3	24	10	60
7	40	0.1	-	18	69

<sup>a</sup>G II 15 mol%, in DCE (60 °C) or DCM (40 °C) for 2 d; <sup>b</sup>determined from analytical HPLC chromatogram: 30-70% aqueous MeCN with 0.1% TFA over 40 min; <sup>c</sup>additional side product peaks were observed in the product mixture (see Appendix 1); <sup>d</sup>SM: starting material; <sup>e</sup>- < 10%

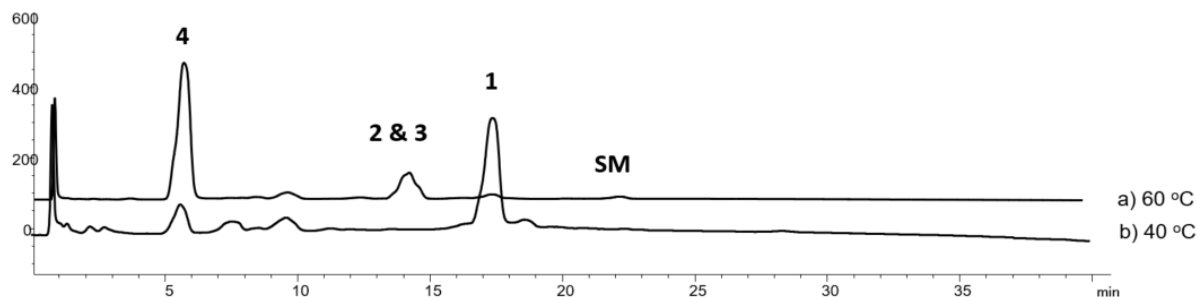


Figure 4.4 Chromatograms of the RCM product mixture following RCM at a) 60 °C and b) 40 °C at a 3 mM catalyst concentration (Table 4.2). Structures of **1-4** are shown in Figure 4.3.

We subsequently explored the use of phenol and 1,4-benzoquinone, additives that are reported to effectively suppress olefin isomerization during olefin metathesis reactions.<sup>30,46</sup> Catalyst degradation products such as ruthenium hydrides have been implicated in olefin isomerization during olefin metathesis.

Even in the presence of the additive phenol, the temperature dependence of catalyst degradation was evident in the low RCM product yields, at 60 °C (Table 4.3). This is consistent with previous reports of increased catalyst degradation at similarly higher temperatures giving rise to isomerized products.<sup>51</sup> As previously observed (Table 4.2), minimal amounts of the RCM product were observed at 60 °C. Even in the presence of phenol, substantial amounts of desallyl products were obtained, indicating that phenol did not effectively suppress desallyl side products formation at the higher temperature (Table 4.3). The RCM product yield was low (<15%) while appreciable desallyl products (25-55%) and starting material (23-39%) were observed. Reactions in toluene did not show improved yields of the RCM product. Negligible amounts of RCM product were observed in toluene.

Conversely, further experiments with phenol revealed higher RCM product yields (31-79%, Table 4.3) at the lower temperature (40 °C), suggesting a robust suppression of isomerization accompanied by substantial conversion to the desired RCM product. The highest yields were observed at a catalyst concentration of 0.3 mM at 40 °C with phenol. Improved yields of the RCM product at the lower temperature but not the higher temperature indicate the temperature dependent effect of the additive phenol with G II as the catalyst.

Table 4.3 Effect of phenol, temperature,<sup>a,b</sup> and catalyst concentration on model dipeptide RCM product yields.

Entry	[Cat.] (mM) <sup>c</sup>	Yield (%) <sup>d</sup>			
		Additive (1 equiv)	RCM pdt.	Total desallyl pdt.	SM <sup>e</sup>
1	3	phenol	42	20	- <sup>f</sup>
2	1	phenol	60	-	-
3	0.3	phenol	79	-	-
4	0.1	phenol	31	15	43

<sup>a</sup>Results shown are in DCM at 40 °C for 2 d; <sup>b</sup>at 60 °C in DCE, phenol did not effectively suppress desallyl side products formation; <sup>c</sup>15 mol% G II for 2 d; <sup>d</sup>additional side product peaks were observed in the product mixture (see Appendix 1); <sup>e</sup>SM: starting material; <sup>f</sup>- < 10%

With 1,4-benzoquinone as the additive, negligible quantities of desallyl products were observed but low RCM product yield was observed at both 60 °C and 40 °C. Starting material was predominant in the product profile at both 60 °C (67%) and 40 °C (76%), indicating poor conversion of starting material to the RCM product. Thus, 1,4-benzoquinone was effective at suppressing isomerization, but poor in supporting conversion of reactant to the desired RCM product. This is consistent with previous results where 1,4-benzoquinone suppressed both catalyst activity and olefin isomerization.<sup>36</sup> The marked disparities (Figure 4.5) here suggest different operative mechanisms of action for the two additives.

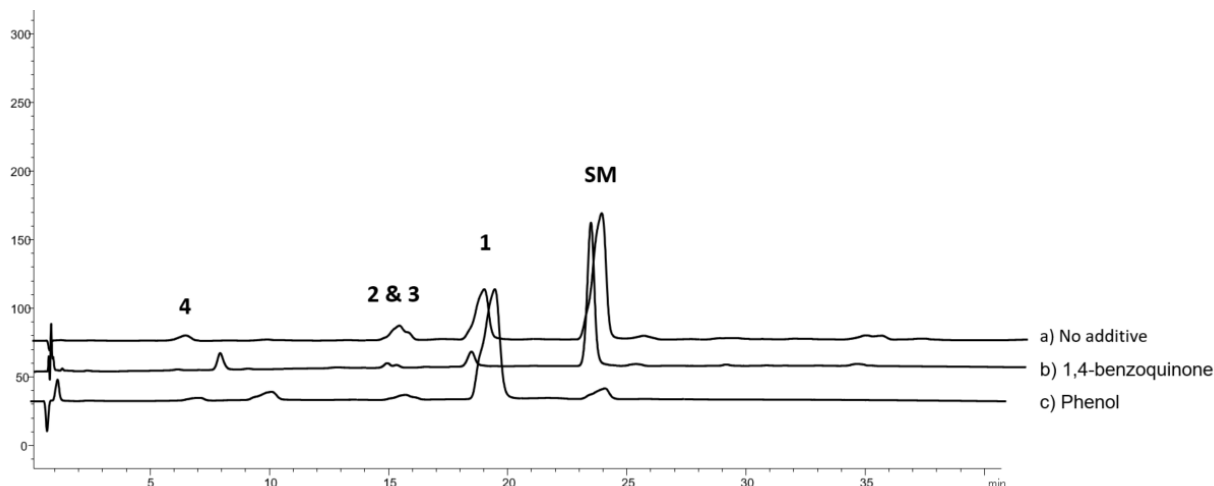


Figure 4.5 Chromatograms of the RCM product mixture following RCM (G II 15 mol% in DCM at 40 °C for 2 d) in the presence or absence of the additives 1,4-benzoquinone and phenol (1 equiv each). SM: starting material. Structures of **1-4** are shown in Figure 4.3.

Given the poor conversion to the RCM product at elevated temperatures we explored the use of Hoveyda-Grubbs II (HG II) that is reported to have higher thermal stability.<sup>11</sup> Notably HG II has an isopropoxy ether chelated to the metal center while G II has a coordinating phosphine ligand (Figure 4.6). We explored the performance of HG II at 60 °C and 40 °C and the effect of adding phenol (Table 4.4).

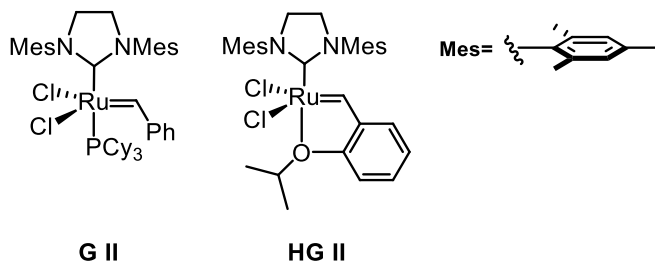


Figure 4.6 Structures of Grubbs 2<sup>nd</sup> generation (G II) and Hoveyda-Grubbs 2<sup>nd</sup> generation (HG II) catalysts

Whereas temperature dependent catalyst activity was observed for G II (Table 4.2), HG II exhibited comparable catalytic activity at both temperatures examined, particularly in the absence of an additive (Table 4.4). At the higher temperature and in the absence of phenol, HG II exhibited drastic improvements in the RCM product yield (Table 4.4) compared to GII (Table 4.2); this is

consistent with the greater thermal stability of HG II. The presence of phenol at 60 °C, however, interfered with product formation, presumably due to competing chelating effects of phenol and the isopropyl ether ligand which in turn affects thermal stability and catalyst degradation. On the other hand, substantial RCM product yield was observed at 40 °C with phenol, as previously observed for G II (Table 4.3) under similar reaction conditions. In contrast to G II, however, higher yields of the RCM product were observed without phenol, consistent with the increased stability of HG II.

Table 4.4 Model dipeptide RCM product yields with HG II at 40 and 60 °C.<sup>a</sup>

Entry	Temp. (°C)	Additive (1 equiv)	RCM pdt.	Total desallyl pdt.	S.M <sup>b</sup>
1	60	-	86	-	- <sup>c</sup>
2 <sup>d</sup>	60	phenol	17	32	-
3	40	-	80	-	-
4	40	phenol	72	15	-

<sup>a</sup> 0.3 mM 15 mol% HG II in DCE (60 °C) or DCM (40 °C) for 2 d; <sup>b</sup> SM: starting material; <sup>c</sup> - < 10%; <sup>d</sup> additional side product peaks were observed in the product mixture (see Appendix 1)

We subsequently explored the utility of the optimized conditions on cyclization of a tripeptide with Tyr(All) residues (Figure 4.7). Reasonably high yields of the RCM product (65-84%) were generally observed at 40 °C with both G II and HG II; interestingly, much lower yields were observed with HG II at 60 °C (Table 4.5). Consistent with the model dipeptide study, the highest yields were observed at the lower temperature examined. Overall, satisfactory RCM product yields were observed at 40 °C under the optimized conditions.

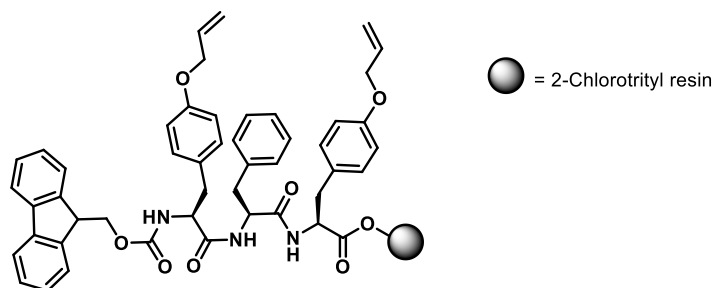


Figure 4.7 Structure of model tripeptide Fmoc-Tyr(All)-Phe-Tyr(All).

Table 4.5 Tripeptide RCM product yields under optimized conditions with G II and HG II.<sup>a</sup>

Entry	Catalyst	Temp.(°C)	Additive (1 equiv)	RCM Pdt.	Total desallyl pdt.
1 <sup>b</sup>	HG II	60	-	27	28
2	HG II	40	-	84	- <sup>c</sup>
3	HG II	40	phenol	67	-
4	G II	40	phenol	65	-

<sup>a</sup>0.3 mM 15 mol% G II or HG II in DCE (60 °C) or DCM (40 °C) for 2 d; <sup>b</sup>additional side product peaks were observed in the product mixture (see Appendix 1); <sup>c</sup>< 10%

### 4.3 Conclusions

The model dipeptide study illustrated several important modifications to improve yields of the desired product. Particularly, we observed the superior efficiency of phenol compared to 1,4-benzoquinone to suppress deallylation, the temperature dependent effectiveness of phenol with G II, as well as the influence of the thermal stability of the catalyst. As a result, we had optimized conditions at 40 °C with G II in the presence of phenol. Furthermore, we identified conditions that resulted in appreciable yields of the RCM product with HG II. Overall the optimized conditions from the model dipeptide using G II and HG II were effective and gave satisfactory yields of the RCM product. The best yields were obtained in DCM at 40 °C in both the model dipeptide and the tripeptide; notably, phenol was required with G II but not with HG II to suppress deallylation.



Further synthesis of arodyn analogs containing Tyr(All) using the optimized conditions for pharmacological evaluation was undertaken (see Chapter 5). The methodology presented here could be beneficial in RCM reactions where olefin isomerization complicates purification and could enhance the yields of the desired RCM product, particularly for peptidic substrates.

## 4.4 Experimental

### Materials and methods

The Rink amide ChemMatrix resin was purchased from Biotage (Charlotte, NC), the Fmoc-protected PAL-PEG-PS was purchased from APPTec LLC (Louisville, KY), and the 2-chlorotrityl chloride resin was purchased from Chem-Impex International (Wood Dale, IL). All standard protected amino acids were purchased from Bachem (King of Prussia, PA), EMD Millipore Chemicals (San Diego, CA), Peptides International (Louisville, KY), or Chem-Impex International. Fmoc-L-Tyr(All)-OH was purchased from Chem-Impex International. The coupling agent benzotriazol-1-yl-oxy-tris-pyrrolidino-phosphonium hexafluorophosphate (PyBOP) and the coupling additive 1-hydroxybenzotriazole hydrate (HOBt) were obtained from Peptides International. Dichloromethane (DCM), *N,N*-diisopropylethylamine (DIEA), dimethylformamide (DMF), diethyl ether, acetonitrile, methanol, and trifluoroacetic acid (TFA) were purchased from Fisher Scientific (Hampton, NH). All other chemicals were purchased from Aldrich Chemical Co. (Milwaukee, WI).

### Instruments

Electrospray ionization mass spectrometry (ESI/MS) was performed on an LCT Premier (Waters Corp., Milford MA) instrument with a time of flight mass analyzer or the Advion expression L compact MS (Advion, Inc. Ithaca, NY). A Voyager DE STR high performance

matrix-assisted laser desorption time-of-flight mass spectrometer (MALDI-TOFMS) was used for MALDI analysis.

Analytical HPLC was performed on an Agilent 1200 system fitted with a Grace Vydac analytical column (C18, 300 Å, 5 µm, 4.6 mm x 50 mm) equipped with a Vydac C18 guard cartridge. HPLC chromatograms were monitored at 214 nM.

### **Solid phase peptide synthesis (SPPS) on the 2-chlorotrityl chloride resin**

Peptides were prepared by the Fmoc (9-fluorenylmethoxycarbonyl) solid-phase synthesis strategy. The general method reported previously (Scheme 4.1) for the synthesis of linear peptides on 2-chlorotrityl resin<sup>52,53</sup> on a custom-made manual peptide synthesizer (CHOIR) was followed in the synthesis of the following dipeptides and tripeptide: Fmoc-Tyr(All)-Tyr(All)-OH, Fmoc-Tyr(All)-Tyr-OH, Fmoc-Tyr-Tyr(All)-OH, Fmoc-Tyr-Tyr-OH, and Fmoc-Tyr(All)-Phe-Tyr(All)-OH (Table 4.6). Briefly, after swelling of the resin in DCM (2×10 min), the Fmoc-protected C-terminal amino acid (2 equiv in DCM/DMF(4/1)) and DIEA, 5 equiv) were added to the resin, the reaction mixture was agitated with nitrogen gas for 6 h with addition of DCM every 30 min to maintain solvent volume. DIEA (5 equiv) was added every 2 h. MeOH (15 %) and DIEA (5 %) in DCM (2×10 min) were then used to cap unreacted sites on the resin, after which the resin was washed with DCM/DMF (1:1, 5x). After Fmoc deprotection (20% piperidine, 1 x 5 min, 2 x 20 min), the resin was washed with DMF (5x), DCM/DMF (1:1, 5x) and DCM (5x).

Cycles of Fmoc deprotection and amino acid couplings (2 equiv in DCM/DMF, 4/1) were performed to add amino acids to the growing peptide chain. Amino acid couplings were performed using PyBOP (2 equiv), HOBt (2 equiv), and DIEA (5 equiv) in DCM/DMF (1/1) for 2–4 h. Nitrogen gas was used to agitate the mixture during coupling. To cleave the peptide from the resin,

1% TFA in DCM was bubbled through the resin (5 mL x 10, 2 min each), then drained into a round bottom flask and evaporated.

Table 4.6 Analytical data of synthesized linear and cyclic peptides.

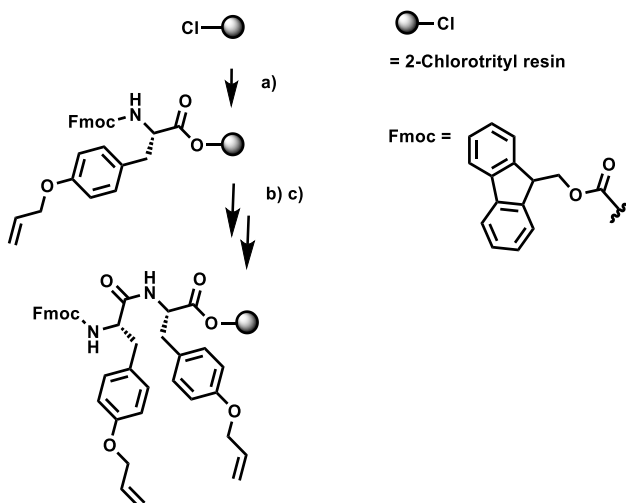
Peptide	HPLC $t_R$ (min) <sup>a</sup>	Mass ( $m/z$ )	
		Calculated	Observed
<i>cyclo</i> -Fmoc-Tyr(All)-Tyr(All)-OH	18.0	[M+Na] <sup>+</sup> 641.22	[M+Na] <sup>+</sup> 641.22
Fmoc-Tyr(All)-Tyr-OH	14.6	[M+Na] <sup>+</sup> 629.22	[M+Na] <sup>+</sup> 629.90
Fmoc-Tyr-Tyr(All)-OH	14.4	[M+Na] <sup>+</sup> 629.22	[M+Na] <sup>+</sup> 629.80
Fmoc-Tyr-Tyr-OH	6.0	[M+Na] <sup>+</sup> 589.19	[M+Na] <sup>+</sup> 589.19
Fmoc-Tyr(All)-Tyr(All)-OH	23.0	[M+Na] <sup>+</sup> 669.25	[M+Na] <sup>+</sup> 669.25
Fmoc-Tyr(All)-Phe-Tyr(All)-OH	26.4	[M+Na] <sup>+</sup> 816.32	[M+Na] <sup>+</sup> 816.33
<i>cyclo</i> -Fmoc-Tyr(All)-Phe-Tyr(All)-OH	21.6	[M+Na] <sup>+</sup> 788.29	[M+Na] <sup>+</sup> 788.29
[Tyr(All) <sup>2,3</sup> ]arodyn	32.2 <sup>b</sup>	[M+H] <sup>+</sup> 1647.01	[M+H] <sup>+</sup> 1647.86
<i>cyclo</i> [Tyr(All) <sup>2,3</sup> ]arodyn	29.3 <sup>b</sup>	[M+3H] <sup>3+</sup> 540.30	[M+3H] <sup>3+</sup> 540.50

<sup>a</sup>30-70% aqueous MeCN with 0.1% TFA over 40 min; <sup>b</sup>5-50% aqueous MeCN with 0.1% TFA over 45 min

### Synthesis of Fmoc-Tyr(All)-Tyr(All)-OH

SPPS was performed as described above on the 2-chlorotrityl resin (1 g, 0.84 mmol, 0.84 mmol/g). Fmoc-Tyr(All)-OH (2 equiv 745 mg, 1.68 mmol) was loaded following the general method for the first amino acid loading on 2-chlorotrityl resin SPPS as described above. After Fmoc-deprotection, Fmoc-Tyr(All)-OH (2 equiv 745 mg, 1.68 mmol) was coupled to the resin to extend the peptide chain followed by Fmoc deprotection as described in the general procedure for SPPS to give Fmoc-Tyr(All)-Tyr(All)-OH ESI/MS  $m/z$  669.25 observed, 669.25 calculated (M+Na)<sup>+</sup>, HPLC  $t_R$  = 23.0 min (30-70% aqueous MeCN with 0.1% TFA over 40 min at a flow rate of 1 mL/min).

Scheme 4.1 Synthesis of Fmoc-Tyr(All)-Tyr(All)-OH.



a) Fmoc-Tyr(All)-OH, DIEA, DCM, rt, 6-8 h; b) Piperidine/DMF (1:4), (1 x 5 min, 2 x 20 min ) rt; c) Fmoc-Tyr(All)-OH, PyBop, HOBt, DIEA, DCM/DMF, rt, 2-6 h.

### SPPS of [Tyr(All)<sup>2,3</sup>]arodyn

[Tyr(All)<sup>2,3</sup>]arodyn was prepared by the Fmoc SPPS strategy using the automated Biotage microwave peptide synthesizer (Initiator+ Alstra; Biotage, Sweden) on a 0.14 mmol scale. Rinkamide ChemMatrix (0.45-0.52 mmol/g) or Fmoc-PAL-PEG-PS resin (0.18-0.20 mmol/g) resin was swollen for 20 min at 70° C in DMF prior to cycles of amino acid coupling and deprotection (prior to the coupling reaction, the Fmoc group was removed from the Fmoc-PAL-PEG-PS resin). Coupling reactions were performed using Fmoc amino acids (4 equiv, 0.5 M), activated with PyBOP (4 equiv, 0.5 M) and HOBt (4 equiv, 0.5 M) in the presence of DIPEA (8 equiv in NMP, 0.5 M), for 5 min at 75 °C. Fmoc deprotection was performed at room temperature with 20% 4-methylpiperidine in DMF (4.5 mL, 1 x 3 min; 4.5 mL, 2 x 10 min). The side chains of Lys and Arg were protected with *tert*-butoxycarbonyl (Boc) and 2,2,4,6,7-pentamethyldihydrobenzofuran-5-sulfonyl (Pbf), respectively. N-Acetylation was performed using acetic anhydride (5 M in DMF) and DIEA (2 M in NMP) for 20 min at room temperature.

The resulting peptide-resin was washed with DMF (5 mL, 3 x 45 sec) and DCM (5 mL, 3 x 45 sec). Generally, crude peptides were cleaved from the resin using acidic cleavage cocktails for at least 2h and then precipitated in cold ether following filtration. For the Rinkamide ChemMatrix resin, crude peptides were cleaved from the resin using TFA/triisopropylsilane(TIPS)/H<sub>2</sub>O (95/2.5/2.5). For Fmoc-PAL-PEG-PS resin, crude peptides were cleaved from the resin using TFA/phenol/H<sub>2</sub>O/TIPS (88/5/5/2); for cleavage of aliquots, the solution was diluted with 10% aqueous acetic acid (3–5 mL) and then extracted with diethyl ether (3 × 5 mL) following filtration.

### **General procedure for RCM**

Generally, second-generation Grubbs' catalyst (15 mol%) or second-generation Hoveyda Grubbs' catalyst (15 mol%) was dissolved in DCM and added to Fmoc-Tyr(All)-Tyr(All)-2-chlorotrityl resin (0.56 mmol/g) or Fmoc-Tyr(All)-Phe-Tyr(All)-2-chlorotrityl resin (0.51 mmol/g). Catalyst loading was calculated relative to the resin-bound peptide loading. Additives (phenol or 1,4-benzoquinone) were added to the reaction mixture along with the catalyst, and the reaction mixture was heated as indicated for the respective reaction conditions for 2 days under nitrogen gas with gentle stirring. The solvent volume was varied according to the quantity of resin used in order to give the desired catalyst concentration for the reaction. After the specified reaction time, the resin was transferred to a 15 mL polypropylene syringe fitted with a polytetrafluoroethylene (PTFE) frit on a manual peptide synthesizer and washed with MeOH (3 x 5 mL) and DCM (10 x 5 mL), with N<sub>2</sub> agitation, to remove the catalyst. Following aliquot cleavage of the dried resin, analytical HPLC was performed using a linear gradient of 30-70% aqueous MeCN with 0.1% TFA over 40 min for the model dipeptide and tripeptide or 5-50% aqueous MeCN with 0.1% TFA over 45 min for [Tyr(All)<sup>2-3</sup>]arodyn. Yields for the respective reactions

were determined from analytical HPLC chromatograms (Appendix 1); in some cases, baseline resolution was not achieved so yields shown are an estimate.

#### 4.5 References

(1) Ghalit, N.; Rijkers, D. T. S.; Liskamp, R. M. J. Alkene- and alkyne-bridged mimics of nisin as potential peptide-based antibiotics. *J Mol Catal A: Chem* **2006**, *254*, 68-77.

(2) Wels, B.; Kruijtzter, J. A. W.; Garner, K.; Nijenhuis, W. A. J.; Gispén, W. H.; Adan, R. A. H.; Liskamp, R. M. J. Synthesis of a novel potent cyclic peptide MC4-ligand by ring-closing metathesis. *Bioorg Med Chem Lett* **2005**, *13*, 4221-4227.

(3) Nomura, W.; Aikawa, H.; Ohashi, N.; Urano, E.; Métifiot, M.; Fujino, M.; Maddali, K.; Ozaki, T.; Nozue, A.; Narumi, T.; Hashimoto, C.; Tanaka, T.; Pommier, Y.; Yamamoto, N.; Komano, J. A.; Murakami, T.; Tamamura, H. Cell-Permeable Stapled Peptides Based on HIV-1 Integrase Inhibitors Derived from HIV-1 Gene Products. *ACS Chem Biol* **2013**, *8*, 2235-2244.

(4) Kim, Y.-W.; Grossmann, T. N.; Verdine, G. L. Synthesis of all-hydrocarbon stapled [ $\alpha$ ]-helical peptides by ring-closing olefin metathesis. *Nat Protoc* **2011**, *6*, 761-771.

(5) Pérez de Vega, M. J.; García-Aranda, M. I.; González-Muñiz, R. A role for ring-closing metathesis in medicinal chemistry: Mimicking secondary architectures in bioactive peptides. *Med Res Rev* **2011**, *31*, 677-715.

(6) Brik, A. Metathesis in Peptides and Peptidomimetics. *Adv Synth Catal* **2008**, *350*, 1661-1675.

(7) Rijkers, D. S. Synthesis of Cyclic Peptides and Peptidomimetics by Metathesis Reactions In Synthesis of Heterocycles by Metathesis Reactions

Prunet, J., Ed.; Springer Berlin Heidelberg: Cham, 2017, p 191-244.

(8) Lin, Y. A.; Davis, B. G. Vignette: Extending the Application of Metathesis in Chemical Biology – The Development of Site-Selective Peptide and Protein Modifications In Handbook of Metathesis; Wiley-VCH Verlag GmbH & Co. KGaA: 2015, p 295-309.

(9) Hoveyda, A. H.; Zhugralin, A. R. The remarkable metal-catalysed olefin metathesis reaction. *Nature* **2007**, *450*, 243-251.

- (10) Miller, S. J.; Blackwell, H. E.; Grubbs, R. H. Application of Ring-Closing Metathesis to the Synthesis of Rigidified Amino Acids and Peptides. *J Am Chem Soc* **1996**, *118*, 9606-9614.
- (11) Vougioukalakis, G. C.; Grubbs, R. H. Ruthenium-Based Heterocyclic Carbene-Coordinated Olefin Metathesis Catalysts. *Chem Rev* **2010**, *110*, 1746-1787.
- (12) Manzini, S.; Fernández-Salas, J. A.; Nolan, S. P. From a Decomposition Product to an Efficient and Versatile Catalyst: The [Ru( $\eta^5$ -indenyl)(PPh<sub>3</sub>)<sub>2</sub>Cl] Story. *Acc Chem Res* **2014**, *47*, 3089-3101.
- (13) Wang, Z. J.; Jackson, W. R.; Robinson, A. J. A simple and practical preparation of an efficient water soluble olefin metathesis catalyst. *Green Chem* **2015**, *17*, 3407-3414.
- (14) Olszewski, T. K.; Bieniek, M.; Skowerski, K.; Grela, K. A New Tool in the Toolbox: Electron-Withdrawing Group Activated Ruthenium Catalysts for Olefin Metathesis. *Synlett* **2013**, *24*, 903-919.
- (15) Fanelli, R.; Jeanne-Julien, L.; René, A.; Martinez, J.; Cavelier, F. Stereoselective synthesis of unsaturated  $\alpha$ -amino acids. *Amino Acids* **2015**, *47*, 1107-1115.
- (16) Aillard, B.; Robertson, N. S.; Baldwin, A. R.; Robins, S.; Jamieson, A. G. Robust asymmetric synthesis of unnatural alkenyl amino acids for conformationally constrained  $\alpha$ -helix peptides. *Org Biomol Chem* **2014**, *12*, 8775-8782.
- (17) Williams, R. M.; Im, M. N. Asymmetric synthesis of monosubstituted and  $\alpha,\alpha$ -disubstituted  $\alpha$ -amino acids via diastereoselective glycine enolate alkylations. *J Am Chem Soc* **1991**, *113*, 9276-9286.
- (18) Jacobsen, O.; Klaveness, J.; Rongved, P. Structural and pharmacological effects of ring-closing metathesis in peptides. *Molecules* **2010**, *15*, 6638-6677.
- (19) Kirshenbaum, K.; Arora, P. S. Cross-dressing proteins by olefin metathesis. *Nat Chem Biol* **2008**, *4*, 527-528.
- (20) Kim, Y. W.; Kutchukian, P. S.; Verdine, G. L. Introduction of all-hydrocarbon  $i,i+3$  staples into  $\alpha$ -helices via ring-closing olefin metathesis. *Org Lett* **2010**, *12*, 3046-3049.
- (21) Schafmeister, C. E.; Po, J.; Verdine, G. L. An All-Hydrocarbon Cross-Linking System for Enhancing the Helicity and Metabolic Stability of Peptides. *J Am Chem Soc* **2000**, *122*, 5891-5892.

- (22) Blackwell, H. E.; O'Leary, D. J.; Chatterjee, A. K.; Washenfelder, R. A.; Bussmann, D. A.; Grubbs, R. H. New Approaches to Olefin Cross-Metathesis. *J Am Chem Soc* **2000**, *122*, 58-71.
- (23) van Lierop, B. J.; Whelan, A. N.; Andrikopoulos, S.; Mulder, R. J.; Jackson, W. R.; Robinson, A. J. Methods for Enhancing Ring Closing Metathesis Yield in Peptides: Synthesis of a Dicarba Human Growth Hormone Fragment. *Int J Pept Res Ther* **2010**, *16*, 133-144.
- (24) Blackwell, H. E.; Grubbs, R. H. Highly Efficient Synthesis of Covalently Cross-Linked Peptide Helices by Ring-Closing Metathesis. *Angew Chem Int Ed* **1998**, *37*, 3281-3284.
- (25) Abell, A. D.; Alexander, N. A.; Aitken, S. G.; Chen, H.; Coxon, J. M.; Jones, M. A.; McNabb, S. B.; Muscroft-Taylor, A. Synthesis of macrocyclic beta-strand templates by ring closing metathesis. *J Org Chem* **2009**, *74*, 4354-4356.
- (26) Illesinghe, J.; Guo, C. X.; Garland, R.; Ahmed, A.; van Lierop, B.; Elaridi, J.; Jackson, W. R.; Robinson, A. J. Metathesis assisted synthesis of cyclic peptides. *Chem Commun* **2009**, 295-297.
- (27) Robinson, A. J.; Elaridi, J.; Van Lierop, B. J.; Mujcinovic, S.; Jackson, W. R. Microwave-assisted RCM for the synthesis of carbocyclic peptides. *J Pept Sci* **2007**, *13*, 280-285.
- (28) Mangold, S. L.; O'Leary, D. J.; Grubbs, R. H. Z-Selective Olefin Metathesis on Peptides: Investigation of Side-Chain Influence, Preorganization, and Guidelines in Substrate Selection. *J Am Chem Soc* **2014**, *136*, 12469-12478.
- (29) Mangold, S. L.; O'Leary, D. J.; Grubbs, R. H. Z-Selective olefin metathesis on peptides: investigation of side-chain influence, preorganization, and guidelines in substrate selection. *J Am Chem Soc* **2014**, *136*, 12469-12478.
- (30) Hong, S. H.; Sanders, D. P.; Lee, C. W.; Grubbs, R. H. Prevention of Undesirable Isomerization during Olefin Metathesis. *J Am Chem Soc* **2005**, *127*, 17160-17161.
- (31) Collins, S. K. Solvent and Additive Effects on Olefin Metathesis In Handbook of Metathesis; Wiley-VCH Verlag GmbH & Co. KGaA: 2015, p 343-377.
- (32) Schrodi, Y. Mechanisms of Olefin Metathesis Catalyst Decomposition and Methods of Catalyst Reactivation In Handbook of Metathesis; Wiley-VCH Verlag GmbH & Co. KGaA: 2015, p 323-342.



- (33) Ascic, E.; Jensen, J. F.; Nielsen, T. E. Synthesis of Heterocycles through a Ruthenium-Catalyzed Tandem Ring-Closing Metathesis/Isomerization/N-Acylium Cyclization Sequence. *Angew Chem Int Ed* **2011**, *50*, 5188-5191.
- (34) Mallagaray, Á.; Domínguez, G.; Gradillas, A.; Pérez-Castells, J. Tandem RCM–Isomerization– Cyclopropanation Reactions. *Org Lett* **2008**, *10*, 597-600.
- (35) Donohoe, T. J.; O’Riordan, T. J. C.; Rosa, C. P. Ruthenium-Catalyzed Isomerization of Terminal Olefins: Applications to Synthesis. *Angew Chem Int Ed* **2009**, *48*, 1014-1017.
- (36) Hemelaere, R.; Carreaux, F.; Carboni, B. Synthesis of Alkenyl Boronates from Allyl-Substituted Aromatics Using an Olefin Cross-Metathesis Protocol. *J Org Chem* **2013**, *78*, 6786-6792.
- (37) Cadot, C.; Dalko, P. I.; Cossy, J. Olefin isomerization by a ruthenium carbenoid complex. Cleavage of allyl and homoallyl groups. *Tetrahedron Lett* **2002**, *43*, 1839-1841.
- (38) Fang, W.-J.; Murray, T. F.; Aldrich, J. V. Design, synthesis, and opioid activity of arodyn analogs cyclized by ring-closing metathesis involving Tyr(allyl). *Bioorg Med Chem* **2018**, *26*, 1157-1161.
- (39) Bennett, M. A.; Murray, T. F.; Aldrich, J. V. Identification of Arodyn, a Novel Acetylated Dynorphin A-(1–11) Analogue, as a  $\kappa$  Opioid Receptor Antagonist. *J Med Chem* **2002**, *45*, 5617-5619.
- (40) Aldrich, J. V.; McLaughlin, J. P. Peptide kappa opioid receptor ligands: potential for drug development. *AAPS J* **2009**, *11*, 312-322.
- (41) Fang, W. J.; Cui, Y. J.; Murray, T. F.; Aldrich, J. V. Design, Synthesis, and Pharmacological Activities of Dynorphin A Analogues Cyclized by Ring-Closing Metathesis. *J Med Chem* **2009**, *52*, 5619-5625.
- (42) De Rosa, M.; Unge, J.; Motwani, H. V.; Rosenquist, A.; Vrang, L.; Wallberg, H.; Larhed, M. Synthesis of P1'-functionalized macrocyclic transition-state mimicking HIV-1 protease inhibitors encompassing a tertiary alcohol. *J Med Chem* **2014**, *57*, 6444-6457.
- (43) Schulz, M.; Atkinson, M. J.; Elsey, R.; Thuo, M. Copper(I) halides inhibit olefin isomerized by-products from phosphine-based Grubbs’ metathesis catalysts in polar protic solvents. *Transition Met Chem* **2014**, *39*, 763-767.

(44) ten Brink, H. T.; Rijkers, D. T.; Kemmink, J.; Hilbers, H. W.; Liskamp, R. M. Ring-closing metathesis for the synthesis of side chain knotted pentapeptides inspired by vancomycin. *Org Biomol Chem* **2004**, *2*, 2658-2663.

(45) Schmidt, B. Catalysis at the Interface of Ruthenium Carbene and Ruthenium Hydride Chemistry: Organometallic Aspects and Applications to Organic Synthesis. *Eur J Org Chem* **2004**, *2004*, 1865-1880.

(46) Schmidt, B.; Hauke, S. Cross metathesis of allyl alcohols: how to suppress and how to promote double bond isomerization. *Org Biomol Chem* **2013**, *11*, 4194-4206.

(47) Bilel, H.; Hamdi, N.; Zagrouba, F.; Fischmeister, C.; Bruneau, C. Eugenol as a renewable feedstock for the production of polyfunctional alkenes via olefin cross-metathesis. *RSC Adv* **2012**, *2*, 9584-9589.

(48) Voigtritter, K.; Ghorai, S.; Lipshutz, B. H. Enhanced Olefin Cross Metathesis Reactions: The Copper Iodide Effect. *J Org Chem* **2011**, *76*, 4697-4702.

(49) Reichwein, John F.; Liskamp, Rob M. J. Synthesis of Cyclic Dipeptides by Ring-Closing Metathesis. *Eur J Org Chem* **2000**, *2000*, 2335-2344.

(50) Kadyrov, R. Low Catalyst Loading in Ring-Closing Metathesis Reactions. *Chem Eur J* **2013**, *19*, 1002-1012.

(51) Lehman Jr, S. E.; Schwendeman, J. E.; O'Donnell, P. M.; Wagener, K. B. Olefin isomerization promoted by olefin metathesis catalysts. *Inorg Chim Acta* **2003**, *345*, 190-198.

(52) Ross, N. C.; Kulkarni, S. S.; McLaughlin, J. P.; Aldrich, J. V. Synthesis of CJ-15,208, a novel  $\kappa$ -opioid receptor antagonist. *Tetrahedron Lett*, *51*, 5020-5023.

(53) Aldrich, J. V.; Kulkarni, S. S.; Senadheera, S. N.; Ross, N. C.; Reilley, K. J.; Eans, S. O.; Ganno, M. L.; Murray, T. F.; McLaughlin, J. P. Unexpected Opioid Activity Profiles of Analogues of the Novel Peptide Kappa Opioid Receptor Ligand CJ-15,208. *ChemMedChem* **2011**, *6*, 1739-1745.

**Chapter 5 - Conformational constraint of aromatic residues in the “message” sequence of the kappa opioid receptor antagonist arodyn using RCM**

## 5.1 Introduction

The last chapter described the use of a model dipeptide to explore reaction conditions that suppress deallylation during RCM and therefore enhance cyclization yields. Notably, cyclic constraints are generally incorporated at non-critical residues, typically with AllGly when using RCM. This chapter focuses on the constraint of aromatic residues in arodyn analogs with the goal of examining the pharmacological effect of these constrained analogs. Such a constraint could potentially stabilize the bioactive conformation in addition to improving metabolic stability of the kappa opioid receptor (KOR) antagonist arodyn.

Aromatic residues in arodyn contribute to KOR affinity, as observed in the alanine scan where a 3- to 4-fold loss in KOR affinity resulted upon substitution of Phe<sup>1</sup> and Phe<sup>3</sup>; Phe<sup>2</sup> substitution, however, had minimal effect.<sup>1</sup> Aromatic residues are critical components of the opioid pharmacophore according to the “message-address” concept applied to opioid peptides by Chavkin and Goldstein.<sup>2</sup> The “message”, which consists of two aromatic residues and a spacer, is common to all mammalian opioid peptides. The “message” binds to and activates the receptor, in contrast to the “address” which enhances affinity for a particular receptor. Of note, there are limited reports of cyclization of aromatic residues in opioid peptides.<sup>3,4</sup>

Chimeric peptides with increased selectivity for the KOR have been developed based on the “message-address” concept. The chimeric peptide JVA 901 (now called venorphan), a KOR antagonist, was developed by combining the “message” sequence of a tetrapeptide with weak KOR antagonism, derived from cobra venom, with the address sequence of [D-Ala<sup>8</sup>]Dyn A 1-11.<sup>5</sup> Venorphan reversed agonism of Dyn A (1-13)NH<sub>2</sub> in a concentration dependent manner and showed KOR selectivity comparable to [D-Ala<sup>8</sup>]Dyn A 1-11 despite having 100-fold lower KOR affinity ( $K_i = 19.8$  nM).<sup>5</sup>

Similarly, extacet was developed by replacing the N-terminal “message” sequence of [D-Ala<sup>8</sup>]-Dyn A 1-11 with Ac-Arg-Phe-Met-Trp-Met-Arg-NH<sub>2</sub> ([Arg<sup>6</sup>]acetalin), which shows potent mu opioid receptor (MOR) antagonism.<sup>6</sup> A 65-fold increase in affinity for KOR (K<sub>i</sub> = 6.6 nM) was observed for extacet, but it also retained high MOR affinity (K<sub>i</sub> = 1.12 nM). Further modifications and SAR on the “message” sequence in a combinatorial library led to the discovery of arodyn, Ac[Phe<sup>1,2,3</sup>, Arg<sup>4</sup>,D-Ala<sup>8</sup>]Dyn A-(1-11)NH<sub>2</sub>, a relatively potent (K<sub>i</sub> = 10 nM) and selective KOR antagonist (K<sub>i</sub> ratio (κ/μ/δ) = 1/174/583).<sup>7</sup> *In vivo* studies following intracerebroventricular injection demonstrated that arodyn prevents stress-induced reinstatement of cocaine-seeking behavior.<sup>8</sup>

Previous cyclization of [Ile<sup>8</sup>]arodyn using RCM in the “message” sequence indicated that cyclization between adjacent aromatic residues was tolerated by the KOR, whereas cyclization between Tyr(All)<sup>3</sup> and AllGly<sup>5</sup> resulted in a substantial decrease (>39-fold) in KOR affinity.<sup>4</sup> Like arodyn, potent KOR antagonism in the [<sup>35</sup>S]GTPγS assay was observed for arodyn analogs cyclized between aromatic residues 2 and 3 (K<sub>B</sub> = 3.2 nM), as well as between residues 1 and 2 (K<sub>B</sub> = 27.5 nM). Whereas these analogs retained affinity at KOR, they exhibited some loss in affinity compared to arodyn, possibly due to the Ile<sup>8</sup> substitution. This chapter describes arodyn analogs with D-Ala in place of Ile<sup>8</sup>, which is expected to increase affinity to KOR (Bennet MA, Murray TF, Aldrich JV, unpublished results).

To constrain aromatic residues using RCM, we employed Tyr(All) residues to give an alkene bridge. The alkene bridge could be introduced between any of the three aromatic residues (Figure 5.1). Initial cyclization of [Tyr(All)<sup>2,3</sup>]arodyn using Grubbs 2<sup>nd</sup> generation catalyst (G II) resulted in desallyl products, which complicated purification and compromised the product yield. This chapter describes the synthesis of arodyn analogs using conditions that suppress deallylation

during RCM. Based on docking studies, cyclization was explored between adjacent aromatic residues where the rings were modified by using *meta*- or *para*-substituted allyl tyrosine precursors (Figure 5.2).

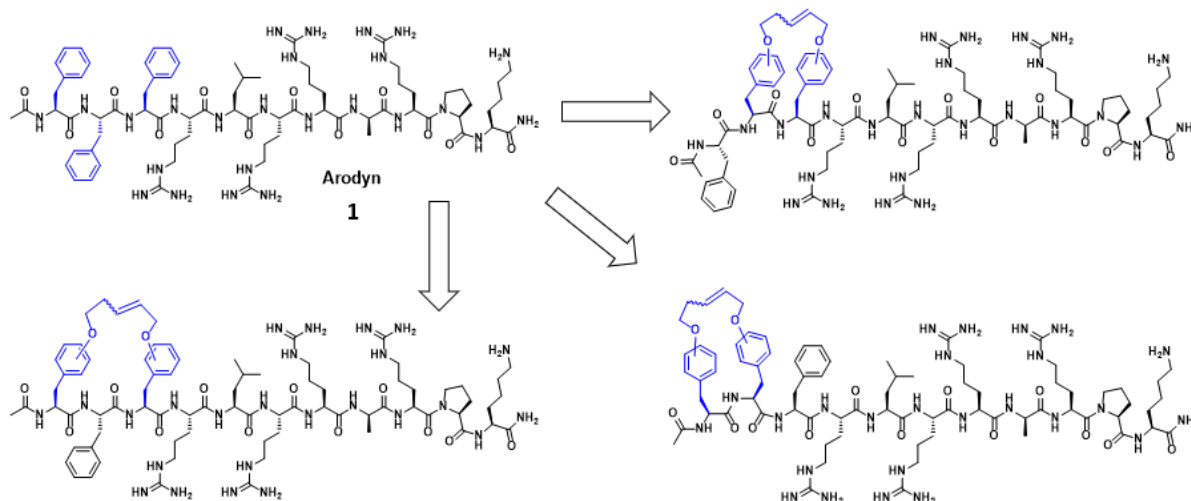
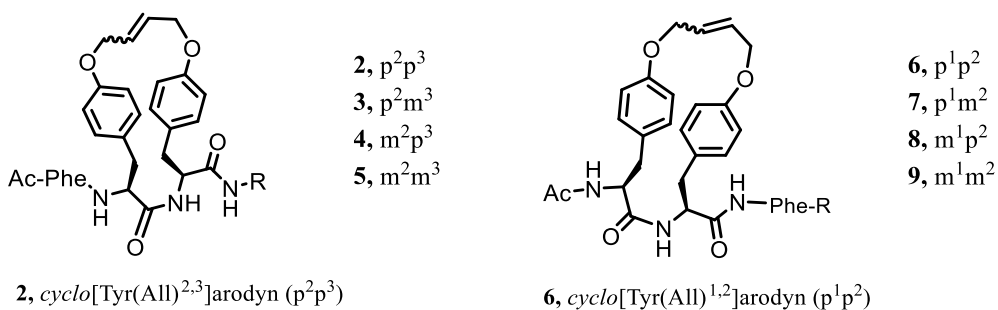


Figure 5.1 Structures of arodyn analogs and possible constraint of aromatic residues.



R = Arg-Leu-Arg-Arg-D-Ala-Arg-Pro-Lys-NH<sub>2</sub>

Figure 5.2 Arodyn analogs cyclized at adjacent tyrosine residues.

## 5.2 Results and discussion

### 5.2.1 Pharmacophore generation and docking study

To generate a pharmacophore with key structural features, we used the KOR X-ray crystal structure that was solved in its inactive state with the antagonist JD<sub>T</sub>ic bound at the orthosteric site.<sup>9</sup> We made several important assumptions and developed criteria to inform and guide the docking study (see Appendix 2 for details of modeling methods). First, rather than dock the full peptides, which is computationally expensive, we docked the corresponding tetrapeptide fragment for arodyn (Ac-Phe-Phe-Phe-Arg-NHCH<sub>3</sub>) and each of its cyclic analogs to assess how the “message” sequence may interact with KOR. Importantly, Arg<sup>4</sup> is included as part of the modeled fragments, as it is the first amino acid residue to likely interact with nonconserved acidic residues that directly flank the orthosteric site (Glu209 in extracellular loop 2 and/or Glu297<sup>6,58</sup>).<sup>10</sup> Many KOR ligands possess basic sites – including arodyn – that are hypothesized to interact with nonconserved acidic residues (Glu203, Asp206, Asp216, Asp217, and/or Asp218) that line extracellular loop 2 (ECL2). While these potential interactions are not considered in the current modeling approach, docking poses that direct the C terminus of the fragment peptide away from ECL2 were eliminated from further evaluation.

The binding mode of arodyn and its analogs to KOR is somewhat unique, as these peptides do not possess the prototypical phenol or N-terminal basic amine that is present in most opioid ligands. Surprisingly, arodyn analogs containing these groups demonstrated diminished affinity for the KOR.<sup>1</sup> We created a pharmacophore consisting of two basic sites (adjacent to Glu209 and Glu297) and two aromatic sites (see Appendix 2 for details on pharmacophore generation) to position the basic guanidinium and two of the three aromatic groups into regions of the pocket known to bind these moieties.<sup>9-12</sup>

Arodyn analogs with modifications in the “message” sequence exhibit binding affinities within 1- to 7-fold that of arodyn.<sup>1</sup> An alanine scan of arodyn indicated that while the “address” sequence contributed substantially to binding at the KOR, aromatic residues Phe<sup>1</sup> and Phe<sup>3</sup> also contribute to KOR affinity.<sup>1</sup> Accordingly, it is possible that the “message” sequence for the different analogs binds in similar conformations. The backbone and the side chains of Phe<sup>1</sup> and Phe<sup>3</sup> are oriented such that cyclizations may not appreciably change the positions of these groups in the receptor binding pocket among arodyn and its cyclic analogs.

While many different conformations and docking poses of cyclic arodyn analogs were observed in the study (including some with slightly better docking scores), only one common molecular architecture (Figures 5.3 and 5.4a-d) emerged that satisfied all the pharmacophore criteria. In this arrangement, no moieties of the docked molecules formed contacts with the conserved Asp138<sup>3,32</sup> residue, as expected from the SAR. While this ligand-receptor contact is present in all opioid receptor crystal structures which all contain basic opioid ligands, it does not appear to be important for the binding of noncationic ligands.<sup>13</sup>

In this arrangement, the side chains of the first residue in arodyn (Phe) and its analogs (Phe, Tyr or *m*-Tyr) adopt similar *anti* conformations (similar  $\chi_1$  angles, see Table A2.1a in Appendix 2, Figure 5.5). These groups overlap with the tetrahydroisoquinoline of JD<sub>Tic</sub> and, by extension, the phenols of the other opioid ligands in other crystal structures. The side chains of the second residue (Phe<sup>2</sup>, Tyr<sup>2</sup>, or *m*-Tyr<sup>2</sup>) do not appear to have a common conformation (different  $\chi_1$  and  $\chi_2$  angles, see Table A2.1b in Appendix 2) among the docked species; in this case, the cyclizations seem to perturb the conformation of this side chain.



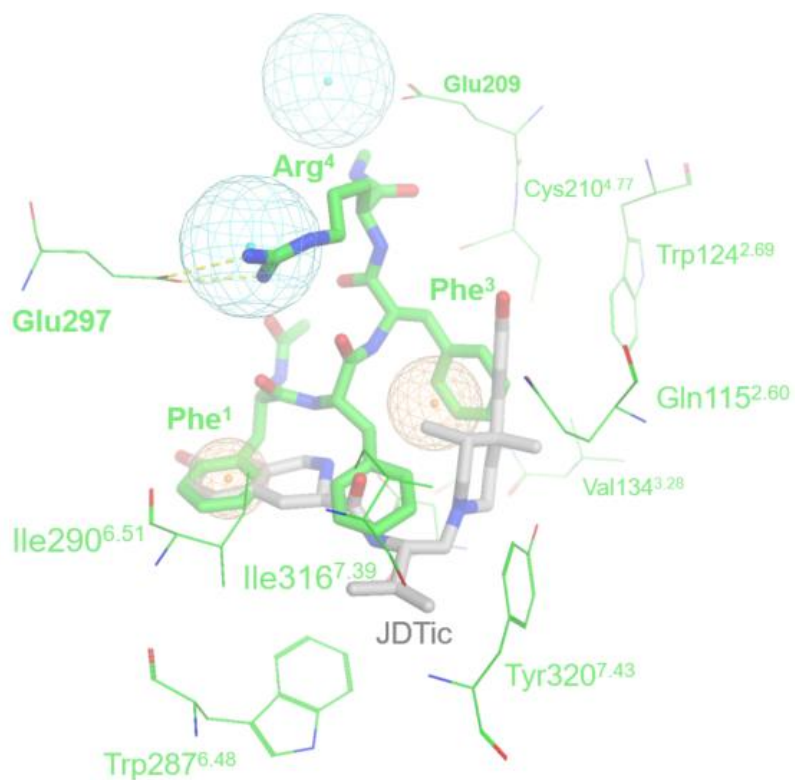


Figure 5.3 Docked structure of arodyn (thick green sticks) docked in the KOR model. In this pose, Phe<sup>1</sup> and Phe<sup>3</sup> of arodyn occupy the two aromatic pharmacophoric sites (orange spheres); the guanidinium of Arg<sup>4</sup> lies in one of the basic sites of the pharmacophore (cyan sphere), forming an ionic contact (yellow lines) with Glu297. JDtic (thick gray sticks) and the important nonconserved acidic residues Glu209 and Glu297 – as well as the conserved residues within 5.0 Å of Phe<sup>1</sup>, Phe<sup>2</sup>, and Phe<sup>3</sup> of arodyn – of the minimized receptor are also shown (thin green sticks).

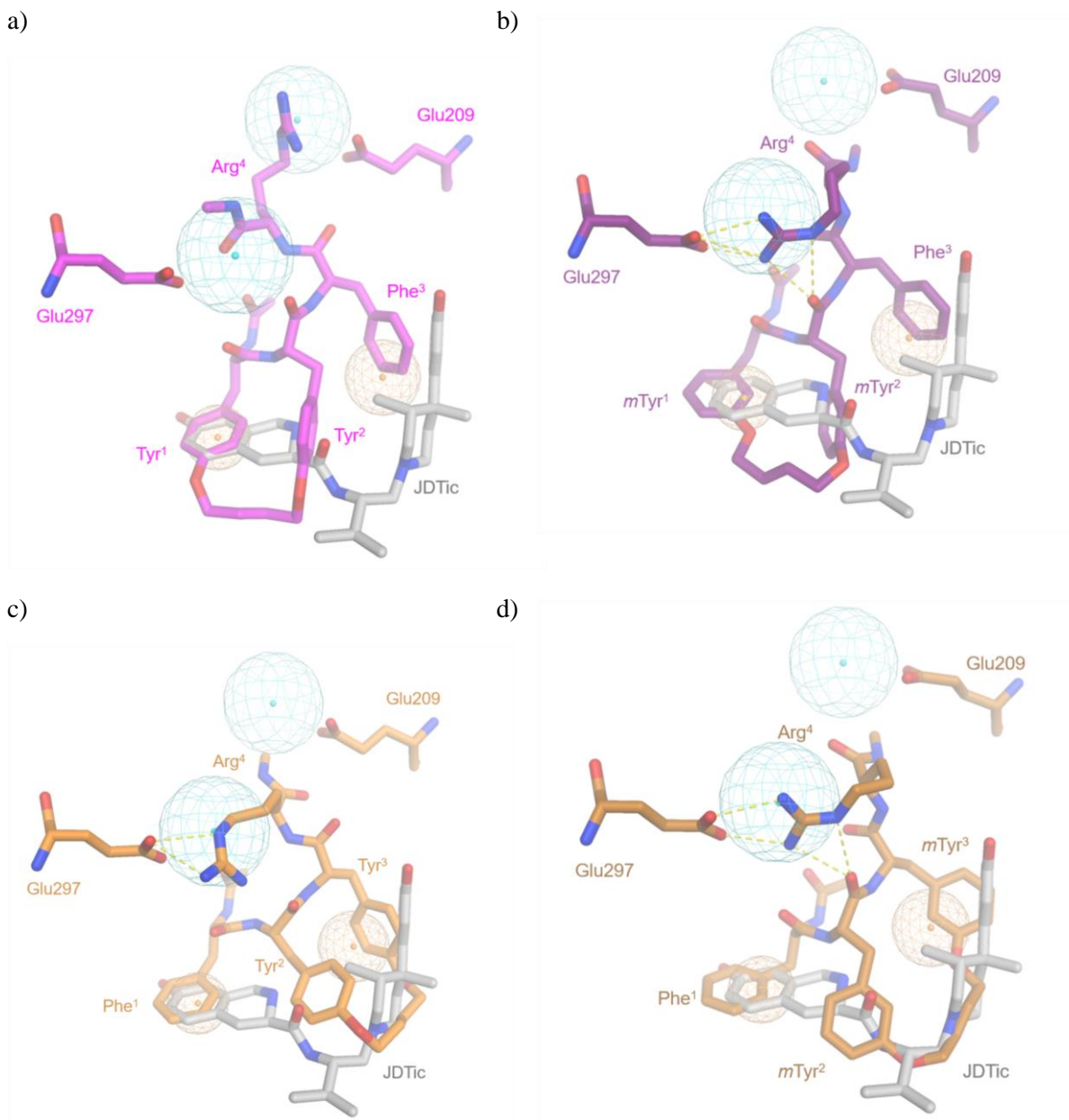


Figure 5.4 Structure of the a)  $p^1p^2$  (magenta sticks), b)  $m^1m^2$  (purple sticks), c)  $p^2p^3$  (orange sticks), and d)  $m^2m^3$  (brown sticks) cyclic arodyn analogs when docked inside the KOR model (not shown). In these poses, Phe<sup>1</sup> and Phe<sup>3</sup> of the analogs occupy the two pharmacophoric aromatic sites (orange spheres) while the guanidinium of Arg<sup>4</sup> lies in one of the basic sites of pharmacophore (cyan sphere); Glu209 and Glu297 of the minimized receptor are also shown. The guanidinium of Arg<sup>4</sup> forms an ionic contact (yellow lines) with the nearby Glu297 in all analogs except a) the  $p^1p^2$  analog. In b) and d) the guanidinium of Arg<sup>4</sup> also forms an intramolecular ion-dipole interaction with the carbonyl of *m*-Tyr<sup>2</sup> (yellow lines).

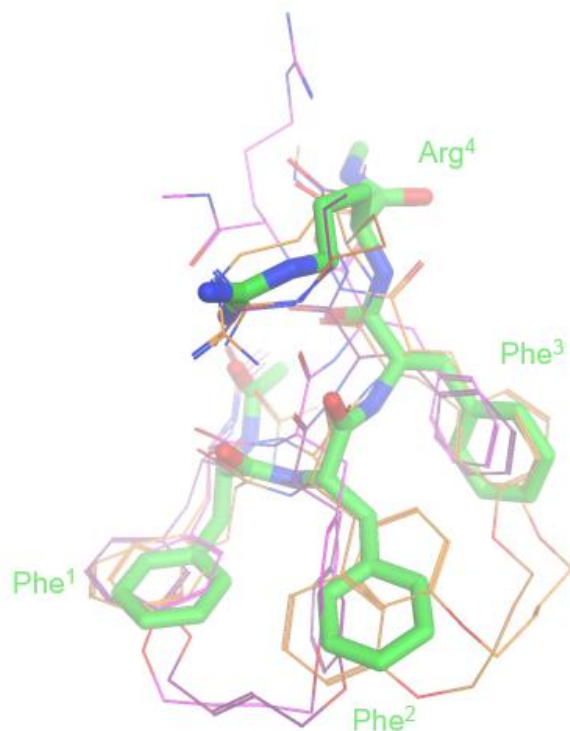


Figure 5.5 Overlay of arodyn and its analogs following docking in the KOR model (not shown). Arodyn (green) and its p<sup>1</sup>p<sup>2</sup> (magenta), m<sup>1</sup>m<sup>2</sup> (purple), p<sup>2</sup>p<sup>3</sup> (orange), and m<sup>2</sup>m<sup>3</sup> (brown) analogs have similar conformations. The acetyl group and backbone of residues 1-3 generally have a similar backbone across the analogs. The side chains of residues 1 and 3 ( $\chi_1$ ,  $\chi_2$ ) are generally similar, while the conformation of the side chain of residue 2 varies substantially. The conformation of Arg<sup>4</sup> also varies among the different species; only the p<sup>1</sup>p<sup>2</sup> analog does not appear to form an ionic contact with the side chain of Glu297.

The side chains of the third residue (Phe, Tyr, or *m*-Tyr), in contrast to Phe<sup>1</sup>, were found to adopt a common gauche (-) conformation (observed  $\chi_1$  angles, see Table A2.1c in Appendix 2). When superimposed on the corresponding crystal structures, the side chains overlay closely with the pendant phenyl ring of BU72 and the Phe<sup>3</sup> side chain of DIPP-NH<sub>2</sub>, crystallized bound to the MOR and DOR, respectively.<sup>11,12</sup> These two phenyl groups do not appear to impart selectivity to BU72 and DIPP-NH<sub>2</sub>, as they lie in a conserved region of the pocket (Gln115<sup>2,60</sup>, W124<sup>2,69</sup>, Val134<sup>3,28</sup>, Leu135<sup>3,29</sup>, Asp138<sup>3,32</sup>, Cys210<sup>4,77</sup>). In fact, BU72 is actually a mixed MOR and KOR agonist;<sup>14</sup> DIPP-NH<sub>2</sub> is a mixed DOR antagonist and MOR agonist, achieving its modest

selectivity for DOR via the phenyl moiety of its Tic<sup>2</sup> residue.<sup>15</sup> Overall, the phenyl groups of arodyn occupy a region in the receptor lined with conserved residues (Gln115<sup>2.60</sup>, Asp138<sup>3.32</sup>, Trp287<sup>6.48</sup>, Ile290<sup>6.51</sup>, Ile316<sup>7.39</sup>, Tyr320<sup>7.43</sup>) that flank the amide of JDtic in the KOR crystal structure.<sup>9</sup>

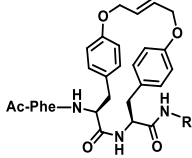
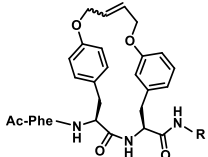
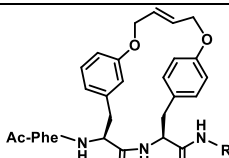
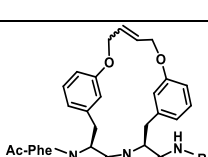
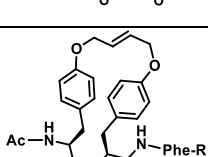
Given that arodyn lacks the prototypical phenol or N-terminal basic amine common in opioid ligands, the docked arodyn analogs provided further insight into the possible binding mode of arodyn at the KOR. The proposed docking poses (Figures 5.4a-d) suggested that cyclization between aromatic residues would be compatible binding to the KOR. We therefore used RCM to introduce conformational constraint in arodyn between aromatic residues.

### 5.2.2 Chemistry

While RCM is a powerful technique to install C-C bonds, there is a lack of general conditions that guarantee successful metathesis.<sup>16,17</sup> Of particular interest, ruthenium catalysts can also promote non-metathesis transformations,<sup>18</sup> including olefin isomerization.<sup>19</sup> that is problematic, especially in alkenes with allylic heteroatoms or aromatic groups.<sup>20</sup> Jacobsen and Rongved have extensively reviewed RCM in peptidic systems, particularly the impact of intramolecular RCM bridges on structure and pharmacological activity.<sup>21</sup> A vast majority of RCM reactions are performed in solution phase, and a low concentration of substrate (2 mM) is typically used. Initial solid phase RCM of dynorphin A<sup>22</sup> and arodyn analogs<sup>23</sup> used a DCM/DMF solvent mixture which allows for higher reaction temperatures, compatibility with hydrophilic peptides and on-resin cyclization. In later studies, low catalyst concentration and phenol as an isomerization suppressant<sup>24</sup> were found to enhance RCM product formation and suppress side products, as demonstrated in the model dipeptide study (Chapter 4). In the model dipeptide study the highest yields of RCM product were obtained using DCM and a 0.3 mM catalyst concentration in the

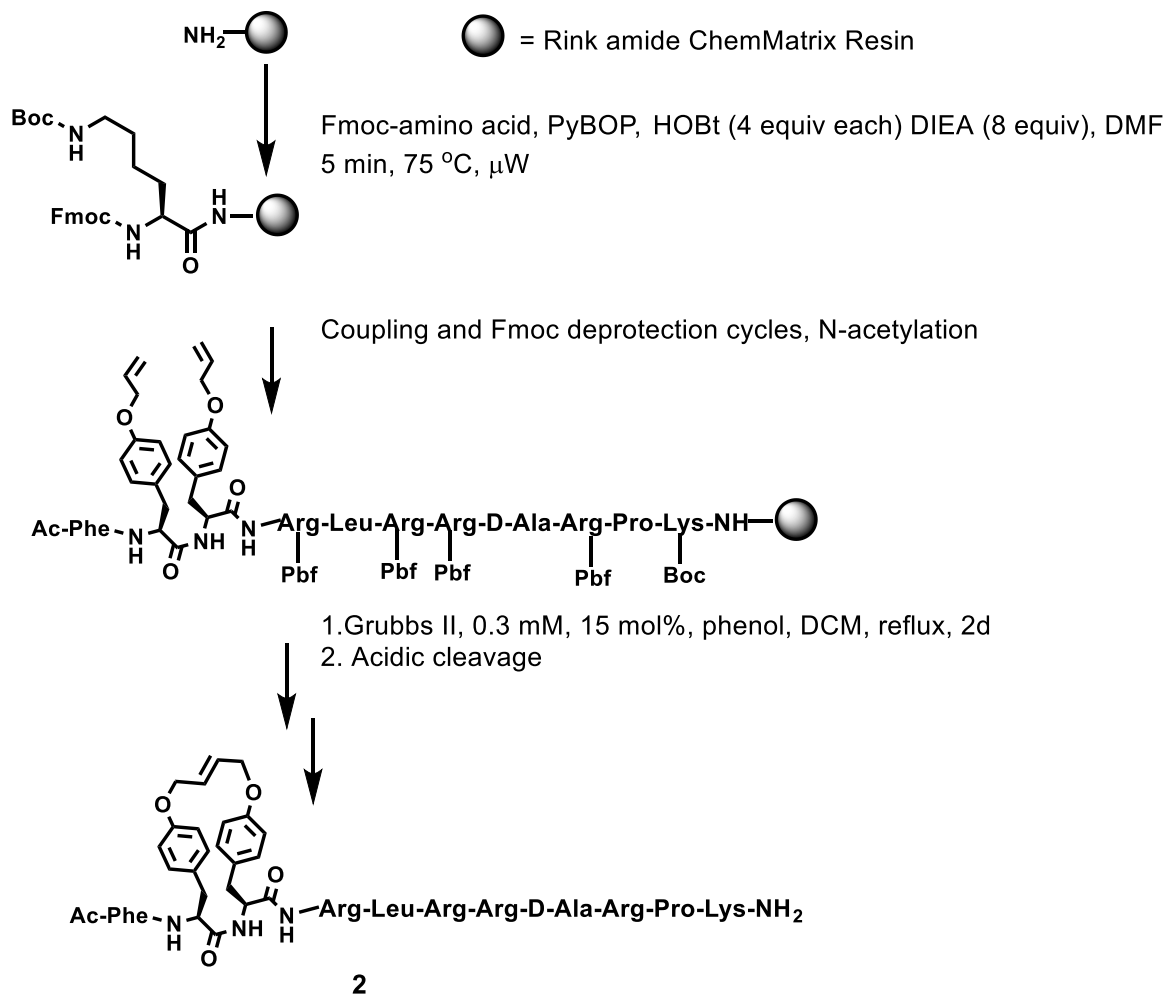
presence of phenol. A series of cyclic arodyn analogs (Table 5.1, Scheme 5.1) were synthesized by conventional heating using these conditions developed for a model dipeptide.

Table 5.1 Structures of the arodyn analogs cyclized by RCM under conventional heating and their linear precursors. In some cases a mixture of *cis/trans* analogs were obtained (indicated by a wavy bond).

Peptide	Arodyn analog	Structure
<b>1, arodyn</b>		Ac-Phe-Phe-Phe-R
<b>2</b>	<i>cyclo</i> [Tyr(All) <sup>2,3</sup> ]	
<b>3</b>	<i>cyclo</i> [Tyr(All) <sup>2</sup> , <i>m</i> -Tyr(All) <sup>3</sup> ]	
<b>4</b>	<i>cyclo</i> [ <i>m</i> -Tyr(All) <sup>2</sup> , Tyr(All) <sup>3</sup> ]	
<b>5</b>	<i>cyclo</i> [ <i>m</i> -Tyr(All) <sup>2,3</sup> ]	
<b>6</b>	<i>cyclo</i> [Tyr(All) <sup>1,2</sup> ]	
Linear arodyn analogs		
<b>10</b>	[Tyr(All) <sup>2,3</sup> ]	Ac-Phe-Tyr(All)-Tyr(All)-R
<b>11</b>	[Tyr(All) <sup>2</sup> , <i>m</i> -Tyr(All) <sup>3</sup> ]	Ac-Phe-Tyr(All)- <i>m</i> -Tyr(All)-R
<b>12</b>	[ <i>m</i> -Tyr(All) <sup>2</sup> , Tyr(All) <sup>3</sup> ]	Ac-Phe- <i>m</i> -Tyr(All)-Tyr(All)-R
<b>13</b>	[ <i>m</i> -Tyr(All) <sup>2,3</sup> ]	Ac-Phe- <i>m</i> -Tyr(All)- <i>m</i> -Tyr(All)-R
<b>14</b>	[Tyr(All) <sup>1,2</sup> ]	Ac-Tyr(All)-Tyr(All)-Phe-R

R= Arg-Leu-Arg-Arg-D-Ala-Arg-Pro-Lys-NH<sub>2</sub>

Scheme 5.1 Synthesis of the p<sup>2</sup>p<sup>3</sup> analog **2** by RCM with conventional heating using optimized conditions from the model dipeptide study.



### 5.2.2.1 RCM by conventional heating

The optimized conditions found for the dipeptide were explored for RCM of arodyn analogs using conventional heating. As observed in the model dipeptide, lowering the temperature, reducing the catalyst loading, and using phenol as an isomerization suppressant with the 2<sup>nd</sup> generation Grubbs catalyst (G II) contributed to an increase in the RCM product **2** (Table 5.2). As observed in the model dipeptide reasonable yields were observed using both G II and the 2<sup>nd</sup> generation Hoveyda-Grubbs catalyst (HG II) (Table 5.2). The optimized conditions from the model dipeptide resulted in a 2-fold increase in the RCM product compared to the original

conditions (Table 5.2). The optimized conditions with G II in the presence of phenol (Table 5.2) were subsequently used in the synthesis of **2-6** for pharmacological evaluation (Figure 5.6 and Table 5.3).

Conformational effects influenced the cyclization efficiency of arodyn analogs. Varying yields of the respective cyclizations were observed indicating sequence dependent effects; notably, cyclization of **7** resulted in low yields under conventional heating. Sequence dependent effects were most prominent in the p<sup>1</sup>p<sup>3</sup> analog **15** where no cyclization was observed even after 5 days of heating under the optimized conditions using G II. The bis-desallyl product was observed as the major product following RCM for 5 days.

Table 5.2 Results for RCM of **10** using various reaction conditions.

Entry	Solvent	Temp. (°C)	[Cat.] (mM)	Cat. <sup>a</sup> mol %	Additive	RCM Pdt.
1	DCM/DMF	60	3	40	-	34
2	DCM	40	0.3	15	phenol	71
3	DCM	40	0.3	15 <sup>b</sup>	-	64

<sup>a</sup>G II catalyst; <sup>b</sup>HG II catalyst

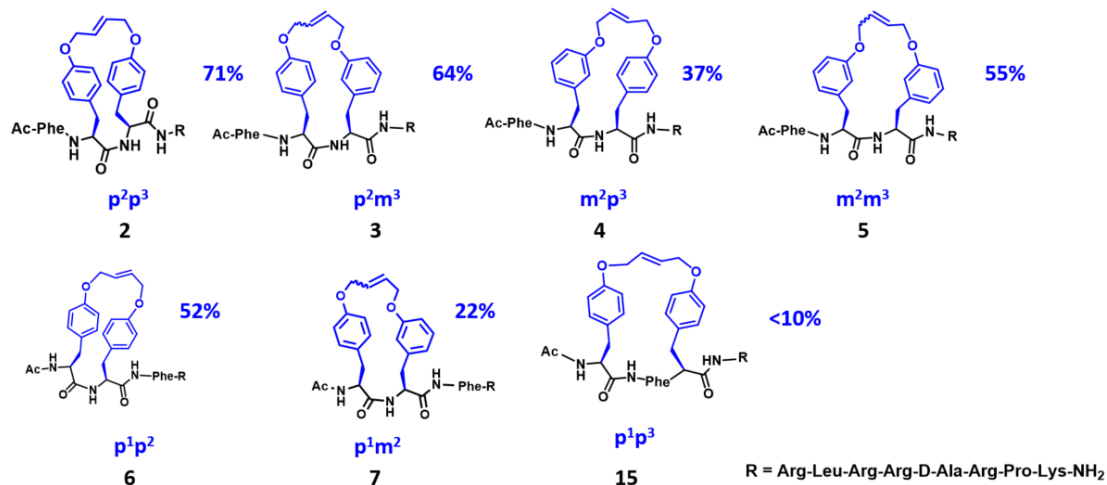


Figure 5.6 Arodyn analogs cyclized via conventional heating, showing the corresponding yields.

Table 5.3 Analytical data of purified cyclic peptides **2-6** and their linear analogs.

Peptide	UPLC $t_R$ (min)		Mass ( $m/z$ )	
	System 1 <sup>a</sup> (% purity)	System 2 <sup>b</sup> (% purity)	Calculated	Observed
<b>2</b>	8.38 (97.8)	9.47 (99.8)	[M+3H] <sup>3+</sup> 540.3	[M+3H] <sup>3+</sup> 540.5
<b>3</b>	8.95 (97.5)	9.24/9.48 (98.7) <sup>c</sup>	[M+H] <sup>1+</sup> 1619.0	[M+H] <sup>1+</sup> 1619.5
<b>4</b>	8.88 (96.8)	9.22 (98.5)	[M+H] <sup>1+</sup> 1619.0	[M+H] <sup>1+</sup> 1619.4
<b>5</b>	8.88 (96.6)	9.04/9.14 (99.7) <sup>c</sup>	[M+H] <sup>1+</sup> 1619.0	[M+H] <sup>1+</sup> 1619.5
<b>6</b>	8.60 (97.7)	9.15 (99.8)	[M+H] <sup>1+</sup> 1619.0	[M+H] <sup>1+</sup> 1619.6
<b>10</b>	8.99 (99.4)	10.09 (99.6)	[M+H] <sup>1+</sup> 1647.0	[M+H] <sup>1+</sup> 1647.9
<b>11</b>	9.15 (99.7)	10.35 (99.3)	[M+H] <sup>1+</sup> 1647.0	[M+H] <sup>1+</sup> 1647.5
<b>12</b>	9.12 (99.2)	10.48 (97.0)	[M+H] <sup>1+</sup> 1647.0	[M+H] <sup>1+</sup> 1647.3
<b>13</b>	9.47 (99.7)	10.13 (99.9)	[M+H] <sup>1+</sup> 1647.0	[M+H] <sup>1+</sup> 1647.5
<b>14</b>	9.29 (99.9)	10.46 (96.3)	[M+H] <sup>1+</sup> 1647.0	[M+H] <sup>1+</sup> 1647.4

<sup>a</sup>5-55% aqueous MeCN with 0.1% TFA over 10 min, 1 mL/min; <sup>b</sup>25-75% aqueous MeOH with 0.1% TFA over 10 min, 1 mL/min; <sup>c</sup>*trans/cis*

Given the low yield observed for analog **7** (Figure 5.6) under conventional heating, reaction conditions using microwave heating were also explored. Microwave heating has been shown to improve RCM reactions of resin-bound peptides with low catalyst loadings and short reaction times.<sup>25</sup> Two modes of microwave irradiation, open vessel and closed vessel microwave heating, were explored.

### 5.2.2.2 Microwave Assisted RCM

Generally, HG II performed better than G II in the model dipeptide under microwave heating (Table 5.3) and was thus adopted for microwave assisted RCM using the optimized conditions established in the model dipeptide study. Cyclization of the model dipeptide, **16**, using HG II under open vessel heating at 60 °C resulted in 68% of the cyclic product after 2 h and 82%



after 3 h (Table 5.4), which was comparable to heating for 2 d under conventional heating. HG II, which is more stable than G II,<sup>26</sup> was therefore used in subsequent microwave assisted RCM. Whereas the dipeptide was rapidly cyclized, the tripeptide, **17**, required a longer reaction time (5 h) to achieve a similar cyclization yield; a 50% yield was observed after 3 h and increased to 79% after 5 h heating (Table 5.4).

Cyclization of **10** also required a longer reaction time than the dipeptide, but only 30% of the cyclic product was observed after 5 h (Table 5.4). Additionally, a 2-fold increase in the catalyst loading (30 mol%) was required to obtain a reasonable yield of **2** (53%), suggesting catalyst decomposition under open vessel conditions. Closed vessel microwave heating was therefore explored to enhance cyclization yields. Of note, due to instrument design, closed vessel microwave heating allowed higher reaction temperatures in contrast to open vessel microwave heating.

Table 5.4 Comparison of RCM product yields following cyclization of model dipeptide, tripeptide, and arodyn analogs under conventional heating using G II and with microwave irradiation using HG II.<sup>a</sup>

Peptide	Substrate	RCM Pdt (%)		
		conventional heating <sup>b</sup>	microwave heating <sup>c</sup>	
			open vessel	closed vessel
<b>16</b>	Fmoc-Tyr(All)-Tyr(All) <sup>d</sup>	80	82 <sup>e</sup>	-
<b>17</b>	Fmoc-Tyr(All)-Phe-Tyr(All) <sup>d</sup>	65	50 <sup>e</sup> , 79	-
<b>10</b>	[Tyr(All) <sup>2,3</sup> ]arodyn <sup>f</sup>	71	29, 53 <sup>g</sup>	72, 72 <sup>h</sup>
<b>18</b>	[Tyr(All) <sup>1</sup> , <i>m</i> -Tyr(All) <sup>2</sup> ]arodyn <sup>f</sup>	22	-	44, 67 <sup>h</sup>
<b>19</b>	[ <i>m</i> -Tyr(All) <sup>1</sup> , Tyr(All) <sup>2</sup> ]arodyn <sup>f</sup>	-	-	56 <sup>h</sup>
<b>20</b>	[ <i>m</i> -Tyr(All) <sup>1,2</sup> ]arodyn <sup>f</sup>	-	-	66 <sup>h</sup>

<sup>a</sup> Initial RCM experiments using G II catalyst under open vessel heating resulted in negligible conversion of the model dipeptide; <sup>b</sup> G II (15 mol%, 0.3 mM) in DCM, phenol 40 °C, 2 d (optimized conditions from Chapter 4); <sup>c</sup> HG II (15 mol%, 0.3 mM) in dichloroethane, 60 °C, 5 h unless otherwise specified; <sup>d</sup> peptide on 2-chlorotriptyl resin; <sup>e</sup> 3 h; <sup>f</sup> peptide on Rink amide ChemMatrix resin; <sup>g</sup> HG II (30 mol%, 0.3 mM); <sup>h</sup> 75 °C, 2 h

Closed vessel microwave heating under the optimized conditions resulted in a similar yield (72%) in 5 h to that obtained by conventional heating compared to only 30% under open vessel microwave heating (Table 5.4). Furthermore, a 2-fold increase in the cyclization yield of **18** compared to conventional heating was observed under the optimized conditions (Chapter 4). An additional improvement in the yield of **18** was observed following microwave irradiation at 75 °C for 2 h (Table 5.4). Similarly, high cyclization yields were observed after **19** and **20** were cyclized for 2 h at 75 °C (Table 5.4). Presumably, closed vessel microwave heating limited the catalyst decomposition that could occur under open vessel heating and facilitated enhanced yields in the cyclization of **18**. Microwave irradiation therefore facilitated the synthesis of arodyn analogs involving *m*-Tyr(All) in the cyclic constraint for pharmacological evaluation (Tables 5.5 and 5.6). Notably, however, the cyclization of [Tyr(All)<sup>1,3</sup>]arodyn was negligible under both open vessel and closed vessel microwave irradiation. This suggests that [Tyr(All)<sup>1,3</sup>]arodyn adopts a conformation that does not bring the alkene precursors in close proximity to facilitate cyclization to form **15**.

Table 5.5 Structures of arodyn analogs containing *m*-Tyr(All) in positions 1 and 2 cyclized by RCM under microwave irradiation and their linear precursors.

Peptide	Arodyn analog	Structure
7	<i>cyclo</i> [Tyr(All) <sup>1</sup> , <i>m</i> -Tyr(All) <sup>2</sup> ]	
8	<i>cyclo</i> [ <i>m</i> -Tyr(All) <sup>1</sup> ,Tyr(All) <sup>2</sup> ]	
9	<i>cyclo</i> [ <i>m</i> -Tyr(All) <sup>1,2</sup> ]	
Linear arodyn analogs		
18	[Tyr(All) <sup>1</sup> , <i>m</i> -Tyr(All) <sup>2</sup> ]	Ac-Tyr(All)- <i>m</i> -Tyr(All)-Phe-R
19	[ <i>m</i> -Tyr(All) <sup>1</sup> ,Tyr(All) <sup>2</sup> ]	Ac- <i>m</i> -Tyr(All)-Tyr(All)-Phe-R
20	[ <i>m</i> -Tyr(All) <sup>1,2</sup> ]	Ac- <i>m</i> -Tyr(All)- <i>m</i> -Tyr(All)-Phe-R
R= Arg-Leu-Arg-Arg-D-Ala-Arg-Pro-Lys-NH <sub>2</sub>		

Table 5.6 HPLC and MS data of purified arodyn analogs **7-9** and their linear analogs **18-20**.

Peptide	HPLC $t_R$ (min)		ESI-MS ( $m/z$ )	
	System 1 <sup>a</sup> (% purity)	System 2 <sup>b</sup> (% purity)	Calculated	Observed
<b>7</b>	28.9;29.9 <sup>c</sup> (98.1)	22.63 (95.0)	[M+3H] <sup>3+</sup> 540.3	[M+3H] <sup>3+</sup> 540.7
			[M+2H] <sup>2+</sup> 405.5	[M+2H] <sup>2+</sup> 405.8
<b>8</b>	29.1 (98.6)	23.3 (98.2)	[M+3H] <sup>3+</sup> 540.3	[M+3H] <sup>3+</sup> 540.7
			[M+2H] <sup>2+</sup> 405.5	[M+2H] <sup>2+</sup> 405.8
<b>9</b>	29.5 (98.7)	23.8 (95.1)	[M+3H] <sup>3+</sup> 540.3	[M+3H] <sup>3+</sup> 540.7
			[M+2H] <sup>2+</sup> 405.5	[M+2H] <sup>2+</sup> 405.8
<b>18</b>	33.7 (95.2)	29.3 (95.2)	[M+3H] <sup>3+</sup> 549.7	[M+3H] <sup>3+</sup> 550.3
			[M+2H] <sup>2+</sup> 412.5	[M+2H] <sup>2+</sup> 413.0
<b>19</b>	32.8 (98.0)	28.2 (98.9)	[M+3H] <sup>3+</sup> 549.7	[M+3H] <sup>3+</sup> 550.3
			[M+2H] <sup>2+</sup> 412.5	[M+2H] <sup>2+</sup> 412.7
<b>20</b>	33.3 (99.9)	29.0 (98.2)	[M+3H] <sup>3+</sup> 549.7	[M+3H] <sup>3+</sup> 550.1
			[M+2H] <sup>2+</sup> 412.5	[M+2H] <sup>2+</sup> 412.9

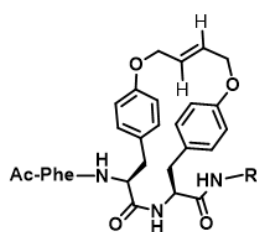
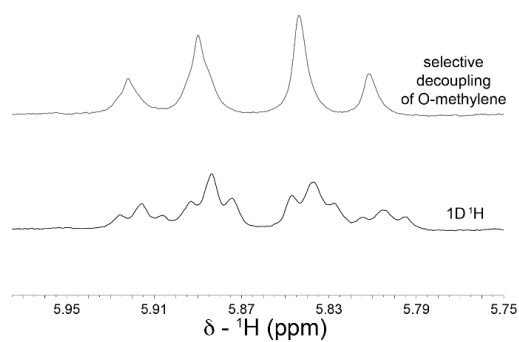
<sup>a</sup> 5-50% aqueous MeCN with 0.1% TFA over 45 min, 1 mL/min; <sup>b</sup> 25-70% aqueous MeOH with 0.1% TFA over 45 min, 1 mL/min; <sup>c</sup> *cis/trans* mixture

### 5.2.2.3 NMR analysis

NMR J-couplings and chemical shifts were employed to determine the *cis/trans* configuration of the olefins (Appendix 3). For some spectra, multiplets were not well separated likely because the difference in chemical shifts was not significantly larger than the scalar coupling constants, thereby giving non-first order effects. In these instances, we performed homonuclear decoupling experiments, as illustrated for **2** (Figure 5.7a and b); as a result, we assigned the coupling constant, 16 Hz (<sup>3</sup>J<sub>olefin</sub>), indicating a *trans* olefin. The same logic was applied to other cyclic analogs. Generally, the chemical shifts of vinyl protons were between 5.5 and 6.05 ppm for the cyclic analogs (Table 5.7). The olefins were predominantly in the *trans* configuration except

in RCM between adjacent *m*-Tyr(All) residues where appreciable quantities of the *cis* isomer (Table 5.6) were observed (Appendix 3).

a)



R=Arg-Leu-Arg-Arg-D-Ala-Arg-Pro-Lys-NH<sub>2</sub>

b)

2

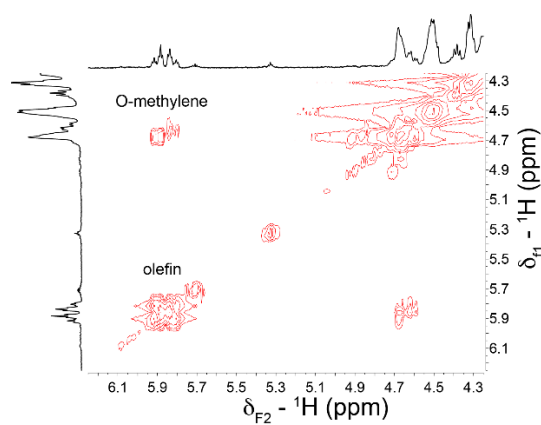
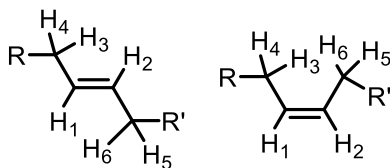


Figure 5.7 a) <sup>1</sup>H NMR of **2** showing olefin protons and the spectrum following homonuclear decoupling; b) COSY of **2**.

Table 5.7 <sup>1</sup>H NMR data for cyclic aroldyn analogs **2-9**.



Compound		Chemical shifts ( $\delta$ ) of olefinic protons	$J$ (Hz)	<i>cis/trans</i> ratio
<b>2</b>	<b>2-trans</b>	H <sub>1</sub> = 5.82	$J_{12}$ = 16.0	-
		H <sub>2</sub> = 5.90	$J_{21}$ = 15.9	
<b>3</b>	<b>3-cis</b>	H <sub>1</sub> = 5.74	$J_{12}$ = 11.2	1
		H <sub>2</sub> = 5.87	$J_{21}$ = 11.3	
	<b>3-trans</b>	H <sub>1</sub> = 5.52	$J_{12}$ = 15.8	3
		H <sub>2</sub> = 5.95	$J_{21}$ = 16.1	
<b>4</b>	<b>4-trans</b>	H <sub>1</sub> = 5.71	$J_{12}$ = 16.1	-
		H <sub>2</sub> = 5.88	$J_{21}$ = 16.3	
<b>5</b>	<b>5-cis</b>	H <sub>1</sub> = 5.71	$J_{12}$ = 11.0	1
		H <sub>2</sub> = 5.91	$J_{21}$ = 11.4	
	<b>5-trans</b>	H <sub>1</sub> = 5.78	$J_{12}$ = 16.0	1
		H <sub>2</sub> = 5.99 <sup>a</sup>	-	
<b>6</b>	<b>6-trans</b>	H <sub>1</sub> = 5.80	$J_{12}$ = 16.2	-
		H <sub>2</sub> = 5.87	$J_{21}$ = 15.8	
<b>7</b>	<b>7-cis<sup>a</sup></b>	H <sub>1</sub> = 5.74	-	1

		H <sub>2</sub> = 6.05	-	
	<b>7-trans</b>	H <sub>1</sub> = 5.62	J <sub>12</sub> = 16.1	4
		H <sub>2</sub> = 5.89	J <sub>21</sub> = 16.1	
<b>8</b>	<b>8-cis</b>	H <sub>1</sub> = 5.61	J <sub>12</sub> = 11.6	1
		H <sub>2</sub> = 5.63	J <sub>21</sub> = 10.8	
	<b>8-trans</b>	H <sub>1</sub> = 5.76	J <sub>12</sub> = 16.2	67
		H <sub>2</sub> = 5.82	J <sub>21</sub> = 16.0	
<b>9</b>	<b>9-cis</b>	H <sub>1</sub> = 5.77	J <sub>12</sub> = 11.2	1
		H <sub>2</sub> = 5.96	J <sub>21</sub> = 11.2	
	<b>9-trans</b>	H <sub>1</sub> = 5.83	J <sub>12</sub> = 15.8	2
		H <sub>2</sub> = 6.04	J <sub>21</sub> = 15.7	
<sup>a</sup> Coupling constants could not be obtained due to poor resolution of the fine structure				

### 5.2.3 Affinity

#### In vitro pharmacological evaluation

The opioid receptor affinities of the cyclic arodyn analogs and their linear precursors were evaluated using Chinese hamster ovary (CHO) cells stably expressing cloned opioid receptors. Initial results indicate that cyclizations involving the aromatic residues were generally well tolerated at the KOR; cyclized analogs displayed affinities within 4-fold that of arodyn with the exception of **7** and **9** with *meta*-substituted Tyr(All) at positions 2 and positions 1 and 2, respectively (Table 5.8). Some analogs gained affinity for MOR, thus exhibiting reduced selectivity for KOR (Table 5.8). Reduced selectivity for KOR was observed for *meta*-substituted Tyr(All) derivatives **3** and **5** compared to their linear counterparts. The cyclic *para* substituted analogs **2** and **6** displayed the highest selectivity for the KOR relative to the MOR among the cyclic analogs evaluated to date.

The docking studies of arodyn and its cyclic analogs to the KOR crystal structure<sup>9</sup> (Figure 5.4) suggested that the binding mode does not change appreciably upon cyclization. The similar KOR affinities of the cyclic arodyn analogs are consistent with the results of the docking study.

Table 5.8 Opioid receptor binding affinities of arodyn analogs cyclized by RCM and their linear counterparts.

Peptide (cyclic)	K <sub>i</sub> <sup>a</sup>		K <sub>i</sub> ratio (MOR/KOR)	Peptide (linear)	K <sub>i</sub> <sup>a</sup>		K <sub>i</sub> ratio (MOR/KOR)
	KOR	MOR			KOR	MOR	
				<b>1</b> <sup>b</sup>	10.0 ± 3.0	1740 ± 130	174
<b>2 (p<sup>2</sup>p<sup>3</sup>)</b>	14.7 ± 5.6	1372 ± 329	93	<b>10</b>	18.9 ± 3.6	1224 ± 239	65
<b>3 (p<sup>2</sup>m<sup>3</sup>)</b>	19.8 ± 6.8	607 ± 28	31	<b>11</b>	11.7 ± 3.3	1384 ± 145	118
<b>4 (m<sup>2</sup>p<sup>3</sup>)</b>	39.2 ± 12.9	1958 ± 207	50	<b>12</b>	41.2 ± 14.3	1326 ± 106	32
<b>5 (m<sup>2</sup>m<sup>3</sup>)</b>	15.4 ± 3.4	828 ± 125	54	<b>13</b>	3.3 ± 0.3	838 ± 77	255
<b>6 (p<sup>1</sup>p<sup>2</sup>)</b>	11.7 ± 2.7	1434 ± 402	123	<b>14</b>	12.1 ± 4.3	221 ± 17	18
<b>7 (p<sup>1</sup>m<sup>2</sup>)</b>	56.7 ± 15.3	ND <sup>c</sup>	-	<b>18</b>	62.2 ± 5.1	ND	-
<b>8 (m<sup>1</sup>p<sup>2</sup>)</b>	29.2 ± 3.5	ND	-	<b>19</b>	43.2 ± 5.5	ND	-
<b>9 (m<sup>1</sup>m<sup>2</sup>)</b>	68.2 ± 10.4	ND	-	<b>20</b>	65.8 ± 18.1	ND	-

<sup>a</sup> Mean K<sub>i</sub> values ± SEM from at least 3 independent experiments; <sup>b</sup> from ref.<sup>7</sup>; <sup>c</sup> not determined

Negligible efficacies were observed in GTPγS screening at KOR at 10 μM for analogs **2-6** and **10-14**, indicating that both linear and cyclic analogs have minimal agonist activity at KOR. Further determination of binding affinities and further testing of all cyclized analogs is in progress. Of note, the originally prepared cyclic arodyn analogs **21** and **22** exhibited 5- and 7-fold losses, respectively, in affinity relative to arodyn (Table 5.9).<sup>23</sup> D-Ala<sup>8</sup> substitution was expected to improve affinity to KOR from earlier studies (Bennet, Murray, Aldrich, unpublished results). Compounds **2** and **6** exhibited similar affinity to arodyn, indicating increased affinity following D-Ala<sup>8</sup> substitution (Table 5.8). D-Ala substitution also affected KOR selectivity and a marked difference in selectivity for the KOR was observed; 93-fold for **2** (Table 5.8) and 16-fold for **21**



(Table 5.9), indicating increased selectivity with D-Ala<sup>8</sup> in the cyclized arodyn analogs. A similar substantial difference in selectivity was observed between **6** (Table 5.8) and **22** (Table 5.9) cyclized between residues 1 and 2.

Table 5.9 Opioid receptor binding affinities of *cyclo*[Tyr(All)<sup>x,y</sup>,Ile<sup>8</sup>] analogs cyclized by RCM.<sup>23</sup>

Compound number	Peptide	K <sub>i</sub> ± SEM (nM) <sup>a</sup>		K <sub>i</sub> ratio (MOR/KOR)
		KOR	MOR	
<b>1<sup>b</sup></b>	arodyn	10.0 ± 3.0	1740 ± 130	174
<b>21 (p<sup>2</sup>p<sup>3</sup>)</b>	<i>cyclo</i> [Tyr(All) <sup>2,3</sup> ,Ile <sup>8</sup> ]arodyn	55.4 ± 4.1	903 ± 34	16
<b>22 (p<sup>1</sup>p<sup>2</sup>)</b>	<i>cyclo</i> [Tyr(All) <sup>1,2</sup> ,Ile <sup>8</sup> ]	71.7 ± 5.2	1920 ± 150	27

<sup>a</sup> Mean K<sub>i</sub> values ± SEM from at least three independent experiments; from ref.<sup>7</sup>

### 5.3 Conclusions

The studies discussed in this chapter were aimed at examining the effect of constraining aromatic residues that contribute to the KOR affinity of arodyn. We successfully introduced a local constraint in the N-terminus of arodyn using conditions developed in a model dipeptide system to suppress olefin isomerization during RCM. The resulting non-native C-C bond is metabolically stable and is different from standard peptide cyclization approaches such as lactam or disulfide bridges. Additionally, while RCM is typically done at non-critical residues using AllGly, we used Tyr(All) residues to restrict the conformation of residues contributing to KOR affinity to potentially stabilize the bioactive conformation. Of note, docking studies suggested constrained aromatic residues would be compatible with binding to KOR.

Optimized conditions from the model dipeptide study and microwave heating facilitated the synthesis of arodyn analogs with constrained aromatic residues using RCM. Accordingly, varying cyclization yields were observed due to sequence and conformationally dependent effects that lowered cyclization efficiency in some analogs. Microwave irradiation was vital in improving

the yields of peptide RCM while reducing the reaction times, particularly for cyclizations between the first two residues involving *m*-Tyr(All).

The resulting cyclic arodyn analogs generally retained affinity at the KOR with binding affinities within 7-fold of arodyn. Cyclizations involving Tyr(All) between adjacent residues displayed the highest affinity and selectivity for KOR. In contrast, among the analogs evaluated to date, cyclizations involving *m*-Tyr(All) exhibited reduced selectivity for KOR. The general retention of KOR affinity in the cyclic arodyn analogs is consistent with modeling studies which suggested similar positioning of the aromatic groups of the different analogs in the KOR binding site.

Incorporation of D-Ala<sup>8</sup> improved KOR binding affinities compared to the corresponding analogs containing Ile<sup>8</sup>, indicating the contribution of this modification in the “address” sequence. A 5.5-fold improvement in affinity was observed for **2** relative to **21** while about a 6-fold improvement was observed for **6** relative to **22**. Additionally, **2** was at least 7-fold more selective for KOR relative to MOR than **21** while **6** was about 4-fold more selective for the KOR than **22** as a result of increased KOR affinity. Overall, proposed binding modes from the docking study provide a plausible explanation as to why the cyclizations between aromatic residues in the “message” sequence was generally well tolerated at the KOR.

## 5.4 Experimental

### Materials and methods.

The Rink amide ChemMatrix resin was purchased from Biotage (Charlotte, NC), the Fmoc-protected PAL-PEG-PS was purchased from APPTec LLC (Louisville, KY), and the 2-chlorotrityl chloride resin was purchased from Chem-Impex International (Wood Dale, IL). All

standard protected amino acids were purchased from Bachem (King of Prussia, PA), EMD Millipore Chemicals (San Diego, CA), Peptides International (Louisville, KY), or Chem-Impex International. Fmoc-L-Tyr(All)-OH was purchased from Chem-Impex International, and Fmoc-*m*-Tyr(All) was purchased from PepTech Corporation (Bedford, MA, USA). The coupling agent benzotriazol-1-yl-oxy-tris-pyrrolidino-phosphonium hexafluorophosphate (PyBOP) and the coupling additive 1-hydroxybenzotriazole hydrate (HOBt) were obtained from Peptides International. Dichloromethane (DCM), *N,N*-diisopropylethylamine (DIEA), *N,N*-dimethylformamide (DMF), diethyl ether, acetonitrile, methanol, and trifluoroacetic acid (TFA) were purchased from Fisher Scientific (Hampton, NH). All other chemicals were purchased from Aldrich Chemical Co. (Milwaukee, WI).

### **Instruments.**

Open vessel microwave assisted RCM was performed on a Biotage microwave peptide synthesizer (Initiator+ Alstra; Biotage, Sweden). Closed vessel microwave assisted RCM was performed on a Biotage Initiator+ SP Wave microwave synthesizer.

Electrospray ionization mass spectrometry (ESI/MS) was performed on an LCT Premier (Waters Corp., Milford, MA) instrument with a time of flight mass analyzer or on the Advion expression L compact MS (Advion, Inc., Ithaca, NY). A Voyager DE STR high performance matrix-assisted laser desorption time-of-flight mass spectrometer (MALDI-TOFMS) was used for MALDI MS analysis.

<sup>1</sup>H NMR spectra of these compounds (0.5–2 mg) were obtained at 27 °C in DMSO-*d*<sub>6</sub> on a Bruker Avance III 600 MHz equipped with a 5 mm cryoprobe in the McKnight Brain Institute at the National High Magnetic Field Laboratory's AMRIS facility at the University of Florida or

a Bruker AVANCE DRX-500 spectrometer (500.13 MHz proton frequency) equipped with a 5 mm z-gradient cryoprobe. <sup>1</sup>H chemical shifts were referenced to the residual DMSO signal at 2.49 ppm, and coupling constants were extracted from the 1D spectra.

Analytical HPLC was performed on two instruments: an Acquity UPLC system (Waters Corp., Milford MA) fitted with an Acquity UPLC Ethylene Bridged Hybrid (BEH) column (C18, 130 Å, 1.7 µm, 2.1 mm x 50 mm) or an Agilent 1200 system fitted with a Grace Vydac analytical column (C18, 300 Å, 5 µm, 4.6 mm x 50 mm) equipped with a Vydac C18 guard cartridge. Preparative HPLC was performed on a Vydac C18 column (10 µm, 300 Å, 22 x 250 mm) equipped with a Vydac C18 guard cartridge using a Waters HPLC system (Waters Corp., Milford MA) or an LC-AD Shimadzu liquid chromatography system at a flow rate of 20 mL/min. HPLC chromatograms were monitored at 214 nM.

### **Solid phase peptide synthesis (SPPS) on the 2-chlorotrityl chloride resin**

The general method reported previously for synthesis of linear peptides on the 2-chlorotrityl resin (0.84-1.0 mmol/g loading),<sup>27,28</sup> using the Fmoc (9-fluorenylmethoxycarbonyl) strategy was followed in the synthesis of the dipeptide Fmoc-Tyr(All)-Tyr(All) and the tripeptide Fmoc-Tyr(All)-Phe-Tyr(All) (Table 5.10). Briefly, after swelling of the resin in DCM (2×10 min), the Fmoc-protected C-terminal amino acid (2 equiv in DCM/DMF(4/1)) and DIEA, 5 equiv) were added to the resin, and the reaction mixture was agitated with nitrogen gas for 6 h with addition of DCM every 30 min to maintain solvent volume. DIEA (5 equiv) was added every 2 h. Unreacted sites on the resin were capped with 15% MeOH and 5% DIEA in DCM (2×10 min) after which the resin was washed with DCM/DMF (1:1, 5x). After Fmoc deprotection (20% piperidine, 1 x 5 min, 2 x 20 min), the resin was washed with DMF (5x), DCM/DMF (1:1, 5x) and DCM (5x).

Cycles of Fmoc deprotection and amino acid couplings (2 eq. in DCM/DMF(4/1)) were performed to add to the growing peptide chain. Amino acid couplings were performed using PyBOP (2 equiv), HOBT (2 equiv), and DIEA (5 equiv) in DCM/DMF (1:1) for 2–4 h. Nitrogen gas was used to agitate the mixture during couplings. To cleave the peptide from the resin, 1% TFA in DCM was bubbled through the resin (5 mL x 10, 2 min each) then drained into a round bottom flask and evaporated.

### **Ring Closing Metathesis (RCM) of the resin-bound model dipeptide and tripeptide**

Generally, second-generation Grubbs' catalyst (G II) (3.6 mg, 0.004 mmol, 849.0 g/mol, 0.15 equiv) or second-generation Hoveyda-Grubbs' catalyst (HG II) (2.6 mg, 0.004 mmol, 626.6 g/mol, 0.15 equiv) was dissolved in degassed DCM or 1,2-dichloroethane (DCE) (14 mL, 0.3 mM) and added to Fmoc-Tyr(All)-Tyr(All)-2-chlorotrityl resin (50 mg, 0.028 mmol, 0.56 mmol/g) or Fmoc-Tyr(All)-Phe-Tyr(All)-2-chlorotrityl resin (50 mg, 0.026 mmol, 0.51 mmol/g). Catalyst loading was calculated relative to the resin-bound peptide loading. The additive phenol (1 equiv) was added to the reaction mixture when using G II and the reaction mixture was heated for 2 days under nitrogen gas with gentle stirring. Open vessel microwave assisted RCM was performed on a Biotage microwave peptide synthesizer (Initiator+ Alstra; Biotage, Sweden) in PTFE reaction vials. Following RCM, the resin was washed with MeOH (3 x 5 mL) and DCM (10 x 5 mL) before drying and cleavage from the solid support. Analytical HPLC was performed using a linear gradient of 30-70% solvent B (solvent A, water (0.1% TFA) and solvent B, MeCN (0.1% TFA) at a flow rate of 1 mL/min.

Table 5.10. Analytical data for linear peptides synthesized on the 2-chlorotrityl resin and their cyclic analogs.

Entry	Retention time <sup>a</sup>	ESI-MS ( <i>m/z</i> )		
		Calculated	Observed	
1	Fmoc-Tyr(All)-Tyr(All)-OH	23.0	[M+Na] <sup>+</sup> 669.26	[M+Na] <sup>+</sup> 669.26
2	<i>cyclo</i> -Fmoc-Tyr(All)-Tyr(All)-OH	18.0	[M+Na] <sup>+</sup> 641.22	[M+Na] <sup>+</sup> 641.22
3	Fmoc-Tyr(All)-Phe-Tyr(All)-OH	26.4	[M+Na] <sup>+</sup> 816.32	[M+Na] <sup>+</sup> 816.33
4	<i>cyclo</i> -Fmoc-Tyr(All)-Phe-Tyr(All)-OH	21.6	[M+Na] <sup>+</sup> 788.29	[M+Na] <sup>+</sup> 788.30

<sup>a</sup>30-70% aqueous MeCN with 0.1% TFA over 40 min at 1 mL/min on an Agilent 1200 system

### Solid phase peptide synthesis (SPPS) of arodyn analogs

The Rinkamide ChemMatrix (0.45-0.52 mmol/g) or Fmoc-PAL-PEG-PS resin (0.18-0.20 mmol/g) was swollen for 20 min at 70 °C in DMF prior to cycles of amino acid coupling and deprotection (prior to the coupling reaction, the Fmoc group was removed from the Fmoc-PAL-PEG-PS resin) on a Biotage microwave peptide synthesizer (Initiator+ Alstra; Biotage, Sweden). Coupling reactions were performed using Fmoc amino acids (4 equiv, 0.5 M), activated with PyBOP (4 equiv, 0.5 M) and HOBt (4 equiv, 0.5 M) in the presence of DIEA (8 equiv in NMP, 0.5 M), for 5 min at 75 °C. Fmoc deprotection was performed at room temperature with 20% 4-methylpiperidine in DMF (4.5 mL, 1 x 3 min; 4.5 mL, 2 x 10 min). The side chains of Lys and Arg were protected with *tert*-butoxycarbonyl (Boc) and 2,2,4,6,7-pentamethyldihydrobenzofuran-5-sulfonyl (Pbf), respectively. N-Acetylation was performed using acetic anhydride (5 M in DMF) and DIEA (2 M in NMP) for 20 min at room temperature. The resulting peptide resin was washed with DMF (5 mL, 3 x 45 sec) and DCM (5 mL, 3 x 45 sec). Generally, crude peptides were cleaved from the resin using acidic cleavage cocktails for at least 2 h and then precipitated in cold ether following filtration. For the Rinkamide ChemMatrix resin, crude peptides were cleaved from the resin using 4 mL TFA/triisopropylsilane(TIPS)/H<sub>2</sub>O (95/2.5/2.5). For Fmoc-PAL-PEG-PS resin,

crude peptides were cleaved from the resin using 4 mL TFA/phenol/H<sub>2</sub>O/TIPS (88/5/5/2); for cleavage of aliquots, the solution was diluted with 10% aqueous acetic acid (3–5 mL) and then extracted with diethyl ether (3 × 5 mL) following filtration.

### **Ring Closing Metathesis (RCM) of arodyn analogs**

Generally, a solution of degassed DCM or 1,2-dichloroethane (DCE) containing Hoveyda-Grubbs-II catalyst (3.0 mg, 0.3 mM, 0.15 equiv) or Grubbs-II catalyst (4.0 mg, 0.3 mM, 0.15 equiv) was added to the resin-bound peptide (150 mg, 0.21 mmol/g) before heating. Conventional heating under N<sub>2</sub> was performed for 2 days. Open vessel microwave assisted RCM was performed on a Biotage microwave peptide synthesizer (Initiator+ Alstra; Biotage, Sweden) in PTFE reaction vials while closed vessel microwave assisted RCM was performed on a Biotage Initiator+ SP Wave microwave synthesizer in capped microwave reaction vials. Following the reaction, the resin was washed with MeOH (3 x 5 mL) and DCM (10 x 5 mL) before drying and cleavage from the solid support. Analytical HPLC was performed using a linear gradient of 5-50% solvent B (solvent A, water (0.1% TFA) and solvent B, MeCN (0.1% TFA) at a flow rate of 1 mL/min.

### **Synthesis of cyclic peptides 2-6**

Following assembly of the protected peptide on the resin by SPPS as described above, the peptide was subjected to RCM as follows. A solution of degassed DCM containing Grubbs-II catalyst (4.0 mg, 0.3 mM, 0.15 equiv) and phenol (3.0 mg, 0.03 mmol, 1 equiv) was added to the resin-bound peptide (150 mg, 0.21 mmol/g) before heating, and conventional heating at 40 °C was performed under N<sub>2</sub> for 2 days. The crude peptide was cleaved from the resin and isolated as described above under the procedures for SPPS and RCM of arodyn analogs.

## Synthesis of cyclic peptides 7-9

Following assembly of the protected peptide on the resin by SPPS as described above, the peptide was subjected to RCM as follows. A solution of degassed 1,2-dichloroethane (DCE) containing Hoveyda-Grubbs-II catalyst (3.0 mg, 0.3 mM, 0.15 equiv) was added to the resin-bound peptide (150 mg, 0.21 mmol/g) before heating at 75 °C for 2 h under closed vessel microwave heating. Closed vessel microwave assisted RCM was performed on a Biotage Initiator+ SP Wave microwave synthesizer in capped microwave reaction vials. The crude peptide was cleaved from the resin and isolated as described above under the procedures for SPPS and RCM of arodyn analogs.

## Purification and analysis of purified peptides

The crude peptides were purified by preparative reversed-phase HPLC using a Waters HPLC system (Waters Corp., Milford MA) or an LC-AD Shimadzu liquid chromatography system on a Vydac C18 column (10  $\mu$ , 300 Å, 22 x 250 mm). A linear gradient of 25–45% aqueous MeCN (containing 0.1% TFA) over 40 min (0.5% MeCN/min) for crude linear peptides and 20–35% over 60 min (0.25%/min) for crude cyclic peptides was used for purification (cyclic peptides were isolated as *cis/trans* mixtures). The purifications were monitored at 214 nm.

Analytical HPLC to verify the purity of the final peptides was performed on an Agilent 1200 series liquid chromatograph system using a Vydac 218-TP column (5  $\mu$ , 300 Å, 4.6 mm x 50 mm) equipped with a Vydac guard cartridge or an Acquity UPLC Ethylene Bridged Hybrid (BEH) column (C18, 130 Å, 1.7  $\mu$ m, 2.1 mm x 50 mm). The two systems used for analysis on the Agilent 1200 series liquid chromatograph system were: a linear gradient of 5-50% solvent B (solvent A = aqueous 0.1% TFA and solvent B = MeCN containing 0.1% TFA) over 45 min at a



flow rate of 1 mL/min (system 1), and a linear gradient of 25-70% solvent B (solvent A = aqueous 0.1% TFA and solvent B = MeOH containing 0.1% TFA) over 45 min at a flow rate of 1.0 mL/min (system 2). On the Acquity UPLC system the two systems used for analysis were: a linear gradient of 5-55% solvent B (solvent A = aqueous 0.1% TFA and solvent B = MeCN containing 0.1% TFA) over 10 min at a flow rate of 0.2 mL/min (system 1), and a linear gradient of 25-75% solvent B (solvent A = aqueous 0.1% TFA and solvent B = MeOH containing 0.1% TFA) over 10 min at a flow rate of 0.2 mL/min (system 2). The final purity of the peptides by both methods was greater than 95%. Molecular weights of the peptides were determined by ESI-MS (Advion CMS) or MALDI (Voyager DE STR).

## **Pharmacological evaluation**

### **Radioligand binding assay**

Competitive inhibition of [<sup>3</sup>H]diprenorphine and [<sup>3</sup>H]DAMGO ([D-Ala<sup>2</sup>,MePhe<sup>4</sup>,glyol]enkephalin) was employed to determine binding affinities at KOR and MOR receptors, respectively. The receptors were expressed on Chinese hamster ovary (CHO) cells. Radioligand binding assays were performed for arodyn analogs cyclized by RCM and their corresponding linear precursors. Incubations were carried out in triplicate with varying concentrations of peptides (0.1-10,000 nM) for 90 min at RT in the presence of peptidase inhibitors (10 μM bestatin, 30 μM captopril, and 50 μM L-leucyl-L-leucine) and 3 mM Mg<sup>2+</sup>. Nonspecific binding was determined in the presence of 10 μM unlabeled Dyn A-(1-13)NH<sub>2</sub> and DAMGO for KOR and MOR, respectively. IC<sub>50</sub> values were determined by nonlinear regression analysis fit to a logistic equation for the competition data using Prism software (GraphPad Software Inc., San Diego, CA). K<sub>i</sub> values were calculated from the IC<sub>50</sub> values by the Cheng and Prusoff equation<sup>29</sup> using K<sub>D</sub> values of 0.45 and 0.49 for [<sup>3</sup>H]diprenorphine and [<sup>3</sup>H]DAMGO respectively. Arodyn

has low affinity for the  $\delta$  opioid receptor (DOR) ( $K_i > 5 \mu\text{M}$ );<sup>5</sup> therefore binding affinities of the analogs were not evaluated for this receptor.

### **GTP $\gamma$ S assay**

The binding of the GTP analog [<sup>35</sup>S]GTP $\gamma$ S to membranes containing KOR was assayed as described previously.<sup>30</sup> The assay mixture contained 50 mM HEPES, pH 7.4, 1 mM EDTA, 5 mM magnesium acetate, 1  $\mu\text{M}$  GDP, 1 mM dithiothreitol, 100 mM NaCl, 10  $\mu\text{M}$  bestatin, 30  $\mu\text{M}$  captopril, 50  $\mu\text{M}$  Leu-Leu, 1 mg/mL bovine serum albumin, and approximately 100,000 disintegrations per min (dpm) [<sup>35</sup>S]GTP $\gamma$ S (0.08 - 0.15 nM). Approximately 10  $\mu\text{g}$  of KOR expressing CHO cell membrane protein was used per tube. Following 90 min incubation at 22 °C, the assay was terminated by filtration under vacuum on a Brandel (Gaithersburg, MD) model M-48R cell harvester using Schleicher and Schuell Inc. (Keene, NH) number 32 glass fiber filters. The filters were rinsed five times (4 mL for each wash) with ice-cold (5 °C) 50 mM Tris HCl, pH 7.4, containing 5 mM MgCl to remove unbound [<sup>35</sup>S]GTP $\gamma$ S. Filter disks were then placed into counting vials to which 8 mL of Biocount scintillation fluid (Research Products International Corp., Mount Prospect, IL) was added. Filter-bound radioactivity was determined by liquid scintillation counting (Beckman Instruments, Fullerton, CA) following overnight extraction at room temperature. The amount of radioligand bound was less than 10% of the total added in all experiments. Specific binding was defined as total binding minus that occurring in the presence of 3  $\mu\text{M}$  unlabeled GTP $\gamma$ S. Nonspecific binding was approximately 1% of the total binding at 0.1 nM [<sup>35</sup>S]GTP $\gamma$ S.

### **5.5 References**

(1) Bennett, M. A.; Murray, T. F.; Aldrich, J. V. Structure–activity relationships of arodyn, a novel acetylated kappa opioid receptor antagonist. *J Pept Sci* **2005**, *65*, 322-332.

- (2) Chavkin, C.; Goldstein, A. Specific receptor for the opioid peptide dynorphin: structure--activity relationships. *Proc Natl Acad Sci U.S.A.* **1981**, *78*, 6543-6547.
- (3) Siemion, I. Z.; Szewczuk, Z.; Herman, Z. S.; Stachura, Z. To the problem of biologically active conformation of enkephalin. *Molecular and Cellular Biochemistry* **1981**, *34*, 23-29.
- (4) Fang, W.-J.; Murray, T. F.; Aldrich, J. V. Design, synthesis, and opioid activity of arodyn analogs cyclized by ring-closing metathesis involving Tyr(allyl). *Bioorg Med Chem* **2018**, *26*, 1157-1161.
- (5) Wan, Q.; Murray, T. F.; Aldrich, J. V. A novel acetylated analogue of dynorphin A-(1-11) amide as a kappa-opioid receptor antagonist. *J Med Chem* **1999**, *42*, 3011-3013.
- (6) Kulkarni, S. S. C.; H. Murray, T. F.; DeLander, G. E.; Aldrich, J. V. The use of the message-address concept in the design of potential antagonists based on dynorphin A In *Peptides: Chemistry, Structure and Biology* (Proceedings of the 14th American Peptide Symposium); Hodges, R. S., Kaumaya, P. T. P., Eds.; Mayflower Scientific Ltd.: England, 1996, p 655-656.
- (7) Bennett, M. A.; Murray, T. F.; Aldrich, J. V. Identification of Arodyn, a Novel Acetylated Dynorphin A-(1-11) Analogue, as a  $\kappa$  Opioid Receptor Antagonist. *J Med Chem* **2002**, *45*, 5617-5619.
- (8) Carey, A. N.; Borozny, K.; Aldrich, J. V.; McLaughlin, J. P. Reinstatement of Cocaine Place-Conditioning Prevented by the Peptide kappa-Opioid Receptor Antagonist Arodyn. *Eur J Pharmacol* **2007**, *569*, 84-89.
- (9) Wu, H.; Wacker, D.; Mileni, M.; Katritch, V.; Han, G. W.; Vardy, E.; Liu, W.; Thompson, A. A.; Huang, X.-P.; Carroll, F. I.; Mascarella, S. W.; Westkaemper, R. B.; Mosier, P. D.; Roth, B. L.; Cherezov, V.; Stevens, R. C. Structure of the human kappa-opioid receptor in complex with JDTic. *Nature* **2012**, *485*, 327-332.
- (10) Metzger, T. G.; Paterlini, M. G.; Ferguson, D. M.; Portoghese, P. S. Investigation of the selectivity of oxymorphone- and naltrexone-derived ligands via site-directed mutagenesis of opioid receptors: exploring the "address" recognition locus. *J Med Chem* **2001**, *44*, 857-862.
- (11) Huang, W.; Manglik, A.; Venkatakrisnan, A. J.; Laeremans, T.; Feinberg, E. N.; Sanborn, A. L.; Kato, H. E.; Livingston, K. E.; Thorsen, T. S.; Kling, R. C.; Granier, S.; Gmeiner, P.; Husbands, S. M.; Traynor, J. R.; Weis, W. I.; Steyaert, J.; Dror, R. O.; Kobilka, B. K. Structural insights into mu-opioid receptor activation. *Nature* **2015**, *524*, 315-321.
- (12) Fenalti, G.; Zatsopin, N. A.; Betti, C.; Giguere, P.; Han, G. W.; Ishchenko, A.; Liu, W.; Guillemin, K.; Zhang, H.; James, D.; Wang, D.; Weierstall, U.; Spence, J. C. H.; Boutet, S.; Messerschmidt, M.; Williams, G. J.; Gati, C.; Yefanov, O. M.; White, T. A.; Oberthuer, D.; Metz, M.; Yoon, C. H.; Barty, A.; Chapman, H. N.; Basu, S.; Coe, J.; Conrad, C. E.; Fromme, R.; Fromme, P.; Tourwé, D.; Schiller, P. W.; Roth, B. L.; Ballet, S.; Katritch, V.; Stevens, R. C.; Cherezov, V. Structural

basis for bifunctional peptide recognition at human  $\delta$ -opioid receptor. *Nat Struct Mol Biol* **2015**, *22*, 265-268.

(13) Vardy, E.; Mosier, P. D.; Frankowski, K. J.; Wu, H.; Katritch, V.; Westkaemper, R. B.; Aube, J.; Stevens, R. C.; Roth, B. L. Chemotype-selective modes of action of kappa-opioid receptor agonists. *J Biol Chem* **2013**, *288*, 34470-34483.

(14) Neilan, C. L.; Husbands, S. M.; Breeden, S.; Ko, M. C.; Aceto, M. D.; Lewis, J. W.; Woods, J. H.; Traynor, J. R. Characterization of the complex morphinan derivative BU72 as a high efficacy, long-lasting mu-opioid receptor agonist. *Eur J Pharmacol* **2004**, *499*, 107-116.

(15) Schiller, P. W.; Fundytus, M. E.; Merovitz, L.; Weltrowska, G.; Nguyen, T. M. D.; Lemieux, C.; Chung, N. N.; Coderre, T. J. The opioid mu agonist/delta antagonist DIPP-NH<sub>2</sub>[Psi] produces a potent analgesic effect, no physical dependence, and less tolerance than morphine in rats. *J Med Chem* **1999**, *42*, 3520-3526.

(16) Gradillas, A.; Pérez-Castells, J. Macrocyclization by Ring-Closing Metathesis in the Total Synthesis of Natural Products: Reaction Conditions and Limitations. *Angew Chem Int Ed* **2006**, *45*, 6086-6101.

(17) Kadyrov, R. Low Catalyst Loading in Ring-Closing Metathesis Reactions. *Chem Eur J* **2013**, *19*, 1002-1012.

(18) Martínez-Amezaga, M.; Delpiccolo, C.; Méndez, L.; Dragutan, I.; Dragutan, V.; Mata, E. Unprecedented Multifunctionality of Grubbs and Hoveyda–Grubbs Catalysts: Competitive Isomerization, Hydrogenation, Silylation and Metathesis Occurring in Solution and on Solid Phase. *Catalysts* **2017**, *7*, 111.

(19) Hong, S. H.; Sanders, D. P.; Lee, C. W.; Grubbs, R. H. Prevention of Undesirable Isomerization during Olefin Metathesis. *J Am Chem Soc* **2005**, *127*, 17160-17161.

(20) Higman, C. S.; Plais, L.; Fogg, D. E. Isomerization During Olefin Metathesis: An Assessment of Potential Catalyst Culprits. *ChemCatChem* **2013**, *5*, 3548-3551.

(21) Jacobsen, Ø.; Klaveness, J.; Rongved, P. Structural and Pharmacological Effects of Ring-Closing Metathesis in Peptides. *Molecules* **2010**, *15*, 6638-6677.

(22) Fang, W.-J.; Cui, Y.; Murray, T. F.; Aldrich, J. V. Design, Synthesis, and Pharmacological Activities of Dynorphin A Analogues Cyclized by Ring-Closing Metathesis. *J Med Chem* **2009**, *52*, 5619-5625.

(23) Fang, W.-J.; Murray, T. F.; Aldrich, J. V. Design, Synthesis, and Opioid Activity of Aroclon Analogs Cyclized by Ring-Closing Metathesis involving Tyr(Allyl). *Bioorg Med Chem Lett* **2017**, *XX*, in press.

- (24) Schmidt, B.; Hauke, S. Cross metathesis of allyl alcohols: how to suppress and how to promote double bond isomerization. *Org Biomol Chem* **2013**, *11*, 4194-4206.
- (25) Robinson, A. J.; Elaridi, J.; Van Lierop, B. J.; Mujcinovic, S.; Jackson, W. R. Microwave-assisted RCM for the synthesis of carbocyclic peptides. *J Pept Sci* **2007**, *13*, 280-285.
- (26) Vougioukalakis, G. C.; Grubbs, R. H. Ruthenium-Based Heterocyclic Carbene-Coordinated Olefin Metathesis Catalysts. *Chem Rev* **2010**, *110*, 1746-1787.
- (27) Ross, N. C.; Kulkarni, S. S.; McLaughlin, J. P.; Aldrich, J. V. Synthesis of CJ-15,208, a novel  $\kappa$ -opioid receptor antagonist. *Tetrahedron Lett* **2010**, *51*, 5020-5023.
- (28) Aldrich, J. V.; Kulkarni, S. S.; Senadheera, S. N.; Ross, N. C.; Reilley, K. J.; Eans, S. O.; Ganno, M. L.; Murray, T. F.; McLaughlin, J. P. Unexpected Opioid Activity Profiles of Analogues of the Novel Peptide Kappa Opioid Receptor Ligand CJ-15,208. *ChemMedChem* **2011**, *6*, 1739-1745.
- (29) Cheng, Y.; Prusoff, W. H. Relationship between the inhibition constant ( $K_1$ ) and the concentration of inhibitor which causes 50 per cent inhibition ( $I_{50}$ ) of an enzymatic reaction. *Biochem Pharmacol* **1973**, *22*, 3099-3108.
- (30) Ross, N. C.; Reilley, K. J.; Murray, T. F.; Aldrich, J. V.; McLaughlin, J. P. Novel opioid cyclic tetrapeptides: Trp isomers of CJ-15,208 exhibit distinct opioid receptor agonism and short-acting kappa opioid receptor antagonism. *Br J Pharmacol* **2012**, *165*, 1097-1108.

## **Chapter 6 - Head to side chain cyclization of arodyn using RCM**

## 6.1 Introduction

Arodyn is a potent and highly selective kappa opioid receptor (KOR) antagonist and has been used as a lead peptide to generate conformationally constrained KOR ligands.<sup>1, 2</sup> Lactam-based cyclization of arodyn has been limited to side chain to side chain motifs, while RCM-based cyclizations have covered both side chain to side chain and head to side chain motifs involving non-critical residues 2, 5, and 8.<sup>3</sup> Unlike the lactam strategy, RCM cyclizations involving residues 2, 5, and 8 have met with varying degrees of success due to sequence dependent effects. Of note, cyclizations using RCM between Tyr(All) residues at positions 2 and 3 as well as between AllGly residues at positions 5 and 8 were KOR selective and reasonably well-tolerated at KOR ( $\leq 5$ -fold loss in affinity compared to arodyn).<sup>2, 3</sup>

Previous work on head to side chain cyclization by RCM in arodyn suggested considerable sequence dependence in these cyclizations. RCM between an N-terminal vinylacetyl/Alloc group and an allylglycine residue at position 2, 5, or 8 were largely unsuccessful using Grubbs 2<sup>nd</sup> generation catalyst (G II) in DCM/DMF (4:1) under conventional heating for 2 days (Table 6.1).<sup>3</sup> The only analog obtained in this series was *cyclo*<sup>N,2</sup>[COOCH<sub>2</sub>(CH=CH-)Ala<sup>2</sup>,NMePhe<sup>1</sup>,Ile<sup>8</sup>]arodyn, **4** (Table 6.1). Evidently, this N-methylated arodyn derivative could adopt a conformation that facilitates cyclization. Interestingly, NMePhe<sup>1</sup> arodyn analogs are prone to deletion of AcNMePhe under acidic conditions, but the introduction of a heteroatom-containing group such as CH<sub>3</sub>OCO conferred acid stability.<sup>4</sup> *cyclo*<sup>N,2</sup>[COOCH<sub>2</sub>(CH=CH-)Ala<sup>2</sup>,NMePhe<sup>1</sup>,Ile<sup>8</sup>]arodyn displayed a 20-fold loss in affinity for the KOR ( $K_i = 208 \pm 14$ ) compared to arodyn.

Table 6.1 Attempted cyclizations of head to side chain arodyn analogs. Only **4** was obtained.<sup>3</sup>

Peptide	Arodyn analog	Structure
<b>1</b>	$cyclo^{N,2}[\text{COCH}_2(\text{CH}=\text{CH}-)\text{Ala}^2, \text{Ile}^8]$	
<b>2</b>	$cyclo^{N,5}[\text{COCH}_2(\text{CH}=\text{CH}-)\text{Ala}^5, \text{Ile}^8]$	
<b>3</b>	$cyclo^{N,8}[\text{COCH}_2(\text{CH}=\text{CH}-)\text{Ala}^8]$	
<b>4</b>	$cyclo^{N,2}[\text{COOCH}_2(\text{CH}=\text{CH}-)\text{Ala}^2, \text{NMePhe}^1, \text{Ile}^8]$	
<b>5</b>	$cyclo^{N,5}[\text{COOCH}_2(\text{CH}=\text{CH}-)\text{Ala}^5, \text{NMePhe}^1, \text{Ile}^8]$	
<b>6</b>	$cyclo^{N,8}[\text{COOCH}_2(\text{CH}=\text{CH}-)\text{Ala}^8]$	

R = Phe-Arg-Leu-Arg-Arg-Ile-Arg-Pro-Lys-NH<sub>2</sub>; R<sup>1</sup> = Arg-Arg-Ile-Arg-Pro-Lys-NH<sub>2</sub>; R<sup>2</sup> = Arg-Pro-Lys-NH<sub>2</sub>



The difficulty of accessing the head to side chain cyclic analogs of arodyn (Table 6.1) is another illustration of the conformational and sequence dependent effects on RCM cyclization efficiency. In this section we describe the synthesis of head to side chain cyclized arodyn analogs using Tyr(All) and AllGly residues to further probe effects of cyclization on KOR affinity, selectivity, and efficacy. We employed microwave assisted heating (Chapter 5) to explore improving yields of difficult cyclizations in arodyn analogs.

## **6.2 Results and discussion**

### **6.2.1 Head to side chain analogs using RCM involving Tyr(All)**

Head to side chain cyclizations involving an aromatic residue and N-terminal 4-penteneoic or 5-hexenoic acid were explored to constrain the N-terminal segment of arodyn via RCM using Hoveyda-Grubbs 2<sup>nd</sup> generation catalyst (HG II). Microwave conditions previously developed for arodyn analogs containing Tyr(All) (15 mol% HG II in DCE, 0.3 mM, 75 °C, 2 h) were employed. The low yields observed in this series suggest that the reactive termini could not adopt a conformation favorable for cyclization except for **10** (Table 6.2). The generally low yields in this series also illustrate the sequence dependence of cyclization efficiency, as was observed for the previous cyclizations in the N-terminal segment of arodyn described above (Table 6.1). Notably, cyclization at higher temperature did not improve the reaction yields, but increased degradation products. Similarly, cyclization for 5 h at 60 °C did not improve the product yield. The apparent poor conversion to the RCM product suggests that conformational limitations preclude efficient cyclization in these arodyn analogs which could not be overcome by microwave assisted heating.

Table 6.2 Attempted cyclizations of head to side chain analogs of arodyn involving Tyr(All).<sup>a</sup>

Compound	Arodyn analog	Structure
<b>7<sup>b</sup></b>	[4pent,Tyr(All) <sup>1</sup> ]	
<b>8<sup>c</sup></b>	[5hex,Tyr(All) <sup>1</sup> ]	
<b>9</b>	[4pent,Tyr(All) <sup>2</sup> ]	
<b>10</b>	[5hex,Tyr(All) <sup>2</sup> ]	
<b>11</b>	[4pent,Tyr(All) <sup>3</sup> ]	
<b>12</b>	[5hex,Tyr(All) <sup>3</sup> ]	

R= Arg-Leu-Arg-Arg-D-Ala-Arg-Pro-Lys-NH<sub>2</sub>; <sup>a</sup> yields of the RCM product of various ring sizes, ranging from 14 to 21 atoms, were less than 25% with the exception of **10** (45%); <sup>b</sup> 4pent:4-pentenoic acid; <sup>c</sup>5hex: 5-hexenoic acid

### 6.2.2 Head to sidechain cyclization involving AllGly

Head to side chain cyclizations of arodyn analogs containing the all-hydrocarbon RCM bridge were synthesized by incorporating allylglycine as the 5<sup>th</sup> residue, while 4-pentenoic acid or

5-pentenoic acid were incorporated at the N-terminus (Table 6.3). Various cyclization conditions were explored under microwave heating to maximize the RCM product yields. In the synthesis of **13**, minimal conversion to product was observed after long heating times (2 and 5 h) at 75 °C, but shorter reaction times at elevated temperatures considerably increased cyclization yields (Figure 6.1), consistent with the temperature dependence of the 2<sup>nd</sup> generation Hoveyda-Grubbs catalyst (HG II).<sup>5, 6</sup> However, elevated temperatures also increased side reaction products.

Table 6.3 Attempted cyclizations of head to side chain analogs of arodyn involving AllGly and their linear precursors.

Compound	Arodyn analog	Structure
<b>13</b>	$cyclo^{N,5}[4pent,AllGly^5]$	
<b>14</b>	$cyclo^{N,5}[5hex,AllGly^5]$	
<b>15</b>	$[4pent,AllGly^5]$	4pent-Phe-Phe-Phe-Arg-R <sup>1</sup>
<b>16</b>	$[5hex,AllGly^5]$	5hex-Phe-Phe-Phe-Arg-R <sup>1</sup>
R= Arg-Arg-D-Ala-Arg-Pro-Lys-NH <sub>2</sub> R <sup>1</sup> = AllGly-Arg-Arg-D-Ala-Arg-Pro-Lys-NH <sub>2</sub> .		

Cyclization involving AllGly required at least 100 °C for 2 h before any substantial product was formed (Figure 6.1, Table 6.4). In the RCM of **15**, further heating at 150 °C shortened the reaction time while giving similar yields to microwave heating at 100 °C for 2 h, but with more side products (Figure 6.1, Table 6.4). LC-MS analysis revealed that the side products were ring contraction (**17**) and ring expansion products (**14**) consistent with CH<sub>2</sub> deletion and insertion, respectively (Figures 6.1 and 6.2, Table 6.5). Schroeder and co-workers reported similar CH<sub>2</sub>

deletions and insertions resulting in chain shortened and homologated side products, presumably due to ruthenium hydride formation during olefin metathesis.<sup>7</sup> Additionally, Schroeder and co-workers found higher degrees of isomerization and homologation in longer-chain substrates. In another example, Hanson *et al.* reported olefin isomerization and ring contraction products following RCM in the synthesis of dolabelide C.<sup>8</sup>

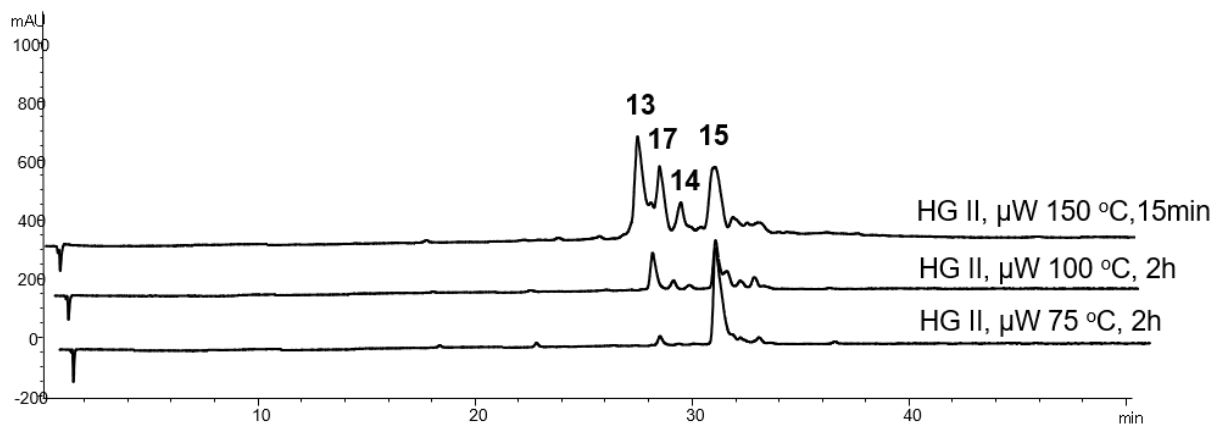


Figure 6.1 Representative chromatograms showing the RCM of **15** at various temperatures under microwave heating.

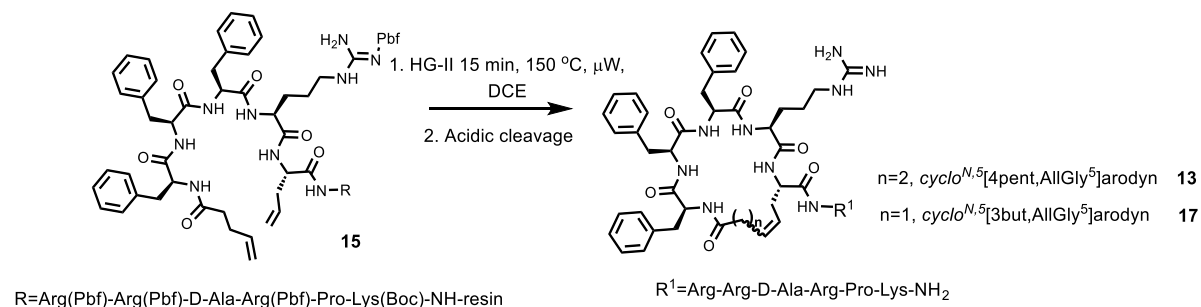


Figure 6.2 Structures of the major products following microwave assisted RCM of **15** at 150 °C. 3but = 3-butenic acid.

Table 6.4 Cyclization yields following RCM of **15** under various microwave heating conditions.

Entry	Temp (°C) <sup>a</sup>	Time	Yields of major pdts. <sup>b,c</sup>	
			<b>13</b>	<b>17</b>
1	60	5h	- <sup>d</sup>	-
2	75	2h	-	-
3	100	2h	29	-
4	120	2h	31	16
5	150	15 min	34	19
6	150 <sup>e</sup>	15 min	29	11

<sup>a</sup>15 mol% HG II, 0.3 mM DCE; <sup>b</sup> analytical HPLC conditions: 5-50% aqueous MeCN (0.1% TFA) over 45 min; <sup>c</sup> < 10% of **14** (Figure 6.1) was observed; <sup>d</sup> < 10%; <sup>e</sup> 15 mol% HG II, 1 mM

Table 6.5 Analytical data of the major products following microwave assisted RCM of **15** at 150 °C. LC-MS analysis facilitated identification of the ring contraction product **17**.<sup>a</sup>

Compound	HPLC $t_R$ (min) <sup>a</sup>	ESI-MS		Yield (%) <sup>b</sup>
		Calc.	Obsvd.	
<b>13</b>	27.4	[M+2H] <sup>2+</sup> 765.9	[M+2H] <sup>2+</sup> 766.4	34
		[M+3H] <sup>3+</sup> 511.0	[M+3H] <sup>3+</sup> 511.3	
		[M+4H] <sup>4+</sup> 383.5	[M+4H] <sup>4+</sup> 383.8	
<b>17</b>	28.4	[M+2H] <sup>2+</sup> 758.9	[M+2H] <sup>2+</sup> 759.3	19
		[M+3H] <sup>3+</sup> 506.3	[M+3H] <sup>3+</sup> 506.6	
		[M+4H] <sup>4+</sup> 379.9	[M+4H] <sup>4+</sup> 380.1	

<sup>a</sup> ESI-MS from the LC-MS of the crude reaction mixture; <sup>b</sup> analytical HPLC conditions: 5-50% aqueous MeCN (0.1% TFA) over 45 min.

CH<sub>2</sub> deletions and insertions were also observed in the RCM of **16** (Figures 6.3 and 6.4, Table 6.6) in addition to a similar temperature dependence to that observed in the RCM of **15**

(Figure 6.1). Minimal cyclization (<10%) was observed after microwave heating at 75 °C for 2 h, while a considerable increase in yield was observed following heating at 150 °C for 15 min (Figure 6.3). Of note, negligible quantities (<10%) of the linear precursor **16** (Figure 6.3) were observed, in contrast to a considerable amount (20%) of **15** (Figure 6.1) observed following its RCM at 150 °C. The observed differences in depletion of the linear precursor during RCM suggest increased cyclization efficiency of the homologated analog **16** compared to **15**.

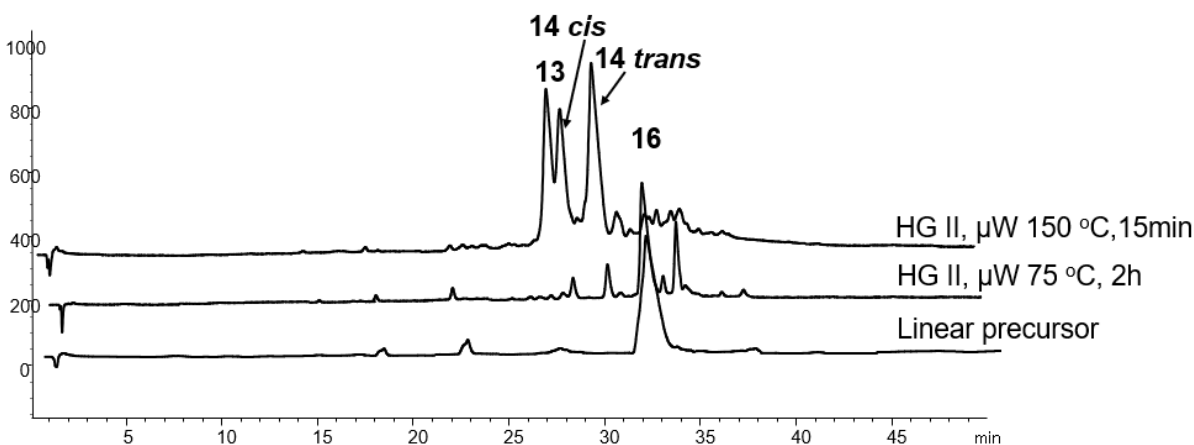


Figure 6.3 Representative chromatograms showing the RCM of **16** at various temperatures under microwave heating.

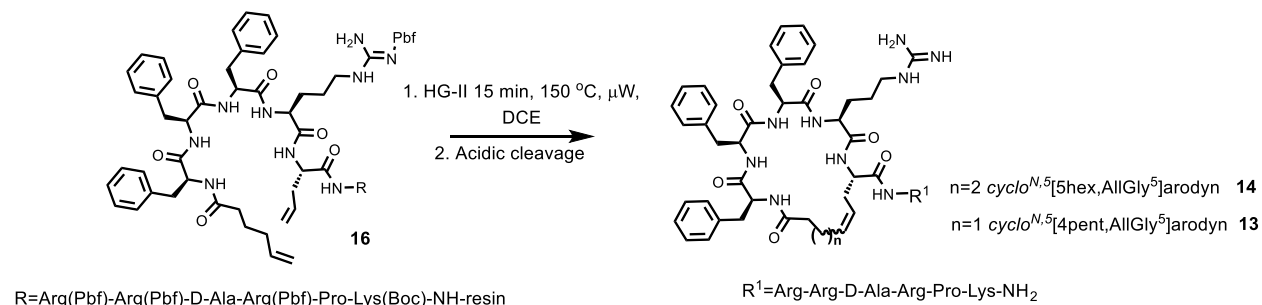


Figure 6.4 Structures of the major products following microwave assisted RCM of **16** at 150 °C.

Table 6.6 Analytical data of the major products following microwave assisted RCM of **16** at 150 °C.<sup>a</sup>

Compound	HPLC $t_R$ (min) <sup>a</sup>	ESI-MS <sup>b</sup>		Yield <sup>b</sup> (%)
		Calc.	Obsvd.	
<b>13</b>	27.2	[M+3H] <sup>3+</sup> 511.2 [M+4H] <sup>4+</sup> 383.5	[M+3H] <sup>3+</sup> 511.2 [M+4H] <sup>4+</sup> 383.9	24
<b>14 cis</b>	27.9	[M+3H] <sup>3+</sup> 515.6 [M+4H] <sup>4+</sup> 386.9	[M+3H] <sup>3+</sup> 516.1 [M+4H] <sup>4+</sup> 387.3	24
<b>14 trans</b>	29.6	[M+3H] <sup>3+</sup> 515.6 [M+4H] <sup>4+</sup> 386.9	[M+3H] <sup>3+</sup> 516.1 [M+4H] <sup>4+</sup> 387.2	35

<sup>a</sup> HPLC on an Agilent 1200 series liquid chromatography system; <sup>b</sup> ESI-MS from the LC-MS of the crude reaction mixture; <sup>b</sup> analytical HPLC conditions: 5-50% aqueous MeCN (0.1% TFA) over 45 min

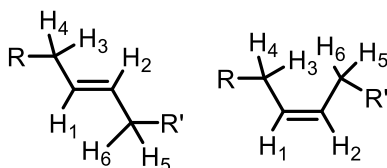
Olefin isomerization is widely reported as a side reaction of degradation products of Grubbs catalysts<sup>9-11</sup> and can result in complex mixtures necessitating elaborate purification steps. Despite an increase in the desired RCM product, elevated temperatures were accompanied by multiple RCM products. This is presumably due to catalyst degradation which occurs at higher temperatures. Olefin isomerization products resulted in ring contraction which was the major side product in the cyclizations of both **15** and **16** (Figures 6.2 and 6.4).

Following RCM of **16**, the *cis/trans* isomers of **14** (Table 6.7, Appendix 4) were purified using a linear gradient of 20-40% aqueous MeCN (0.1% TFA) over 80 min using at a flow rate of 20 mL/min (Table 6.8). The slow gradient was used to separate the *cis* isomer (**14 cis**) from the ring contraction product **13** (Figure 6.3); however, **13** could not be sufficiently purified.

Initial evaluation of KOR binding affinity indicates that the *cis/trans* isomers of **14** retain similar affinities at the KOR (Table 6.9) which were 5-fold lower than arodyn. The linear peptide

16 displayed roughly 3-fold lower affinity than arodyn. Further pharmacological evaluation of the geometrical isomers of **14** and the linear precursor is in progress.

Table 6.7 <sup>1</sup>H NMR data of cyclic arodyn analogs **14 cis** and **14 trans**.



Compound	Chemical shift of olefinic protons ( $\delta$ )	$J_{\text{olefin}}$ (Hz)	<i>cis/trans</i> ratio <sup>a</sup>
<b>14 cis</b>	H <sub>1</sub> = 5.21	$J_{12}$ = 10.4	1
	H <sub>2</sub> = 5.38	$J_{21}$ = 10.0	
<b>14 trans</b>	H <sub>1</sub> = 5.30	$J_{12}$ = 15.2	1.5
	H <sub>2</sub> = 5.39	$J_{21}$ = 15.3	
<sup>a</sup> Determined through peak integration from HPLC analysis of the crude reaction mixture			

Table 6.8 Analytical data of purified **14** and its linear precursor **16**.

Compound	HPLC $t_R$ (min) <sup>a</sup>		ESI-MS	
	System 1 <sup>b</sup> (% purity)	System 2 <sup>c</sup> (% purity)	Calcd.	Obsvd.
<b>14 cis</b>	24.8 (99.9)	17.3 (99.9)	$[M+2H]^{2+}$ 772.9	$[M+2H]^{2+}$ 773.2
			$[M+3H]^{3+}$ 515.6	$[M+3H]^{3+}$ 515.9
<b>14 trans</b>	26.2 (99.9)	21.1 (99.9)	$[M+2H]^{2+}$ 772.9	$[M+2H]^{2+}$ 773.1
			$[M+3H]^{3+}$ 515.6	$[M+3H]^{3+}$ 515.8
<b>16</b>	26.3 (98.9)	20.5 (99.9)	$[M+2H]^{2+}$ 787.0	$[M+2H]^{2+}$ 786.9
			$[M+3H]^{3+}$ 525.0	$[M+3H]^{3+}$ 525.2
<sup>a</sup> HPLC on an Agilent 1290 series liquid chromatography system; <sup>b</sup> 5-50% aqueous MeCN (0.1% TFA) over 45 min; <sup>c</sup> 25-70% aqueous MeOH (0.1% TFA) over 45 min				



Table 6.9 Preliminary KOR binding affinities of *cyclo*<sup>N,5</sup>[5hex,AllGly<sup>5</sup>]arodyn and the linear precursor.

Compound number	Arodyn analog	K <sub>i</sub> ± SEM (nM) <sup>a</sup>
		KOR
	arodyn <sup>b</sup>	10.0 ± 3.0
<b>14 cis</b>	<i>cyclo</i> <sup>N,5</sup> [5hex,AllGly <sup>5</sup> ]	47.7 ± 3.6
<b>14 trans</b>	<i>cyclo</i> <sup>N,5</sup> [5hex,AllGly <sup>5</sup> ]	46.4 ± 7.2
<b>16</b>	[5hex,AllGly <sup>5</sup> ]	26.9 ± 7.6

<sup>a</sup> Mean K<sub>i</sub> values ± SEM from at least 3 independent experiments; <sup>b</sup> from ref<sup>12</sup>

### 6.3 Conclusions

Cyclization of arodyn in the N-terminal “message” sequence was explored using RCM in a head to side chain motif with varying yields under microwave heating. Cyclizations involving a Tyr(All) residue in position 1, 2 or 3 were negatively impacted by sequence dependent effects, thereby limiting the analogs that could be obtained in appreciable yield. Longer range cyclizations involving AllGly at position 5 resulted in considerable product yields, but required elevated temperatures. Higher temperatures were, however, accompanied by side products, mainly ring contraction products presumably due to olefin isomerization. The resulting cyclic arodyn analogs exhibit interesting novel topologies. Initial KOR binding data indicated a 5-fold decrease in affinity for both geometrical isomers of *cyclo*<sup>N,5</sup>[5hex,AllGly<sup>5</sup>]arodyn (**14**) compared to arodyn. Pharmacological analysis to determine the effects on MOR affinity, selectivity, and efficacy at KOR are in progress.

### 6.4 Experimental

#### Materials

Fmoc-L-Tyr(All)-OH and Fmoc-AllGly-OH were purchased from Chem-Impex International (Wood Dale, IL). The coupling agent benzotriazol-1-yl-oxy-tris-pyrrolidino-phosphonium hexafluorophosphate (PyBOP) was obtained from P3 BioSystems (Louisville, KY) while the coupling agent 2-(1H-benzotriazol-1-yl)-1,1,3,3-tetramethyluronium

hexafluorophosphate (HBTU) was obtained from Peptides International. The coupling additive 1-hydroxybenzotriazole hydrate (HOBt) was obtained from Chem-Impex International. The sources of other materials are listed in Chapter 5.

## **Instruments**

Microwave assisted RCM was performed on a Biotage Initiator+ SP Wave microwave synthesizer and solid phase peptide synthesis (SPPS) was performed on a Biotage microwave peptide synthesizer (Initiator+ Alstra; Biotage, Sweden).

Electrospray ionization mass spectrometry (ESI/MS) was performed on an Advion expression L compact MS (Advion, Inc. Ithaca NY).

<sup>1</sup>H NMR spectra of these compounds (0.5–2 mg) were obtained at 27 °C in DMSO-*d*<sub>6</sub> on a Bruker Avance III 600 MHz equipped with a 5 mm cryoprobe in the McKnight Brain Institute at the National High Magnetic Field Laboratory's AMRIS facility at the University of Florida. <sup>1</sup>H chemical shifts were referenced to the residual DMSO signal at 2.50 ppm, and coupling constants were extracted from the 1D spectra.

Analytical HPLC was performed on an Agilent 1200 system or an Agilent 1290 system fitted with a Grace Vydac analytical column (C18, 300 Å, 5 µm, 4.6 mm x 50 mm) equipped with a Vydac C18 guard cartridge. Yields for the respective reactions were determined from analytical HPLC chromatograms monitored at 214 nM; in some cases, baseline resolution was not achieved so yields shown are an estimate.

## **Solid Phase Peptide Synthesis (SPPS)**

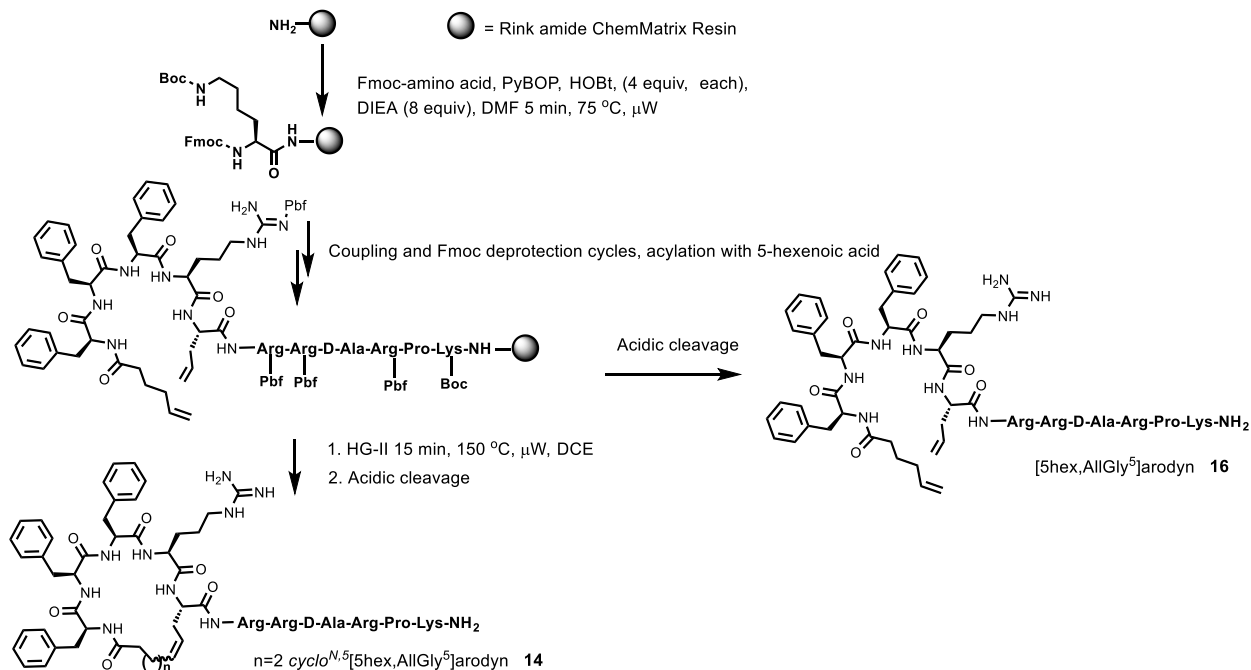
Aroclon analogs were prepared by the Fmoc (9-fluorenylmethoxycarbonyl) SPPS strategy using the automated Biotage microwave peptide synthesizer (Initiator+ Alstra; Biotage, Sweden) on a 0.14 mmol scale. Rink amide ChemMatrix resin (0.45-0.54 mmol/g) was swelled for 20 min

at 70° C in DMF prior to cycles of amino acid coupling and deprotection. Coupling reactions were performed using Fmoc amino acids (4 equiv, 0.5 M), activated with PyBOP (4 equiv, 0.5 M) and HOBt (4 equiv, 0.5 M) in DMF in the presence of DIEA (8 equiv in NMP) for 5 min at 75 °C. Fewer equivalents were used in the coupling of Fmoc-AllGly (2 equiv). Fmoc deprotection was performed at room temperature with 20% 4-methylpiperidine in DMF (4.5 mL, 1 x 3 min; 4.5 mL, 2 x 10 min). The side chains of Lys and Arg were protected with *tert*-butoxycarbonyl (Boc) and 2,2,4,6,7-pentamethyldihydrobenzofuran-5-sulfonyl (Pbf), respectively. Acylation was performed using 4-pentenoic anhydride or 5-hexenoic acid as described below. Synthesis of [5hex,AllGly<sup>5</sup>]arodyn (**16**) is shown in scheme 6.1 as an example.

#### **Acylation with 4-pentenoic anhydride**

Following synthesis of [AllGly<sup>5</sup>]arodyn using SPPS as described above, DIEA (1.4 mmol, 10 equiv) was added to a 4-pentenoic anhydride solution in (0.35 M) in DMF (3 mL) and the resulting solution was added to the resin-bound peptide (150 mg, 0.14 mmol, 0.54 mmol/g). Acylation was performed for 20 min at room temperature, and the resin-bound peptide was then washed with DMF (5 mL, 3 x 45 sec) and DCM (5 mL, 3 x 45 sec) to give [4pent,AllGly<sup>5</sup>]arodyn (**15**); ESI/MS  $m/z$  520.8 observed, 520.3 calculated  $[M+3H]^{3+}$ , HPLC  $t_R$  = 30.2 min (5-50% aqueous MeCN with 0.1% TFA over 45 min at a flow rate of 1 mL/min).

Scheme 6.1 Synthesis of [5hex,AllGly<sup>5</sup>]arodyn (**16**) and *cyclo*<sup>N,5</sup>[5hex,AllGly<sup>5</sup>]arodyn (**14**).



### Acylation with 5-hexenoic acid

Following synthesis of [AllGly<sup>5</sup>]arodyn using SPPS as described above, DIEA (1.12 mmol, 8 equiv) was added to a solution of 5-hexenoic acid (0.70 mmol, 5 equiv) and HBTU (0.69, 4.9 equiv) in DMF (3.5 mL). The mixture was added to the resin-bound peptide (0.14 mmol) and subjected to microwave irradiation (Biotage Initiator+ Alstra) for 5 min at 75 °C, and the resin-bound peptide was washed with DMF (5 mL, 3 x 45 sec) and DCM (5 mL, 3 x 45 sec) to give [5hex,AllGly<sup>5</sup>]arodyn (**16**); ESI/MS  $m/z$  525.2 observed, 525.0 calculated  $[M+3H]^{3+}$ , HPLC  $t_R$  = 31.6 min (5-50% aqueous MeCN with 0.1% TFA over 45 min at a flow rate of 1 mL/min).

### Ring Closing Metathesis (RCM)

A solution of degassed 1,2-dichloroethane (DCE) containing 15 mol % (0.15 equiv) of Hoveyda-Grubbs II catalyst (0.3 mM) was added to the resin-bound peptide (150 mg, 0.21 mmol/g) before heating. Closed vessel microwave assisted RCM was performed on a Biotage Initiator+ SP Wave microwave synthesizer in capped microwave reaction vials for the indicated

amount of time at the indicated temperatures. Synthesis of *cyclo*<sup>N,5</sup>[5hex,AllGly<sup>5</sup>]arodyn (**14**) is shown in scheme 6.1 as an example. The resin was washed with MeOH (3 x 5 mL) and DCM (10 x 5 mL) before drying and cleavage. Yields were determined from analytical HPLC chromatograms using a linear gradient of 5-50% solvent B (solvent A = aqueous 0.1% TFA and solvent B = MeCN containing 0.1% TFA) over 45 min at a flow rate of 1 mL/min (Figures 6.1 and 6.3).

#### **Synthesis of *cyclo*<sup>N,5</sup>[5hex,AllGly<sup>5</sup>]arodyn (**14**)**

[AllGly<sup>5</sup>]arodyn was synthesized using SPPS and acylated to give [5hex,AllGly<sup>5</sup>]arodyn (**16**) as described above. The resin-bound [5hex,AllGly<sup>5</sup>]arodyn (**16**, 150 mg, 0.03 mmol, 0.21 mmol/g) was subjected to RCM as described in the RCM procedure for 15 min at 150 °C (Scheme 6.1) to give *cyclo*<sup>N,5</sup>[5hex,AllGly<sup>5</sup>]arodyn (**14**) (see Table 6.6 for analytical data).

#### **Cleavage, purification and analysis of purified peptides**

Crude peptides (Scheme 6.1) were cleaved from the resin in TFA/triisopropylsilane (TIPS)/water (95/2.5/2.5) for at least 2 h and then precipitated in cold ether following filtration. The crude peptides were purified by preparative reversed-phase HPLC on a Shimadzu liquid chromatograph system, equipped with a CBM-20A system controller, LC-20AR solvent delivery module and SPD-20A UV-Vis detector, on a Vydac C18 column (10 μ, 300 Å, 22 x 250 mm). A linear gradient of 20–40 % aqueous MeCN (containing 0.1% TFA) over 80 min at a flow rate of 20 mL/min was used with purifications, which were monitored at 214 nm. Analytical HPLC on an Agilent 1290 series liquid chromatograph system was performed to verify the purity of the final peptides using a Vydac 218-TP column (5 μ, 300 Å, 4.6 mm x 50 mm) equipped with a Vydac guard cartridge. Two systems, a linear gradient of 5-50% solvent B (solvent A = aqueous 0.1% TFA and solvent B = MeCN containing 0.1% TFA) over 45 min at a flow rate of 1 mL/min (system

1), and a linear gradient of 25-70% solvent B (solvent A = aqueous 0.1% TFA and solvent B = MeOH containing 0.1% TFA) over 45 min at a flow rate of 1.0 mL/min (system 2), were used for the analyses. The final purity of all peptides by both methods was greater than 99% (Table 6.8). Molecular weights of the peptides were determined by ESI-MS (Advion CMS).

### Pharmacological assays

Radioligand binding assays were performed using cloned rat  $\kappa$  opioid receptors stably expressed in CHO cells as described in Chapter 5.

### 6.5 References

1. Bennett, M. A.; Murray, T. F.; Aldrich, J. V. Identification of Arodyn, a Novel Acetylated Dynorphin A-(1-11) Analogue, as a  $\kappa$  Opioid Receptor Antagonist. *J Med Chem* **2002**, 45, 5617-5619.
2. Fang, W.-J.; Murray, T. F.; Aldrich, J. V. Design, synthesis, and opioid activity of arodyn analogs cyclized by ring-closing metathesis involving Tyr(allyl). *Bioorg Med Chem* **2018**, 26, 1157-1161.
3. Fang, W. Design and Synthesis of Novel Linear and Cyclic Peptide Ligands for Kappa Opioid Receptors. University of Kansas, 2008.
4. Fang, W. J.; Bennett, M. A.; Aldrich, J. V. Deletion of Ac-NMePhe<sup>1</sup> from [NMePhe<sup>1</sup>]arodyn under acidic conditions, part 1: Effects of cleavage conditions and N-terminal functionality. *Biopolymers* **2011**, 96, 97-102.
5. Dimartino, G.; Wang, D.; Chapman, R. N.; Arora, P. S. Solid-Phase Synthesis of Hydrogen-Bond Surrogate-Derived  $\alpha$ -Helices. *Org Lett* **2005**, 7, 2389-2392.
6. Chapman, R. N.; Arora, P. S. Optimized Synthesis of Hydrogen-Bond Surrogate Helices: Surprising Effects of Microwave Heating on the Activity of Grubbs Catalysts. *Org Lett* **2006**, 8, 5825-5828.
7. O'Doherty, I.; Yim, J. J.; Schmelz, E. A.; Schroeder, F. C. Synthesis of Caeliferins, Elicitors of Plant Immune Responses: Accessing Lipophilic Natural Products via Cross Metathesis. *Org Lett* **2011**, 13, 5900-5903.

8. Hanson, P. R.; Chegondi, R.; Nguyen, J.; Thomas, C. D.; Waetzig, J. D.; Whitehead, A. Total Synthesis of Dolabelide C: A Phosphate-Mediated Approach. *J Org Chem* **2011**, *76*, 4358-4370.
9. Hong, S. H.; Sanders, D. P.; Lee, C. W.; Grubbs, R. H. Prevention of Undesirable Isomerization during Olefin Metathesis. *J Am Chem Soc* **2005**, *127*, 17160-17161.
10. Martinez-Amezaga, M.; Delpiccolo, C.; Méndez, L.; Dragutan, I.; Dragutan, V.; Mata, E. Unprecedented Multifunctionality of Grubbs and Hoveyda–Grubbs Catalysts: Competitive Isomerization, Hydrogenation, Silylation and Metathesis Occurring in Solution and on Solid Phase. *Catalysts* **2017**, *7*, 1-14.
11. Courchay, F. C.; Sworen, J. C.; Ghiviriga, I.; Abboud, K. A.; Wagener, K. B. Understanding Structural Isomerization during Ruthenium-Catalyzed Olefin Metathesis: A Deuterium Labeling Study. *Organometallics* **2006**, *25*, 6074-6086.
12. Bennett, M. A.; Murray, T. F.; Aldrich, J. V. Identification of arodyn, a novel acetylated dynorphin A-(1-11) analogue, as a kappa opioid receptor antagonist. *J Med Chem* **2002**, *45*, 5617-5619.

## **Chapter 7 - Synthesis of bicyclic arodyn analogs**



## 7.1 Introduction

Cyclization restricts conformational mobility and can potentially stabilize a bioactive conformation in addition to imparting proteolytic resistance. Accordingly, cyclic peptides are gathering increasing interest due to their selectivity and increased binding affinity in addition to enhanced permeability.<sup>1-3</sup> More importantly, linear peptides can be rapidly metabolized and cyclization can impart metabolic stability which improves bioavailability.<sup>4</sup>

Bicyclization imparts additional conformational constraint which can further enhance metabolic stability. This can be particularly important to limit proteolytic degradation observed in monocyclic peptides with larger ring sizes.<sup>5</sup> For example, a bicyclic derivative of the HIV fusion inhibitor enfuvirtide displayed an 82-fold enhancement in proteolytic stability relative to the linear peptide and several-fold higher stability compared to a monocyclic derivative.<sup>6</sup> Additionally, bicyclization can allow incorporation of an additional pharmacophore as demonstrated by fusion of a peptidyl–prolyl *cis–trans* isomerase (Pin1) inhibitor and a cell penetrating peptide.<sup>7</sup> This potential and interest in bicyclic peptides has led to the development of numerous bicyclization methods to improve structural diversity.<sup>5</sup> Furthermore, structural diversity can be increased by using various linkers and varying the location of reactive groups in the linear precursor of a polycyclic peptide.

Of particular note, there are currently no known polycyclic opioid receptor ligands possibly due to the shorter peptide chain of the best studied opioid peptides;<sup>8</sup> however, analogs of dynorphin A (Dyn A) are a promising starting point due to their longer peptide chain. Accordingly, analogs of dynorphin A such as arodyn lend themselves to the synthesis of polycyclic analogs due to the multitude of residues available for cyclization. In this initial synthesis of polycyclic derivatives of arodyn, we limited our design to involve positions where previous cyclizations were tolerated by

the kappa opioid receptor (KOR). To this effect, we explored using RCM and lactam chemistries in the synthesis of bicyclic KOR ligands.

Structure-activity relationships (SAR) of arodyn,<sup>9, 10</sup> particularly with respect to the effects of cyclization on KOR affinity, selectivity, and efficacy, was informative in the design of a bicyclic opioid receptor ligand based on Dyn A (Tables 7.1 and 7.2). Generally, the cyclizations involving AllGly at position 2 of arodyn displayed substantial losses in KOR affinity (Table 7.1). Notably, however, the *cis* isomer of **4** (Table 7.1) was tolerated at the KOR unlike the *trans* analog, which highlights the effect of ligand conformation on KOR affinity. The binding assay results further indicate that both isomers of **4** lost selectivity for KOR over MOR relative to arodyn. Interestingly, preliminary results suggest that cyclization had mixed effects on KOR activation in the GTP $\gamma$ S assay, further exemplifying the effects of ligand conformation on biological activity (Table 7.2). Whereas arodyn displayed negligible KOR activation, cyclizations between AllGly at positions 2 and either 5 or 8 activated the KOR (Table 7.2). For example, both isomers of **4** displayed appreciable KOR activation in the GTP $\gamma$ S assay. The SAR of cyclic arodyn analogs was therefore particularly informative in the design of a bicyclic arodyn analog. Importantly, cyclizations that individually had not resulted in considerable loss of KOR binding affinity are promising starting points for an effective bicyclic KOR ligand.

Table 7.1 Binding affinities of monocyclic RCM arodyn analogs.

Compound	Arodyn analog		K <sub>i</sub> ± SEM (nM) <sup>a</sup>		K <sub>i</sub> ratio (μ/κ)
			κ	μ	
<b>1</b>	arodyn <sup>b</sup>		10.0 ± 3.0	1750 ± 130	174
Cyclic arodyn analogs <sup>c</sup>					
<b>2</b>	<i>cyclo</i> <sup>2,5</sup> [Ala <sup>2</sup> (-CH=CH-)Ala <sup>5</sup> ,Ile <sup>8</sup> ]	<i>cis</i>	131 ± 22	2310 ± 440(4)	18
		<i>trans</i>	410 ± 54	>10,000	>24
<b>3</b>	<i>cyclo</i> <sup>2,5</sup> [D-Ala <sup>2</sup> (-CH=CH-)Ala <sup>5</sup> ,Ile <sup>8</sup> ]	<i>cis</i>	202 ± 12	>10,000	>50
		<i>trans</i>	130 ± 20	>10,000	>77
<b>4</b>	<i>cyclo</i> <sup>2,8</sup> [Ala <sup>2</sup> (-CH=CH-)Ala <sup>8</sup> ]	<i>cis</i>	59.9 ± 12.9	13.9 ± 3.0 (5)	0.2
		<i>trans</i>	453 ± 22	425 ± 74	0.9
<b>5</b>	<i>cyclo</i> <sup>2,8</sup> [D-Ala <sup>2</sup> (-CH=CH-)Ala <sup>8</sup> ]	<i>trans</i>	4960 ± 170	ND	
<b>6</b>	<i>cyclo</i> <sup>5,8</sup> [Ala <sup>5</sup> (-CH=CH-)Ala <sup>8</sup> ]	<i>cis</i>	54.0 ± 3.9	>10,000	185
		<i>trans</i>	63.0 ± 6.3	9370 ± 590	149
<b>7</b>	<i>cyclo</i> <sup>N,5</sup> [COOCH <sub>2</sub> (CH=CH-)Ala <sup>5</sup> ,NMePhe <sup>1</sup> ,Ile <sup>8</sup> ]		208 ± 14	2850 ± 360	14
<b>8</b>	<i>cyclo</i> <sup>3,5</sup> [Tyr <sup>3</sup> (-CH=CH-)Ala <sup>5</sup> ,Ile <sup>8</sup> ] <sup>d,e</sup>		398 ± 40	3460 ± 300	9
<b>9</b>	<i>cyclo</i> <sup>1,2</sup> [Tyr <sup>1</sup> (-CH=CH-)Tyr <sup>2</sup> ,Ile <sup>8</sup> ] <sup>d,e</sup>		71.7 ± 5.2	1920 ± 150	27
<b>10</b>	<i>cyclo</i> <sup>1,2</sup> [Tyr <sup>1</sup> (-CH=CH-)Tyr <sup>2</sup> ] <sup>d,f</sup>		11.7 ± 2.7	1434 ± 402	123
<b>11</b>	<i>cyclo</i> <sup>2,3</sup> [Tyr <sup>2</sup> (-CH=CH-)Tyr <sup>3</sup> ,Ile <sup>8</sup> ] <sup>d,e</sup>		55.4 ± 4.1	903 ± 34	16
<b>12</b>	<i>cyclo</i> <sup>2,3</sup> [Tyr <sup>2</sup> (-CH=CH-)Tyr <sup>3</sup> ] <sup>d,f</sup>		14.7 ± 5.6	1372 ± 328	93
<sup>a</sup> The results are expressed as the mean ± SEM of 3 independent experiments except where noted;					
<sup>b</sup> from ref <sup>11</sup> ; <sup>c</sup> from ref <sup>9</sup> unless otherwise indicated; <sup>d</sup> <i>trans</i> ; <sup>e</sup> from ref <sup>10</sup> ; <sup>f</sup> Chapter 5					

Table 7.2 Preliminary results for activity of cyclic arodyn analogs in the GTP $\gamma$ S assay.

Compound number	GTP $\gamma$ S binding @ 10 $\mu$ M <sup>a</sup>
<b>1, arodyn<sup>b</sup></b>	11 $\pm$ 6%
<b>2 cis</b>	84 $\pm$ 6%
<b>2 trans</b>	24 $\pm$ 24%
<b>3 cis</b>	<10%
<b>3 trans</b>	ND
<b>4 cis</b>	68 $\pm$ 8%
<b>4 trans</b>	84 $\pm$ 14%
<b>5 trans</b>	ND
<b>6 cis</b>	-18 $\pm$ 18%
<b>6 trans</b>	-39 $\pm$ 19%
<b>7</b>	ND
<b>8</b>	<10%
<b>9</b>	<10%
<b>10</b>	<10%
<b>11</b>	<10%
<b>12</b>	<10%
<sup>a</sup> Compared to Dyn A (1-13)NH <sub>2</sub> (100%); <sup>b</sup> From ref <sup>11</sup>	

## 7.2 Synthesis of a bicyclic arodyn analog using RCM

Various strategies have been employed in the synthesis of polycyclic peptides to achieve regioselectivity including sequential RCM<sup>12</sup> and orthogonal metathesis.<sup>13</sup> Based upon the KOR binding affinity and selectivity data for the monocyclic derivatives of arodyn (Table 7.1), constraints between positions 2 and 3 as well as positions 5 and 8 were chosen for the synthesis of a bicyclic analog cyclized using RCM (Figure 7.1). Binding affinities at the KOR indicate that these cyclizations were tolerated by the KOR and the resulting monocyclic analogs displayed negligible KOR activation, similar to arodyn. RCM using Hoveyda-Grubbs 2<sup>nd</sup> generation catalyst

(HG II) was used sequentially to install the cyclic constraints (Scheme 7.1) to limit unwanted cyclizations.

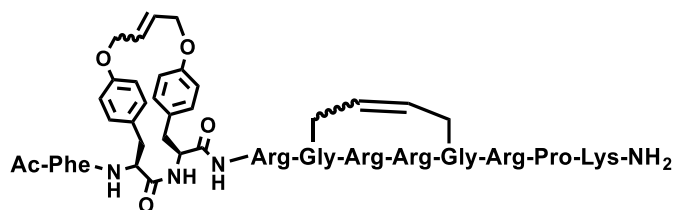
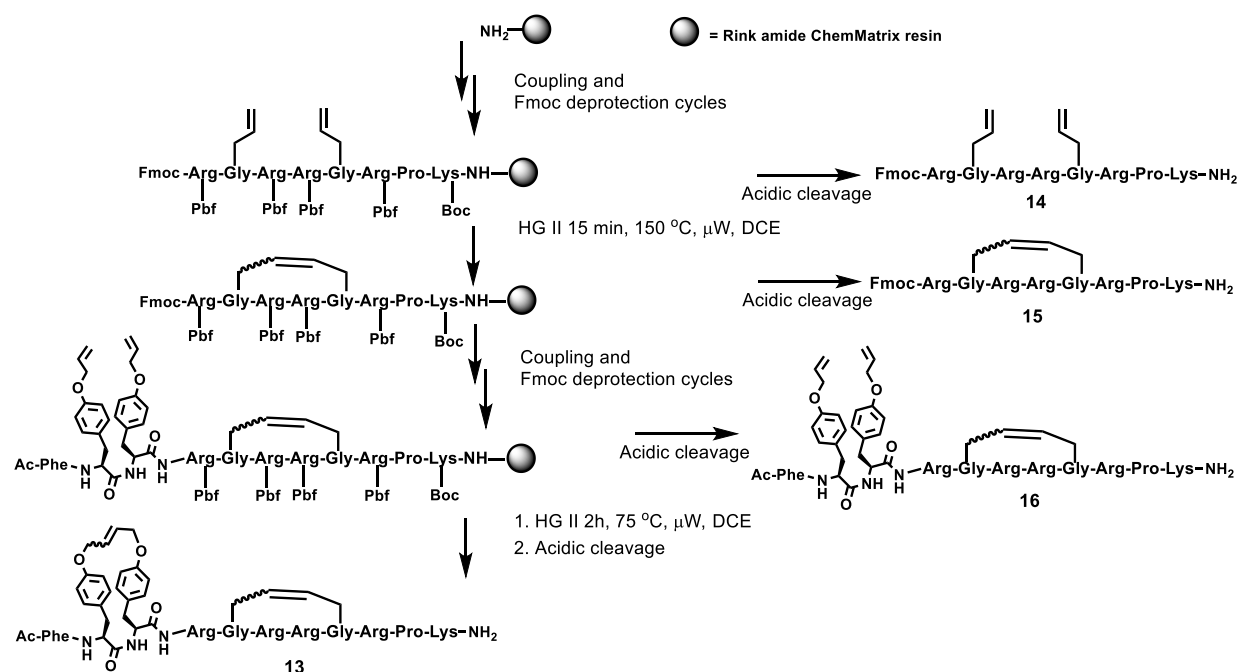


Figure 7.1 Structure of bicyclic arodyn analog *cyclo*[Tyr(All)<sup>2,3</sup>,AllGly<sup>5,8</sup>]arodyn (**13**).

Scheme 7.1 Synthesis of *cyclo*[Tyr(All)<sup>2,3</sup>,AllGly<sup>5,8</sup>]arodyn (**13**) using sequential RCM. PyBOP = benzotriazol-1-yl-oxy-tris-pyrrolidino-phosphonium hexafluorophosphate, HOBT = 1-hydroxybenzotriazole, Boc = *tert*-butoxycarbonyl and Pbf = 2,2,4,6,7-pentamethyldihydrobenzofuran-5-sulfonyl.



## 7.2.1 Results and discussion

The C-terminal and N-terminal cyclic constraints were installed sequentially to limit unwanted regioisomers. Accordingly, the synthesis of the C-terminal segment **15** under various conditions (Figure 7.2) was explored to optimize reaction yields before synthesis of the

heteroatom-containing RCM bridge (Scheme 7.1). Notably, optimized conditions for the synthesis of the cyclic N-terminal segment had been previously developed (Chapter 5).

A temperature dependent increase in yield similar to that observed in the head to sidechain arodyn analogs containing AllGly (Chapter 6) was observed in the synthesis of **15**. The RCM product yields increased with increasing temperature (Figure 7.3, Tables 7.3 and 7.4). Doubling the temperature drastically increased conversion to the RCM product, consistent with the temperature dependent activity of Grubbs catalysts.<sup>14, 15</sup> At 150 °C reaction times from 5 min to 30 min resulted in appreciable RCM product yields (63-73%). Further increasing the temperature did not improve the RCM product yield, suggesting that catalyst activity peaks at 150 °C. Arora and coworkers observed a similar temperature dependence in the synthesis of hydrogen-bond surrogate helices using RCM; yields in cyclized peptide peaked at 200 °C for HG II.<sup>15</sup>

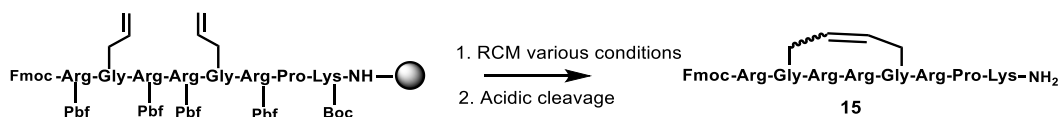


Figure 7.2 Synthesis of *cyclo*[Fmoc-AllGly<sup>5,8</sup>]arodyn<sup>4-11</sup> (**15**).

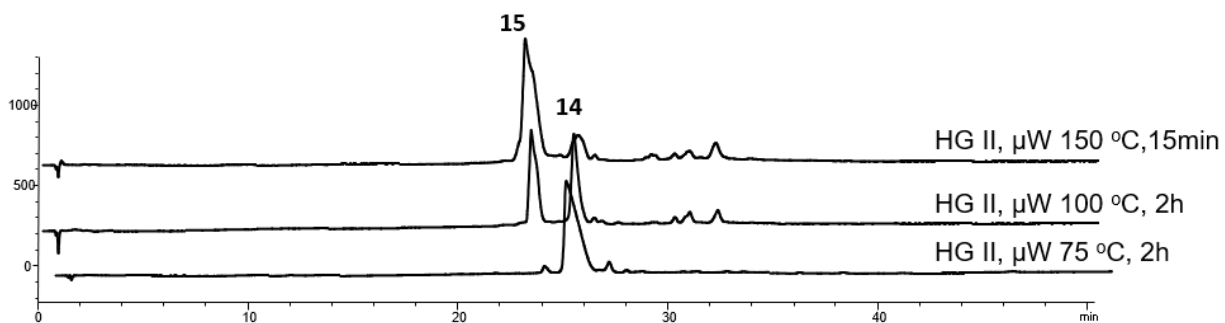


Figure 7.3 Representative chromatograms showing RCM of **14** at various temperatures under microwave heating.

Table 7.3 Analytical data for **14** and **15**.

Compound	HPLC $t_R$ (min) <sup>a</sup>	ESI-MS	
		Calcd.	Obsvd.
<b>14</b>	25.3	[M+3H] <sup>3+</sup> 428.6	[M+3H] <sup>3+</sup> 428.7
<b>15</b>	23.3	[M+3H] <sup>3+</sup> 419.2	[M+3H] <sup>3+</sup> 419.5
<sup>a</sup> 5-50% aqueous MeCN (0.1% TFA) over 45 min			

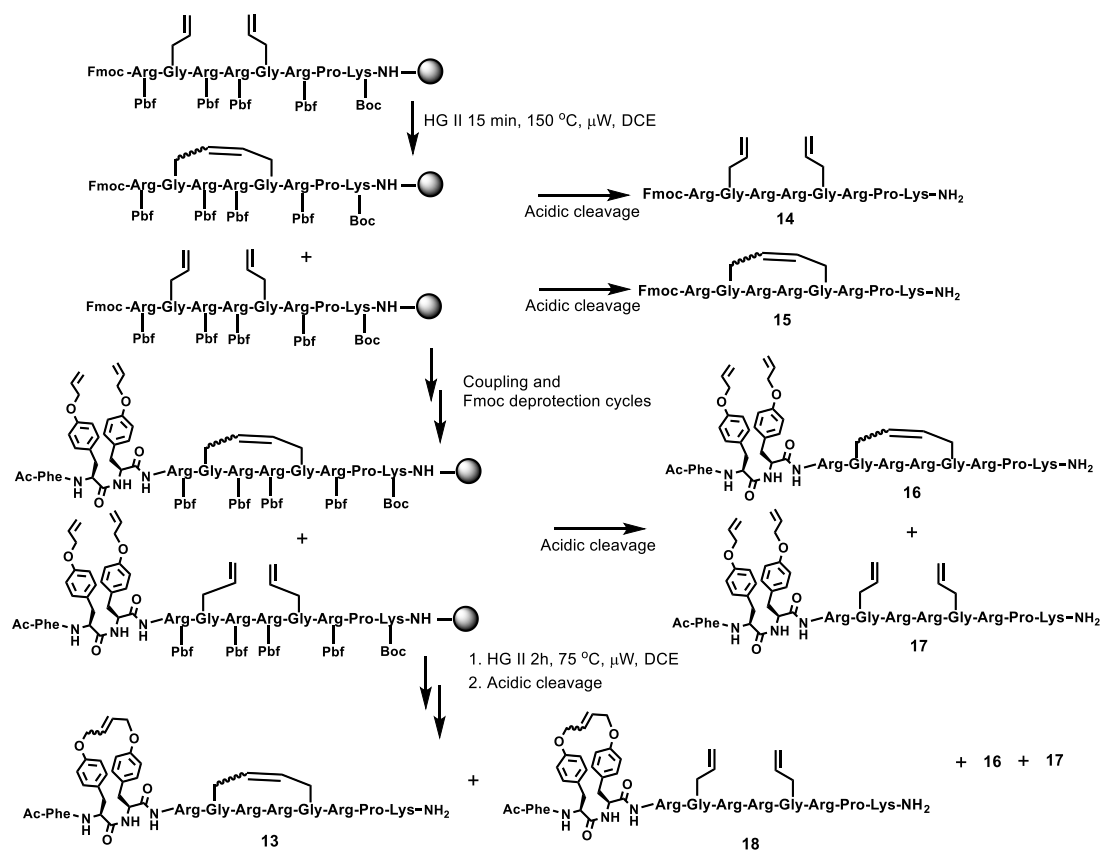
Table 7.4 Synthesis of **15** under various microwave heating conditions.

Entry	Temp (°C) <sup>a</sup>	Time	RCM Pdt yield (%)
1	75	2h	_ <sup>b</sup>
2	100	2h	46
3	150	5 min	63
4	150	15 min	73
5	150	30 min	73
6	175	15 min	67
<sup>a</sup> 15 mol% HG II 0.3 mM in DCE; <sup>b</sup> <10%			

Following synthesis of **15** in appreciable yields (Table 7.4), the resin-bound peptide containing **15** plus residual **14** was subjected to further solid phase peptide synthesis (SPPS) to incorporate the N-terminal residues containing Tyr(All) resulting in **16** and **17** (Scheme 7.2). The mixture containing resin-bound protected forms of **16** and **17** was then subjected to RCM using conditions previously established to install the heteroatom-containing RCM bridge involving Tyr(All) (Chapter 5, Scheme 7.2). Encouragingly, the bicyclic RCM product **13** was obtained in reasonable yields (52%, Figure 7.4). LC-MS analysis indicated that the product mixture also contained **16**, **17**, and **18** (Figure 7.4, Table 7.5). Peptide **18** is the cyclization product of **17** and

was observed as the major side product; this is consistent with previously observed minimal RCM of AllGly residues at 75 °C for 2 h (Table 7.4). Purification was performed using a linear gradient of aqueous MeCN (0.1% TFA) over 80 min (20-40%) at a flowrate of 20 mL/min. Of note, **13** was purified as a mixture of *cis/trans* isomers as these isomers could not be separated. Future experiments will include NMR analysis to establish the ratio for each linkage.

Scheme 7.2 Synthesis of **13** using sequential RCM showing structures of major products in the reaction mixture.





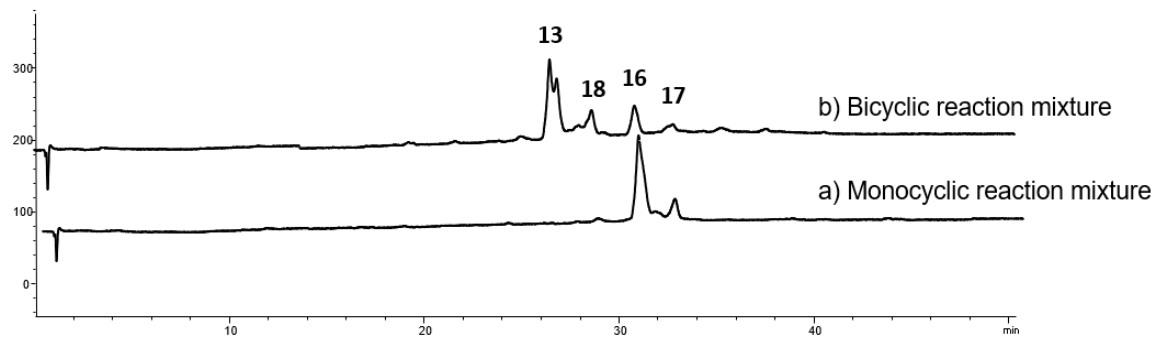


Figure 7.4 Chromatograms of the synthesis of the **13** showing major components of the reaction mixtures a) before and b) after RCM involving Tyr(All) residues.

Table 7.5 Analytical data of major components of the RCM product mixture following the synthesis of **13**.

Compound	HPLC $t_R$ (min) <sup>a</sup>	ESI-MS	
		Calcd.	Obsvd.
<b>13</b>	27.0	$[M+2H]^{2+}$ 801.5	$[M+2H]^{2+}$ 801.7
		$[M+3H]^{3+}$ 534.6	$[M+3H]^{3+}$ 534.9
<b>16</b>	30.8	$[M+3H]^{3+}$ 544.0	$[M+3H]^{3+}$ 543.9
		$[M+4H]^{4+}$ 408.2	$[M+4H]^{4+}$ 408.2
<b>17</b>	32.9	$[M+3H]^{3+}$ 553.3	$[M+3H]^{3+}$ 553.2
		$[M+4H]^{4+}$ 415.3	$[M+4H]^{4+}$ 415.2
<b>18</b>	28.7	$[M+2H]^{2+}$ 815.5	$[M+2H]^{2+}$ 815.4
		$[M+3H]^{3+}$ 544.0	$[M+3H]^{3+}$ 543.9
<sup>a</sup> 5-50% aqueous MeCN (0.1% TFA) over 45 min			

Encouragingly, the bicyclic analog *cyclo*[Tyr(All)<sup>2,3</sup>,AllGly<sup>5,8</sup>]arodyn (**13**) retained affinity at the KOR, displaying higher affinity for the KOR than the corresponding monocyclic derivatives **6** and **11**. (Table 7.6). Additional pharmacological evaluation of the synthesized bicyclic arodyn analog **13** to probe effects on KOR selectivity, efficacy, and antagonist potency is in progress.

Table 7.6 Initial evaluation of receptor affinity of bicyclic arodyn analog **13** and related arodyn analogs.

Compound number	Arodyn analog	$K_i \pm \text{SEM}$ (nM)	
		$\kappa$	$\mu$
<b>1</b>	arodyn <sup>a</sup>	10.0 ± 3.0	1750 ± 130
<b>6</b>	<i>cyclo</i> [AllGly <sup>5,8</sup> ] <sup>b</sup>	<i>cis</i>	54.0 ± 3.9
		<i>trans</i>	63.0 ± 6.3
<b>11</b>	<i>cyclo</i> [Tyr(All) <sup>2,3</sup> , Ile <sup>8</sup> ] <sup>c,d</sup>	55.4 ± 4.1	903 ± 34
<b>13</b>	<i>cyclo</i> [Tyr(All) <sup>2,3</sup> , AllGly <sup>5,8</sup> ] <sup>e</sup>	26.4 ± 5.9	ND <sup>f</sup>
<sup>a</sup> from ref <sup>11</sup> ; <sup>b</sup> from ref <sup>9</sup> ; <sup>c</sup> <i>trans</i> ; <sup>d</sup> from ref <sup>10</sup> ; <sup>e</sup> mean $K_i$ values ± SEM from at least 3 independent experiments; <sup>f</sup> not determined			

### 7.3 Synthesis of a bicyclic arodyn analog using lactam chemistry

Various cyclizations can impart different conformations to the peptide and influence binding topology at the target. Trivalent rigid linkers including tris(bromomethyl)benzene (TBMB) and benzene-1,3,5-tricarboxylic acid (trimesic acid) have been utilized in the synthesis of bicyclic peptides, particularly in bicyclic peptide libraries.<sup>16, 17</sup> TBMB has been used in crosslinking three cysteine residues,<sup>16</sup> whereas trimesic acid has been used to crosslink the *N*-terminal amine to lysine and 1,3-diaminopropionic (Dap) residues.<sup>17</sup> Furthermore, increasing varieties of chemical linkers have been developed for the synthesis of bicyclic peptides and peptide libraries.<sup>18</sup> In the initial design and synthesis of a lactam-based bicyclic KOR ligand based on arodyn, we used a trimesic acid scaffold. Additionally, we used pharmacological data from previous monocyclic derivatives as an important guide to choose the location of the cyclic constraints.

Binding affinity data were available for multiple monocyclic lactam derivatives of arodyn, therefore making arodyn an excellent lead peptide to explore bicyclization motifs and their effects on KOR affinity, efficacy, and selectivity. Notably, cyclizations incorporating a lactam bridge

displayed substantial losses in KOR affinity with the exception of *cyclo*[Asp<sup>5</sup>,Dap<sup>8</sup>]arodyn ( $K_i = 61.0 \pm 23.7$  nM) and *cyclo*[D-Asp<sup>5</sup>,Dap<sup>8</sup>]arodyn ( $K_i = 55.3 \pm 15.1$  nM, Table 7.7). In particular, side chain to side chain lactams involving position 2 of arodyn were not tolerated by the KOR similar to analogs cyclized using RCM (Table 7.1). Similar substantial losses in affinity have been observed in head to side chain cyclizations of Dyn A analogs involving the third or fifth residues; this suggests unfavorable interactions with functionalities in the constraint or an unfavorable conformation.<sup>19</sup> In contrast, it should be noted that cyclodyn, a head to side chain (Glu<sup>5</sup>) cyclized KOR antagonist based on Dyn A, retains affinity at the KOR ( $K_i = 26.8 \pm 2.8$  nM) but is less selective for KOR (KOR/MOR/DOR=1/12/>330) than arodyn.<sup>20</sup>

Table 7.7 Binding affinities of monocyclic lactam arodyn analogs.

Compound	Arodyn analog	$K_i \pm \text{SEM}$ (nM) <sup>a</sup>		$K_i$ ratio ( $\mu/\kappa$ )
		$\kappa$	$\mu$	
<b>19</b>	Arodyn <sup>b</sup>	10.0 $\pm$ 3.0	1750 $\pm$ 130	175
	Cyclic arodyn analogs <sup>c</sup>			
<b>20</b>	<i>cyclo</i> [D-Asp <sup>2</sup> ,Dap <sup>5</sup> ,Ile <sup>8</sup> ]	2460 $\pm$ 300 (5)	>10,000	>4
<b>21</b>	<i>cyclo</i> [Asp <sup>2</sup> ,Dap <sup>5</sup> ,Ile <sup>8</sup> ]	580 $\pm$ 150	>10,000	>17
<b>22</b>	<i>cyclo</i> [Asp <sup>2</sup> ,Lys <sup>5</sup> ,Ile <sup>8</sup> ]	862 $\pm$ 284 (4)	ND	ND
<b>23</b>	<i>cyclo</i> [D-Asp <sup>2</sup> ,Dap <sup>8</sup> ]	677 $\pm$ 38	375 $\pm$ 83	0.6
<b>24</b>	<i>cyclo</i> [Asp <sup>2</sup> ,Dap <sup>8</sup> ]	373 $\pm$ 43	1540 $\pm$ 160	4
<b>25</b>	<i>cyclo</i> [D-Asp <sup>5</sup> ,Dap <sup>8</sup> ]	55.3 $\pm$ 15.1	>10,000	>182
<b>26</b>	<i>cyclo</i> [Asp <sup>5</sup> ,Dap <sup>8</sup> ]	61.0 $\pm$ 23.7	>10,000 (5)	>163

<sup>a</sup>The results are expressed as the mean  $\pm$  SEM of 3 independent experiments except where noted; <sup>b</sup>From ref<sup>11</sup>; <sup>c</sup>From ref<sup>9</sup>

### 7.3.1 Results and discussion

Trimesic acid (TMA) was employed as a rigid linker for the synthesis of a lactam-based bicyclic arodyn analog. 2-Methyltrityl (Mtt) protected diaminopropionic (L-Dap) residues were incorporated at positions 5 and 8 of arodyn to facilitate formation of the bicycle. TMA was coupled to the N-terminus of protected [Dap<sup>5,8</sup>]arodyn, followed by selective deprotection of the Dap residues (Scheme 7.3). Cyclization with PyBOP and HOBt afforded the bicyclic peptide in one step under microwave heating (Table 7.8, Figure 7.5) with >90% conversion. Purification was performed using a linear gradient of aqueous MeCN (0.1% TFA) over 80 min (20-40%) at a flow rate of 20 mL/min (see experimental).

Scheme 7.3 Synthesis of *cyclo*<sup>N,5,8</sup>[TMA,Dap<sup>5,8</sup>]arodyn (**29**).

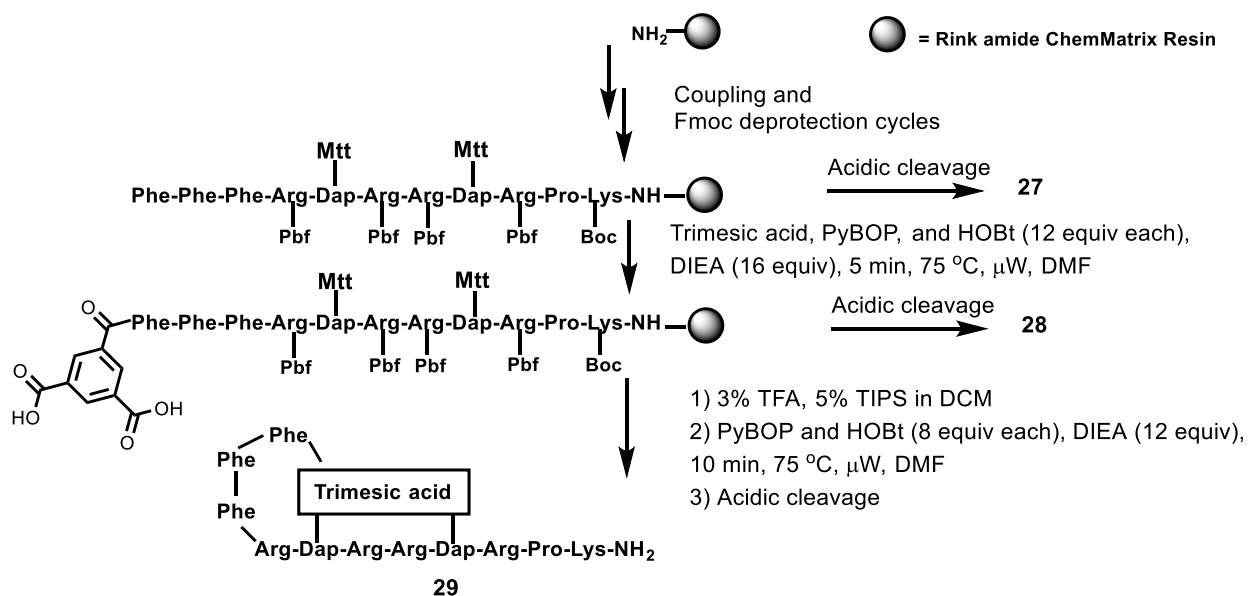


Table 7.8 Analytical data of **27**, **28**, and **29**.

Compound	Arodyn analog	HPLC $t_R$ (min) <sup>a</sup>	ESI-MS	
			Calcd.	Obsvd.
<b>27</b>	[Dap <sup>5,8</sup> ]arodyn	20.5	[M+3] <sup>3+</sup> 494.6 [M+4] <sup>4+</sup> 371.2	[M+3] <sup>3+</sup> 494.7 [M+4] <sup>4+</sup> 371.4
<b>28</b>	[TMA,Dap <sup>5,8</sup> ]arodyn <sup>b</sup>	25.5	[M+3] <sup>3+</sup> 558.3 [M+4] <sup>4+</sup> 419.0	[M+3] <sup>3+</sup> 558.7 [M+4] <sup>4+</sup> 419.3
<b>29</b>	<i>cyclo</i> <sup>N,5,8</sup> [TMA,Dap <sup>5,8</sup> ]arodyn	30.4	[M+2H] <sup>2+</sup> 819.4 [M+3H] <sup>3+</sup> 546.6	[M+2H] <sup>2+</sup> 819.7 [M+3H] <sup>3+</sup> 547.0

<sup>a</sup>5-50% aqueous MeCN (0.1% TFA) over 45 min; <sup>b</sup>TMA=trimesic acid

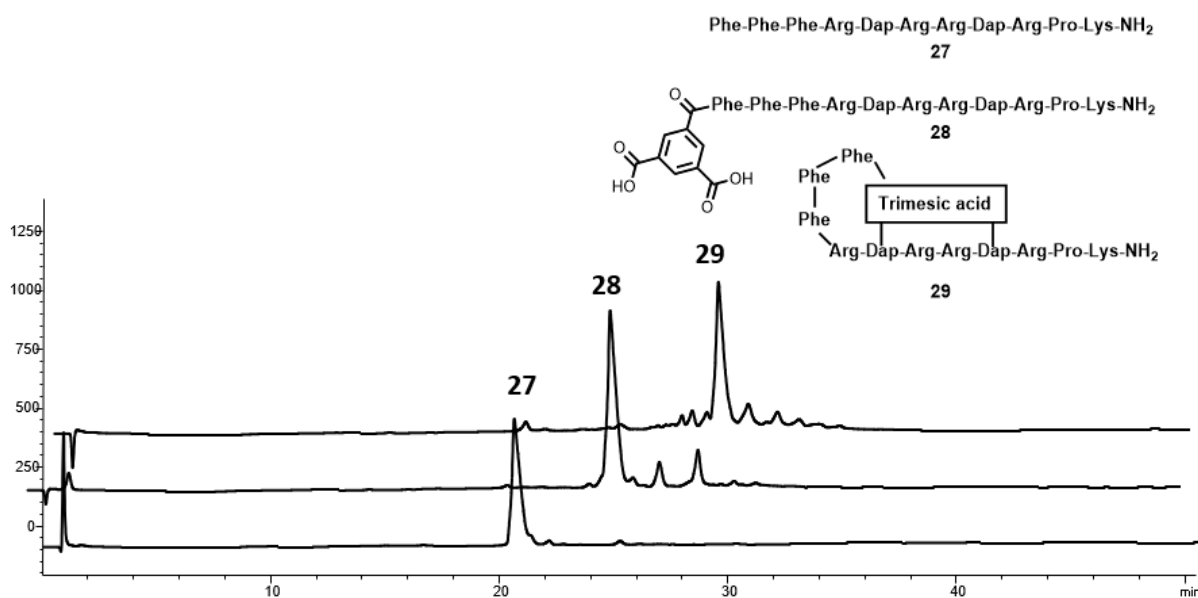


Figure 7.5 Chromatograms and structures of the lactam-based bicyclic arodyn analog and the corresponding linear precursors.

In preliminary receptor affinity evaluation, however,  $cyclo^{N,5,8}$ [TMA,Dap<sup>5,8</sup>]arodyn (**29**,  $K_i=514\pm 149$  nM) displayed a 51-fold loss in affinity compared to arodyn. Of note, RCM cyclizations involving the N-terminus and residue 5 of arodyn retained affinity at KOR (Chapter 6) and cyclodyn, a head to side chain (Glu<sup>5</sup>) cyclized Dyn A derivative, also retained affinity at KOR.<sup>20</sup> The substantial loss in affinity exhibited by  $cyclo^{N,5,8}$ [TMA,Dap<sup>5,8</sup>]arodyn was similar to those found for arodyn analogs with lactam constraints involving residue 2 in the “message” sequence (Table 7.7). Only cyclizations between residues 5 and 8 were tolerated at the KOR displaying much less drastic decreases in KOR affinity (Table 7.7). Monocyclic lactam derivatives with the rigid linker isophthalic acid (benzene-1,3-dicarboxylic acid) between the N-terminus and residue 5, the N-terminus and residue 8, as well as between residues 5 and 8 could give further insight on the effects of the different cyclization positions on KOR affinity.

## 7.4 Conclusions

Polycyclic peptides are an emerging class of macrocycles whose unique attributes can be leveraged to modulate biological targets. Of particular interest, polycyclic peptides are promising therapeutics and chemical probes with enhanced proteolytic stability which can improve pharmacokinetic properties.<sup>5, 21</sup>

In this initial study, we designed and synthesized two bicyclic opioid KOR ligands derived from the Dyn A-based antagonist arodyn and report the first bicyclic opioid receptor ligands (Schemes 7.1 and 7.3). Based on previous SAR of arodyn analogs, we limited the positions involved in the cyclizations to those where the constraint was both tolerated at the KOR and maintained KOR selectivity. Microwave heating facilitated cyclization of two bicyclic arodyn analogs, resulting in appreciable yields. Sequential RCM was utilized for regioselective cyclization of one bicyclic analog, while a rigid aromatic linker, trimesic acid, was employed in the synthesis of a lactam-based arodyn bicycle. Initial receptor affinity evaluation indicate that these two bicyclic arodyn analogs displayed vastly different affinities for the KOR that are likely due to differences in peptide topology. Whereas the RCM-based bicyclic analog **13** retained KOR affinity, the TMA bicyclic analog **29** displayed a considerable loss in KOR affinity. Future bicycles could expand the structural diversity of these KOR ligands by combining lactam and RCM cyclizations. In addition, proteolytic stability studies will be important, given that linear Dyn A derivatives can be rapidly metabolized.<sup>22</sup>

## 7.5 Experimental

### Materials

Fmoc-Dap(Mtt) was purchased from Anaspec (Fremont, CA). The sources of other materials are listed in chapter 5.

### Instruments

Microwave assisted RCM was performed on a Biotage Initiator+ SP Wave microwave synthesizer and solid phase peptide synthesis (SPPS) was performed on a Biotage microwave peptide synthesizer (Initiator+ Alstra; Biotage, Sweden).

Electrospray ionization mass spectrometry (ESI/MS) was performed on an Advion expression L compact MS (Advion, Inc. Ithaca NY).

Analytical HPLC was performed on an Agilent 1200 system fitted with a Grace Vydac analytical column (C18, 300 Å, 5 µm, 4.6 mm x 50 mm) equipped with a Vydac C18 guard cartridge. Yields for respective reactions were determined from analytical HPLC chromatograms monitored at 214 nm; in some cases, baseline resolution was not achieved so yields shown are an estimate.

### Solid Phase Peptide Synthesis (SPPS)

Aroclon analogs were prepared by the Fmoc (9-fluorenylmethoxycarbonyl) SPPS strategy using the automated Biotage microwave peptide synthesizer (Initiator+ Alstra; Biotage, Sweden) on a 0.14 mmol scale. The Rink amide ChemMatrix resin (0.14 mmol, 0.52 mmol/g) was swelled for 20 min at 70 °C in DMF prior to cycles of amino acid coupling and deprotection. Coupling reactions were performed using Fmoc amino acids (4 equiv, 0.5 M), activated with PyBOP (4 equiv, 0.5 M) and HOBt (4 equiv, 0.5 M) in DMF in the presence of DIPEA (8 equiv in NMP) for 5 min at 75 °C. Fewer equivalents were used in the coupling of Fmoc-Dap(Mtt) (2 equiv). Fmoc



deprotection was performed at room temperature with 20% 4-methylpiperidine in DMF (4.5 mL, 1 x 3 min; 4.5 mL, 2 x 10 min). The side chains of Dap, Lys and Arg were protected with methyltrityl (Mtt), *tert*-butoxycarbonyl (Boc) and 2,2,4,6,7-pentamethyldihydrobenzofuran-5-sulfonyl (Pbf), respectively. N-Terminal acetylation was performed using acetic anhydride (5 M in DMF) and DIEA (2 M in NMP) for 10 minutes at room temperature. The resulting peptides were washed with DMF (5 mL, 3 x 45 sec) and DCM (5 mL, 3 x 45 sec). Crude peptides were cleaved from the resin using TFA/ triisopropylsilane (TIPS)/water (95/2.5/2.5) for at least 2 h and then precipitated with cold ether following filtration.

### Ring Closing Metathesis (RCM)

A solution of degassed 1,2-dichloroethane (DCE) containing 15 mol % (0.15 equiv) of Hoveyda-Grubbs II catalyst (0.3 mM) was added to the resin-bound peptide (150 mg, 0.21 mmol/g) before heating. Closed vessel microwave assisted RCM was performed on a Biotage Initiator+ SP Wave microwave synthesizer in capped microwave reaction vials for the indicated amount of time at the indicated temperatures, sequential RCM was performed as indicated in scheme 7.1. The resin was washed with MeOH (3 x 5 mL) and DCM (10 x 5 mL) before drying and cleavage.

### Synthesis of *cyclo*[Tyr(All)<sup>2,3</sup>,AllGly<sup>5,8</sup>] (13)

[Fmoc-AllGly<sup>5,8</sup>]arodyn<sup>4-11</sup> (14) was synthesized using SPPS as described above and the protected resin-bound peptide (150 mg, 0.03 mmol, 0.23 mmol/g) was subjected to RCM for 15 min at 150 °C as described in the RCM procedure (Scheme 7.2, see Figure 7.3 and Table 7.3 for analytical data). SPPS of the resin-bound peptide was performed to extend the peptide chain, and the resulting full length resin-bound peptide mixture (150 mg, 0.03 mmol, 0.21 mmol/g) was

subjected to RCM for 2 h at 75 °C as described in the RCM procedure (Scheme 7.2, see Table 7.5 for analytical data). The final peptide was cleaved from the resin as described above and purified as described below.

### Synthesis of *cyclo*<sup>N,5,8</sup>[TMA,Dap<sup>5,8</sup>]arodyn (**29**)

Following synthesis of [Dap<sup>5,8</sup>]arodyn (**27**, Scheme 7.3), DIEA (388 μL, 2.24 mmol, 16 equiv) was added to a solution of trimesic acid (117.6 mg, 0.56 mmol, 4 equiv), PyBOP (873 mg, 1.68 mmol, 12 equiv), and HOBt (257 mg, 1.68 mmol, 12 equiv) in DMF (3.5 mL). The mixture was added to the N-terminal free amine of protected [Dap<sup>5,8</sup>]arodyn (0.14 mmol, 1 equiv) and subjected to microwave irradiation (Biotage Initiator+ Alstra ) for 5 min at 75 °C as indicated in scheme 7.3. See Table 7.8 for analytical data of [TMA,Dap<sup>5,8</sup>]arodyn (**28**) following aliquot cleavage.

The protected resin-bound peptide, [TMA,Dap(Mtt)<sup>5,8</sup>]arodyn, was washed with 3% TFA/5% TIS in DCM (3 mL, 10 x 2min) to selectively remove the Mtt protecting group after which the resin was washed with DCM (3mL, 5 x 2 min). Following Mtt deprotection, DIEA (291 μL, 1.68 mmol, 12 equiv) was added to a solution of PyBOP (582 mg, 1.12 mmol, 8 equiv), and HOBt (171 mg 1.12 mmol, 8 equiv) in DMF (3.5 mL). The mixture was added to the resin-bound peptide [TMA, Dap<sup>5,8</sup>]arodyn (0.14 mmol, 1 equiv) and subjected to microwave irradiation (Biotage Initiator+ Alstra ) for 10 min at 75 °C. The resin-bound peptide was washed with DMF (5 mL, 3 x 45 sec) and DCM (5 mL, 3 x 45 sec). See Table 7.8 for analytical data.

### Purification and analysis of purified peptides

The crude peptides **13** and **29** were purified by preparative reversed-phase HPLC on a Shimadzu liquid chromatograph system equipped with a CBM-20A system controller, LC-20AR

solvent delivery module and SPD-20A UV-Vis detector on a Vydac C18 column (10  $\mu$ , 300 Å, 22 x 250 mm) fitted with a C18 guard cartridge. A linear gradient of 20–40 % aqueous MeCN (containing 0.1% TFA) over 80 min at a flow rate of 20 mL/min was used for purification of both bicyclic peptides **13** and **29** (Table 7.9). The purifications were monitored at 214 nm. Analytical HPLC was used to verify the purity of the final peptides using a Vydac 218-TP column (5  $\mu$ , 300 Å, 4.6 mm x 50 mm) equipped with a Vydac guard cartridge. Two systems, a linear gradient of 5-50% solvent B (solvent A = aqueous 0.1% TFA and solvent B = MeCN containing 0.1% TFA) over 45 min at a flow rate of 1 mL/min (system 1), and a linear gradient of 25-70% solvent B (solvent A = aqueous 0.1% TFA and solvent B = MeOH containing 0.1% TFA) over 45 min at a flow rate of 1.0 mL/min (system 2), were used for the analyses. The final purity of all peptides by both methods was greater than 99% (Table 7.7). Molecular weights of the peptides were determined by ESI-MS (Advion CMS).

Table 7.9 Analytical data of bicyclic arodyn analogs.

Compound	HPLC $t_R$ (min) <sup>a</sup>		ESI-MS	
	System 1 <sup>a</sup> (% purity)	System 2 <sup>b</sup> (% purity)	Calcd.	Obsvd.
<b>13</b>	27.0 (99.9)	13.4 (99.9)	[M+2H] <sup>2+</sup> 801.5	[M+2H] <sup>2+</sup> 801.7
			[M+3H] <sup>3+</sup> 534.6	[M+3H] <sup>3+</sup> 534.9
<b>29</b>	30.4 (99.9)	26.9 (99.9)	[M+2H] <sup>2+</sup> 819.4	[M+2H] <sup>2+</sup> 819.7
			[M+3H] <sup>3+</sup> 546.6	[M+3H] <sup>3+</sup> 547.0
<sup>a</sup> 5-50% aqueous MeCN (0.1% TFA) over 45 min; <sup>b</sup> 25-70% aqueous MeOH (0.1% TFA) over 45 min				

### Pharmacological assays

Radioligand binding assays were performed using cloned rat  $\kappa$  opioid receptors stably expressed in CHO cells as described in Chapter 5.

## 7.6 References

1. Zorzi, A.; Deyle, K.; Heinis, C. Cyclic Peptide Therapeutics: Past, Present and Future. *Curr Opin Chem Biol* **2017**, *38*, 24-29.
2. Ong, Y. S.; Gao, L.; Kalesh, K. A.; Yu, Z.; Wang, J.; Liu, C.; Li, Y.; Sun, H.; Lee, S. S. Recent Advances in Synthesis and Identification of Cyclic Peptides for Bioapplications. *Curr Top Med Chem* **2017**, *17*, 2302-2318.
3. Alaofi, A.; On, N.; Kiptoo, P.; Williams, T. D.; Miller, D. W.; Siahaan, T. J. Comparison of Linear and Cyclic His-Ala-Val Peptides in Modulating the Blood-Brain Barrier Permeability: Impact on Delivery of Molecules to the Brain. *J Pharm Sci* **2016**, *105*, 797-807.
4. Nielsen, D. S.; Shepherd, N. E.; Xu, W.; Lucke, A. J.; Stoermer, M. J.; Fairlie, D. P. Orally Absorbed Cyclic Peptides. *Chem Rev* **2017**, *117*, 8094-8128.
5. Rhodes, C. A.; Pei, D. Bicyclic Peptides as Next-Generation Therapeutics. *Chem Eur J* **2017**, *23*, 12690-12703.
6. Bird, G. H.; Madani, N.; Perry, A. F.; Princiotta, A. M.; Supko, J. G.; He, X.; Gavathiotis, E.; Sodroski, J. G.; Walensky, L. D. Hydrocarbon double-stapling remedies the proteolytic instability of a lengthy peptide therapeutic. *Proc Natl Acad Sci* **2010**, *107*, 14093-14098.
7. Lian, W.; Jiang, B.; Qian, Z.; Pei, D. Cell-Permeable Bicyclic Peptide Inhibitors against Intracellular Proteins. *J Am Chem Soc* **2014**, *136*, 9830-9833.
8. Remesic, M.; Lee, Y. S.; Hruby, V. J. Cyclic Opioid Peptides. *Curr Med Chem* **2016**, *23*, 1288-1303.
9. Fang, W. Design and Synthesis of Novel Linear and Cyclic Peptide Ligands for Kappa Opioid Receptors. University of Kansas, 2008.
10. Fang, W.-J.; Murray, T. F.; Aldrich, J. V. Design, synthesis, and opioid activity of arodyn analogs cyclized by ring-closing metathesis involving Tyr(allyl). *Bioorg Med Chem* **2018**, *26*, 1157-1161.
11. Bennett, M. A.; Murray, T. F.; Aldrich, J. V. Identification of Arodyn, a Novel Acetylated Dynorphin A-(1-11) Analogue, as a  $\kappa$  Opioid Receptor Antagonist. *J Med Chem* **2002**, *45*, 5617-5619.

12. Pattabiraman, V. R.; Stymiest, J. L.; Derksen, D. J.; Martin, N. I.; Vederas, J. C. Multiple On-Resin Olefin Metathesis to Form Ring-Expanded Analogues of the Lantibiotic Peptide, Lacticin 3147 A2. *Org Lett* **2007**, *9*, 699-702.
13. Cromm, P. M.; Schaubach, S.; Spiegel, J.; Furstner, A.; Grossmann, T. N.; Waldmann, H. Orthogonal ring-closing alkyne and olefin metathesis for the synthesis of small GTPase-targeting bicyclic peptides. *Nat Commun* **2016**, *7*, 11300.
14. Dimartino, G.; Wang, D.; Chapman, R. N.; Arora, P. S. Solid-Phase Synthesis of Hydrogen-Bond Surrogate-Derived  $\alpha$ -Helices. *Org Lett* **2005**, *7*, 2389-2392.
15. Chapman, R. N.; Arora, P. S. Optimized Synthesis of Hydrogen-Bond Surrogate Helices: Surprising Effects of Microwave Heating on the Activity of Grubbs Catalysts. *Org Lett* **2006**, *8*, 5825-5828.
16. Heinis, C.; Rutherford, T.; Freund, S.; Winter, G. Phage-encoded combinatorial chemical libraries based on bicyclic peptides. *Nat Chem Biol* **2009**, *5*, 502-507.
17. Lian, W.; Upadhyaya, P.; Rhodes, C. A.; Liu, Y.; Pei, D. Screening Bicyclic Peptide Libraries for Protein-Protein Interaction Inhibitors: Discovery of a Tumor Necrosis Factor- $\alpha$  Antagonist. *J Am Chem Soc* **2013**, *135*, 11990-11995.
18. Chen, S.; Morales-Sanfrutos, J.; Angelini, A.; Cutting, B.; Heinis, C. Structurally Diverse Cyclisation Linkers Impose Different Backbone Conformations in Bicyclic Peptides. *ChemBioChem* **2012**, *13*, 1032-1038.
19. Vig, B. S.; Murray, T. F.; Aldrich, J. V. Synthesis of novel basic head-to-side-chain cyclic dynorphin A analogs: strategies and side reactions. *Biopolymers* **2003**, *71*, 620-637.
20. Vig, B. S.; Murray, T. F.; Aldrich, J. V. A novel N-terminal cyclic dynorphin A analogue cyclo<sup>N,5</sup>[Trp<sup>3</sup>,Trp<sup>4</sup>,Glu<sup>5</sup>] dynorphin A-(1-11)NH<sub>2</sub> that lacks the basic N-terminus. *J Med Chem* **2003**, *46*, 1279-1282.
21. Loktev, A.; Haberkorn, U.; Mier, W. Multicyclic Peptides as Scaffolds for the Development of Tumor Targeting Agents. *Curr Med Chem* **2017**, *24*, 2141-2155.
22. Aldrich, J. V.; McLaughlin, J. P. Peptide Kappa Opioid Receptor Ligands: Potential for Drug Development. *AAPS J* **2009**, *11*, 312-322.

## **Chapter 8 - Conclusions and future studies**

## 8.1 Introduction

The objective of this dissertation was the synthesis of conformationally constrained analogs of the KOR antagonist arodyn that could be potentially useful in the development of drug abuse therapy as well as pharmacological tools to study KOR receptors. Arodyn (Figure 8.1) is a potent and selective KOR antagonist that was shown to block stress-induced reinstatement of cocaine-seeking *in vivo*.<sup>1,2</sup> Conformational constraint using ring closing metathesis (RCM), which can potentially stabilize a bioactive conformation, increase metabolic stability, and increase membrane permeability,<sup>3</sup> was explored (Figure 8.1). Conformationally constrained arodyn analogs could facilitate further *in vivo* studies.

## 8.2 Conclusions and future studies

RCM is widely used, but side reactions such as olefin isomerization due to catalyst degradation products can limit yields of the RCM product in addition to complicating purification.<sup>4-6</sup> During the synthesis of arodyn analogs with constrained aromatic residues desallyl products due to olefin isomerization compromised RCM product yields (Figures 8.2 and 8.3). Therefore, we explored modifications of reaction parameters and the use of additives<sup>5,6</sup> to enhance yields of the RCM product in RCM involving Tyr(All) residues. In chapter 4, optimized reaction conditions in the model dipeptide studies resulted in a 4-fold increase in the yield of the RCM product compared to the original conditions<sup>7</sup> used to cyclize Dyn A analogs containing AllGly residues. High temperature and high catalyst concentration generally increased side product formation, whereas lower catalyst concentration in the presence of phenol promoted formation of the desired RCM product using Grubbs 2<sup>nd</sup> generation catalyst.

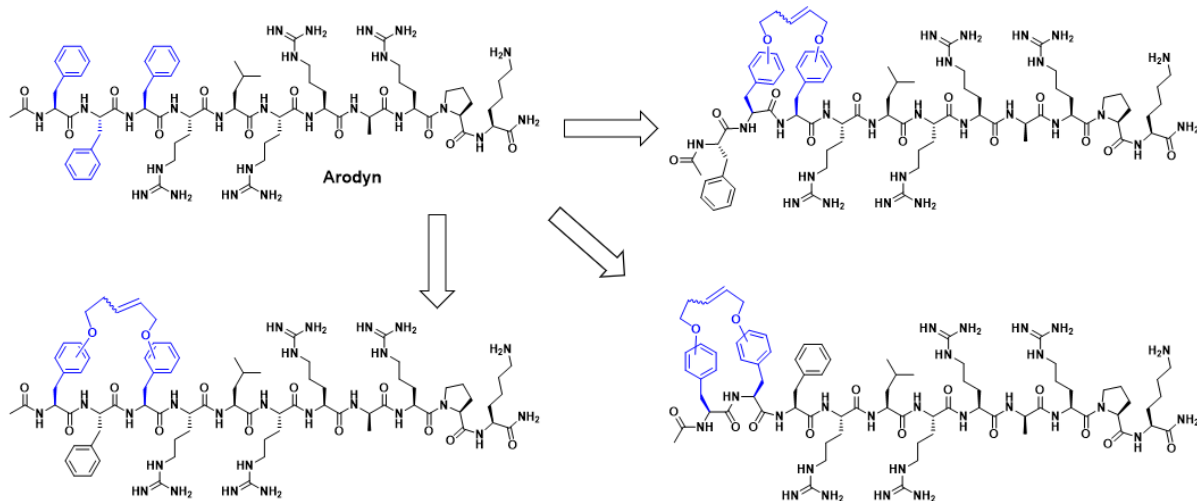


Figure 8.1 Conformational constraints of aromatic residues in arodyn.

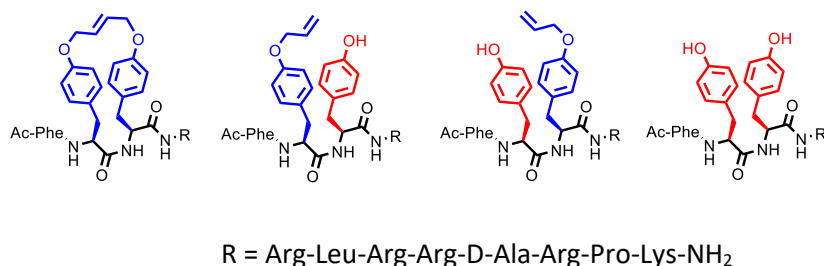


Figure 8.2 Products resulting from RCM of [Tyr(All)<sup>2,3</sup>]arodyn including desallyl products.

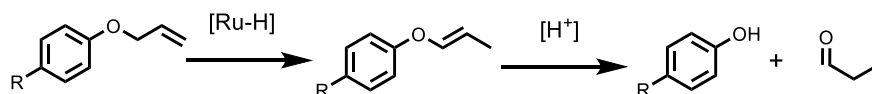


Figure 8.3 Olefin isomerization<sup>8,9</sup> resulting in deallylation during acid catalyzed cleavage from the solid-phase resin.<sup>10</sup>

Optimized RCM reaction conditions from the model dipeptide study and microwave heating were then employed in the synthesis of cyclic arodyn analogs for pharmacological evaluation in chapter 5. Molecular modeling and docking studies suggested that arodyn analogs cyclized between adjacent aromatic residues would retain affinity at the KOR, as these analogs displayed the same general structure as arodyn (Figure 8.4). Accordingly, constrained analogs were synthesized to examine the pharmacological effects of constraining aromatic residues.



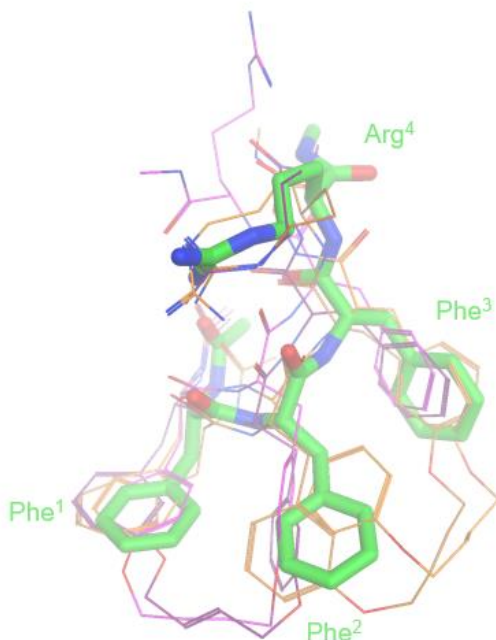


Figure 8.4 Overlay of arodyn and several analogs following docking in the KOR (not shown). Arodyn (green) and its p<sup>1</sup>p<sup>2</sup> (magenta), m<sup>1</sup>m<sup>2</sup> (purple), p<sup>2</sup>p<sup>3</sup> (orange), and m<sup>2</sup>m<sup>3</sup> (brown) analogs have the same general structure (in referring to arodyn analogs, e.g. p<sup>1</sup>p<sup>2</sup>, letters indicate phenyl ring substitution patterns while the superscript indicates residue position in arodyn).

Varying yields of the RCM products were observed using the optimized RCM conditions under conventional heating, especially during RCM involving *m*-Tyr(All) in the 1<sup>st</sup> or 2<sup>nd</sup> position of arodyn. Microwave irradiation was therefore explored to facilitate cyclization of arodyn analogs containing *m*-Tyr(All). Microwave-assisted RCM conditions using Hoveyda-Grubbs 2<sup>nd</sup> generation catalyst (HG II) were identified that resulted in enhanced cyclization yields compared to conventional heating.

Initial pharmacological analysis showed that cyclization between aromatic residues was generally well tolerated at the KOR, with affinities within 1- to 4-fold that of arodyn, with the exception of the p<sup>1</sup>m<sup>2</sup> and m<sup>1</sup>m<sup>2</sup> analogs (which exhibited a 5.7- and 6.8-fold decrease in KOR affinity, respectively). These results are consistent with the similar binding modes of the cyclic analogs in the docking study (Figure 8.4). The cyclic arodyn analogs examined in the GTPγS assay

exhibited negligible activation of KOR similar to arodyn, a potent and selective KOR antagonist. Further pharmacological analysis to determine receptor selectivity and antagonist potency is ongoing.

In chapter 6 head to side chain cyclization motifs involving Tyr(All) and AllGly were explored using microwave heating. Head to side chain cyclizations involving Tyr(All) residues generally resulted in low (<20%) yields, whereas cyclizations involving AllGly exhibited varying yields dependent on reaction temperature. The temperature dependent RCM product yields were consistent with the temperature dependence of Grubbs catalysts.<sup>11</sup> Elevated temperatures increased side products including CH<sub>2</sub> deletions and insertions (Figure 8.5), presumably due to catalyst degradation products.<sup>12</sup> Notably, microwave heating facilitated the synthesis of arodyn analogs that could not be obtained via conventional heating. Initial pharmacological analysis indicates that both the *cis* and *trans* isomers of *cyclo*[5hex,AllGly<sup>5</sup>]arodyn retained affinity at the KOR, exhibiting 5-fold lower affinity compared to arodyn.

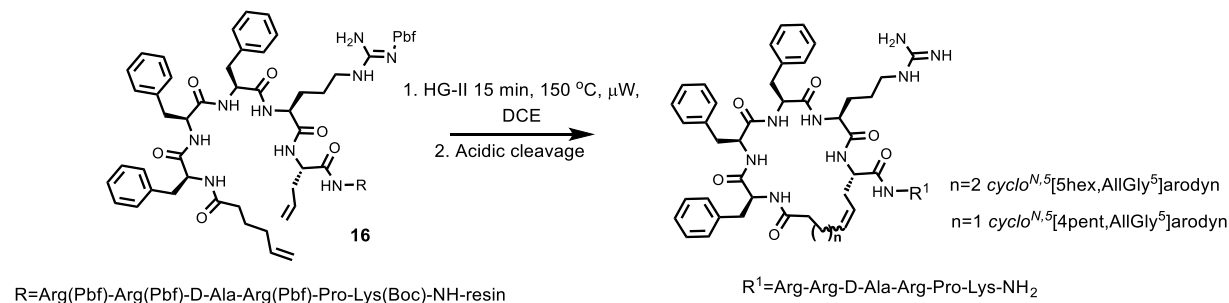


Figure 8.5 Head to side chain arodyn analogs involving AllGly residues showing a ring contraction product. 4pent=4penteoic acid and 5hex=5hexenoic acid.

Lastly, chapter 7 explored the synthesis of bicyclic arodyn analogs with constraints in both the N- and C-terminal segments using microwave irradiation. Polycyclic peptides are particularly promising due to their enhanced metabolic stability which can improve bioavailability.<sup>13, 14</sup> Given that there are no reports of bicyclic opioid peptide ligands,<sup>15</sup> novel bicyclic arodyn analogs with

interesting topologies could potentially be useful pharmacological tools. The structure-activity relationships (SAR) of monocyclic arodyn analogs were used in designing bicyclic arodyn analogs that could interact with KOR. Notably, optimized microwave-assisted RCM conditions from chapters 5 and 6 were successfully used to synthesize a bicyclic arodyn analog, *cyclo*[Tyr(All)<sup>2,3</sup>,AllGly<sup>5,8</sup>]arodyn, with two side-chain to side-chain constraints. Sequential RCM facilitated regioselective cyclization in the synthesis of *cyclo*[Tyr(All)<sup>2,3</sup>,AllGly<sup>5,8</sup>]arodyn, thereby limiting unwanted cyclizations. Encouragingly, initial pharmacological evaluation showed that this bicyclic analog retained affinity at the KOR ( $K_i = 26.4 \pm 5.9$  nM), with slightly higher affinity (approximately 2-fold) than the related monocyclic arodyn analogs *cyclo*[Tyr(All)<sup>2,3</sup>,Ile<sup>8</sup>]arodyn and *cyclo*[AllGly<sup>5,8</sup>]arodyn. Further pharmacological analysis of the synthesized bicyclic arodyn analogs is in progress.

Lactam chemistry was used to synthesize a second bicyclic arodyn analog using trimesic acid (TMA), a rigid aromatic linker. The lactam-based bicyclic arodyn analog *cyclo*<sup>N,5,8</sup>[TMA,Dap<sup>5,8</sup>]arodyn contained head to side-chain and side-chain to side-chain constraints. In initial pharmacological evaluation however, *cyclo*<sup>N,5,8</sup>[TMA,Dap<sup>5,8</sup>]arodyn displayed a substantial loss (51-fold) in KOR affinity, suggesting that the constraint resulted in unfavorable interactions in the KOR similar to arodyn analogs with lactam constraints involving residue 2 in the “message”<sup>16</sup> sequence of arodyn.<sup>10</sup>

This dissertation research has identified several constrained analogs of arodyn that can compliment non-peptide KOR selective ligands, facilitate studying ligand-receptor interactions, and could ultimately aid the development of new therapeutic agents. There has been an increased interest in peptide drug discovery<sup>17</sup> and cyclic peptides<sup>18</sup> in the recent past. Since arodyn can be rapidly metabolized, thus precluding systemic administration, cyclic arodyn analogs could be

useful for further *in vivo* studies. Future studies will also include metabolic stability studies, and metabolically stable arodyn analogs can be examined in blood-brain barrier permeability studies.

### 8.3 References

1. Bennett, M. A.; Murray, T. F.; Aldrich, J. V. Identification of Arodyn, a Novel Acetylated Dynorphin A-(1–11) Analogue, as a  $\kappa$  Opioid Receptor Antagonist. *J Med Chem* **2002**, 45, 5617-5619.
2. Carey, A. N.; Borozny, K.; Aldrich, J. V.; McLaughlin, J. P. Reinstatement of Cocaine Place-Conditioning Prevented by the Peptide kappa-Opioid Receptor Antagonist Arodyn. *Eur J Pharmacol* **2007**, 569, 84-89.
3. Schafmeister, C. E.; Po, J.; Verdine, G. L. An All-Hydrocarbon Cross-Linking System for Enhancing the Helicity and Metabolic Stability of Peptides. *J Am Chem Soc* **2000**, 122, 5891-5892.
4. Hong, S. H.; Day, M. W.; Grubbs, R. H. Decomposition of a Key Intermediate in Ruthenium-Catalyzed Olefin Metathesis Reactions. *J Am Chem Soc* **2004**, 126, 7414-7415.
5. Hong, S. H.; Sanders, D. P.; Lee, C. W.; Grubbs, R. H. Prevention of Undesirable Isomerization during Olefin Metathesis. *J Am Chem Soc* **2005**, 127, 17160-17161.
6. Martinez-Mayorga, K.; Byler, K. G.; Yongye, A. B.; Giulianotti, M. A.; Dooley, C. T.; Houghten, R. A. Ligand/kappa-Opioid Receptor Interactions: Insights From the X-ray Crystal Structure. *Eur J Med Chem* **2013**, 66, 114-121.
7. Fang, W.-J.; Cui, Y.; Murray, T. F.; Aldrich, J. V. Design, Synthesis, and Pharmacological Activities of Dynorphin A Analogs Cyclized by Ring-Closing Metathesis. *J Med Chem* **2009**, 52, 5619-5625.
8. Martinez-Amezaga, M.; Delpiccolo, C.; Méndez, L.; Dragutan, I.; Dragutan, V.; Mata, E. Unprecedented Multifunctionality of Grubbs and Hoveyda–Grubbs Catalysts: Competitive Isomerization, Hydrogenation, Silylation and Metathesis Occurring in Solution and on Solid Phase. *Catalysts* **2017**, 7, 111.
9. Kadyrov, R. Low Catalyst Loading in Ring-Closing Metathesis Reactions. *Chem Eur J* **2013**, 19, 1002-1012.

10. Fang, W. Design and Synthesis of Novel Linear and Cyclic Peptide Ligands for Kappa Opioid Receptors. University of Kansas, 2008.
11. Chapman, R. N.; Arora, P. S. Optimized Synthesis of Hydrogen-Bond Surrogate Helices: Surprising Effects of Microwave Heating on the Activity of Grubbs Catalysts. *Org Lett* **2006**, *8*, 5825-5828.
12. O'Doherty, I.; Yim, J. J.; Schmelz, E. A.; Schroeder, F. C. Synthesis of Caeliferins, Elicitors of Plant Immune Responses: Accessing Lipophilic Natural Products via Cross Metathesis. *Org Lett* **2011**, *13*, 5900-5903.
13. Bird, G. H.; Madani, N.; Perry, A. F.; Princiotta, A. M.; Supko, J. G.; He, X.; Gavathiotis, E.; Sodroski, J. G.; Walensky, L. D. Hydrocarbon Double-Stapling Remedies the Proteolytic Instability of a Lengthy Peptide Therapeutic. *Proc Natl Acad Sci* **2010**, *107*, 14093-14098.
14. Rhodes, C. A.; Pei, D. Bicyclic Peptides as Next-Generation Therapeutics. *Chem Eur J* **2017**, *23*, 12690-12703.
15. Remesic, M.; Lee, Y. S.; Victor, H. J. Cyclic Opioid Peptides. *Curr Med Chem* **2016**, *23*, 1288-1303.
16. Chavkin, C.; Goldstein, A. Specific Receptor for the Opioid Peptide Dynorphin: Structure-Activity Relationships. *Proc Natl Acad Sci* **1981**, *78*, 6543-6547.
17. Henninot, A.; Collins, J. C.; Nuss, J. M. The Current State of Peptide Drug Discovery: Back to the Future? *J Med Chem* **2017**, 1382-1414.
18. Tapeinou, A.; Matsoukas, M.-T.; Simal, C.; Tselios, T. Review Cyclic Peptides on a Merry-Go-Round; Towards Drug Design. *Biopolymers* **2015**, *104*, 453-461.

## **Appendix 1 - Chromatograms of RCM product mixtures from the model dipeptide study<sup>a,b</sup>**

<sup>a</sup>Chromatograms from RCM reaction table entries (baseline resolution was not achieved so yields shown are an estimate)

<sup>b</sup>Compound numbers apply only to this appendix

Table A1.1 Analytical data of synthesized linear and cyclic peptides

Peptide	Compound	HPLC $t_R$ (min) <sup>a</sup>	Mass	
			Calculated	Observed
1	Fmoc-Tyr(All)-Tyr(All)-OH	23.0	[M+Na] <sup>+</sup> 669.25	[M+Na] <sup>+</sup> 669.25
2	<i>cyclo</i> -Fmoc-Tyr(All)-Tyr(All)-OH	18.0	[M+Na] <sup>+</sup> 641.22	[M+Na] <sup>+</sup> 641.22
3	Fmoc-Tyr(All)-Tyr-OH	14.7	[M+Na] <sup>+</sup> 629.22	[M+Na] <sup>+</sup> 629.22
4	Fmoc-Tyr-Tyr(All)-OH	14.7	[M+Na] <sup>+</sup> 629.22	[M+Na] <sup>+</sup> 629.22
5	Fmoc-Tyr-Tyr-OH	6.0	[M+Na] <sup>+</sup> 589.19	[M+Na] <sup>+</sup> 589.19
6	Fmoc-Tyr(All)-Phe-Tyr(All)-OH	26.4	[M+Na] <sup>+</sup> 816.32	[M+Na] <sup>+</sup> 816.33
7	<i>cyclo</i> -Fmoc-Tyr(All)-Phe-Tyr(All)-OH	21.6	[M+Na] <sup>+</sup> 788.29	[M+Na] <sup>+</sup> 788.29
8	[Tyr(All) <sup>2,3</sup> ]arodyn	32.2 <sup>b</sup>	[M+H] <sup>+</sup> 1647.01	[M+H] <sup>+</sup> 1647.86
9	<i>cyclo</i> [Tyr(All) <sup>2,3</sup> ]arodyn	29.3 <sup>b</sup>	[M+3H] <sup>3+</sup> 540.30	[M+3H] <sup>3+</sup> 540.50

<sup>a</sup>30-70% Aqueous MeCN with 0.1% TFA over 40 min  
<sup>b</sup>5-50 Aqueous MeCN with 0.1% TFA over 45 min

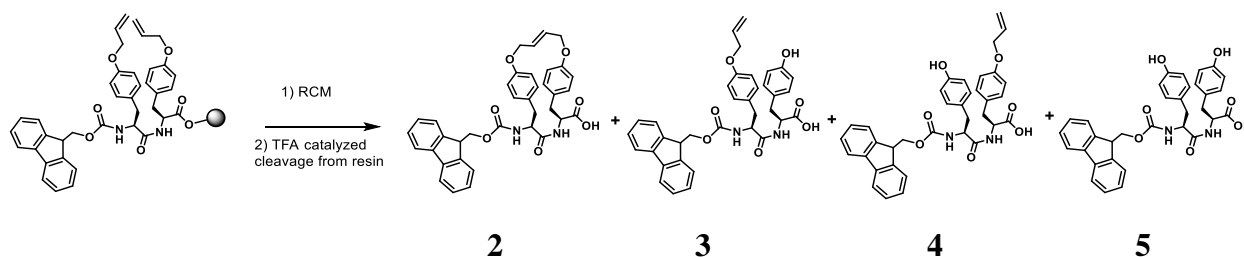


Figure A1.1 Reaction mixture resulting from RCM of **1** showing the RCM product **2** and desallyl products **3**, **4**, and **5**.

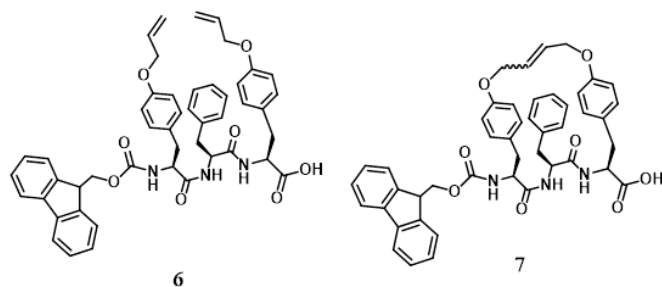
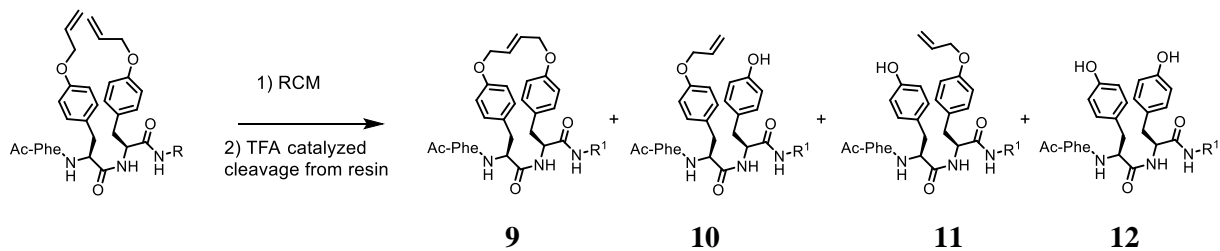


Figure A1.2 Structures of the linear tripeptide **6** and the cyclic tripeptide **7**.



R = Arg(Pbf)-Leu-Arg(Pbf)-Arg(Pbf)-D-Ala-Arg(Pbf)-Pro-Lys(Boc)-NH-resin

R<sup>1</sup> = Arg-Leu-Arg-Arg-D-Ala-Arg-Pro-Lys-NH<sub>2</sub>

Figure A1.3 Reaction mixture resulting from RCM of **8** showing the RCM product **9** and desallyl products **10**, **11**, and **12**.

Table A1.2 Product profiles for RCM using 2<sup>nd</sup> generation Grubbs catalyst (G II).<sup>a</sup>

Entry	Substrate	Temp. (°C)	RCM pdt. (%)	Total desallyl pdt. (%)	SM <sup>b</sup> (%)
1	[Tyr(All) <sup>2,3</sup> ]arodyn <sup>c</sup>	60	32	31	- <sup>c</sup>
2	[Tyr(All) <sup>2,3</sup> ]arodyn <sup>c</sup>	40	18	44	-
3	Fmoc-Tyr(All)-Tyr(All) <sup>c</sup>	60	20	25	-
4	Fmoc-Tyr(All)-Tyr(All) <sup>c</sup>	40	-	18	16

<sup>a</sup>3 mM, 40 mol% G II 2 d, DCM/DMF (4:1); <sup>b</sup>SM: starting material; <sup>c</sup>- < 10%



Table A1.2 entry 1: RCM of **8**; 60 °C, DCM/DMF(4/1), 40 mol %, 3 mM G II

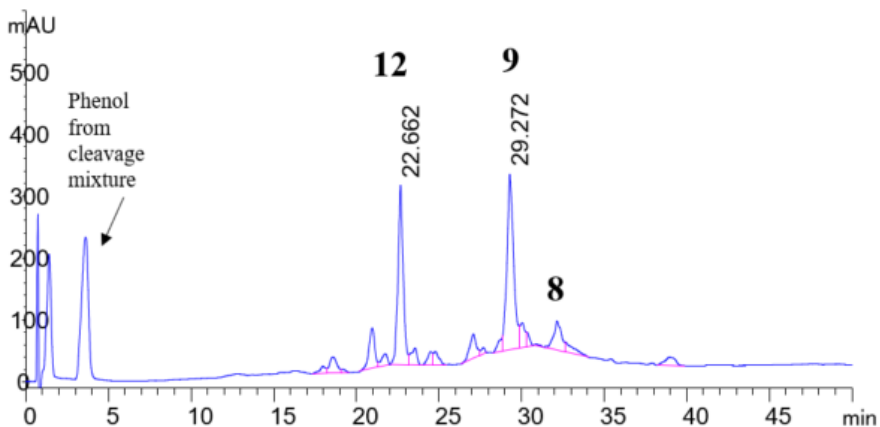


Table A1.2 entry 2: RCM of **8**; 40 °C, DCM/DMF(4/1), 40 mol %, 3 mM G II

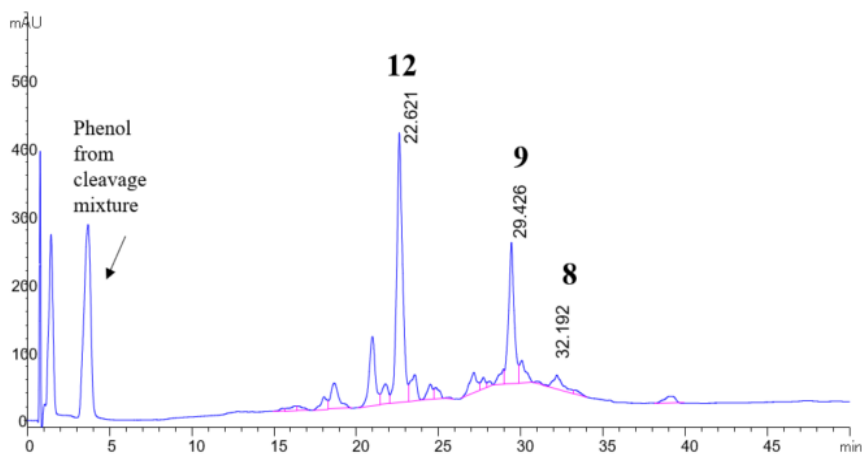


Table A1.2 entry 3: RCM of **1**; 60 °C, DCM/DMF(4/1), 40 mol %, 3 mM G II. Note multiple peaks when DMF is used as solvent.

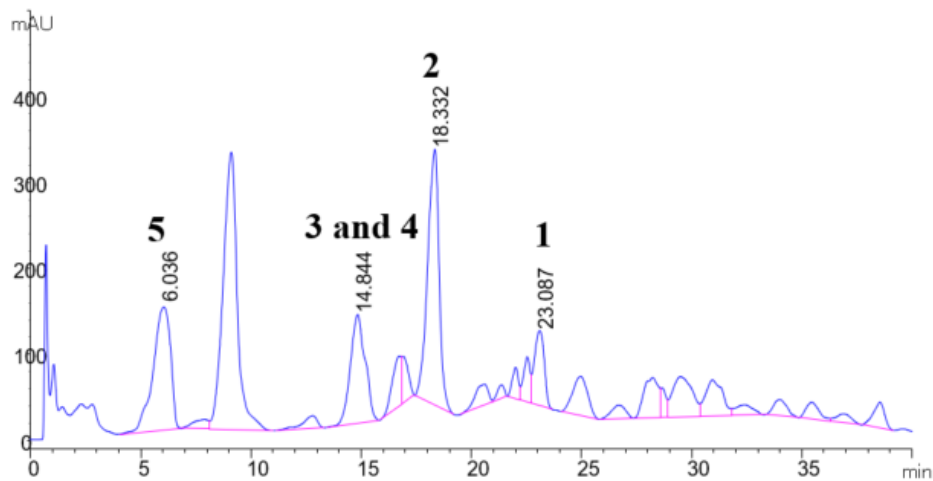


Table A1.2 entry 4: RCM of 1; 40 °C, DCM/DMF(4/1), 40 mol %, 3mM G II.

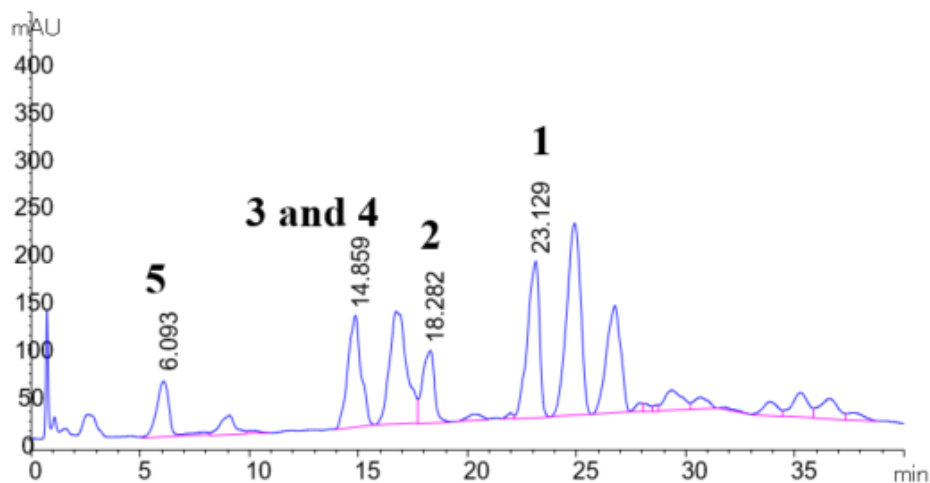


Table A1.3. Effect of temperature and catalyst concentration on model dipeptide RCM product yields.<sup>a</sup>

Entry	Temp. (°C)	[Cat.] (mM)	Yield (%) <sup>b</sup>		
			RCM pdt.	Total desallyl pdt.	S.M <sup>c</sup>
1	60	3	-	82	- <sup>d</sup>
2	60	1	-	39	-
3	60	0.3	-	78	-
4	40	3	63	16	-
5	40	1	55	13	-
6	40	0.3	24	10	60
7	40	0.1	-	18	69

<sup>a</sup> G II 15 mol%, in DCE (60 °C) or DCM (40 °C) for 2d; <sup>b</sup> Determined from HPLC; <sup>c</sup>S.M: Starting material; <sup>d</sup>< 10%

Table A1.3 entry 1: Fmoc-Tyr(All)-Tyr(All) RCM; 60 °C, DCE, 15 mol %, 3 mM G II

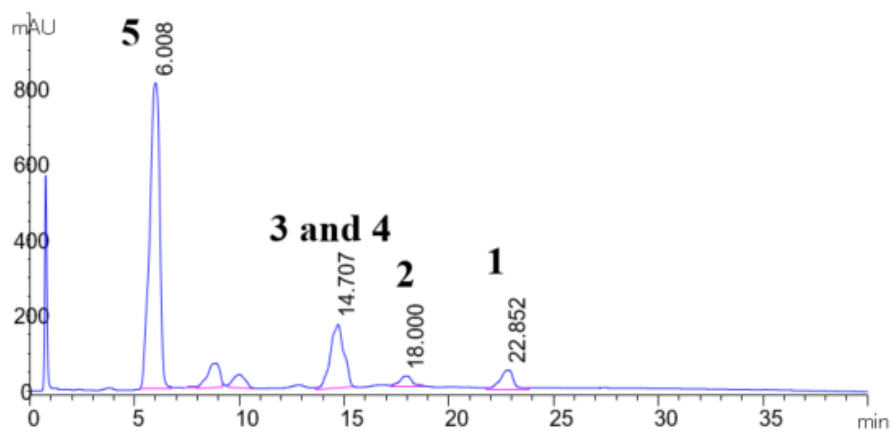


Table A1.3 entry 2: RCM of **1**; 60 °C, DCE, 15 mol %, 1 mM G II

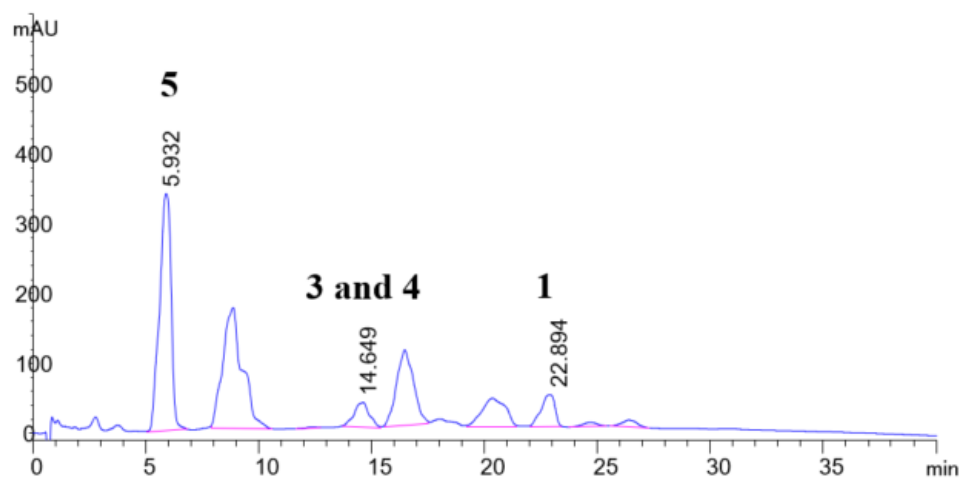


Table A1.3 entry 3: RCM of **1**; 60 °C, DCE, 15 mol %, 0.3 mM G II

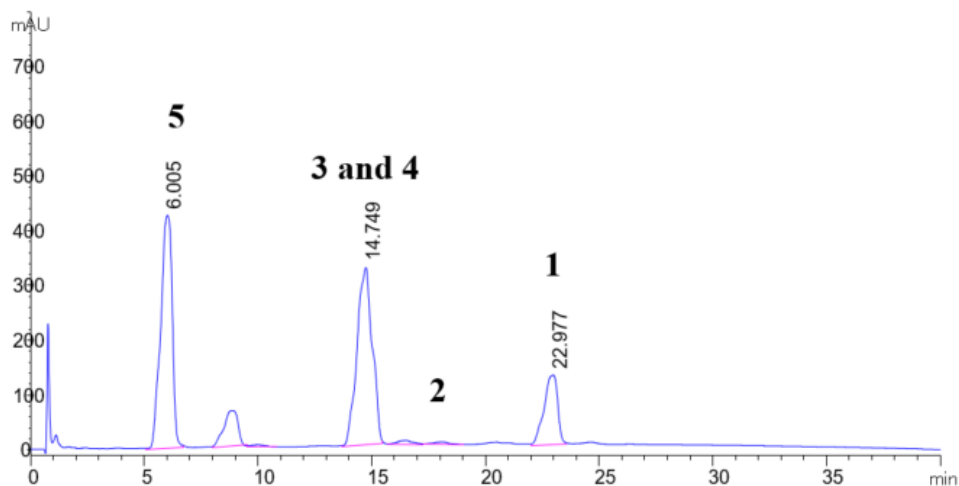


Table A1.3 entry 4: RCM of **1**; 40 °C, DCM, 15 mol %, 3 mM G II

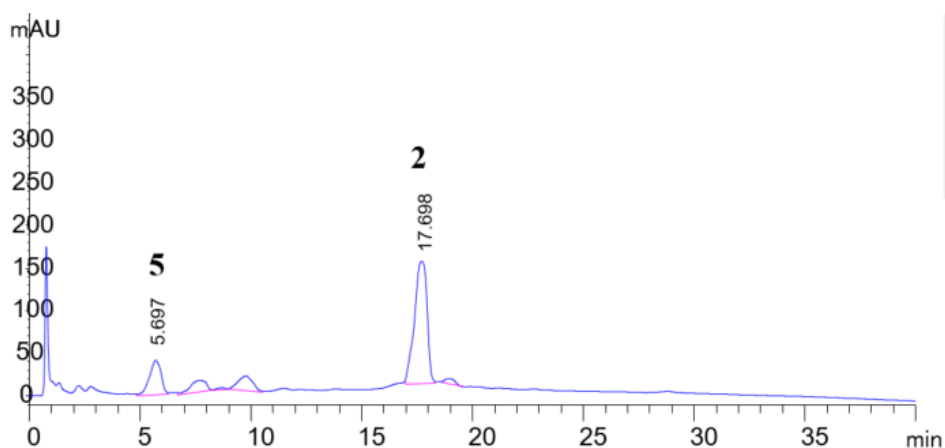


Table A1.3 entry 5: RCM of **1**; 40 °C, DCM, 15 mol %, 1 mM G II

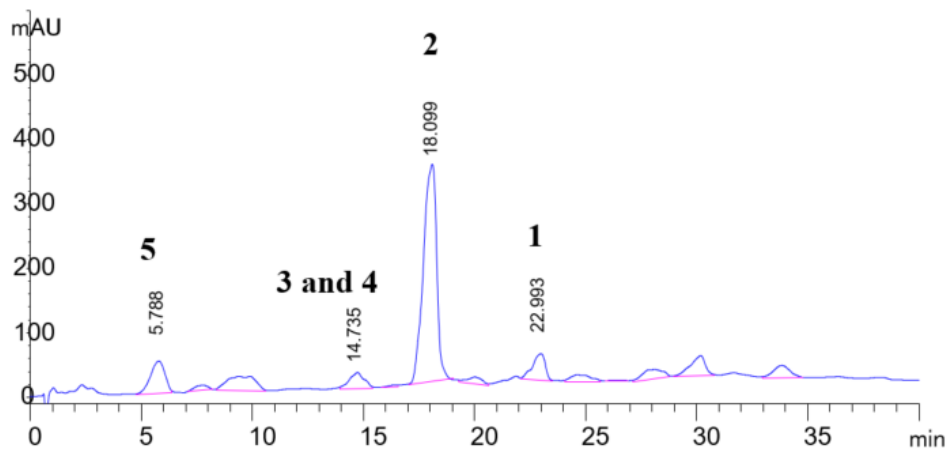


Table A1.3 entry 6: RCM of **1**; 40 °C, DCM, 15 mol %, 0.3 mM G II

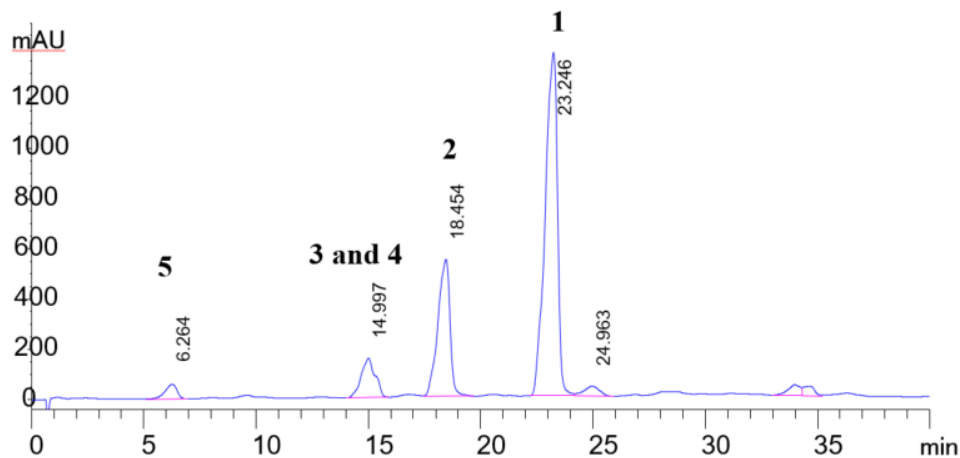


Table A1.3 entry 7: RCM of **1**; 40 °C, DCM, 15 mol %, 0.1 mM G II

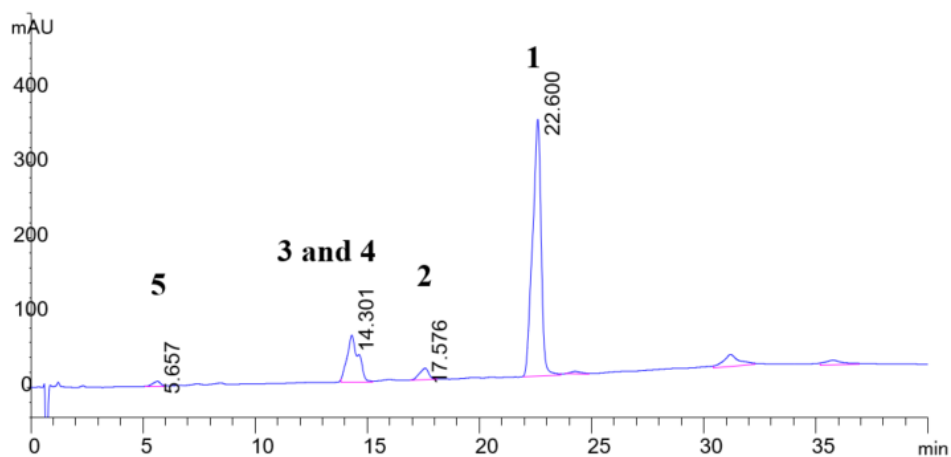


Table A1.4 Effect of phenol, temperature,<sup>a,b</sup> and catalyst concentration on model dipeptide RCM product yields.

Entry	[Cat.] (mM) <sup>c</sup>	Additive (1 equiv)	Yield (%)		SM <sup>d</sup>
			RCM pdt.	Total desallyl pdt.	
1	3	phenol	42	20	- <sup>e</sup>
2	1	phenol	60	-	-
3	0.3	phenol	79	-	-
4	0.1	phenol	31	15	43

<sup>a</sup>Results shown are in DCM at 40 °C for 2 d; <sup>b</sup>at 60 °C in DCE, phenol did not effectively suppress desallyl side products formation; <sup>c</sup>15 mol% G II for 2 d; <sup>d</sup>SM: starting material; <sup>e</sup>- < 10%

Table A1.4 entry 1: RCM of **1**; 40 °C, DCM, 15 mol %, 3 mM G II, phenol

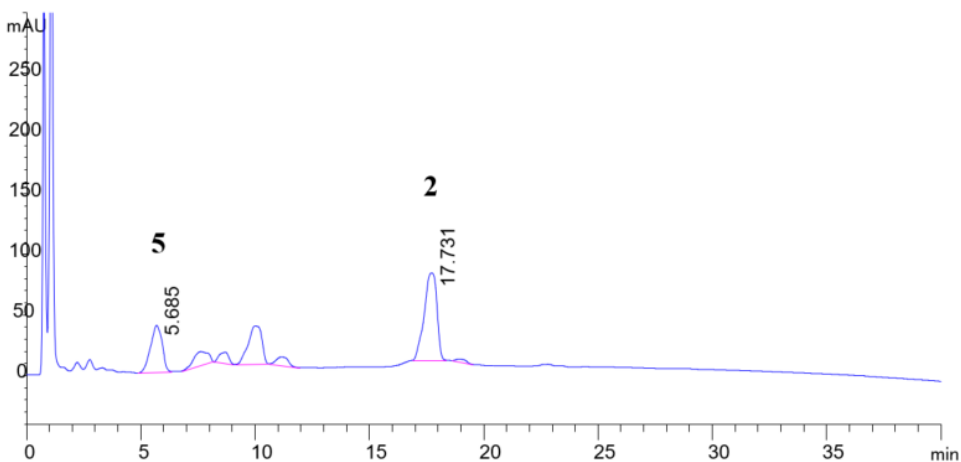


Table A1.4 entry 2: RCM of **1**; 40 °C, DCM, 15 mol %, 1 mM G II, phenol

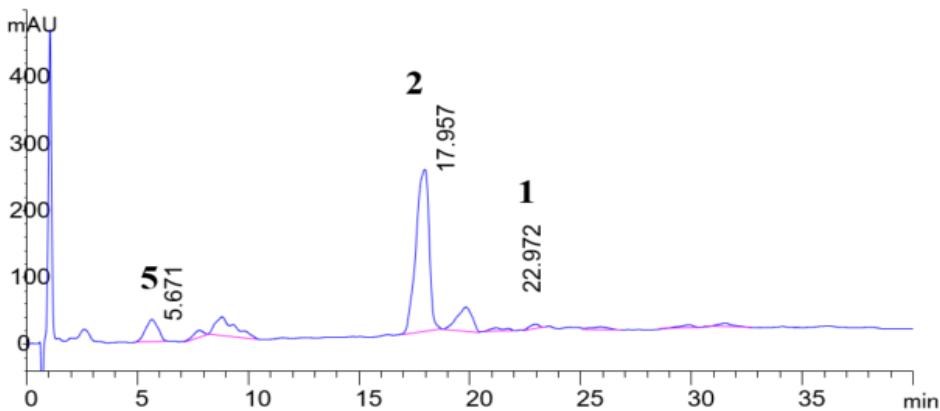


Table A1.4 entry 3: RCM of **1**; 40 °C, DCM, 15 mol %, 0.3 mM G II, phenol

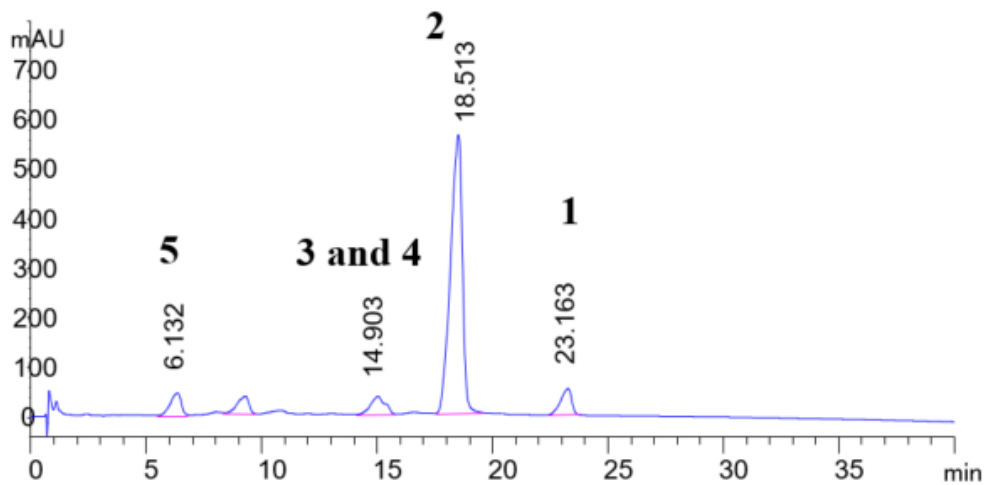


Table A1.4 entry 4: RCM of **1**; 40 °C, DCM, 15 mol %, 0.1 mM G II, phenol

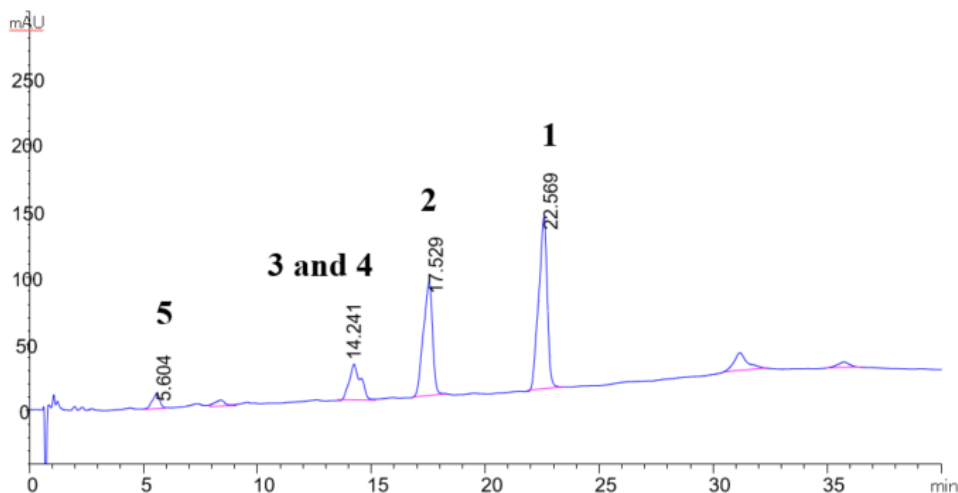


Table A1.5. Model dipeptide RCM product yields with Hoveyda-Grubbs 2<sup>nd</sup> generation catalyst (HG II) at 40 and 60 °C.

Entry	Temp. (°C) <sup>a</sup>	[Cat.] (mM)	Additive (1 equiv.)	RCM pdt.	Total desallyl pdt.	S.M <sup>b</sup>
1	60	0.3	-	86	-	-
2	60	0.3	phenol	25	26	14
3	40	0.3	-	80	-	-
4	40	0.3	phenol	72	15	-

-< 10%; <sup>a</sup> Solvent: DCE for 60, DCM for 40 °C, 2d; <sup>b</sup> S.M: Starting material

Table A1.5 entry 1: RCM of **1**; 60 °C, DCM, 15 mol %, 0.3 mM HG II

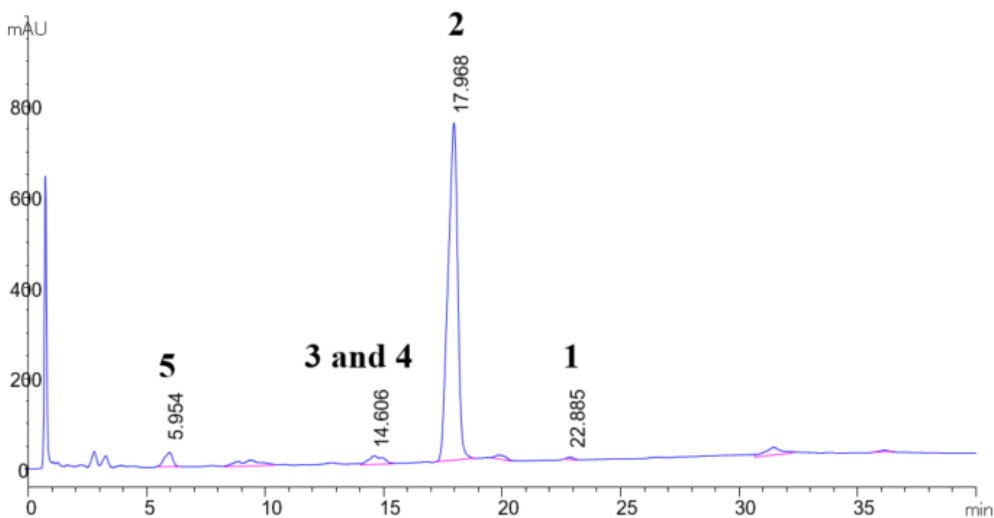


Table A1.5 entry 2: RCM of **1**; 60 °C, DCM, 15 mol %, 0.3 mM HG II, phenol

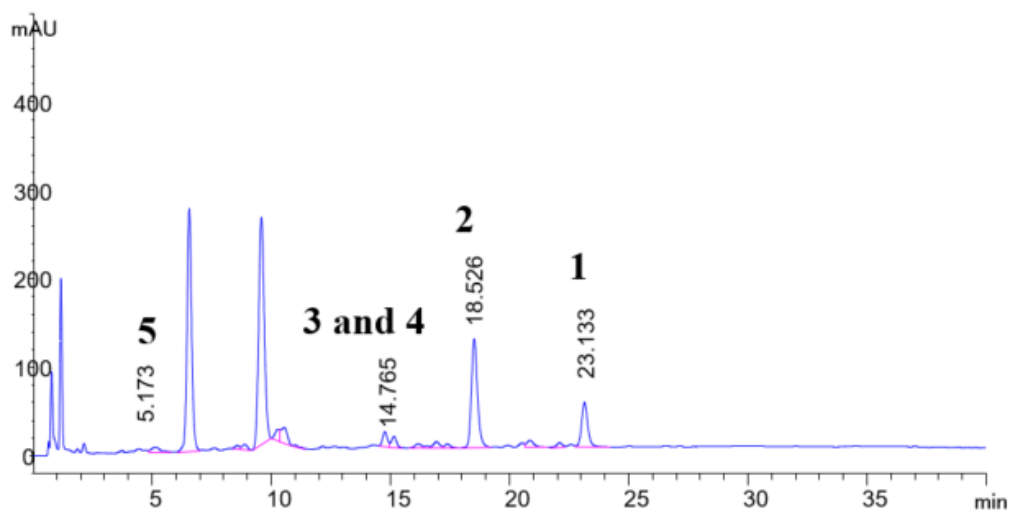


Table A1.5 entry 3: RCM of **1**; 40 °C, DCM, 15 mol %, 0.3 mM HG II

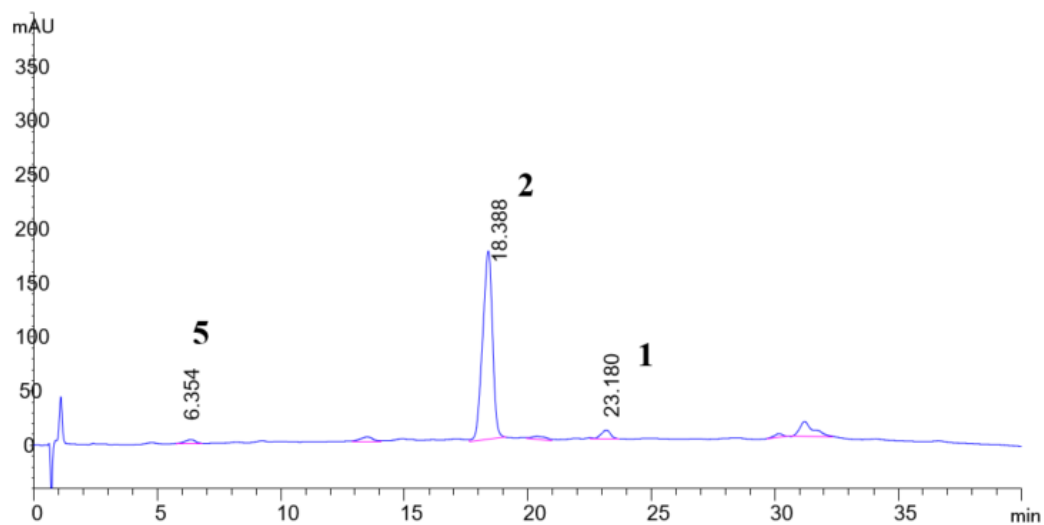




Table A1.5 entry 4: RCM of **1**; 40 °C, DCM, 15 mol %, 0.3 mM HG II, phenol

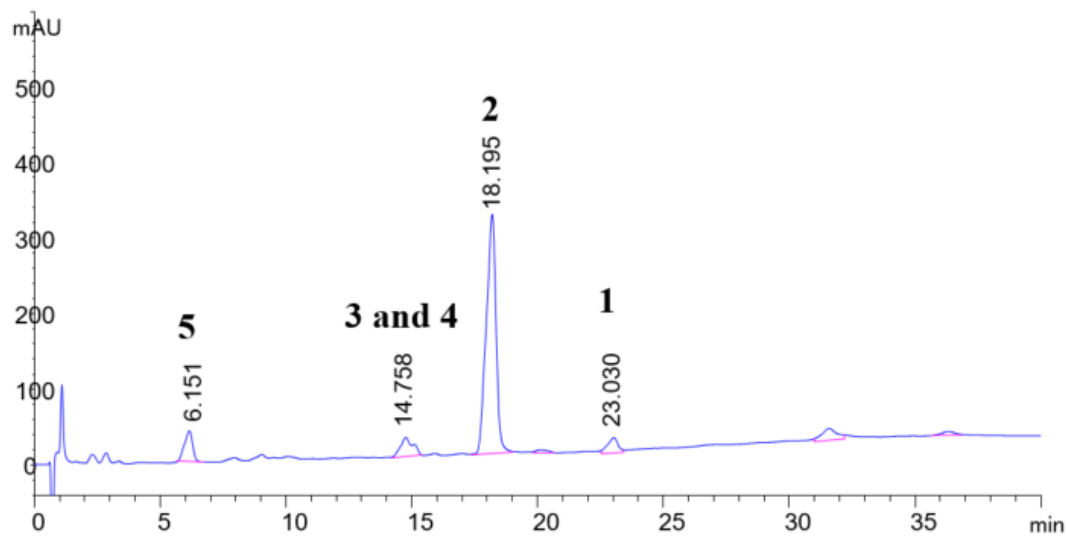


Table A1.6. Tripeptide RCM product yields with optimized conditions with G II and HG II.<sup>a</sup>

Entry	Catalyst	Temp.(°C)	Additive (1 equiv.)	RCM Pdt.	Total desallyl pdt.
1	HG II	60	-	27	28
2	HG II	40	-	84	- <sup>b</sup>
3	HG II	40	phenol	67	-
4	G II	40	phenol	65	-

<sup>a</sup> 0.3 mM 15 mol% G II or HG II in DCE (60 °C) or DCM (40 °C) for 2d; <sup>b</sup> - < 10%;

Table A1.6 entry 1: RCM of **6**; 60 °C, DCM, 15 mol %, 0.3 mM HG II

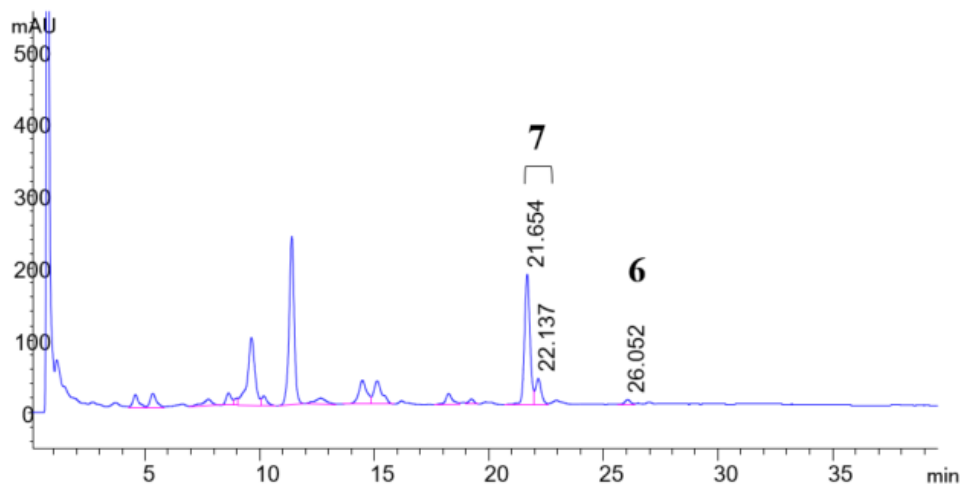


Table A1.6 entry 2: RCM of **6**; 40 °C, DCM, 15 mol %, 0.3 mM HG II, phenol

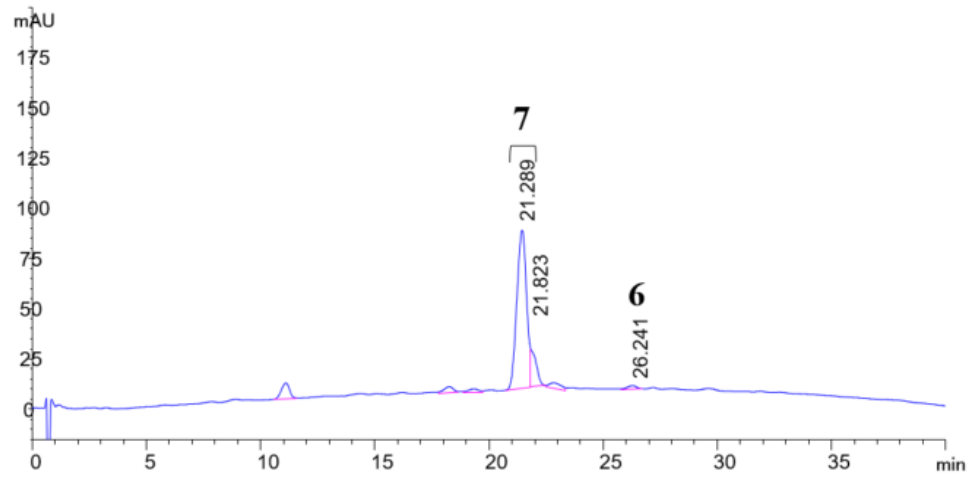


Table A1.6 entry 3: RCM of **6**; 40 °C, DCM, 15 mol %, 0.3 mM HG II, phenol

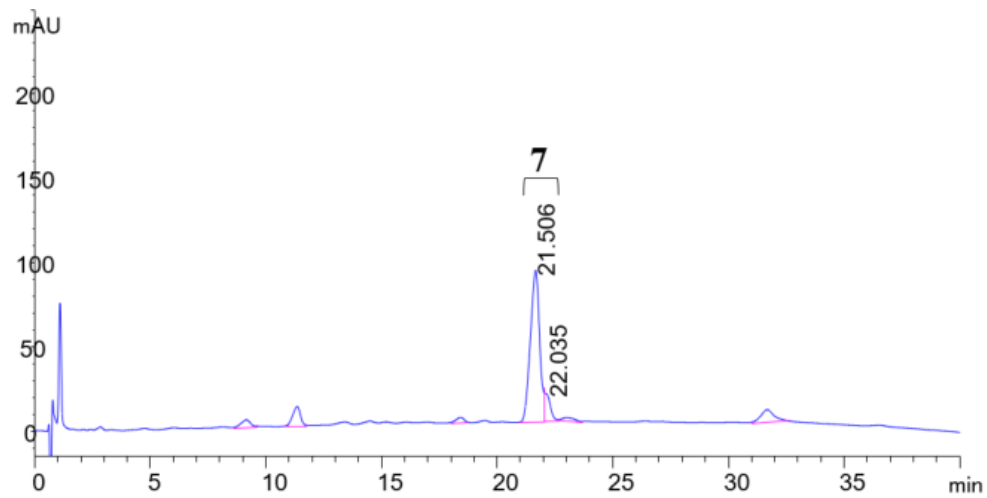


Table A1.6 entry 4: RCM of **6**; 40 °C, DCM, 15 mol %, 0.3 mM G II, phenol

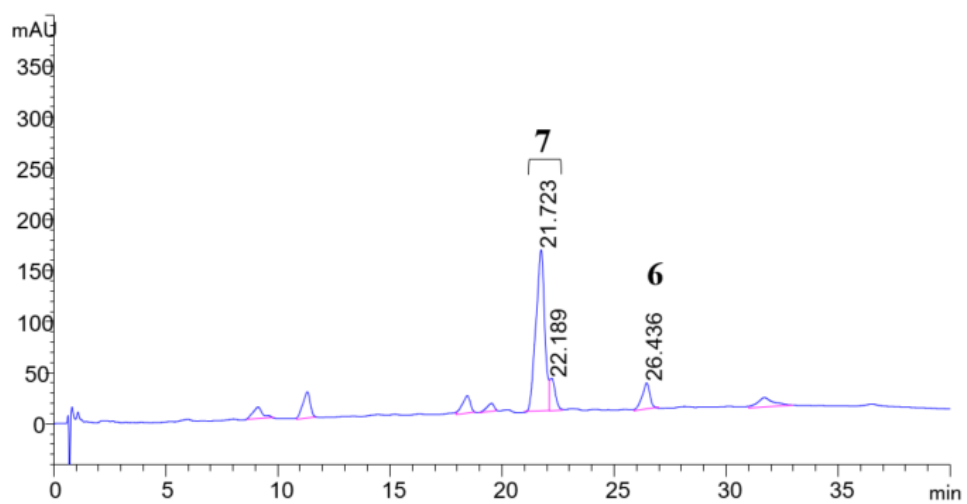


Table A1.7 Summary showing yields<sup>a</sup> of model dipeptide (**1**) RCM under various conditions using Grubbs 2<sup>nd</sup> generation catalyst (G II).

Entry	[Cat. Conc.] (days) <sup>b</sup>	Additive (equiv)	RCM pdt.	Total desall pdt.	SM	Solvent	T (°C)	Catalyst (Mol %)
1	3	-	20	25	- <sup>c</sup>	DCM/DMF(4/1)	60	40
2	3	-	-	50	-	DCE	80	15
3	3	-	-	82	-	DCE	60	15
4	3	1,4-bzq <sup>d</sup> (1)	11	-	67	DCE	60	15
5	3	Phenol (1)	10	55	23	DCE	60	15
6	3	phenol (3)	35	23	-	DCE	60	15
7	3 (1d)	-	30	37	-	DCE	60	15
8	3 (1d)	phenol (10)	38	19	18	DCE	60	15
9	1	-	-	39	-	DCE	60	15
10	1	phenol (1)	11	25	26	DCE	60	15
11	0.3	-	-	78	-	DCE	60	15
12	0.3	phenol (10)	-	18	16	DCE	60	15
13	0.3	phenol (1)	-	35	37	Toluene	60	15
14	0.3	-	-	49	24	Toluene	60	15
15	3	-	-	18	16	DCM/DMF(4/1)	40	40
16	3	-	63	16	-	DCM	40	15
17	3	phenol (1)	42	20	-	DCM	40	15
18	3 (1d)	-	63	-	-	DCM	40	15
19	1	phenol (1)	60	-	-	DCM	40	15
20	1	-	55	13	-	DCM	40	15
21	0.3	1,4-bzq (1)	-	-	81	DCM	40	15
22	0.3	phenol (1)	79	-	-	DCM	40	15
23	0.3	phenol (3)	86	-	-	DCM	40	15
24	0.3	phenol (10)	78	-	-	DCM	40	15
25	0.3	phenol (1)	-	-	69	Toluene	40	15

26	0.3	-	24	10	60	DCM	40	15
27	0.1	phenol (1)	31	15	43	DCM	40	15
28	0.1	-	-	18	69	DCM	40	15
<sup>a</sup> HPLC: 30-70% Aqueous MeCN with 0.1% TFA over 40 min; <sup>b</sup> 2 d unless otherwise indicated; <sup>c</sup> <10 % product; <sup>d</sup> 1,4-benzoquinone								

**Appendix 2 - Modeling of arodyn analogs cyclized by RCM between Tyr(All) residues\***

\*Performed by Dr. Michael Ferracane, Department of Chemistry, University of Redlands, Redlands, California 92373.

## A2.1 Methods

All conformational work was performed using the 2015 Molecular Operating Environment (MOE) software suite.<sup>1</sup> Briefly, the appropriate four residue fragments of arodyn (Ac-Phe-Phe-Phe-Arg-NHCH<sub>3</sub>) and its cyclic p<sup>1</sup>p<sup>2</sup>, m<sup>1</sup>m<sup>2</sup>, p<sup>2</sup>p<sup>3</sup>, and m<sup>2</sup>m<sup>3</sup> analogs were constructed, subjected to conformational search, and docked into the prepared KOR crystal structure (PDB ID: 4DJH) using a pharmacophore.<sup>2</sup> The original crystal structure was solved as a homodimer, and all work was done with the structure 4DJH.A, as it is better resolved than 4DJH.B.

### A2.1.1 Conformational searches

For arodyn and its cyclic analogs, each appropriate fragment was constructed and subjected to 30,000 iterations of stochastic stretching and rotation of its bonds in the Amber10:EHT forcefield.<sup>3</sup> The resulting conformers were considered plausible and unique if they (a) obtained calculated energies within 25 kcal/mol of the species' global minimum, (b) contained only *trans* amide bonds (180±20°) outside the exocyclic region, and (c) possessed heavy atom (C, N, and O) RMSD values greater than 0.05 Å. The calculated energy and atomic coordinates of each species' conformers were saved to a corresponding database that contained between 700-10,000 unique conformers for each of the five species.

### A2.1.2 Receptor preparation

The reported crystal structure of the KOR requires preparation before it can be used in docking experiments. First, the unresolved residues in ECL3 (Thr302-Thr306) were constructed and spliced – in their lowest energy conformation – into the receptor structure. Following this, the first resolved residue of the N terminus (Ser55) and the last resolved residue of the C terminus (Pro347) were “capped” by affixing an acetyl group to the truncated N terminus and an *N*-methyl

amide to the truncated C terminus. Then, any unresolved atoms of side chains (Ile85, Thr88, Lys89, Lys165, Leu167, Phe169, Lys200, Asp217, Arg257, Leu259, Lys265, Arg267, Arg270, Arg271, Val296, Ser301, Thr302, Ser303, His304, Ser305, Thr306, Glu335, Arg342) were added, also in their lowest energy conformation. Finally, hydrogen atoms were added to the receptor, ligand, and solvent so that all atoms achieved their proper valency and charge (pH = 7, T = 300K). This work yielded the prepared  $\kappa$  opioid receptor (KOR), which was used in subsequent docking studies.

### **A2.1.3 Pharmacophore generation**

A pharmacophore (Figure A2.1) was created to guide placement of the conformers into the receptor during docking. The pharmacophore consisted of four elements: two aromatic sites and two cationic sites. The first aromatic element (radius = 1.5 Å) was defined using the atomic coordinates of the phenolic ring of the 7-hydroxytetrahydroisoquinoline moiety of JD<sub>Tic</sub> from its cocrystal structure with the KOR.<sup>2</sup> Following this, the cocrystal structures of BU72 in the  $\mu$  opioid receptor (PDB ID: 5C1M)<sup>4</sup> and DIPP-NH<sub>2</sub> in the  $\delta$  opioid receptor (PDB ID: 4RWA)<sup>5</sup> were overlaid with that of JD<sub>Tic</sub> in the KOR. The second aromatic element (radius = 1.5 Å) was then generated between the pendant phenyl group of BU72 and the phenyl ring of Phe<sup>3</sup> in DIPP-NH<sub>2</sub>, groups with centroids that lie within 2.2 Å of each other when overlaid. The two cationic sites lie adjacent to Glu209 (radius = 2.5 Å) and Glu297 (radius = 2.5 Å), non-conserved acidic residues in ECLs 2 and 3 that flank the orthosteric site.



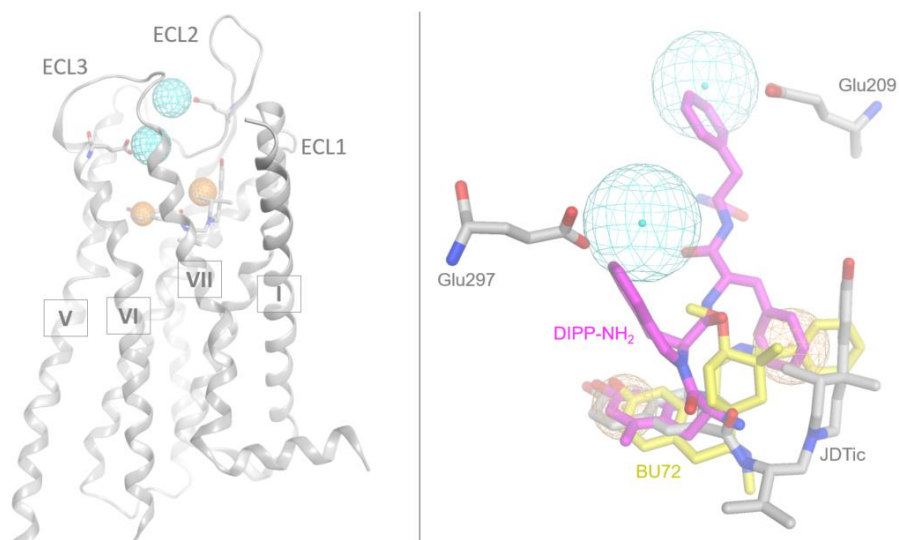


Figure A2.1 Structure of KOR model and pharmacophore for docking. *Left:* KOR model (gray loops) highlighting the acidic residues Glu209 and Glu297 (gray sticks), the crystallized ligand JDtic (gray sticks), and defined pharmacophore elements (colored spheres). *Right:* The KOR model was overlaid with crystal structures of the  $\mu$  and  $\delta$  opioid receptor (not shown). The pharmacophore consists of one aromatic element (orange sphere) in the same site and plane as the phenol of JDtic (gray sticks), a second aromatic site (orange sphere) between the phenyl rings of BU72 (yellow sticks) and DIPP-NH<sub>2</sub> (magenta sticks), and two basic sites (cyan spheres) adjacent to Glu209 and Glu297.

#### A2.1.4 Docking

The pharmacophore was used to guide initial placement of each arodyn/analog conformer into the prepared KOR, holding both the ligand and the receptor fixed. The ligands were required to obtain geometries that positioned an aromatic moiety inside each aromatic site and place the basic guanidinium in either of the two cationic sites. Poses that satisfied these criteria were analyzed to calculate their binding energies using the GBVI/WSA dG scoring function;<sup>6</sup> those that did not were filtered out prior to docking.

The top 1000 ligand-receptor complexes for arodyn and each of its analogs underwent subsequent induced fit docking. Each ligand-receptor complex was minimized (500 iterations) in the Amber10:EHT forcefield. The ligand and receptor residues containing atoms within 9 Å of the ligand were allowed to move freely, while all other atoms were held fixed. Similar to before, any

resulting ligand-receptor complexes that did not fulfill the pharmacophore criteria were filtered out. Each remaining minimized ligand-receptor complex was then rescored using the GBVI/WSA dG scoring function to estimate the binding energy.

## **A2.2 Results and discussion**

### **A2.2.1 Conformational Searches**

The conformational search protocol was designed to generate large libraries of conformers that thoroughly explored the unique conformational space of arodyn and each of its analogs. For each species, the conformational search largely yielded conformers with extended shapes, though there was an oversampling of compacted conformers in which the guanidinium of Arg<sup>4</sup> formed contacts with the carbonyls of the peptide backbone. Interestingly, there were also a number of conformers (~10%) containing higher energy *cis* amides or alkenes. Taken together, these findings demonstrated that our protocol thoroughly explored the spatial and energetic landscape of each species, as each search generated between 700-10,000 unique conformers for arodyn and each of its analogs.

### **A2.2.2 Receptor Preparation**

The X-ray crystal structure of the KOR was originally determined in its antagonist-bound state. JDTic binds in a unique “V” shape, deep in receptor’s orthosteric site. The arodyn analogs, on account of their bulky macrocyclic structure, likely bind to a slightly different conformation of the receptor. Rather than model prospective KOR structures – which we felt would be speculative and complicate interpretation of the docking results – we focused on using an induced fit docking methodology that would hopefully accommodate the unique shape of these ligands. In keeping with this thinking, most alterations made during structure preparation were conservative in nature

and are standard practice (side chain and hydrogen addition) and/or affect residues distant from the orthosteric site (termini capping).

Still, the unresolved residues of ECL3 (Thr302-Thr306) – which flank the orthosteric site – had to be modeled in to properly reflect the environment of the receptor pocket. Differences in the sequence and number of the residues among ECL3 – as well as the arrangement of the helices flanking it – for the  $\kappa$  (GSTSHS),  $\mu$  (ITIPET), and  $\delta$  (VDIDRRD) opioid receptors make extrapolation of the unresolved region's structure challenging. As a result, the missing residues of ECL3 were spliced into the receptor in their lowest energy conformation, a reasonable approximation of the actual structure of this inherently flexible region.

Finally, the water molecules observed in the X-ray crystal structure of the KOR were removed during structure preparation. Importantly, some of these water molecules occupy the orthosteric site, forming a solvent network that connects the side chain of His291<sup>6,52 7</sup> to the phenolic hydroxyl of JDTic. Analogous networks were observed in other opioid receptor crystal structures;<sup>2,4,5,8,9</sup> they similarly connect the conserved His<sup>6,52</sup> residue to each ligand's phenolic hydroxyl group. This functionality is notably absent in arodyn and its analogs, and we anticipate the water network to change accordingly. We opted to leave this site vacant rather than model a hypothetical solvent network. Instead, we used the pharmacophore to prevent ligands from entering this region of the orthosteric site, ultimately approximating the steric environment of a solvated KOR.

### **A2.2.3 Pharmacophore generation and docking**

This discussion is incorporated in chapter 5. Observed  $\chi_1$  and  $\chi_2$  angles are indicated in Tables A2.1a-d)

Table A2.1a Energy scores of arodyn analogs cyclized between adjacent residues and conformational data of the first residue from modeling studies.

Compound	Pose #	Pose Score	Pose Energy	Residue 1				
				$\omega_{Ac}$	$\phi_1$	$\psi_1$	$\chi_1^1$	$\chi_1^2$
<b>Arodyn</b>	63	-10.7718	-217.1639	179.76	-64.07	-57.13	177.28	-87.67
<b>p<sup>1</sup>p<sup>2</sup></b>	72	-11.0986	-205.1700	-176.65	-53.72	-49.68	168.69	-81.48
<b>m<sup>1</sup>m<sup>2</sup></b>	62	-11.0600	-206.1420	-172.62	-63.99	-52.39	171.43	-85.26
<b>p<sup>2</sup>p<sup>3</sup></b>	312	-10.9785	-206.2552	-178.13	-60.36	-29.93	-179.84	-88.18
<b>m<sup>2</sup>m<sup>3</sup></b>	27	-11.9973	-205.7217	-177.70	-70.98	-51.39	-168.21	-103.65

Table A2.1b Conformational data of the second residue in arodyn analogs cyclized between adjacent residues.

Compound	Pose #	Residue 2				
		$\omega_{1,2}$	$\phi_2$	$\psi_2$	$\chi_2^1$	$\chi_2^2$
<b>Arodyn</b>	63	178.14	-81.41	-61.82	-112.24	41.72
<b>p<sup>1</sup>p<sup>2</sup></b>	72	173.28	-87.15	-50.58	-79.91	-81.62
<b>m<sup>1</sup>m<sup>2</sup></b>	62	175.90	-73.04	-51.96	-75.44	-110.78
<b>p<sup>2</sup>p<sup>3</sup></b>	312	-155.83	-126.47	-49.32	-167.01	-82.98
<b>m<sup>2</sup>m<sup>3</sup></b>	27	168.06	-80.05	-42.10	-60.23	170.34

Table A2.1c Conformational data of the third residue in arodyn analogs cyclized between adjacent residues.

Compound	Pose #	Residue 3				
		$\omega_{2,3}$	$\phi_3$	$\psi_3$	$\chi_3^1$	$\chi_3^2$
<b>Arodyn</b>	63	-166.37	-81.54	151.27	-49.73	-95.87
<b>p<sup>1</sup>p<sup>2</sup></b>	72	-151.42	-92.90	19.07	-53.81	-79.10
<b>m<sup>1</sup>m<sup>2</sup></b>	62	-159.16	-87.19	157.90	-66.53	-85.24
<b>p<sup>2</sup>p<sup>3</sup></b>	312	-168.82	-93.21	4.09	-63.18	-90.20
<b>m<sup>2</sup>m<sup>3</sup></b>	27	-163.82	-66.33	131.87	-81.52	-116.36

Table A2.1d Conformational data of the fourth residue in arodyn analogs cyclized between adjacent residues.

Compound	Pose #	Residue 4				
		$\omega_{3,4}$	$\phi_4$	$\psi_4$	$\chi^1$	$\chi^2$
Arodyn	63	-179.67	-92.09	139.48	-80.92	66.26
p <sup>1</sup> p <sup>2</sup>	72	159.58	-144.79	130.05	-156.36	75.97
m <sup>1</sup> m <sup>2</sup>	62	-172.58	-77.85	-27.56	-86.21	62.77
p <sup>2</sup> p <sup>3</sup>	312	-174.85	64.07	154.51	-56.99	-60.38
m <sup>2</sup> m <sup>3</sup>	27	-161.49	-73.25	-30.86	-60.16	-71.47

## A2.4 Conclusions

Among the different species, only the p<sup>1</sup>p<sup>2</sup> analog did not form an ionic contact between the guanidinium of its Arg<sup>4</sup> and the important nonconserved residue Glu297;<sup>10</sup> it instead oriented this moiety toward the side chain of Glu209. This analog is probably capable of forming a contact with Glu297, but our protocol likely undersampled its conformational space and missed that particular binding pose. The side chain of the m<sup>1</sup>m<sup>2</sup> and m<sup>2</sup>m<sup>3</sup> analogs adopted strained conformations to form additional ion-dipole contacts with the carbonyl of *m*-Tyr<sup>2</sup>. Again, the docking experiments were performed using an unsolvated receptor, which biases the ligand-receptor complex toward forming the maximum amount of possible contacts. In reality, there are solvent molecules that must be displaced in order for this interaction to occur, and we question whether this contact is truly relevant *in vivo*.

The four species that formed contacts between Arg<sup>4</sup> and Glu297 positioned their guanidinium groups near the 5' carbon of naltrindole (~2.5 Å from 5' carbon to guanidyl carbon) when overlaid with the crystal structure of naltrindole in the  $\delta$  opioid receptor (Figure A2.2).<sup>8</sup> Interestingly, the analog 5'-guanidinonaltrindole (5'-GNTI) acts as a  $\kappa$ -selective antagonist, and its guanidinium was previously shown to impart selectivity for the  $\kappa$  opioid receptor – via interaction with Glu297 – over the  $\delta$  opioid receptor, which has Trp284 in this position.<sup>11</sup> Taken together,

these results support this orientation of the guanidinium of Arg<sup>4</sup> and the overall binding mode of arodyn and its analogs.

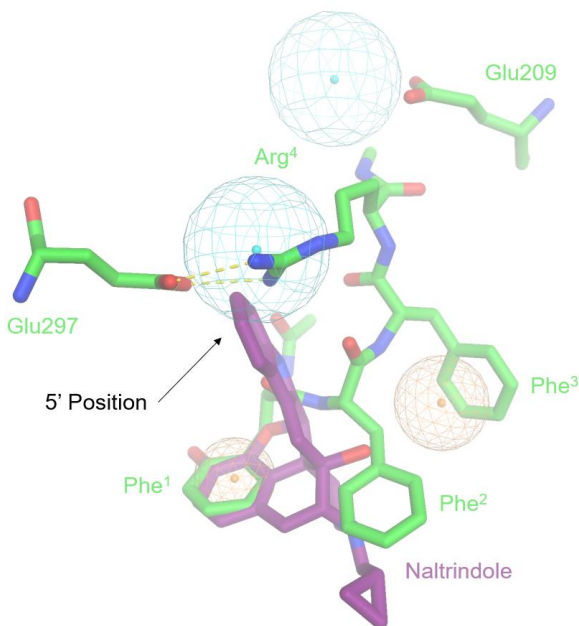


Figure A2.2 Overlay of arodyn (green) docked in the  $\kappa$  opioid receptor model (green) and the crystal structure of naltrindole (purple) in the  $\delta$  opioid receptor (not shown). The guanidinium of Arg<sup>4</sup> is positioned within 2.5 Å of the 5' position of naltrindole, where the guanidinium group of the  $\kappa$ -selective antagonist 5'-guanidinonaltrindole (5'-GNTI) would lie. This moiety was previously found to bind Glu297 of the  $\kappa$  opioid receptor, a finding that – by extension – supports the results from the docking study.

The dihedral angles of the peptide backbones all fell within acceptable Ramachandran values (Table A3.1a-d), including the residues constrained by the macrocycle. The dihedral angles from  $\omega_{Ac-1}$  to  $\phi_3$  are nearly identical among the docked peptides, and the backbones of these analogs overlay well with the backbone of DIPP-NH<sub>2</sub> (Figure A2.3).

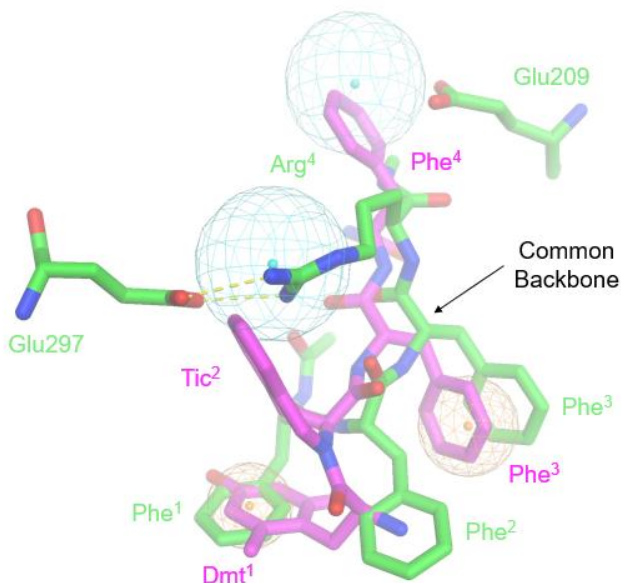


Figure A2.3 Overlay of arodyn (green) docked in the  $\kappa$  opioid receptor model (green) and the crystal structure of DIPP-NH<sub>2</sub> (magenta) in the  $\delta$  opioid receptor (not shown). The two peptidic ligands have different sequences, yet they can arrange the aromatic rings of residues 1 and 3 similarly in the pharmacophore (orange spheres). Interestingly, the backbones of the two peptides are strikingly similar from C $\alpha$ <sup>2</sup> to N<sup>4</sup>, suggesting that peptidic ligands may bind in similar conformations. Phe<sup>4</sup> and Arg<sup>4</sup> of both peptides do not overlay well, although Phe<sup>4</sup> of DIPP-NH<sub>2</sub> was found to occupy different conformations even in the crystal structure.

## A2.5 References

- (1) Brownstein, M. J. A brief history of opiates, opioid peptides, and opioid receptors. *Proc Natl Acad Sci U.S.A.* **1993**, *90*, 5391-5393.
- (2) Wu, H.; Wacker, D.; Mileni, M.; Katritch, V.; Han, G. W.; Vardy, E.; Liu, W.; Thompson, A. A.; Huang, X. P.; Carroll, F. I.; Mascarella, S. W.; Westkaemper, R. B.; Mosier, P. D.; Roth, B. L.; Cherezov, V.; Stevens, R. C. Structure of the human kappa-opioid receptor in complex with JDTic. *Nature* **2012**, *485*, 327-332.
- (3) Weiner, S. J.; Kollman, P. A.; Case, D. A.; Singh, U. C.; Ghio, C.; Alagona, G.; Profeta, S.; Weiner, P. A New Force-Field for Molecular Mechanical Simulation of Nucleic-Acids and Proteins. *J Am Chem Soc* **1984**, *106*, 765-784.
- (4) Huang, W.; Manglik, A.; Venkatakrisnan, A. J.; Laeremans, T.; Feinberg, E. N.; Sanborn, A. L.; Kato, H. E.; Livingston, K. E.; Thorsen, T. S.; Kling, R. C.; Granier, S.;

Gmeiner, P.; Husbands, S. M.; Traynor, J. R.; Weis, W. I.; Steyaert, J.; Dror, R. O.; Kobilka, B. K. Structural insights into mu-opioid receptor activation. *Nature* **2015**, *524*, 315-321.

(5) Fenalti, G.; Zatsopin, N. A.; Betti, C.; Giguere, P.; Han, G. W.; Ishchenko, A.; Liu, W.; Guillemyn, K.; Zhang, H.; James, D.; Wang, D.; Weierstall, U.; Spence, J. C.; Boutet, S.; Messerschmidt, M.; Williams, G. J.; Gati, C.; Yefanov, O. M.; White, T. A.; Oberthuer, D.; Metz, M.; Yoon, C. H.; Barty, A.; Chapman, H. N.; Basu, S.; Coe, J.; Conrad, C. E.; Fromme, R.; Fromme, P.; Tourwe, D.; Schiller, P. W.; Roth, B. L.; Ballet, S.; Katritch, V.; Stevens, R. C.; Cherezov, V. Structural basis for bifunctional peptide recognition at human delta-opioid receptor. *Nat Struct Mol Biol* **2015**, *22*, 265-268.

(6) Corbeil, C. R.; Williams, C. I.; Labute, P. Variability in docking success rates due to dataset preparation. *J Comput Aided Mol Des* **2012**, *26*, 775-786.

(7) Ballesteros, J. A.; Weinstein, H. Integrated methods for the construction of three-dimensional models and computational probing of structure-function relations in G protein-coupled receptors In *Methods in Neurosciences*; Stuart, C. S., Ed.; Academic Press: 1995; Vol. Volume 25, p 366-428.

(8) Fenalti, G.; Giguere, P. M.; Katritch, V.; Huang, X. P.; Thompson, A. A.; Cherezov, V.; Roth, B. L.; Stevens, R. C. Molecular control of delta-opioid receptor signalling. *Nature* **2014**, *506*, 191-196.

(9) Manglik, A.; Kruse, A. C.; Kobilka, T. S.; Thian, F. S.; Mathiesen, J. M.; Sunahara, R. K.; Pardo, L.; Weis, W. I.; Kobilka, B. K.; Granier, S. Crystal structure of the mu-opioid receptor bound to a morphinan antagonist. *Nature* **2012**, *485*, 321-326.

(10) Metzger, T. G.; Paterlini, M. G.; Ferguson, D. M.; Portoghese, P. S. Investigation of the selectivity of oxymorphone- and naltrexone-derived ligands via site-directed mutagenesis of opioid receptors: exploring the "address" recognition locus. *J Med Chem* **2001**, *44*, 857-862.

(11) Sharma, S. K.; Jones, R. M.; Metzger, T. G.; Ferguson, D. M.; Portoghese, P. S. Transformation of a kappa-opioid receptor antagonist to a kappa-agonist by transfer of a guanidinium group from the 5'- to 6'-position of naltrindole. *J Med Chem* **2001**, *44*, 2073-2079.



**Appendix 3 -  $^1\text{H}$  NMR spectra of arodyn analogs cyclized between adjacent residues using RCM**

<sup>a</sup>Compound numbers are the same as those used in Chapter 5

Figure A3.1  $^1\text{H}$ -spectra of **2**. The spectrum of olefinic protons following decoupling of adjacent methylene protons at 4.64 is shown at the bottom as well a COSY showing olefinic and O-methylene protons.

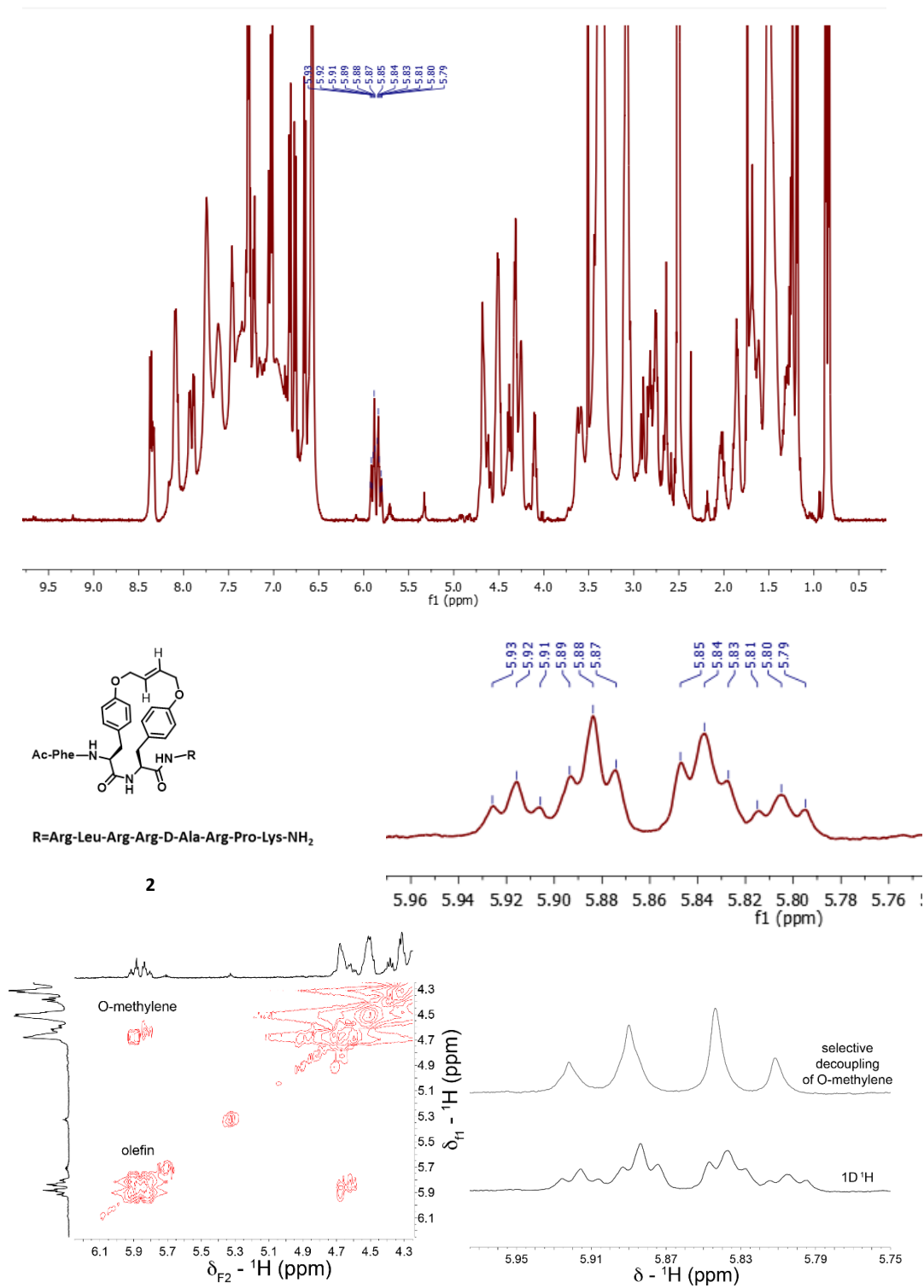


Figure A3.2  $^1\text{H}$ -spectra of **3**.

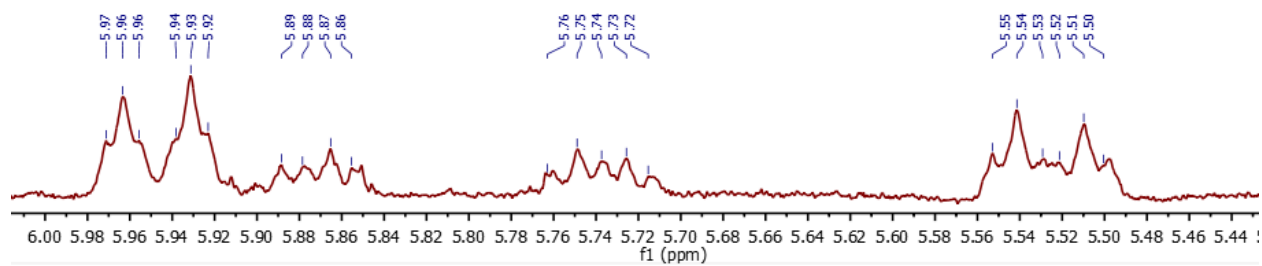
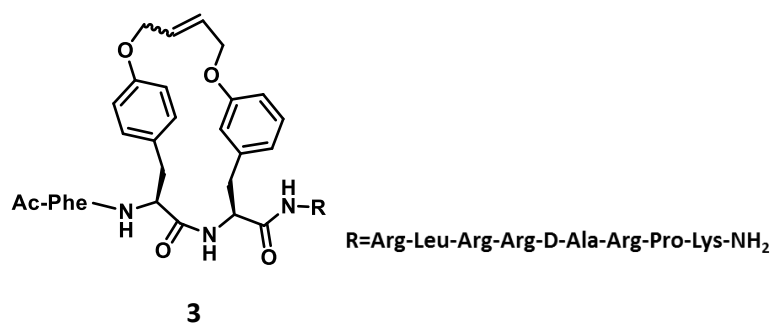
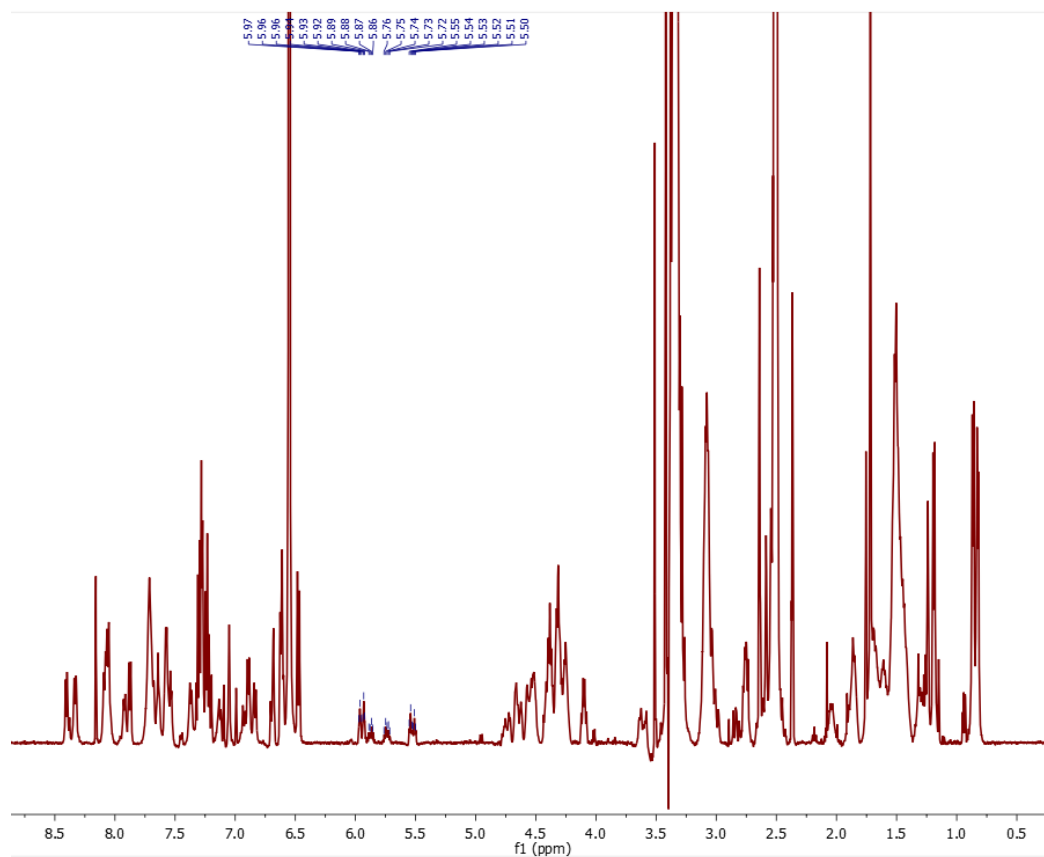


Figure A3.3  $^1\text{H}$ -spectra of **4**.

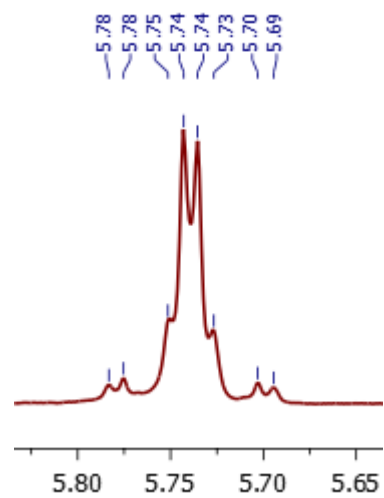
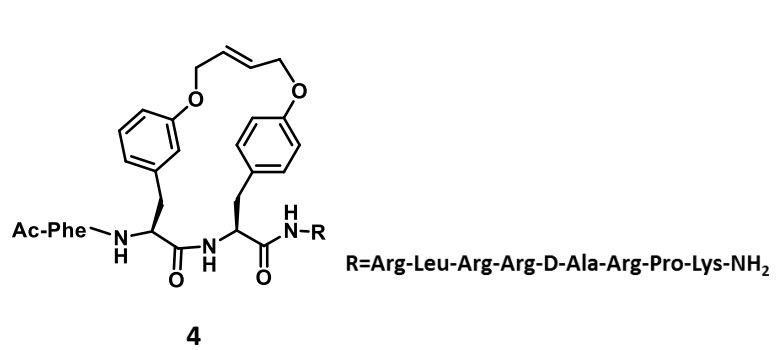
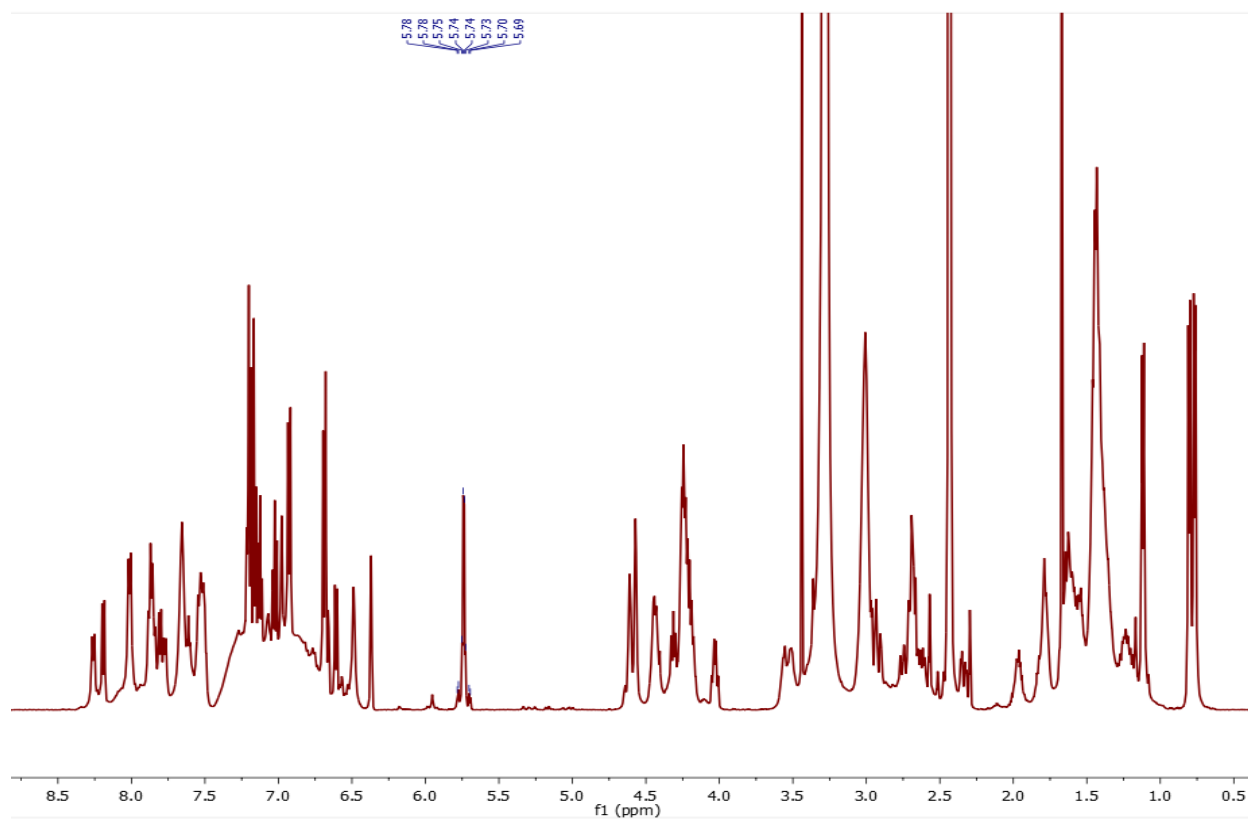


Figure A3.4  $^1\text{H}$ -spectra of **5**.

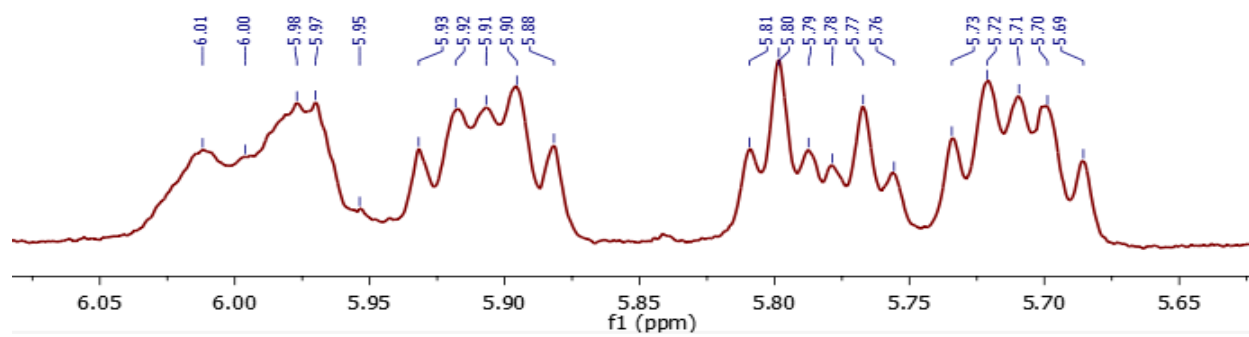
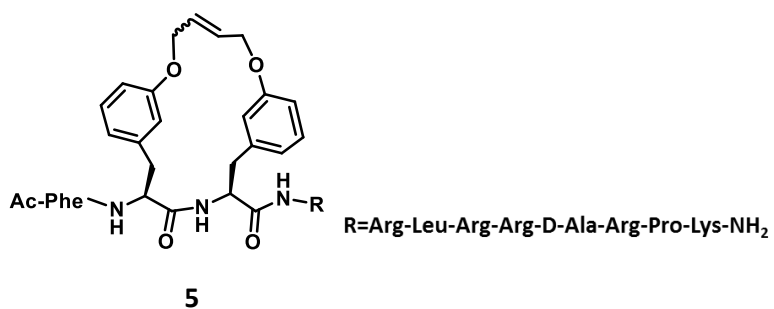
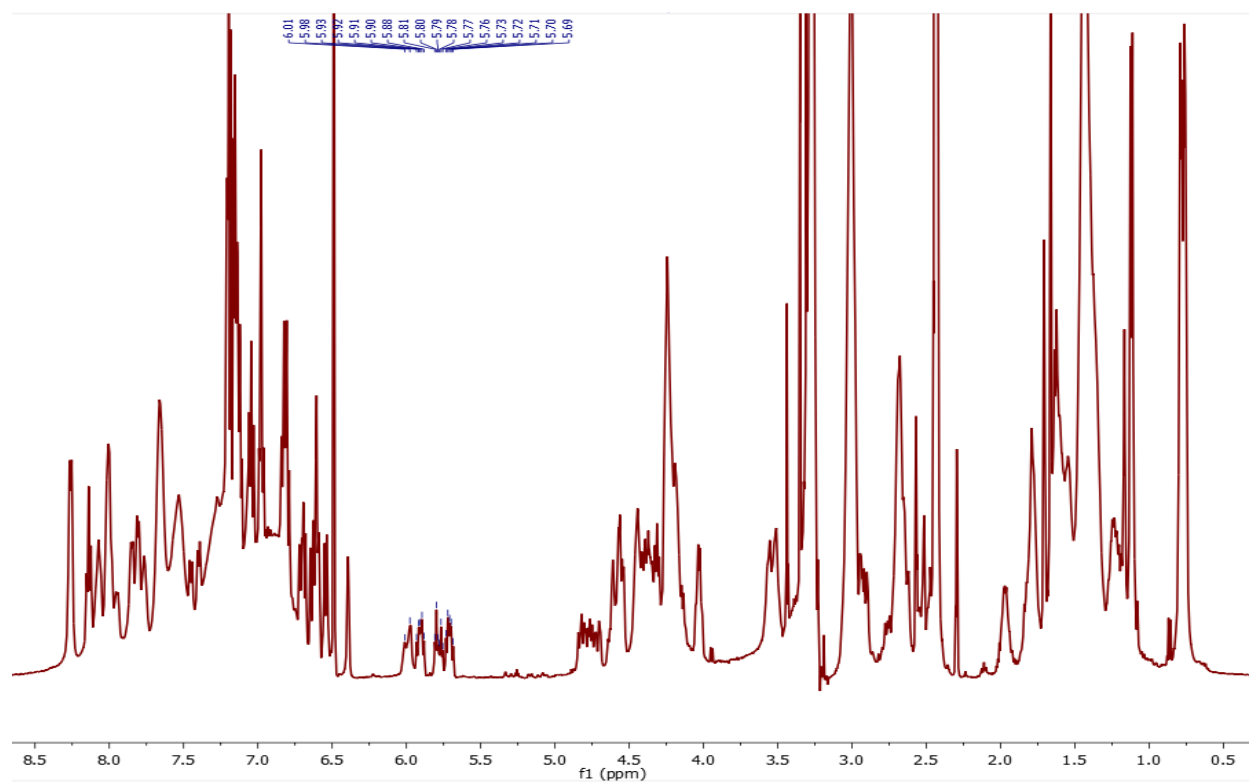
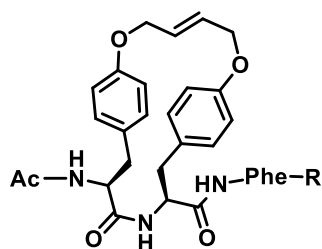
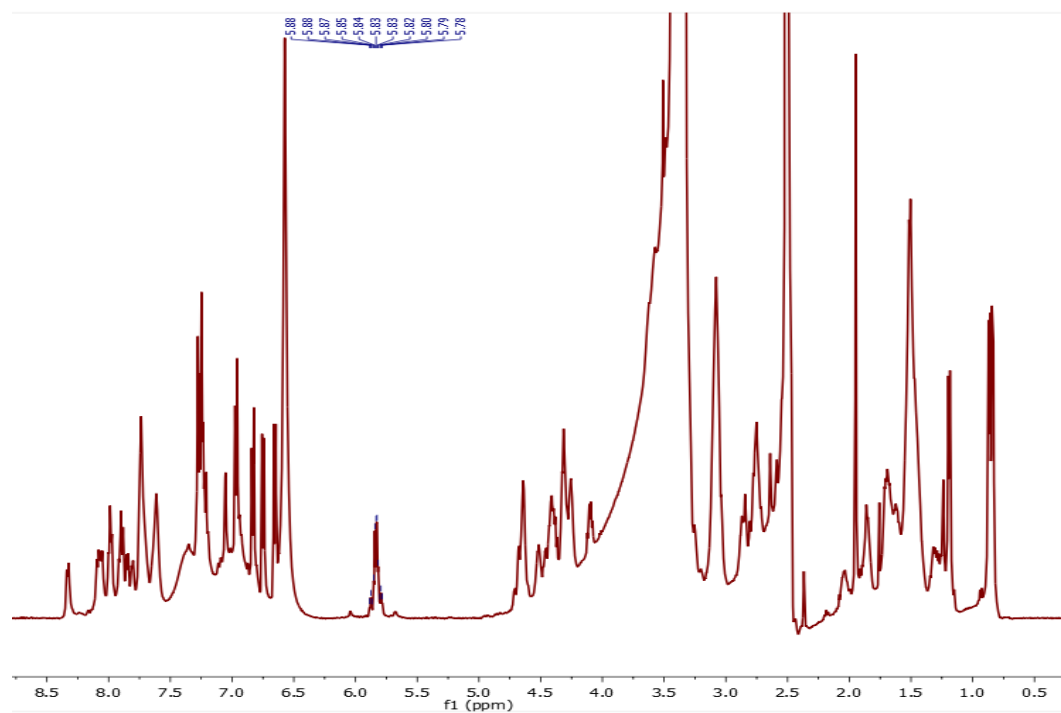


Figure A3.5 <sup>1</sup>H-spectra of **6**. The spectrum of olefinic protons following decoupling of adjacent methylene protons at 4.68 is shown at the bottom.



**6**

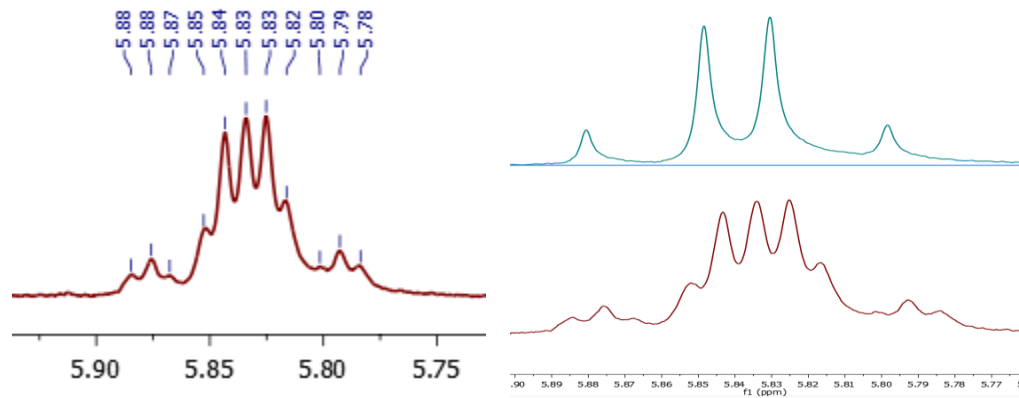
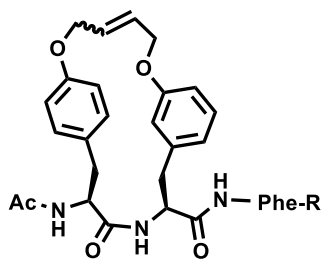
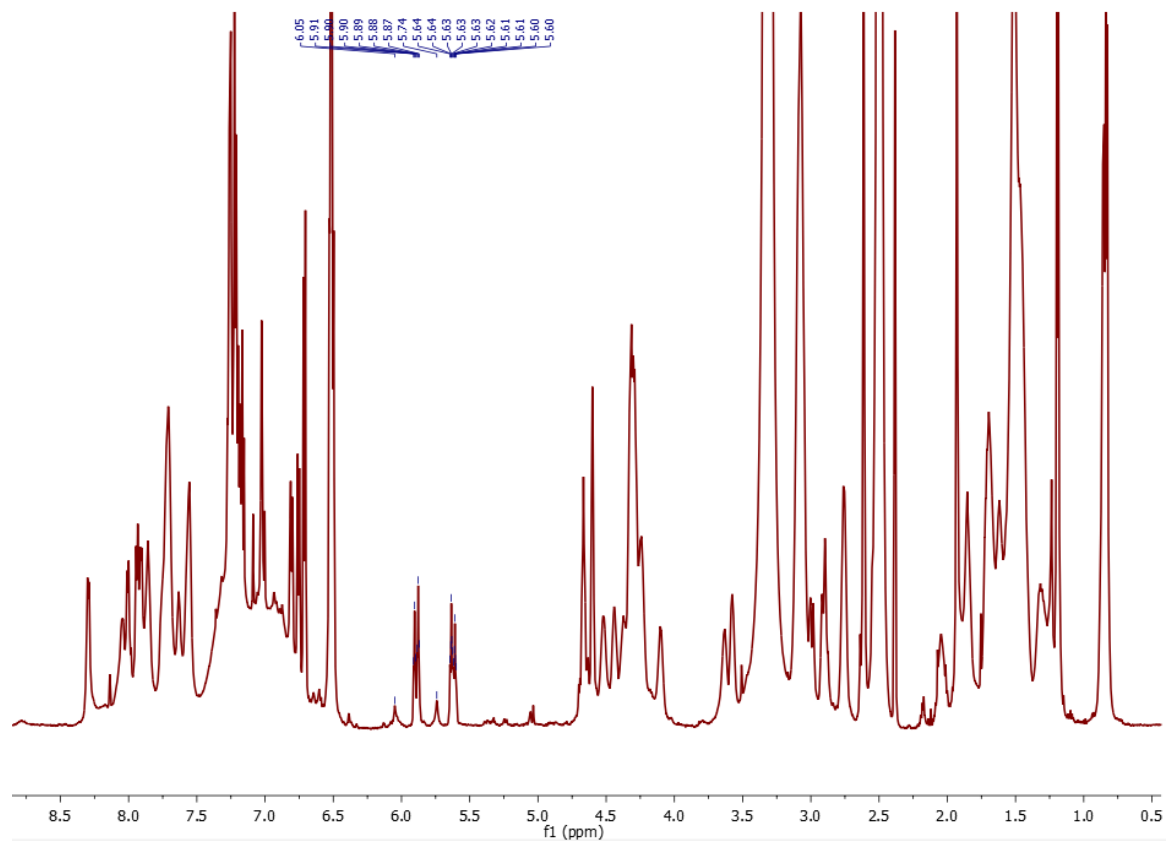


Figure A3.6  $^1\text{H}$ -spectra of **7**.



**7**

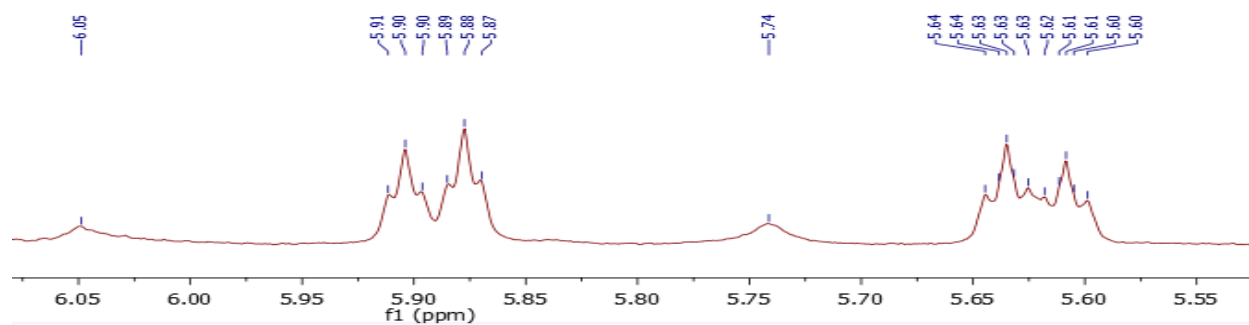
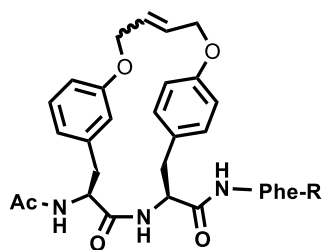
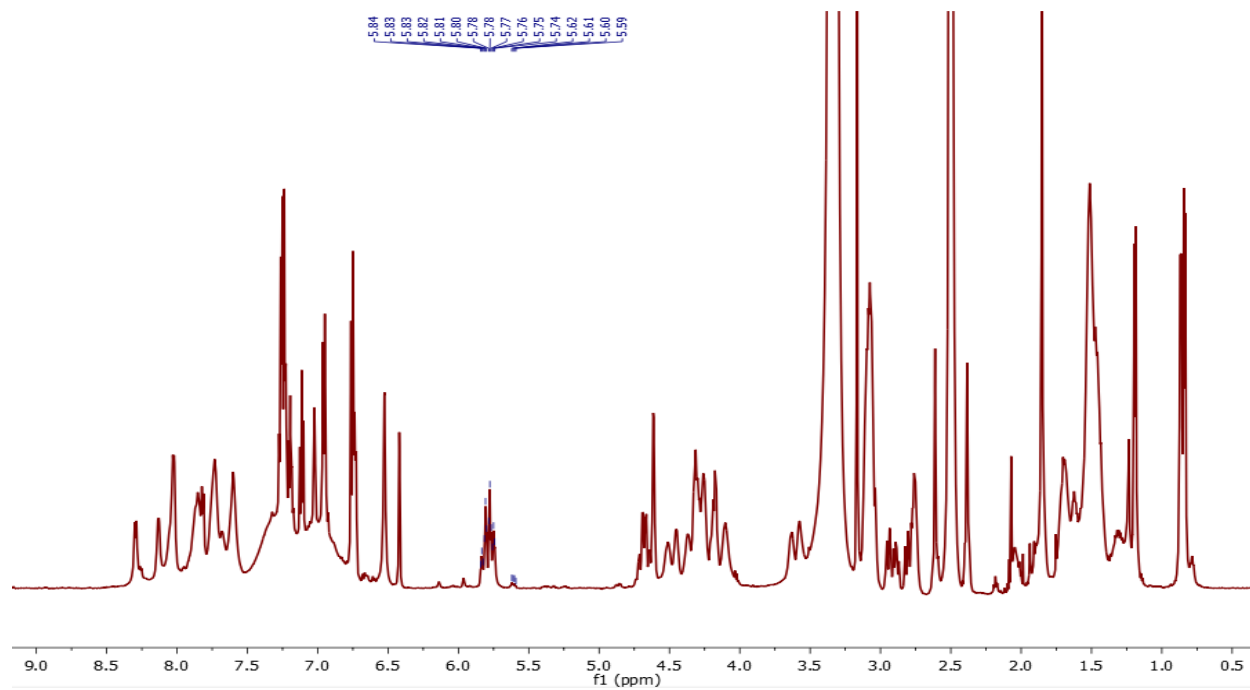


Figure A2.7  $^1\text{H}$ -spectra of **8**.



R=Arg-Leu-Arg-Arg-D-Ala-Arg-Pro-Lys-NH<sub>2</sub>

**8**

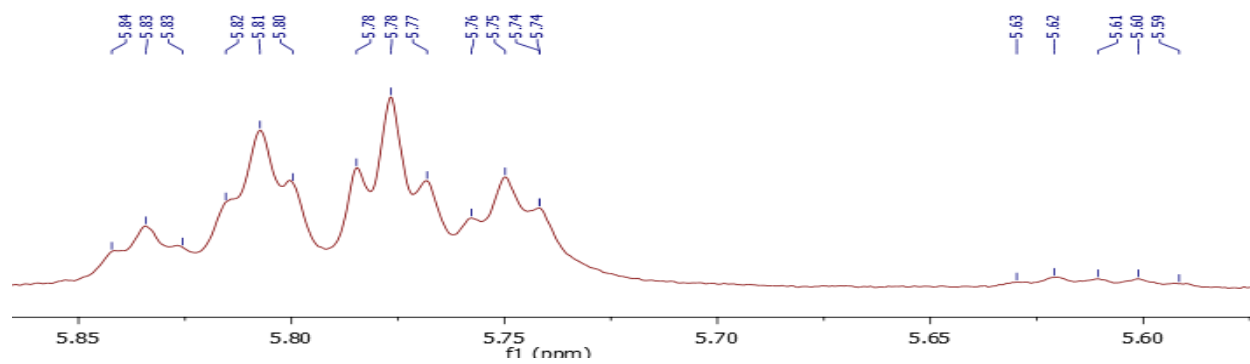
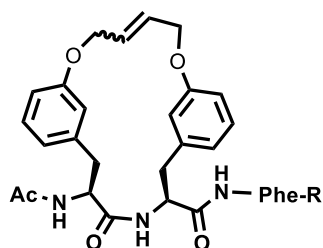
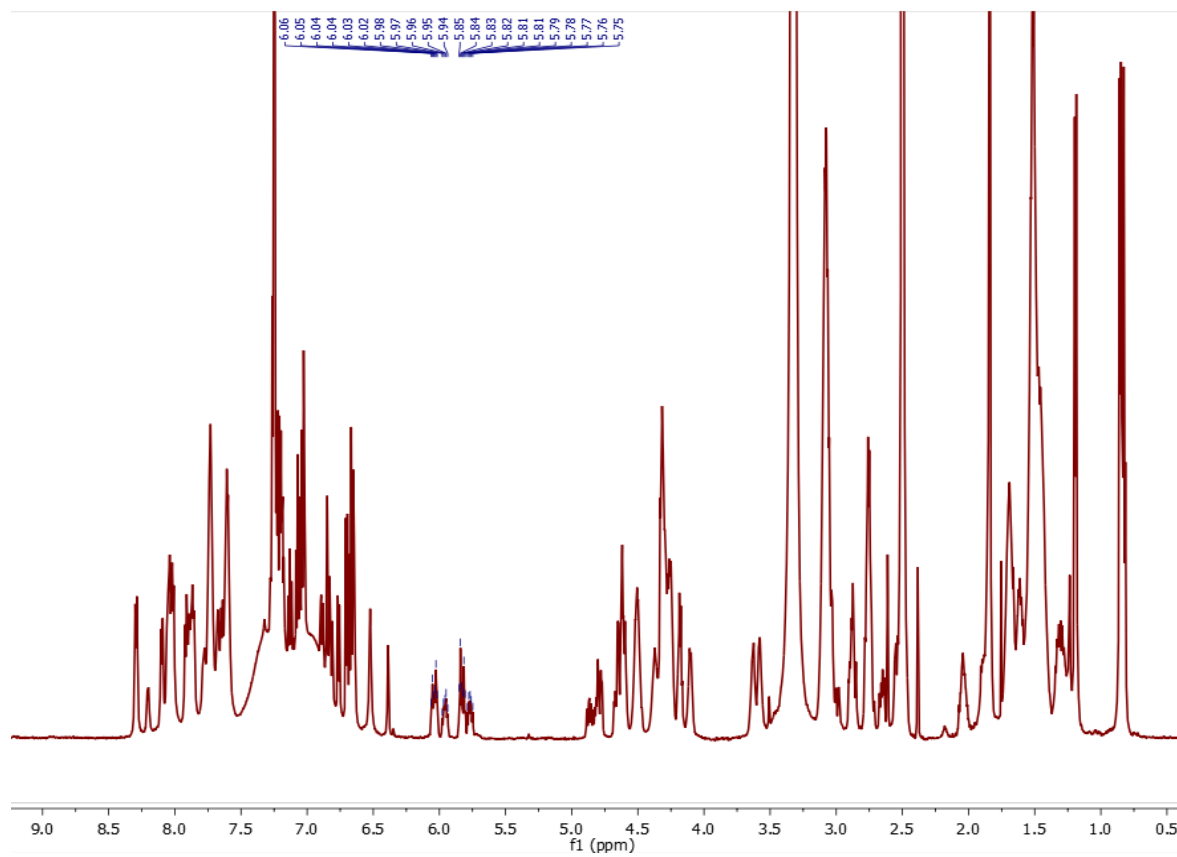


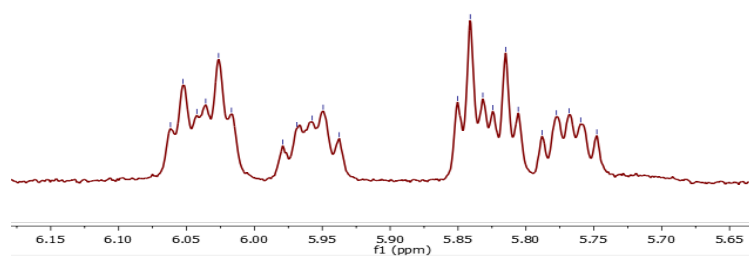


Figure A3.8  $^1\text{H}$ -spectra of **9**.



R=Arg-Leu-Arg-Arg-D-Ala-Arg-Pro-Lys-NH<sub>2</sub>

**9**



**Appendix 4 - <sup>1</sup>H NMR spectra of *cyclo*[5hex,AllGly<sup>5</sup>]arodyn**

<sup>a</sup>Compound numbers are the same as those used in Chapter 6.



Figure A4.2  $^1\text{H}$ -spectra of **14 trans**.

